

***New non-ionic polymers with UCST-
type and complex phase transition
behavior***

DISSERTATION

zur Erlangung des akademischen Grades einer Doktorin/eines

Doktors der Naturwissenschaften (Dr. rer. nat.)

in der Bayreuther Graduiertenschule für Mathematik und Naturwissenschaften

(BayNAT)

der Universität Bayreuth

vorgelegt von

Florian Hermann Ulrich Käfer

aus Tübingen

Bayreuth, 2018

Die vorliegende Arbeit wurde in der Zeit von (*Juni/2014*) bis (*Oktober/2018*) in Bayreuth am Lehrstuhl (*Makromolekulare Chemie 2*) unter Betreuung von Frau Professorin Dr. *Seema Agarwal* angefertigt.

Vollständiger Abdruck der von der Bayreuther Graduiertenschule für Mathematik und Naturwissenschaften (BayNAT) der Universität Bayreuth genehmigten Dissertation zur Erlangung des akademischen Grades einer Doktorin/ eines Doktors der Naturwissenschaften (Dr. rer. nat.).

Dissertation eingereicht am: 16.10.2018

Zulassung durch das Leitungsgremium: 14.11.2018

Wissenschaftliches Kolloquium: 22.05.2019

Amtierender Direktor: Prof. Dr. Dirk Schüler

Prüfungsausschuss:

| | |
|-----------------------------|---------------|
| Prof. Dr. Seema Agarwal | (Gutachterin) |
| Prof. Dr. Matthias Karg | (Gutachter) |
| Prof. Dr. Matthias Breuning | (Vorsitz) |
| Prof. Dr. Peter Strohriegl | |

(Weitere/r Gutachter: Prof. Dr. Andrij Pich

„Alle Schwierigkeiten und Hindernisse sind Stufen auf denen wir in die Höhe steigen.“

Friedrich Nietzsche

Table of Contents

| | | |
|-------|--|----|
| 1 | Summary | 1 |
| 2 | Zusammenfassung | 5 |
| 3 | List of symbols and abbreviations | 9 |
| 4 | Introduction..... | 11 |
| 4.1 | Thermoresponsive polymers | 11 |
| 4.2 | Polymers with a LCST-type phase transition..... | 14 |
| 4.3 | Non-ionic polymers with a UCST-type phase transition..... | 16 |
| 4.4 | Polymers with double (LCST and UCST)-type phase transitions | 23 |
| 4.5 | Thermoresponsive interpenetrating network (IPN) hydrogels..... | 26 |
| 4.6 | Radical polymerization | 29 |
| 4.7 | Aims of the thesis | 33 |
| 5 | Literature | 34 |
| 6 | Synopsis..... | 42 |
| 6.1 | LCST and UCST in One: Double Thermoresponsive Behavior of Block Copolymers of Poly(ethylene glycol) and Poly(acrylamide-co-acrylonitrile) | 44 |
| 6.1.1 | Individual Contribution to Joint Publications..... | 46 |
| 6.2 | Tunable, Concentration-Independent, Sharp, Hysteresis-Free UCST Phase Transition from Poly(<i>N</i> -Acryloyl Glycinamide-Acrylonitrile) System | 47 |
| 6.2.1 | Individual Contribution to Joint Publications..... | 49 |
| 6.3 | Let There be Light: Polymeric Micelles with Upper Critical Solution Temperature as Light-Triggered Heat Nanogenerators for Combating Drug-Resistant Cancer | 50 |
| 6.3.1 | Individual Contribution to Joint Publications..... | 52 |
| 6.4 | Tuning the Phase Transition from UCST-Type to LCST-Type by Composition Variation of Polymethacrylamide Polymers..... | 53 |
| 6.4.1 | Individual Contribution to Joint Publications..... | 55 |

| | | |
|-------|--|-----|
| 6.5 | Controlled-Release LCST-Type Nonwoven Depots via Squeezing-Out Thermal Response..... | 56 |
| 6.5.1 | Individual Contribution to Joint Publications..... | 58 |
| 6.6 | Interpenetrating Thermophobic, Thermophilic Dual Responsive Networks . | 59 |
| 6.6.1 | Individual Contribution to Joint Publications..... | 60 |
| 7 | Reprints of Publications..... | 62 |
| 7.1 | LCST and UCST in One: Double Thermoresponsive Behavior of Block Copolymers of Poly(ethylene glycol) and Poly(acrylamide-co-acrylonitrile) | 63 |
| 7.2 | Tunable, Concentration-Independent, Sharp, Hysteresis-Free UCST Phase Transition from Poly(<i>N</i> -Acryloyl Glycinamide-Acrylonitrile) System | 75 |
| 7.3 | Let There be Light: Polymeric Micelles with Upper Critical Solution Temperature as Light-Triggered Heat Nanogenerators for Combating Drug-Resistant Cancer | 90 |
| 7.4 | Tuning the Phase Transition from UCST-Type to LCST-Type by Composition Variation of Polymethacrylamide Polymers..... | 119 |
| 7.5 | Controlled-Release LCST-Type Nonwoven Depots via Squeezing-Out Thermal Response..... | 132 |
| 7.6 | Interpenetrating Thermophobic, Thermophilic Dual Responsive Networks | 145 |
| 8 | Outlook..... | 154 |
| 9 | Conferences participation..... | 155 |
| 10 | Acknowledgment | 156 |
| 11 | (Eidesstattliche) Versicherung und Erklärungen | 157 |

1 Summary

The research and application of thermoresponsive polymers have been attracting great interest over the last 10 years. As an example, thermoresponsive polymers are used for applications in medicine, biotechnology, and the production of functional materials. Generally, thermoresponsive polymers can be divided into two types: (1) Polymers which dissolve above a critical temperature, i.e. show an upper critical solution temperature, in short UCST, (2) Polymers which dissolve below a certain temperature, i.e. show a lower critical solution temperature, in short LCST. Furthermore, polymers which have both a UCST and LCST are known and are attracting attention in research and development.

This dissertation focused on the synthesis of novel thermoresponsive copolymers and their possible application as a "smart" matrix. The following issues were discussed in detail:

- influence of hydrophilic / hydrophobic groups (comonomers) on thermoresponsive behavior
- temperature dependent change of the polymer morphology
- temperature induced release of active substances / nanoparticles
- fabrication of a double thermoresponsive hydrogel with interpenetrated network structure

In the introductory part of this dissertation, the basics of thermoresponsive polymers are discussed and an overview of the thermoresponsive polymers which are already known in the literature is given. Special attention was directed to non-ionic UCST polymers and polymers with both UCST and LCST. In the following, a short overview

Summary

of methods of controlled radical polymerization, which were used for the synthesis of copolymers in the context of this thesis, is presented.

In the second part of this dissertation, the processed and published results of the subprojects are summarized, and their connection is explained.

The **first** publication deals with the synthesis of a double thermoresponsive poly(ethylene glycol)-*b*-poly(acrylamide-*co*-acrylonitrile) (PEG-*b*-P(AAm-AN)) block copolymer. Based on the known P(AAm-AN) UCST copolymer, the phase transition behavior could be converted into a double thermoresponsive behavior with a UCST and LCST by applying a short hydrophilic PEG block. The double thermoresponsive behavior depends on the length of the PEG block, the acrylamide/acrylonitrile ratio in the copolymer, and on the concentration. Temperature dependent dynamic light scattering (DLS) and transmission electron microscopy (TEM) experiments could illustrate the change of the polymer morphology of micelles to aggregates and to micelles again, which is responsible for the double thermoresponsive behavior.

In the **second** publication, the influence of a hydrophobic comonomer on the thermoresponsive phase behavior of poly(*N*-acryloylglycinamide) (PNAGA) was demonstrated. Using Reversible Addition Fragmentation Transfer (RAFT) polymerization, block-like P(NAGA-AN) copolymers could be synthesized. In contrast to PNAGA, these copolymers exhibit a narrow cooling/heating hysteresis in water, which could be tuned over a temperature range of < 5-40 °C depending on the AN content. Once more, the temperature-dependent change of the polymer morphology could be visualized through TEM and DLS experiments. Interestingly, the copolymers showed no dependence of the cloud point on the concentration, which is rarely observed in UCST polymers.

Summary

On the basis of the first two publications, a PEG-*b*-P(NAGA-AN) block copolymer could be synthesized by free radical polymerization, using a macroinitiator in the **third** publication. Due to the microstructure of the PEG-*b*-P(NAGA-AN) copolymer, the copolymer formed micelles, which could be successfully used to encapsulate the cancer drug doxorubicin (DOX) and a photo-thermal agent. Exposure to near-infrared light resulted in the dissolution of the micelles, which enabled the spatiotemporal controlled release of DOX, and prevented efflux into drug-resistant MCF-7/DOX cells. Thus, an effective prevention of the growth of drug-resistant tumor cells was proven by *in vivo* studies.

In the **fourth** publication, the influence of different *N*-substituted acrylamide-based comonomers on the thermoresponsive behavior of poly(methacrylamide) (PMAAm), which shows a UCST with broad cooling/heating hysteresis, was investigated. The copolymers of MAAm and *N*-cyclohexylacrylamide, respectively *N-tert*-butylacrylamide, were synthesized by free-radical polymerization (FRP), showing a rare phenomenon, in which the type of thermoresponsive behavior could be switched from a UCST to an LCST with regions of complete solubility or insolubility, depending on the copolymer composition.

The **fifth** publication shows the synthesis and application of a terpolymer of MAAm, *N-tert*-butylacrylamide and UV-crosslinkable 4-acryloylbenzophenone. This terpolymer was prepared by FRP and showed LCST behavior. Electrospinning of the terpolymer allowed the fabrication of a nanofiber matrix which, due to a temperature increase, exhibited strong contraction, allowing the controlled release of nanoparticles.

The **sixth** and last publication demonstrates the production of a double thermoresponsive, interpenetrating polymer network (IPN) poly(*N*-acryloylglycinamide)/poly(*N*-isopropylacrylamide) PNAGA/PNIPAAm hydrogel. The

Summary

synthesis was carried out in two, independently of one another, sequential UV induced polymerizations. Mechanical properties of the IPNs showed a clear dependence on temperature and on PNIPAAm content. As a result, it could be shown that better mechanical properties of the IPN are obtained with higher temperatures or a decreasing NIPAAm content.

In the outlook of this thesis, the synthesis and potential application of novel UCST and double thermoresponsive polymers are discussed. In particular, the use of new, acrylamide-based, *N*- and α -substituted comonomers is to the fore.

2 Zusammenfassung

Sowohl die Forschung als auch die Anwendung von thermoresponsiven Polymeren, hat etwa in den letzten 10 Jahren erhebliches Interesse erfahren. So werden heute thermoresponsive Polymere etwa für Anwendungen in der Medizin, Biotechnologie und allgemein zur Herstellung funktioneller Materialien verwendet. Grundsätzlich werden thermoresponsive Polymere in zwei Klassen unterteilt: (1) Polymere welche sich oberhalb einer kritischen Temperatur lösen, also eine (engl. upper critical solution temperature) kurz UCST zeigen, (2) Polymere welche sich unterhalb einer bestimmten Temperatur lösen (engl. lower critical solution temperature) kurz LCST zeigen. Auch Polymere welche beides, eine UCST als auch eine LCST aufweisen, sind bekannt und erfreuen sich zunehmender Aufmerksamkeit in Forschung Entwicklung.

Im Rahmen dieser Dissertation wurde auf die Synthese neuartiger thermoresponsiver Copolymere und deren mögliche Anwendungen als „smarte“ Matrix eingegangen. Hierbei wurde detailliert auf folgende Themengebiete eingegangen.

- Einfluss hydrophiler / hydrophober Gruppen (Comonomere) auf das thermoresponsive Verhalten
- Temperatur abhängige Änderung der Polymer Morphologie in wässriger Umgebung
- Temperatur induzierte Freisetzung von Wirkstoffen / Nanopartikeln
- Darstellung eines doppelt thermoresponsiven Hydrogels mit interpenetrierter Netzwerkstruktur

Im Einleitungsteil dieser Arbeit wird auf die Grundlagen thermoresponsiver Polymere eingegangen und ein Überblick über die in der Literatur bereits bekannten

Zusammenfassung

thermoresponsiven Polymere gegeben. Hier wurde spezielle auf nicht ionische UCST Polymere und Polymere welche UCST und LCST in einem aufweisen, eingegangen. Nachfolgende wird ein kurzer Überblick über Methoden der kontrollierten radikalischen Polymerisation dargelegt, welche zur Synthese von Copolymeren im Rahmen dieser Arbeit angewendet wurde.

Im zweiten Teil dieser Dissertation werden die Ergebnisse der bearbeiteten und veröffentlichten Teilprojekte zusammenfassend dargestellt und deren Zusammenhang erläutert.

Die **erste** Publikation behandelt die Synthese eines neuen doppelt thermoresponsiven Polyethylenglycol-*b*-Poly(acrylamid-*co*-acrylnitril) (PEG-*b*-P(AAm-AN) Blockcopolymer. Ausgehend vom bereits bekannten P(AAm-AN) UCST Copolymer, konnte das UCST Phasenübergangsverhalten durch Anbringen eines kurzen hydrophilen PEG Blocks, in ein doppelt thermoresponsives Verhalten, mit einer UCST und LCST, überführt werden. Hierfür wurde ein PEG-Makroinitiator zur Initiierung der freien radikalischen Polymerisation von Acrylamid mit Acrylnitril verwendet. Dabei zeigt sich, dass das doppelt thermoresponsive Verhalten von der Länge des PEG-Blocks, dem Acrylamid/Acrylnitril Verhältnis im Copolymer, als auch von der Konzentration abhängig ist. Temperaturabhängige Dynamische Lichtstreuexperimente (DLS) und Transmissionselektronenmikroskopie (TEM) Messungen konnten hierbei, die für das doppelt thermoresponsive Verhalten verantwortliche Änderung der Polymorphologie von Mizellen, zu Aggregaten und wieder zu Mizellen, veranschaulichen.

In der **zweiten** Publikation konnte der Einfluss eines hydrophoben Comonomers auf das thermoresponsive Phasenverhalten von Poly(*N*-acryloylglycinamid) gezeigt werden. Unter Verwendung der Reversiblen Additions-Fragmentierung Transfer

Zusammenfassung

(RAFT) Polymerisation konnten blockartige P(NAGA-AN) Copolymere synthetisiert werden. Im Gegensatz zu PNAGA weisen diese Copolymere eine enge Kühl-/Heizhysterese in Wasser auf, die in Abhängigkeit vom AN-Gehalt über einen Temperaturbereich von $< 5-40$ °C eingestellt werden konnte. Wie bereits bei der ersten Arbeit konnte auch hier die temperaturabhängige Änderung der Polymormorphologie mittels TEM und DLS Experimenten veranschaulicht werden. Interessanterweise zeigten die Copolymere keine Abhängigkeit des Trübungspunkt von der Konzentration, was für UCST Polymere selten beobachtet werden konnte.

Auf Grundlage der ersten beiden Publikation, konnte in der **dritten** Publikation mittels freier radikalischer Polymerisation unter der Verwendung eines Makroinitiators ein PEG-*b*-P(NAGA-AN) Blockcopolymer synthetisiert werden. Aufgrund der Mikrostruktur des PEG-*b*-P(NAGA-AN)-Copolymers bildete dieses Mizellen, welche erfolgreich für die Verkapselung des Krebsmedikaments Doxorubicin (DOX) und eines photothermischen Stoffes verwendet werden konnten. Einstrahlung von nahinfrarotem Licht führte zur Auflösung der Mizellen, was die räumlich-zeitliche kontrollierte Freisetzung von DOX ermöglichte und den Ausfluss in arzneimittelresistente MCF-7/DOX-Zellen verhinderte. So wurde eine effektive Vorbeugung des Wachstums von arzneimittelresistenten Tumorzellen durch in-vivo Studien nachgewiesen.

In der **vierten** Publikation, wurde der Einfluss verschiedener *N*-substituierter acrylamidbasierender Comonomere, auf das thermoresponsive Verhalten von Poly(methacrylamid) (PMAAm), welches selbst eine UCST mit breiter Kühl-/Heizhysterese zeigt, untersucht. Die mittels freier radikalischer Polymerisation (FRP) synthetisierten Copolymere aus MAAm und *N*-cyclohexylacrylamid bzw. *N*-*tert*-butylacrylamid zeigten ein seltenes Phänomen, bei dem die Art des

Zusammenfassung

thermoresponsiven Verhaltens in Abhängigkeit der Copolymerzusammensetzung, von einer UCST zu einer LCST, mit Bereichen der vollständige Löslich- bzw. Unlöslichkeit, geändert werden konnte.

Die **fünfte** Publikation, zeigt die Synthese und Anwendung eines Terpolymers aus MAAm, *N-tert*-Butylacrylamid und des durch UV-Licht vernetzbaren 4-Acryloylbenzophenon. Dieses Terpolymer wurde mittels FRP dargestellt und zeigte ein LCST Verhalten. Elektrosponnen des Terpolymers ermöglichte die Fabrikation einer Nanofasermatrix die durch Temperaturerhöhung eine starke Kontraktion aufwies, was zur kontrollierten Freisetzung von Nanopartikeln genutzt werden konnte.

In der **sechsten** und letzten Publikation wird die Herstellung eines doppelt thermoresponsiven, interpenetrierenden Polymernetzwerks (IPN) PNAGA/PNIPAAm Hydrogels aufgezeigt. Die Synthese erfolgte hierbei in zwei unabhängig aufeinander folgenden, UV-Licht induzierten Polymerisationen von NAGA bzw. NIPAAm. Die mechanischen Eigenschaften der IPNs zeigten hierbei eine deutliche Abhängigkeit von der Temperatur und dem PNIPAAm Anteil. So konnte gezeigt werden, dass bei höheren Temperaturen beziehungsweise bei einem abnehmenden NIPAAm-Anteil, bessere mechanische Eigenschaften der IPN erhalten werden.

Im **Ausblick** dieser Arbeit wird auf die Synthese und mögliche Anwendungen neuartiger UCST bzw. doppelt thermoresponsiver Polymere eingegangen. Hier steht vor allem die Verwendung neuer, auf Acrylamid basierenden *N*- und α -substituierten Comonomere im Fokus.

3 List of symbols and abbreviations

| | |
|-------|--------------------------------------|
| AAc | acrylic acid |
| AAm | acrylamide |
| AIBN | azobisisobutyronitrile |
| AN | acrylonitrile |
| ATRP | atom transfer radical polymerization |
| ABP | 4-acryloyloxybenzophenone |
| CMDT | cyanomethyl dodecyl trithiocarbonate |
| CRP | controlled radical polymerization |
| DLS | dynamic light scattering |
| DMSO | dimethyl sulfoxide |
| DOX | Doxorubicin |
| DSC | differential scanning calorimetry |
| eq | equivalents |
| FRP | free radical polymerization |
| GPC | gel permeation chromatography |
| IPN | interpenetrating polymer network |
| LCST | lower critical solution temperature |
| MBA | <i>N,N'</i> -methylenebisacrylamide |
| m, n | degree of polymerization |
| M_n | number average molar mass |
| M_w | weight average molar mass |
| NAGA | <i>N</i> -acryloylglycinamide |

List of symbols and abbreviations

| | |
|----------|--|
| NIPAAm | <i>N</i> -isopropylacrylamide |
| NMRP | nitroxide-mediated radical polymerization |
| NMR | nuclear magnetic resonance |
| PAAc | poly(acrylic acid) |
| PEG | poly(ethylene glycol) |
| PBS | phosphate buffered saline |
| ppm | parts per million |
| PMAAm | poly(methacrylamide) |
| PNAGA | poly(<i>N</i> -acryloylglycinamide) |
| PNIPAAm | poly(<i>N</i> -isopropylacrylamide) |
| RAFT | reversible addition fragmentation chain transfer |
| S | styrene |
| SEM | scanning electron microscopy |
| SLS | static light scattering |
| T_{cp} | cloud point |
| TEM | transmission electron microscopy |
| TEMPO | 2,2,6,6-tetramethylpiperidinyloxy |
| UCST | upper critical solution temperature |
| UV | ultraviolet light |
| Vis | visible light |
| VPTT | volume phase transition temperature |

4 Introduction

“Smart” polymers show a distinct change in solubility, mechanical properties or morphology, owing to small changes of the environment such as temperature, magnetic forces, pH and light irradiation.¹⁻³ Such kind of polymers are mainly used in the field of medicine, biotechnology and sensor technology.^{4, 5} Particular attention was directed to thermoresponsive polymers, as the temperature of the environment can be controlled in a fast and easy way.

In this thesis, the synthesis, properties and application of new thermoresponsive polymers were studied. The main focus of this work was the synthesis of new polymers which show an upper critical solution temperature (UCST), an LCST and UCST in one, as well as either a UCST or LCST, depending on the copolymer composition. Furthermore, we showed the application of thermoresponsive polymers as matrixes for the controlled and temperature triggered release of drugs and nanoparticles.

4.1 Thermoresponsive polymers

In the last decades, the synthesis, characterization and the application of thermoresponsive polymers have made significant progress.^{6, 7} Applications in the field of medicine as drug carrier or as carrier for proteins and enzymes are only a few examples for the wide range of conceivable applications.⁸ Generally, thermoresponsive polymers can be categorized in polymers with an LCST-type or a UCST-type phase transition. The characteristic phase separation of both types is diagrammed with an isobaric, concentration-dependent phase diagram, as shown in (Figure 4.1-1).

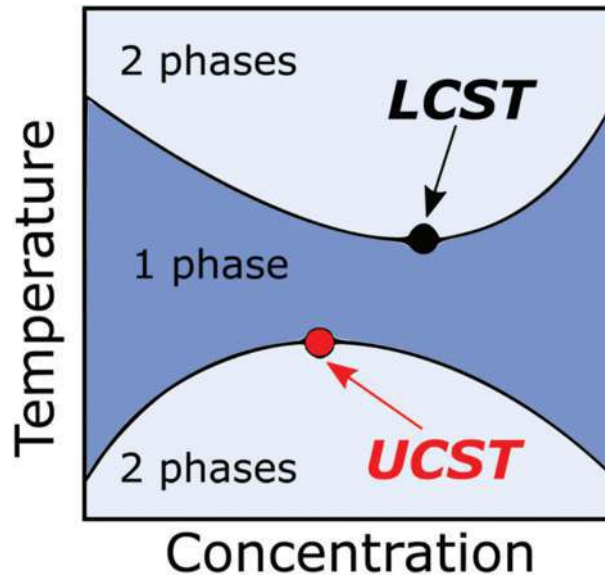


Figure 4.1-1: Concentration-dependent phase diagram for an LCST and UCST polymer in solution. (Reprinted with permission from Ref.¹ Copyright The Royal Society of Chemistry 2016)

The LCST is defined as the minimum of the phase diagram, whereas the UCST is defined as the maximum of the corresponding bimodal curve at a specific polymer solution concentration. In order to understand the mechanism during the phase transition, the inter- and intramolecular interactions have to be discussed on a molecular level. The Flory-Huggins theory, based on the Gibbs equation (Equation 1), describes the free enthalpy of mixing (ΔG_m) for polymer solutions.

$$\Delta G_m = \Delta H_m - T \Delta S_m \quad (1)$$

ΔH_m = change in enthalpy of mixing; ΔS_m = change in entropy of mixing

Introduction

To describe the phase diagram, pure water and pure polymer phases are assumed to be below the UCST as well as above the LCST. Based on this assumption, the free Gibbs energy of mixing must be negative to dissolve a polymer.

For UCST-type copolymers, which are insoluble at low temperature, ΔH_m as well as ΔS_m are positive in the two-phase region of the phase diagram, resulting in positive ΔG_m so that the polymer is insoluble. Upon heating and reaching the maximum of the bimodal curve, the ΔS_m term overweighs, ΔG_m becomes negative and the polymer dissolves. On the molecular scale, the polymer chain changes its conformation from a collapsed globule state to an open coil state.^{9, 10} For LCST-type polymers, it is the contrary. At low temperatures, LCST-type polymers are dissolved as a result of a negative ΔG_m . Heating the solution results in an overweighing positive ΔH_m due to the breakage of the formed water-polymer hydrogen bonds, and the polymer becomes insoluble, appearing as a phase separation. Thus, the ΔS_m and ΔH_m are affected by many factors, such as hydrogen bonds of strong hydrophilic groups and an ordered hydration-shell.¹¹ In contrast, UCST polymers generally show stronger polymer-polymer interaction, which leads to a much smaller change in ΔH_m upon heating.⁹ In order to monitor the phase transition behavior of a polymer solution, different kinds of techniques, such as rheology, light scattering or turbidity measurements can be applied.¹² Turbidity measurements monitor the change in transmittance (%) precipitation of the polymer solution, as shown in Figure 4.1-2.

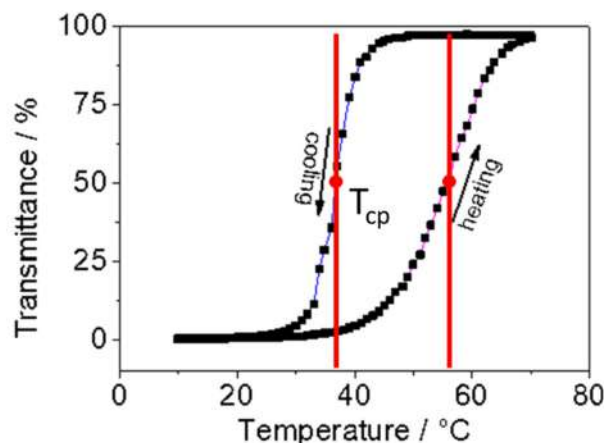


Figure 4.1-2: Turbidity measurement of poly(methacrylamide) with a UCST in aqueous solution showing a broad cooling/heating hysteresis of approx. 25°C.

Typically, the cloud point (T_{cp}), is defined as a point with a specific concentration of the bimodal curve at which the phase separation occurs. The cloud point can be defined as the point of inflection at which the transmittance changed by 50%. The distinction between cloud points in cooling and heating is defined as the cooling/heating hysteresis.

4.2 Polymers with a LCST-type phase transition

Polymers with an LCST in water or in organic solvents are well studied and used in a wide field of applications.^{8, 13} Poly(*N*-isopropylacrylamide) (PNIPAAm) is probably the most studied and used LCST polymer, whereas the thermoresponsive behavior was first shown in 1967 by Scarpa *et al.* and the solution properties were described by Heskins *et al.* in 1968.^{14, 15} In most cases, LCST polymers are based on a poly(*N*-alkyl-(meth) acrylamide) polymer structure.¹³ Roy *et al.* reviewed and listed a number of LCST polymers and copolymers based on the *N*-alkyl (meth) acrylamide structure over a wide temperature range (see Figure 4.2-1).¹⁶ Furthermore, poly(*N*-vinylamide)s,

Introduction

poly(alkylamidoacrylate)s, poly(oxazoline)s and poly(ether)s, such as poly(ethylene glycol) (PEG), are known for displaying an LCST-type phase transition in aqueous solution.^{17, 18}

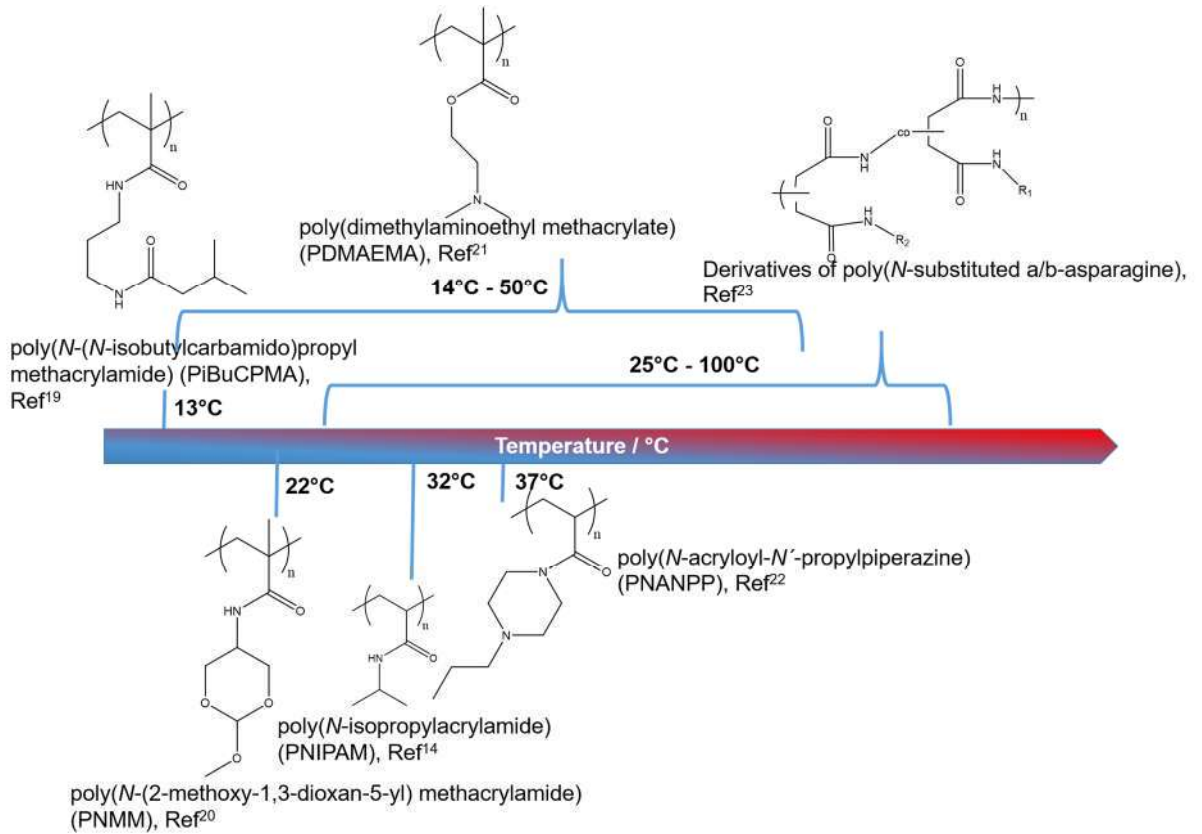


Figure 4.2-1: Representative examples for LCST polymers over a temperature range of 10°C – 100°C.^{14, 19-23}

4.3 Non-ionic polymers with a UCST-type phase transition

Based on ionic interactions (Coulomb interactions) or reversibly strong hydrogen bonds, polymers can exhibit UCST in aqueous solutions.^{9, 24} In comparison to ionic UCST-type polymers, advantages of non-ionic UCST-type polymers are, for example, lower sensitivity to added salts, impurities, pH and a highly repeatable and stable phase transition.^{1, 24} This makes non-ionic UCST-type polymer highly interesting for a great number of applications. Nevertheless, based on the number of publications in the last 10 years (Figure 4.3-1), polymers with a UCST phase transition in water have been studied at a significantly lower level than polymers with an LCST phase transition behavior.

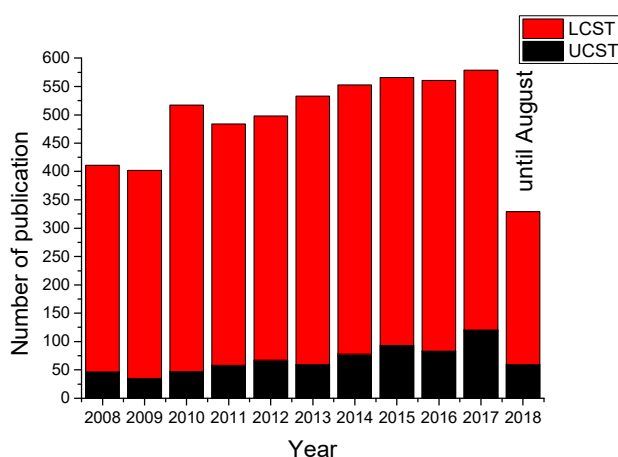


Figure 4.3-1: Number of publications with a general content about LCST and UCST phase transition behavior, respectively, in aqueous solution, non-aqueous solution, gels and applications (based on Scifinder 1st August 2018).

However, the progress made has increased the number of polymers which exhibit a UCST-type phase transition in water. Therefore, a wide temperature range is now available as a result of different cloud points of the novel polymers.⁹ Moreover, cloud

Introduction

points can be tuned by changing the concentration of the solution, varying the molar mass,²⁵ the copolymer composition or by adding salts.¹ One of the most studied UCST polymers is poly(*N*-acryloylglycinamide) (PNAGA), first synthesized by Haas et al.²⁶, whereas UCST behavior was not shown until almost 50 years later by Seuring et al.²⁷ The reason for the delayed observation of the UCST of PNAGA was identified as a result of traces of acrylate and acrylic acid impurities coming from the NAGA monomer synthesis, initiators or chain transfer agents used for the reversible addition-fragmentation chain transfer (RAFT) polymerization.²⁵ However, PNAGA shows a concentration-dependent, sharp UCST-type phase transition in water with a relatively broad cooling/heating hysteresis at a difference of around 12°C in T_{cp} upon cooling/heating (Figure 4.3-2).

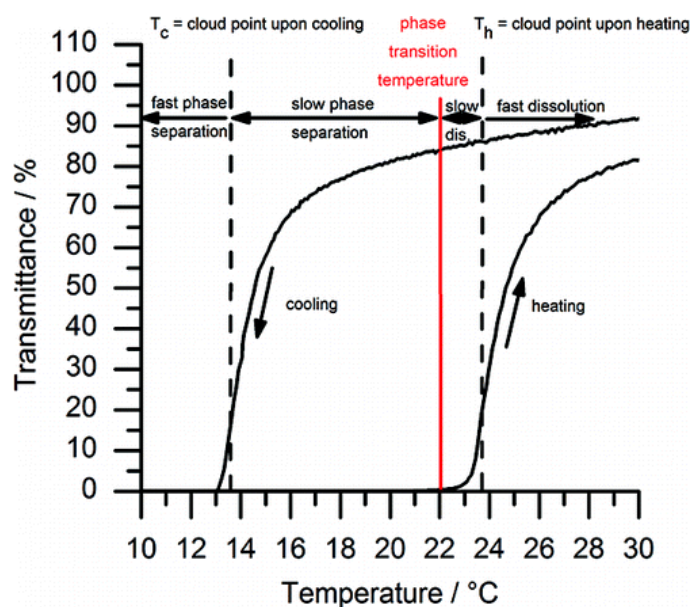


Figure 4.3-2: Cooling/heating hysteresis of PNAGA in aqueous solution. (Reprinted with permission from Ref.²⁸ Copyright 2011 American Chemical Society).

An additional outstanding example is a copolymer of acrylamide (AAm) and the hydrophobic acrylonitrile (AN), whereas the PAAm homopolymer itself is a water

Introduction

soluble polymer.^{29, 30} By changing the copolymer composition, the cloud point is tunable over a wide temperature range of 5°C to around 60°C, which makes it applicable on a broad scale. Furthermore, the copolymers show a sharp transition with an extremely narrow cooling/heating hysteresis in water as well as in physiological buffer solution, as shown in Figure 4.3-3.

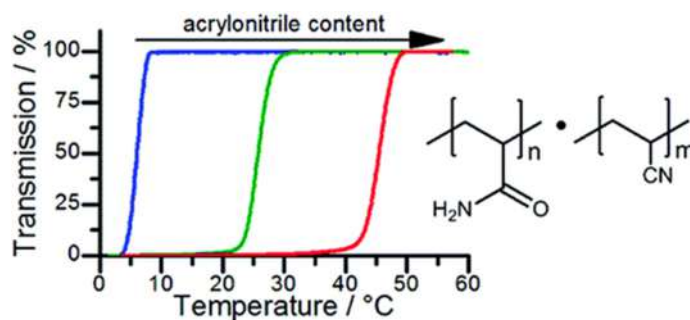
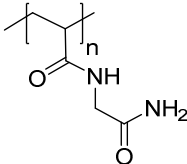
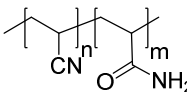
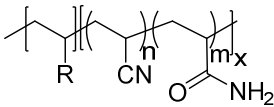
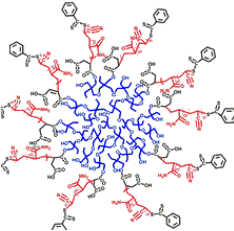
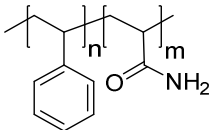


Figure 4.3-3: Turbidity measurement of P(AAm-AN) in PBS buffer solution with a concentration of 1 wt%. The T_{cp} can be tuned within a range of 6-60°C, depending on the molar ratio of acrylamide and acrylonitrile. (Reprinted with permission from Ref.³⁰ Copyright 2012 American Chemical Society).

In comparison to water soluble PAAm, poly(methacrylamide) (PMAAm) is known for showing a UCST-type phase transition in water (see Figure 4.3-3), which was shown by the Agarwal group for the first time.³⁰ Contrary to water soluble PAAm, a broad hysteresis with a UCST type phase transition at around 25°C and a broad hysteresis at a difference of around 25°C when cooled/heated is observed for PMAAm.

In addition to the examples of PNAGA, PMAAm and the copolymer of P(AAm-AN), a literature survey regarding examined non-ionic UCST-polymers, modifications and its application was conducted, which is summarized in Table 1.

Table 1: Literature survey on known non-ionic UCST-type polymers.

| Polymer structure | Properties |
|--|--|
| PNAGA  | Prepared by FRP as well as CRP (ATRP, RAFT), $T_{cp} = 13.7^{\circ}\text{C}$ (cooling); 23°C (heating) for a 1 wt% solution ^{25, 28, 31} |
| P(AAm-AN)  | Copolymers prepared via FRP and RAFT polymerization, $T_{cp} = 6\text{-}60^{\circ}\text{C}$ (depending on AN (mol%) content in polymer) ^{30, 32} |
| P(AAm-AN)- <i>b</i> -PR  <p> 1 R = dimethylacrylamide 2 R = <i>N,N</i>-dimethylaminoethyl methacrylate 3 R = phenyl </p> | Prepared by RAFT, block copolymers undergo micelle formation, $T_{cp} = 14\text{-}48^{\circ}\text{C}$ (dependent on copolymer composition and comonomer) ³² |
| HBPO-star-P(AAm-AN)  | Prepared by RAFT, $T_{cp} = 33.2\text{ - }65.2^{\circ}\text{C}$ with a broad hysteresis (dependent on the amount of AN and the length of the arms) ³³ |
| P(AAm-S)  | Only copolymers made by RAFT, showing a UCST in water due to homogeneity, $T_{cp} = 10\text{-}85^{\circ}\text{C}$ (cooling) (depending on the styrene content) ³⁴ |

Reprinted with permission from, © 2018

American Chemical Society³³

Table 1: Literature survey on known non-ionic UCST-type polymers (continued).

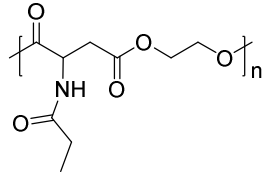
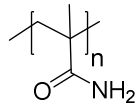
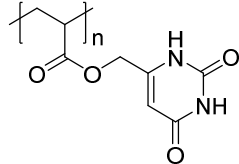
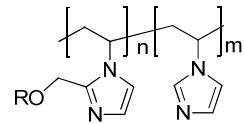
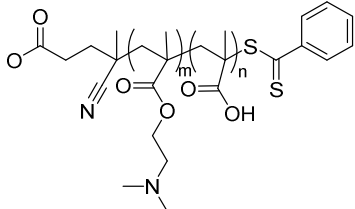
| Polymer structure | Properties |
|--|--|
| <p>PPAE</p>  | <p>The polymer is not cytotoxic.</p> <p>The UCST depends on M_n and the concentration, $T_{cp} = 1.5-37.6^\circ\text{C}$ (can be changed by the amount of NaCl and alcohol amount³⁵)</p> |
| <p>PMAAm</p>  | <p>Broad cooling/heating, $T_{cp} = 35/55^\circ\text{C}$ hysteresis in aqueous solution with a concentration of 1wt%, $T_g = 254^\circ\text{C}$³⁰</p> |
| <p>P(6-(acryloyloxymethyl)-uracil)</p>  | <p>Made by FRP, $T_{cp} \approx 60^\circ\text{C}$ with a concentration of 0.1wt%, T_{cp} is shifted to lower temperatures upon adding urea or adenosine³⁶</p> |
| <p>P(imidazole) based</p>  <p>1 R = H 2 R = H, CONH-cyclodextrine</p> | <p>1: $T_{cp} = 18-40^\circ\text{C}$, 4 wt% in water; (depending on copolymer ratio and pH value, at pH = 2 no T_{cp} observed)</p> <p>2. $T_{cp} = 78^\circ\text{C}$ (depending on copolymer ratio and cyclodextrine side chain content)^{37, 38}</p> |
| <p>P(MAA-DMAEMA)</p>  | <p>Made by RAFT, $T_{cp} = <10-70^\circ\text{C}$ for 5 mg/mL in water/ethanol (depending on the solvent mixture, ethanol 45-75 vol%)³⁹</p> <p>Furthermore, several derivatives are known, showing a UCST in water/ethanol mixtures⁴⁰⁻⁴²</p> |

Table 1: Literature survey on known non-ionic UCST-type polymers (continued).

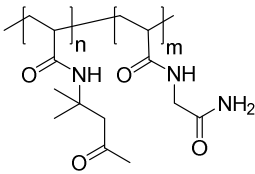
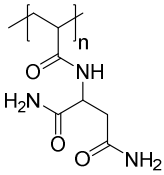
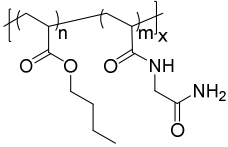
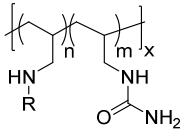
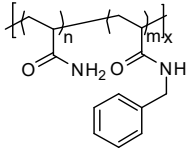
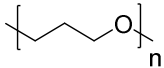
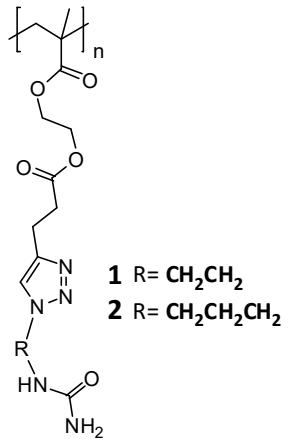
| Polymer structure | Properties |
|---|--|
| <p>P(NAGA₁₇₇-DAAM₉)</p>  | <p>Made by RAFT, ($M_n = 28 \text{ kg} \cdot \text{mol/L}$, $\bar{D} = 1.22$); shows a UCST in water/methanol, T_{cp} (cooling) = 4.5-22.5°C, T_{cp} (heating) = 13.5 to 35.5°C (depending on the composition and M_n)⁴³</p> |
| <p>PNAAM</p>  | <p>Made by RAFT, ($M_n = 17,000 - 118,000$, $\bar{D} = \sim 1.26$, $T_{cp} = 4-24^\circ\text{C}$ (depending on molecular weight and concentration in the range 0.5wt%-3wt%))⁴⁴</p> |
| <p>P(NAGA-BA)</p>  | <p>Made by FRP, $T_{cp} = 9-57^\circ\text{C}$ (depending on composition, concentration), CMC = 66 µg/mL for (NAGA:BA = 0.8:0.2 (n/n))^{30, 45}</p> |
| <p>P(allylurea-R)</p>  <p> 1 R = H, allylamine 2 R = COC₂H₄COOH, succinyl anhydride 3 R = COCH₃, acetyl anhydride </p> | <p>Used to capture proteins under physiological conditions, $T_{cp} = <10-40^\circ\text{C}$ (depending comonomer R, salt concentration and pH)⁴⁶</p> <p>Further derivatives are known⁴⁷</p> |
| <p>P(AAm-benzylAAm)</p>  | <p>Made by FRP-post polymerization modification, $T_{cp} = 7^\circ\text{C}$ for (0.87 mol%, AAm) and (0.13 mol%, benzylAAm) in water⁴⁸</p> |
| <p>PPO</p>  | <p>UCST in water only with concentration above 45 wt%⁴⁹</p> |

Table 1: Literature survey on known non-ionic UCST-type polymers (continued).

| Polymer structure | Properties |
|--|---|
| <p>P(ureido-derivatives)</p>  <p> 1 R= CH₂CH₂ 2 R= CH₂CH₂CH₂ </p> | <p>Made by ATRP and post modification,</p> <p>1. T_{cp} = 76°C, 2. T_{cp} = 96° Partial quaternization with methyl iodide decreased the T_{cp}⁵⁰</p> |

As the examples show, there is a steady growth of non-ionic UCST-type polymers. However, there is still a need to understand in detail the effect of hydrophobic or hydrophilic comonomers on the phase transition behavior of UCST-type polymers in detail. Further research is required in order to understand the influence of these hydrophilic/hydrophobic comonomers on the cooling/heating hysteresis, examples being PMAAm, the T_{cp} and the type of phase transition itself. Copolymers with double thermoresponsive properties as a result of its complex hydrophilic/hydrophobic equilibrium are, among others, to be mentioned here. The following chapter 4.4 gives an overview of such double thermally reacting polymers and describes their synthesis and properties in detail.

4.4 Polymers with double (LCST and UCST)-type phase transitions

In the last few years, polymers which exhibit both an LCST and UCST at the same time became an interesting class of thermoresponsive polymers. These polymers promise a multitude of new application possibilities as a result of its complex change in morphology and its thermoresponsive behavior.^{51, 52} For the synthesis of such polymers, the synthesis of block copolymers consisting of a UCST block and an LCST block or the combination of two LCST and UCST blocks, respectively, was shown.⁵³⁻⁵⁵ Alternatively, a hydrophilic or hydrophobic block can be attached to a known thermoresponsive polymer to obtain a double thermoresponsive polymer. This can be achieved, for example, by controlled polymerization of a second block or by the use of macroinitiator containing hydrophilic or hydrophobic fragments.^{54, 56, 57}

Compared to non-ionic UCST and LCST polymers, the number of double thermoresponsive copolymers is relatively small. In the following, an overview of known double thermoresponsive polymers and its characteristics is given (Table 2).

Table 2: Copolymers with a double thermoresponsive behavior.

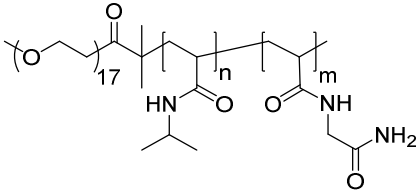
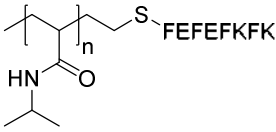
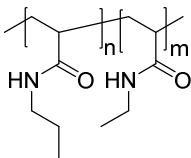
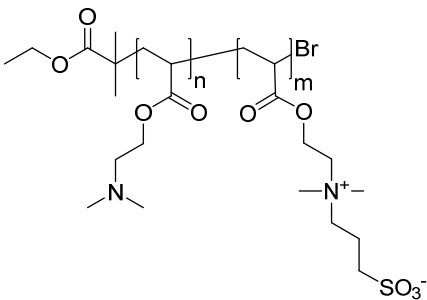
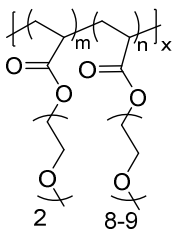
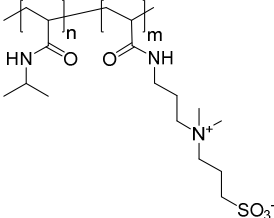
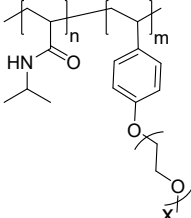
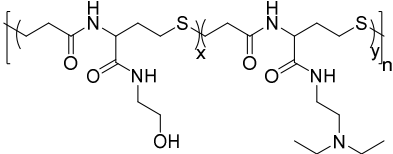
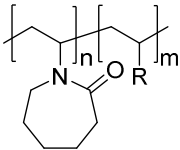
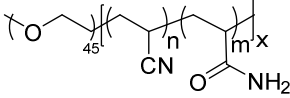
| Polymer structure | Properties |
|---|--|
| <p>PEO-<i>b</i>-PNAGA-<i>b</i>-PNIPAM</p>  | <p>Made by RAFT polymerization using a PEG- macro-RAFT agent, T_{cp}^1 (LCST) = 28.8°C, T_{cp}^2 (UCST) = 7.5°C (depending on the block- length, block- ratio, block-order)⁵⁸</p> |
| <p>PNIPAAm-<i>b</i>-peptide</p>  | <p>Thiol functionalized peptide used for the FRP of NIPAAm, T_{cp}^1 (LCST) = ~30°C, T_{cp}^2 (melting) = ~75°C at a concentration of 200 g/L⁵⁹</p> |
| <p>PNPAM-<i>b</i>-PNEAM</p>  | <p>Made by RAFT polymerization, both T_{cp}^1 (LCST) = 20°C, T_{cp}^2 (LCST) = 70°C (depending on the block-length, block-ratio a concentration of 1 g/L)⁵⁴</p> |
| <p>PDMAEMA-<i>b</i>-PPSBMA</p>  | <p>Made by ATRP, T_{cp}^1 (UCST) = <5-31°C; T_{cp}^2 (LCST) = 48-70°C (depending on the block ratio, pH, salt concentration)⁶⁰</p> |
| <p>P(MEO₂MA - OEGMA)</p>  | <p>Made by FRP, clay nanocomposite hydrogel, T_{cp}^1 and T_{cp}^2 = 5-85°C (depending on the OEGMA content and clay amount)⁶¹</p> |

Table 2: Copolymers with a double thermoresponsive behavior (continued).

| Polymer structure | Properties |
|---|---|
| <p>PSPP₄₃₀-<i>b</i>-PNIPAM₂₀₀</p>  | <p>Made by RAFT polymerization T_{cp}^1 (UCST) = 18°C; T_{cp}^2 (LCST) = 33°C in D₂O and water (depending on the block- length, block- ratio, concentration, electrolyte concentration)^{53, 62}</p> |
| <p>PNIPAAm-<i>b</i>-PpPEGV</p>  | <p>Made by RAFT, NIPAAm; T_{cp}^1 (LCST) = ~30°C, T_{cp}^2 (LCST) = ~44-54°C in water with a concentration of 2wt% (depending on the block- length, block- ratio, length PEG side chain)⁶³</p> |
| <p>P(amido thioether)s</p>  | <p>Made by polyaddition, T_{cp}^1 (LCST) = 36-49°C; T_{cp}^2 (UCST) = ~66°C in water (depending on pH, concentration, composition, CO₂, oxidation)⁶⁴</p> |
| <p>P(NVCL) copolymers</p>  <p>1 R = <i>N</i>-vinylpyrrolidone 2 R = <i>N</i>-methyl-<i>N</i>-vinylacetamide</p> | <p>1-2: Made by cobalt mediated polymerization, (depending on the block ratio, block lengths, salt concentration, comonomer), 1. T_{cp}^1 (LCST) = 25-52°C; T_{cp}^2 (UCST) = 43-70°C, 2. T_{cp}^1 (LCST) = 43-52°C; T_{cp}^2 (UCST) = 70°C^{65, 66}</p> |
| <p>PEG-<i>b</i>-P(AAm-AN)</p>  | <p>Made by FRP using a PEG-macro-initiator, T_{cp}^1 (LCST) = 20-50°C, T_{cp}^2 (UCST) = 23-68°C (depending on PEG block length, AN content, concentration)⁵⁷</p> |

4.5 Thermoresponsive interpenetrating network (IPN) hydrogels

In addition to linear thermoresponsive polymers, thermoresponsive hydrogels, which, as a result of its 3-dimensionally cross-linked structure, are no longer soluble, play an important role in the field of biotechnology and medicine such as sensors and the matrix for cell culturing applications do.⁶⁷⁻⁶⁹

Interpenetrating network hydrogels are, in addition to non-ionic and ionic hydrogels, an interesting group of hydrogels. IPNs consist of at least two independent polymer networks which are not covalently linked and at least one of the two networks is cross-linked or synthesized in the presence of the hydrogel.^{70, 71} Two different variants are conceivable for the synthesis of IPNs, **1**. Stepwise synthesis, the second network being polymerized in the swollen first network, **2**. Simultaneous polymerization of both networks, whereby the two polymerizations are not affecting one another.⁷⁰ The compatibility of the individual polymer properties without the loss of desired specific properties of the polymers makes the application of IPNs as biomaterials, sensors and for tissue engineering highly interesting.⁷¹⁻⁷⁶

Thermoresponsive IPN hydrogels are of interest as they swell and shrink due to slight changes in ambient temperature. PNIPAAm is probably the best-known and most commonly used polymer, which, in the cross-linked state, shows a negative volume phase transition temperature (VPTT), i.e. the gel shrinks above the VPTT.⁷⁷ The synthesis and properties of a PNIPAAm IPN hydrogel were demonstrated by Zhang *et al.*⁷⁸ In this work, a considerable improvement of the mechanical properties resulting from the IPN structure could be achieved when compared to ordinary PNIPAAm. Furthermore, the controlled release of a drug has been demonstrated. The synthesis of PNIPAAm-based IPN hydrogels was shown.⁷⁹ As a result, it was possible to

Introduction

synthesize thermoresponsive IPNs with different additional properties such as conductivity, pH- responsivity, high compressive mechanical properties and fast shrinking.⁸⁰⁻⁸³

A well-known example of a thermoresponsive IPN hydrogel with a UCST phase transition was presented by Li *et al.*⁸⁴ IPNs of poly(acrylic acid)-Graft- β -cyclodextrin (PAAc-*g*- β -CD) and PAAm showed UCST behavior with a T_{cp} at about 35°C. Furthermore, as a result of the IPN structure, a significantly faster release of ibuprofen could be observed with higher temperatures as to when compared to lower temperatures. In addition to the example mentioned, IPNs with a UCST, which are based on PNAGA, are known. One example is an IPN hydrogel of PNAGA and poly(acrylic acid) (PAAc).⁸⁵

PNAGA-based IPN hydrogels are of particular interest due to the good mechanical properties of PNAGA hydrogels.⁸⁶ The exceptionally good mechanical properties are fully based on hydrogen bonds and no chemical cross-linking is required (Figure 4.5-1).

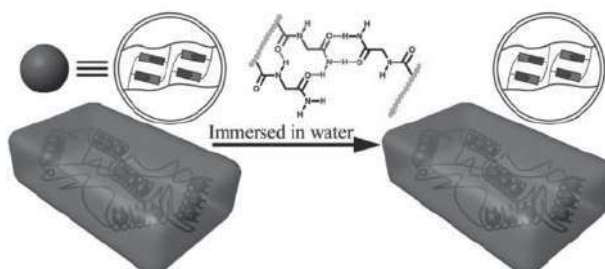


Figure 4.5-1: Physically cross-linked PNAGA hydrogel, based on strong hydrogen bonding. (Reprinted with permission from Ref.⁸⁶ 2015 Copyright WILEY-VCH Verlag GmbH & Co. KGaA, Weinheim).

Introduction

These good mechanical properties of PNAGA have been used, for example, by Wu *et al.* to produce a conductive and highly stretchable IPN hydrogel with self-healing properties.⁸⁷

This was achieved by *in situ* doping of poly(*N*-acryloylglycinamide-co-2-acrylamid-2-methylpropanesulphone) (PNAGA-PAMPS) hydrogels with poly(3,4-ethylenedioxythiophene)-poly(styrenesulfonate) (PEDOT/PSS).

4.6 Radical polymerization

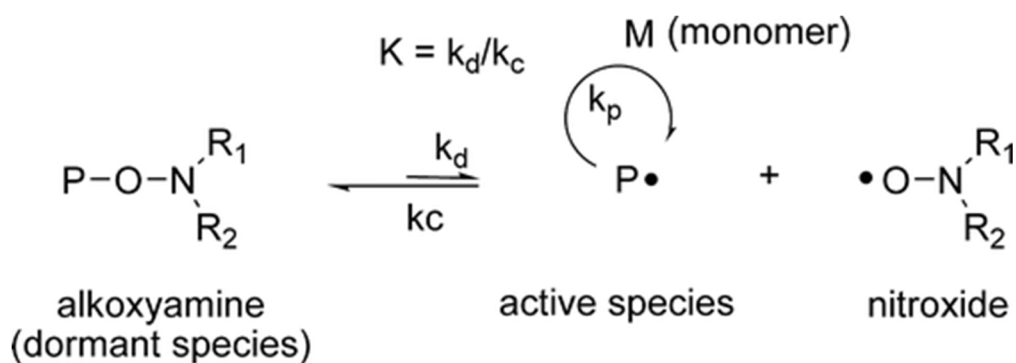
Free-radical polymerization (FRP) is probably the most widely used method for the synthesis of polymers in research and industry. The major advantages of FRP are its fast and relatively simple feasibility, the use of almost all vinyl monomers and the preservation of polymers with a high molar mass.⁸⁸ However, there are also disadvantages of this reaction mechanism. These include the broad molecular weight distribution (\bar{D}) as well as the lack of control over the microstructure of polymers. These properties are a result of the termination and chain transfer, reactions which occur during polymerization.⁸⁸ Controlled radical polymerization (CRP) is a good alternative reaction method to suppress the aforementioned disadvantages of FRP. Thus, the following chapter will deal with the CRP in more detail by showing and discussing various variants of the CRP.

Controlled radical polymerization

CRP is widely used to decrease reactivity of the chain end, leading to a suppression of termination and chain transfer reactions which leads to a controlled molecular weight with lower Dispersity (\bar{D} around 1.3). Different microstructures can be achieved with this polymerization technique which leads to the possibility to obtain block copolymers and defined end groups, which are useful for further reaction steps and applications.⁸⁹ The three most important methods of CRP are presented below. These methods include nitroxide-mediated radical polymerization (NMRP), Reversible Addition-Fragmentation Chain Transfer (RAFT Polymerization) and Atom Transfer Radical Polymerization (ATRP).⁸⁹

Introduction

NMRP is a variant of controlled polymerization, in which a variety of different monomers can be used. Moreover, the advantage of this method lies in the metal-free and effective synthesis of polymers. The reaction mechanism is based on a reversible equilibrium between active species and inactive species, where alkoxyamines, originally 2,2,6,6-tetramethylpiperidinyloxy (TEMPO), are used as inactive species (Scheme 4.6-1).⁹⁰



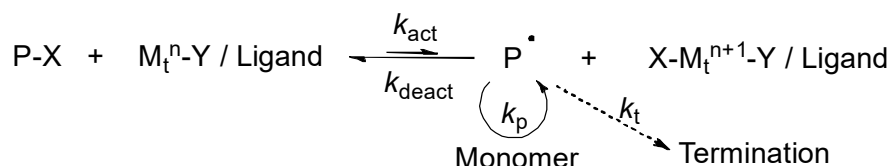
Scheme 4.6-1: Mechanism of NMRP. (Reprinted with permission from Ref.⁹¹ 2008 American Chemical Society).

The disadvantage of using TEMPO resins is the slow reaction rate, high reaction temperatures, and the low number of monomers which can be used.^{92, 93} In recent years, these disadvantages have been reduced by the development of new nitroxides such as *N-tert*-butyl-*N*-(1-diethylphosphono-2,2-dimethylpropyl)-*N*-oxyl (DEPN), 2,2,5,5-tetramethyl-4-phenyl-3-azahexane-3-oxyl (TIPNO), and *N-tert*-butyl-(1-*tert*-butyl-2-ethylsulfinyl)propyl nitroxide (BESN).⁹⁴⁻⁹⁸

Atom Transfer Radical Polymerization (ATRP) is also a known variant of controlled polymerization.⁸⁹ As with NMRP, the reaction mechanism is based on the balance between dormant and propagating species. The deactivated species, alkyl halides

Introduction

macromolecules species (P-X), is converted into the activated species (P·) by a catalytic transition metal complex (Mⁿ-Y/Ligand) where the metal is in its lower oxidation state. In this way, the metal passes into a higher oxidation (X-Mⁿ⁺¹/Ligand) stage and the activated chain can add a monomer before it switches back to the deactivated state (Scheme 4.6-2).⁹⁹



Scheme 4.6-2: Mechanism of the Atomic Transfer Radical Polymerization (ATRP).⁹⁹

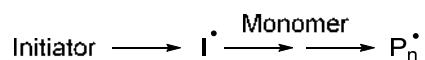
In particular, among others, the Matyjaszewski group has developed a large number of new catalytic transition metal complexes, ligands and initiators in recent decades. Today, these developments enable the broad application of ATRP for the synthesis of polymers with complex structures (block, star, grafted, etc.), the functionalization of polymers and, for example, the modification of functional surfaces.^{89, 99-101}

In addition to NMRP and ATRP, Reversible Addition-Fragmentation Chain Transfer (RAFT) polymerization is another established method for controlled radical polymerization, which was first shown in 1998.¹⁰² The following (Scheme 4.6-3) shows the mechanistic process of RAFT polymerization. As with conventional free radical polymerization, the first step is the disintegration of the initiator and the subsequent initiation by attacking the vinyl group of the monomer, forming an active species (P_n·).¹⁰³ In the next step, this active species (P_n·) is added to the chain transfer agent (CTA) where an active radical (R·) is fragmented off. This, in turn, can re-initiate to form the active species (P_n·) which adds up to the chain transfer agent again with the

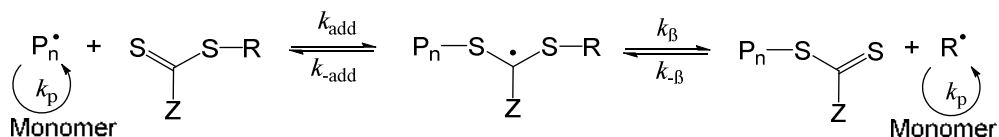
Introduction

elimination of (P_n^\bullet). This step repeats itself during chain propagation until complete consumption of the monomer or upon termination reaction of (P_m) and (P_n).

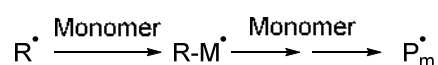
Initiation



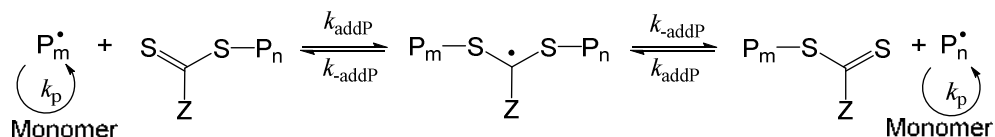
Reversible chain transfer (start reaction)



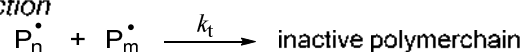
Reinitiation



Chain propagation



Termination reaction



Scheme 4.6-3: Mechanism of the RAFT polymerization process.¹⁰²

Due to the thiocarbonylthio end group of the inactive polymer chain, the subsequent polymerization of another block, the functionalization of surfaces through click reactions and the stabilization of metal nanoparticles are possible.¹⁰⁴⁻¹⁰⁶

4.7 Aims of the thesis

In this thesis, the following topics regarding the synthesis and application of non-ionic UCST-type polymers were addressed:

- effect of hydrophilic and hydrophobic comonomers on the phase transition behavior of the non-ionic UCST-type polymers PNAGA, P(AAm-AN) and PMAAm

- hydrophilic PEG units were introduced to the UCST-type P(AAm-AN) copolymer via a macroinitiator concept
- tuning the cloud point and hysteresis of PNAGA by copolymerization with a hydrophobic comonomer
- changing the type of phase transition behavior of PMAAm from UCST to LCST, depending on the copolymer composition, using hydrophobic *N*-substituted acrylamide comonomers

-applications of the non-ionic UCST- and LCST-type copolymers made with different polymer architectures

- drug release by locally controlled temperature change through light irradiation from UCST-type micelles
- design and characterization of the mechanical properties of an interpenetrating network (IPN) hydrogel with double thermoresponsive properties
- release of nanoparticles due to temperature-induced contraction of a LCST-type nonwoven

5 Literature

1. J. Niskanen and H. Tenhu, *Polymer Chemistry*, 2017, **8**, 220-232.
2. H. Meng and H. Jinlian, *Journal of Intelligent Material Systems and Structures*, 2010, **21**, 859-885.
3. H. Jinlian, M. Harper, L. Guoqiang and I. I. Samuel, *Smart Materials and Structures*, 2012, **21**, 053001.
4. I. Y. Galaev and B. Mattiasson, *Trends in Biotechnology*, 1999, **17**, 335-340.
5. M. A. C. Stuart, W. T. S. Huck, J. Genzer, M. Müller, C. Ober, M. Stamm, G. B. Sukhorukov, I. Szleifer, V. V. Tsukruk, M. Urban, F. Winnik, S. Zauscher, I. Luzinov and S. Minko, *Nature Materials*, 2010, **9**, 101.
6. Y. Deng, Y. Xu, X. Wang, Q. Yuan, Y. Ling and H. Tang, *Macromol Rapid Commun*, 2015, **36**, 453-458.
7. D. Klinger and K. Landfester, *Polymer*, 2012, **53**, 5209-5231.
8. A. Gandhi, A. Paul, S. O. Sen and K. K. Sen, *Asian Journal of Pharmaceutical Sciences*, 2015, **10**, 99-107.
9. J. Seuring and S. Agarwal, *Macromol Rapid Commun*, 2012, **33**, 1898-1920.
10. X. Ye, Y. Lu, L. Shen, Y. Ding, S. Liu, G. Zhang and C. Wu, *Macromolecules*, 2007, **40**, 4750-4752.
11. Y. Okada and F. Tanaka, *Macromolecules*, 2005, **38**, 4465-4471.
12. R. Pamies, K. Zhu, A.-L. Kjøniksen and B. Nyström, *Polymer Bulletin*, 2009, **62**, 487-502.
13. V. Aseyev, H. Tenhu and F. M. Winnik, 2010, **242**, 29-89.
14. J. S. Scarpa, D. D. Mueller and I. M. Klotz, *Journal of the American Chemical Society*, 1967, **89**, 6024-6030.

Literature

15. M. Heskins and J. E. Guillet, *Journal of Macromolecular Science: Part A - Chemistry*, 1968, **2**, 1441-1455.
16. D. Roy, W. L. A. Brooks and B. Sumerlin, *New directions in thermoresponsive polymers*, 2013.
17. C. d. I. H. Alarcón, S. Pennadam and C. Alexander, *Chemical Society Reviews*, 2005, **34**, 276-285.
18. V. Aseyev, H. Tenhu and F. M. Winnik, in *Self Organized Nanostructures of Amphiphilic Block Copolymers II*, eds. A. H. E. Müller and O. Borisov, Springer Berlin Heidelberg, Berlin, Heidelberg, 2011, DOI: 10.1007/12_2010_57, pp. 29-89.
19. A. Yoshikatsu, S. Yasurou, H. Yukio, K. Akihiko and O. Teruo, *Journal of Polymer Science Part A: Polymer Chemistry*, 2008, **46**, 5471-5482.
20. H. Xiaonan, D. Fusheng, J. Rong and L. Zichen, *Macromolecular Rapid Communications*, 2007, **28**, 597-603.
21. M. Okubo, H. Ahmad and T. Suzuki, *Colloid and Polymer Science*, 1998, **276**, 470-475.
22. L. H. Gan, Y. Y. Gan and G. R. Deen, *Macromolecules*, 2000, **33**, 7893-7897.
23. W. Eiji, T. Naoki and U. Hiroshi, *Macromolecular Symposia*, 2007, **249-250**, 509-514.
24. J. Seuring and S. Agarwal, *ACS Macro Letters*, 2013, **2**, 597-600.
25. F. Liu, J. Seuring and S. Agarwal, *Journal of Polymer Science Part A: Polymer Chemistry*, 2012, **50**, 4920-4928.
26. H. H. C. and S. N. W., *Journal of Polymer Science Part B: Polymer Letters*, 1964, **2**, 1095-1096.

Literature

27. J. Seuring and S. Agarwal, *Macromolecular Chemistry and Physics*, 2010, **211**, 2109-2117.
28. J. Seuring, F. M. Bayer, K. Huber and S. Agarwal, *Macromolecules*, 2011, **45**, 374-384.
29. W. M. Kulicke, R. Kniewske and J. Klein, *Progress in Polymer Science*, 1982, **8**, 373-468.
30. J. Seuring and S. Agarwal, *Macromolecules*, 2012, **45**, 3910-3918.
31. F. Liu, J. Seuring and S. Agarwal, *Polymer Chemistry*, 2013, **4**, 3123.
32. H. Zhang, X. Tong and Y. Zhao, *Langmuir*, 2014, **30**, 11433-11441.
33. M. Qi, K. Li, Y. Zheng, T. Rasheed and Y. Zhou, *Langmuir*, 2018, **34**, 3058-3067.
34. B. A. Pineda-Contreras, F. Liu and S. Agarwal, *Journal of Polymer Science Part A: Polymer Chemistry*, 2014, **52**, 1878-1884.
35. Y. Di, X. Ma, C. Li, H. Liu, X. Fan, M. Wang, H. Deng, T. Jiang, Z. Yin and K. Deng, *Macromolecular Chemistry and Physics*, 2014, **215**, 365-371.
36. T. Aoki, K. Nakamura, K. Sanui, A. Kikuchi, T. Okano, Y. Sakurai and N. Ogata, *Polymer Journal*, 1999, **31**, 1185.
37. G. Meiswinkel and H. Ritter, *Macromolecular Rapid Communications*, 2013, **34**, 1026-1031.
38. G. Meiswinkel and H. Ritter, *Macromolecular Chemistry and Physics*, 2013, **214**, 2835-2840.
39. Q. Zhang and R. Hoogenboom, *Chem Commun (Camb)*, 2015, **51**, 70-73.
40. A. Can, Q. Zhang, T. Rudolph, F. H. Schacher, J.-F. Gohy, U. S. Schubert and R. Hoogenboom, *European Polymer Journal*, 2015, **69**, 460-471.

Literature

41. Q. Zhang, F. Tosi, S. Ugduler, S. Maji and R. Hoogenboom, *Macromol Rapid Commun*, 2015, **36**, 633-639.
42. Q. Zhang and R. Hoogenboom, *Progress in Polymer Science*, 2015, **48**, 122-142.
43. W. Sun and P. Wu, *Physical Chemistry Chemical Physics*, 2018, DOI: 10.1039/C8CP04147D.
44. S. Glatzel, A. Laschewsky and J.-F. o. Lutz, *Macromolecules*, 2011, **44**, 413-415.
45. L. Hui, S. Qin and L. Yang, *ACS Biomaterials Science & Engineering*, 2016, **2**, 2127-2132.
46. N. Shimada, M. Nakayama, A. Kano and A. Maruyama, *Biomacromolecules*, 2013, **14**, 1452-1457.
47. N. Shimada, H. Ino, K. Maie, M. Nakayama, A. Kano and A. Maruyama, *Biomacromolecules*, 2011, **12**, 3418-3422.
48. Y. Zhu, A. B. Lowe and P. J. Roth, *Polymer*, 2014, **55**, 4425-4431.
49. H.-N. Lee, B. M. Rosen, G. Fenyvesi and H. B. Sunkara, *Journal of Polymer Science Part A: Polymer Chemistry*, 2012, **50**, 4311-4315.
50. V. Mishra, S.-H. Jung, H. M. Jeong and H.-i. Lee, *Polymer Chemistry*, 2014, **5**, 2411.
51. B. Hu, W. Fu and B. Zhao, *Macromolecules*, 2016, **49**, 5502-5513.
52. P. Schattling, F. D. Jochum and P. Theato, *Polymer Chemistry*, 2014, **5**, 25-36.
53. M. Arotçaréna, B. Heise, S. Ishaya and A. Laschewsky, *Journal of the American Chemical Society*, 2002, **124**, 3787-3793.
54. J. Weiss, C. Böttcher and A. Laschewsky, *Soft Matter*, 2011, **7**, 483-492.
55. J. Weiss and A. Laschewsky, *Macromolecules*, 2012, **45**, 4158-4165.

Literature

56. J. Wang, P. Gao, L. Ye, A.-y. Zhang and Z.-g. Feng, *Polymer Chemistry*, 2011, **2**, 931-940.
57. F. Kafer, F. Liu, U. Stahlschmidt, V. Jerome, R. Freitag, M. Karg and S. Agarwal, *Langmuir*, 2015, **31**, 8940-8946.
58. L. Mäkinen, D. Varadharajan, H. Tenhu and S. Hietala, *Macromolecules*, 2016, **49**, 986-993.
59. F. Stoica, C. Alexander, N. Tirelli, A. F. Miller and A. Saiani, *Chemical Communications*, 2008, DOI: 10.1039/B806782A, 4433-4435.
60. H. Sun, X. Chen, X. Han and H. Liu, *Langmuir*, 2017, **33**, 2646-2654.
61. M. Xia, Y. Cheng, Z. Meng, X. Jiang, Z. Chen, P. Theato and M. Zhu, *Macromol Rapid Commun*, 2015, **36**, 477-482.
62. N. S. Vishnevetskaya, V. Hildebrand, B.-J. Niebuur, I. Grillo, S. K. Filippov, A. Laschewsky, P. Müller-Buschbaum and C. M. Papadakis, *Macromolecules*, 2016, **49**, 6655-6668.
63. Y. Su, Q. Li, S. Li, M. Dan, F. Huo and W. Zhang, *Polymer*, 2014, **55**, 1955-1963.
64. H. Zhang, J. Zhang, W. Dai and Y. Zhao, *Polymer Chemistry*, 2017, **8**, 5749-5760.
65. A. Kermagoret, K. Mathieu, J.-M. Thomassin, C.-A. Fustin, R. Duchêne, C. Jérôme, C. Detrembleur and A. Debuigne, *Polymer Chemistry*, 2014, **5**, 6534-6544.
66. A. Kermagoret, C.-A. Fustin, M. Bourguignon, C. Detrembleur, C. Jérôme and A. Debuigne, *Polymer Chemistry*, 2013, **4**, 2575-2583.
67. F. Ullah, M. B. H. Othman, F. Javed, Z. Ahmad and H. M. Akil, *Materials Science and Engineering: C*, 2015, **57**, 414-433.

Literature

68. J. Pluta and B. Karolewicz, *Polim Med*, 2004, **34**, 63-81.
69. M. W. Tibbitt and K. S. Anseth, *Biotechnology and Bioengineering*, 2009, **103**, 655-663.
70. D. Myung, D. Waters, M. Wiseman, P.-E. Duhamel, J. Noolandi, C. N. Ta and C. W. Frank, *Polymers for Advanced Technologies*, 2008, **19**, 647-657.
71. E. S. Dragan, *Chemical Engineering Journal*, 2014, **243**, 572-590.
72. K. Yasuda, J. Ping Gong, Y. Katsuyama, A. Nakayama, Y. Tanabe, E. Kondo, M. Ueno and Y. Osada, *Biomaterials*, 2005, **26**, 4468-4475.
73. M. A. Haque, T. Kurokawa and J. P. Gong, *Polymer*, 2012, **53**, 1805-1822.
74. M. Prabakaran and J. F. Mano, *Macromolecular Bioscience*, 2006, **6**, 991-1008.
75. Y. Shi, L. Peng and G. Yu, *Nanoscale*, 2015, **7**, 12796-12806.
76. R. A. Green, R. T. Hassarati, J. A. Goding, S. Baek, N. H. Lovell, P. J. Martens and L. A. Poole-Warren, *Macromolecular Bioscience*, 2012, **12**, 494-501.
77. Y. Guan and Y. Zhang, *Soft Matter*, 2011, **7**, 6375-6384.
78. X.-Z. Zhang, D.-Q. Wu and C.-C. Chu, *Biomaterials*, 2004, **25**, 3793-3805.
79. M. A. Haq, Y. Su and D. Wang, *Materials Science and Engineering: C*, 2017, **70**, 842-855.
80. J.-T. Zhang, S.-W. Huang, Y.-N. Xue and R.-X. Zhuo, *Macromolecular Rapid Communications*, 2005, **26**, 1346-1350.
81. J. Zhang and N. A. Peppas, *Macromolecules*, 2000, **33**, 102-107.
82. A. K. Means, D. A. Ehrhardt, L. V. Whitney and M. A. Grunlan, *Macromolecular Rapid Communications*, 2017, **38**, 1700351.
83. Y. Shi, C. Ma, L. Peng and G. Yu, *Advanced Functional Materials*, 2015, **25**, 1219-1225.

Literature

84. Q. Wang, S. Li, Z. Wang, H. Liu and C. Li, *Journal of Applied Polymer Science*, 2009, **111**, 1417-1425.
85. R. Yoshida, Y. Kaneko, K. Sakai, T. Okano, Y. Sakurai, Y. H. Bae and S. W. Kim, *Journal of Controlled Release*, 1994, **32**, 97-102.
86. X. Dai, Y. Zhang, L. Gao, T. Bai, W. Wang, Y. Cui and W. Liu, *Advanced Materials*, 2015, **27**, 3566-3571.
87. Q. Wu, J. Wei, B. Xu, X. Liu, H. Wang, W. Wang, Q. Wang and W. Liu, *Scientific Reports*, 2017, **7**, 41566.
88. R. Braslau, *Journal of the American Chemical Society*, 2003, **125**, 3399-3400.
89. K. Matyjaszewski, *Current Opinion in Solid State and Materials Science*, 1996, **1**, 769-776.
90. C. J. Hawker, A. W. Bosman and E. Harth, *Chemical Reviews*, 2001, **101**, 3661-3688.
91. V. Sciannamea, R. Jérôme and C. Detrembleur, *Chemical Reviews*, 2008, **108**, 1104-1126.
92. M. K. Georges, R. P. N. Veregin, P. M. Kazmaier and G. K. Hamer, *Macromolecules*, 1993, **26**, 2987-2988.
93. P. J. MacLeod, R. P. N. Veregin, P. G. Odell and M. K. Georges, *Macromolecules*, 1998, **31**, 530-531.
94. Y. K. Chong, F. Ercole, G. Moad, E. Rizzardo, S. H. Thang and A. G. Anderson, *Macromolecules*, 1999, **32**, 6895-6903.
95. D. Benoit, S. Grimaldi, S. Robin, J.-P. Finet, P. Tordo and Y. Gnanou, *Journal of the American Chemical Society*, 2000, **122**, 5929-5939.
96. S. Grimaldi, J.-P. Finet, F. Le Moigne, A. Zeghdaoui, P. Tordo, D. Benoit, M. Fontanille and Y. Gnanou, *Macromolecules*, 2000, **33**, 1141-1147.

Literature

97. L. Couvreur, C. Lefay, J. Belleney, B. Charleux, O. Guerret and S. Magnet, *Macromolecules*, 2003, **36**, 8260-8267.
98. C. Le Mercier, S. Acerbis, D. Bertin, F. Chauvin, D. Gigmes, O. Guerret, M. Lansalot, S. Marque, F. Le Moigne, H. Fischer and P. Tordo, *Macromolecular Symposia*, 2002, **182**, 225-247.
99. K. Matyjaszewski and J. Xia, *Chemical Reviews*, 2001, **101**, 2921-2990.
100. K. Matyjaszewski, H. Dong, W. Jakubowski, J. Pietrasik and A. Kusumo, *Langmuir*, 2007, **23**, 4528-4531.
101. K. Matyjaszewski, P. J. Miller, N. Shukla, B. Immaraporn, A. Gelman, B. B. Luokala, T. M. Siclovan, G. Kickelbick, T. Vallant, H. Hoffmann and T. Pakula, *Macromolecules*, 1999, **32**, 8716-8724.
102. J. Chiefari, Y. K. Chong, F. Ercole, J. Krstina, J. Jeffery, T. P. T. Le, R. T. A. Mayadunne, G. F. Meijs, C. L. Moad, G. Moad, E. Rizzardo and S. H. Thang, *Macromolecules*, 1998, **31**, 5559-5562.
103. G. Moad, J. Chiefari, Y. K. Chong, J. Krstina, R. T. A. Mayadunne, A. Postma, E. Rizzardo and S. H. Thang, *Polymer International*, 2000, **49**, 993-1001.
104. G. Moad, Y. K. Chong, A. Postma, E. Rizzardo and S. H. Thang, *Polymer*, 2005, **46**, 8458-8468.
105. G. Moad, E. Rizzardo and S. H. Thang, *Chemistry – An Asian Journal*, 2013, **8**, 1634-1644.
106. C. Barner-Kowollik and S. Perrier, *Journal of Polymer Science Part A: Polymer Chemistry*, 2008, **46**, 5715-5723.

6 Synopsis

The phase transition behavior of established UCST-type polymers was modified by copolymerization with hydrophilic or hydrophobic comonomers to obtain new polymers properties and to tune the T_{cp} , the cooling/heating hysteresis as well as the type of phase transition itself, such as a double thermoresponsive behavior. In the second part of this work, the focus was on the application of synthesized copolymers as thermoresponsive matrixes for the temperature-controlled release of drugs etc. On the whole, this work consists of six linked sub-works (Figure 6-1).

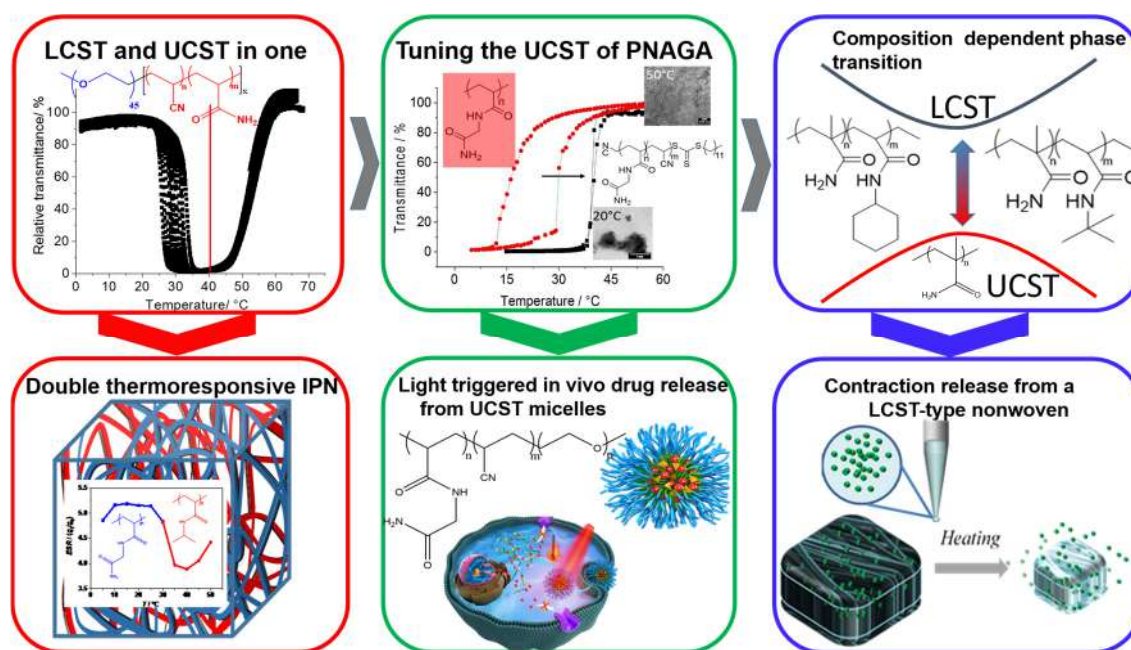


Figure 6-1: Summary of the interlinked research projects in this dissertation.

The first work showed a simple method of making block copolymers of poly(ethylene glycol) (PEG) and P(AAm-AN) by using a PEG based macro-azoinitiator. The copolymer showed dual thermoresponsivity of LCST- and UCST-type in one system, which is stable and highly reproducible for a large number of cycles. (**Publication 1**,

Synopsis

Figure 6-1 top left). The influence of the length of the hydrophilic PEG units on the thermoresponsive behavior as well as on the formation of micelles by means of turbidity measurements and DLS measurements was shown. Moreover, the production and characterization of the mechanical and thermoresponsive properties of a double thermoresponsive interpenetrating network (IPN) hydrogel from PNAGA (UCST) and PNIPAAm (LCST) have been demonstrated (**Publication 6**, Figure 6-1 bottom left).

In the second publication, based on NAGA and AN copolymer using reversible addition-fragmentation chain transfer (RAFT) polymerization, we provide a new polymer system showing highly reproducible, stable and sharp phase transitions for a large number of cycles without any significant hysteresis. Cloud points can be tuned by changing the ratio of the two comonomers without sacrificing the reproducibility and sharpness. Furthermore, changing the concentration and the amount of hydrogen bond suppressing reagent urea were investigated and discussed by using turbidity, cryoTEM and DLS measurements (**Publication 2**, top center Figure 6-1).

(**Publication 3** Figure 6-1, bottom center) shows the application of a PEG-P(NAGA-AN) terpolymer for a localized, light-triggered temperature increase and the resulting local release of drugs to combat drug-resistant cancer cells.

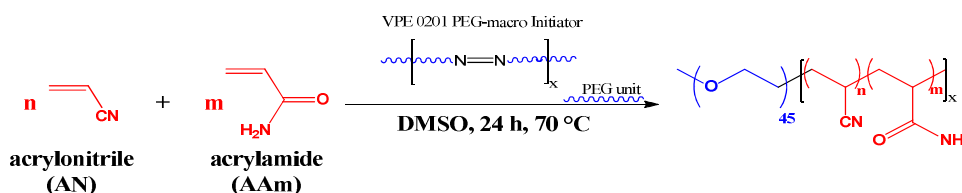
Furthermore, by copolymerization of methacrylamide (MAAm) and *N*-substituted hydrophobic comonomers, the thermoresponsive behavior of PMAAm was transferred from a broad UCST to an LCST phase transition with narrow cooling/heating hysteresis (**Publication 4**, Figure 6-1 top right). By adding a UV-crosslinking comonomer 4-acryloyloxybenzophenone (ABP), the production of a UV-cross linkable electrospun nonwoven with an LCST-type phase transition could be shown (**Publication 5** Figure 6-1 bottom right). As a result of temperature changes, the contraction of the nonwoven demonstrated the temperature-controlled targeted release of nanoparticles.

6.1 LCST and UCST in One: Double Thermoresponsive Behavior of Block Copolymers of Poly(ethylene glycol) and Poly(acrylamide-co-acrylonitrile)

This work was **published** by Käfer, F.; Liu, F.; Stahlschmidt, U.; Jerome, V.; Freitag, R.; Karg, M.; Agarwal, S., in *Langmuir* **2015**, 31 (32), 8940-6.

In this work, we showed a simple method of making block copolymers of poly(ethylene glycol) (PEG) and P(AAm-AN) using a PEG based macro-azoinitiator. The copolymer showed dual thermoresponsivity of LCST- and UCST-type in one system, which is stable and highly reproducible for a large number of cycles. This contrasts with P(AAm-AN) copolymers, which show a UCST-type phase transition in water.

By way of a free radical polymerization of acrylamide with acrylonitrile, PEG-*b*-P(AAm-AN), the block copolymers could be prepared (Scheme 6.1-1).



Scheme 6.1-1: Radical copolymerization of acrylamide/acrylonitrile using a PEG-macroinitiator.

Turbidity measurements (Figure 6.1-1A) and light scattering experiments (Figure 6.1-1B) were used for illustration purposes. It was shown that the double thermoresponsive phase behavior is strongly dependent on the length of the hydrophilic PEG unit and the concentration. In that way, it was reproducible over a large number of cooling/heating cycles with a small hysteresis.

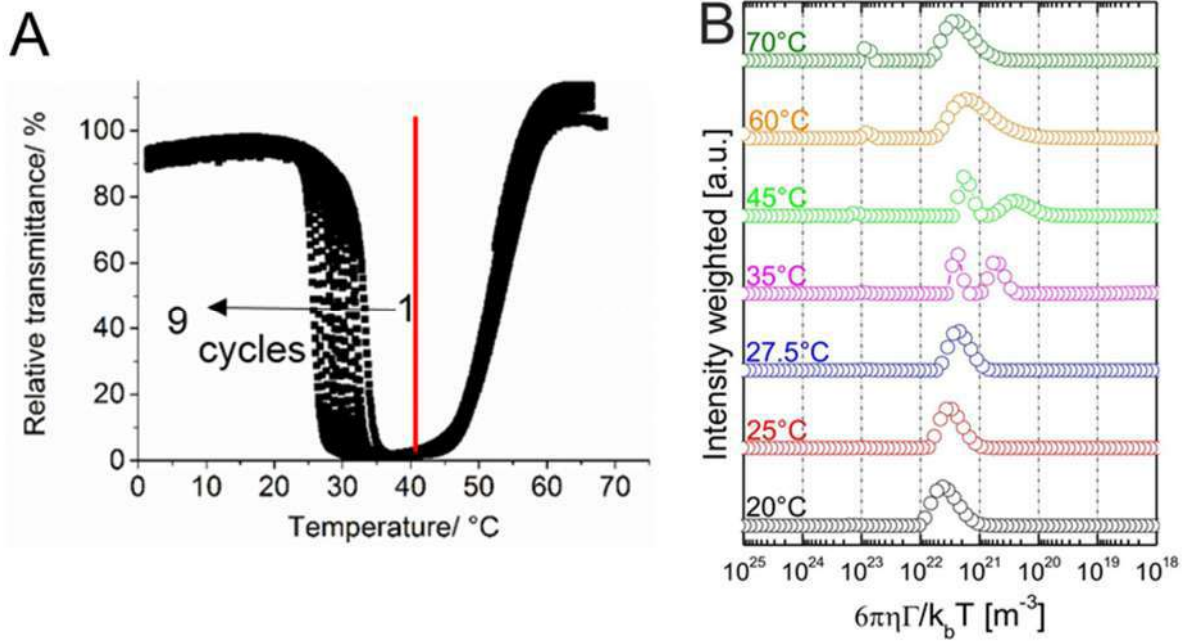


Figure 6.1-1: (A) Turbidity measurements (cooling curves) of PEG-*b*-P(AAm-AN) copolymer in pure water. The concentration was 7 wt%, (B) Relaxation rate distributions normalized by the temperature-dependent solvent viscosity and the temperature.

The double thermoresponsive behavior observed here is essentially based on the temperature-dependent change in morphology (Figure 6.1-2). In this case, the morphology changes with increasing temperature from micellar structures at 25 °C to aggregates (40 °C) and finally back to micellar structures at 64 °C.

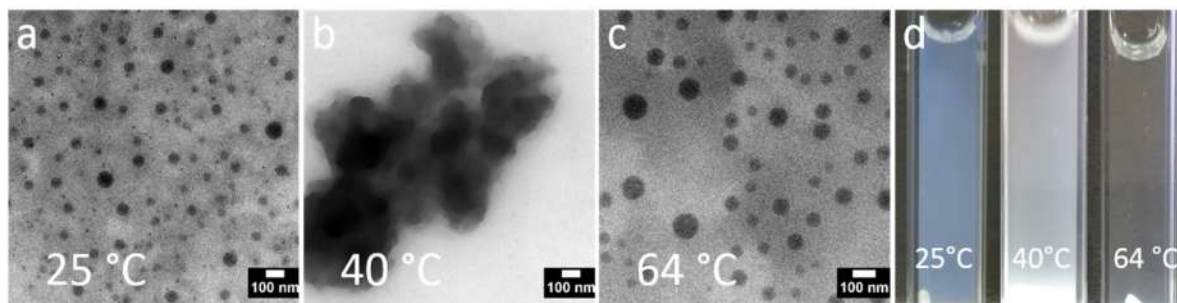


Figure 6.1-2: TEM images of samples prepared at different temperatures with a PEG-*b*-P(AAm-AN) concentration of 7 wt. % at 25 °C (**a**), 40 °C (**b**), 64 °C (**c**) and a visual change of the polymer solution (**d**).

6.1.1 Individual Contribution to Joint Publications

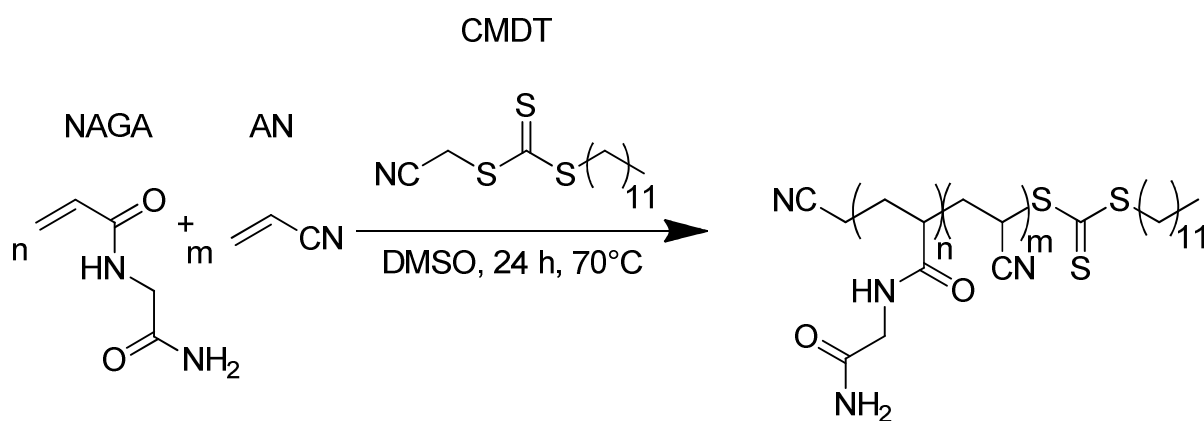
The synthesis of the copolymers and its characterization were carried out by me. The manuscript was also written by me. Dr. Fangyao Liu helped with the discussion and explanation of the results. The toxicity studies were carried out by Ulrich Stahlschmidt and Dr. Valérie Jérôme under the guidance of Prof. Dr. Ruth Freitag. The DLS and static light scattering (SLS) studies were conducted by Arne Lerch under the supervision of Prof. Dr. Matthias Karg. Prof. Dr. Seema Agarwal (corresponding author) was responsible for supervising, participating in the discussion, the designing concept and correcting the manuscript.

6.2 Tunable, Concentration-Independent, Sharp, Hysteresis-Free UCST Phase Transition from Poly(*N*-Acryloyl Glycinamide-Acrylonitrile) System

This work was **published** by **F. Käfer**, A. Lerch, S. Agarwal, in the *Journal of Polymer Science Part A: Polymer Chemistry* **2017**, *55*, 274.

In this work, based on NAGA and AN copolymer, we provide a new polymer system showing a highly reproducible, stable and sharp phase transition for a large number of cycles without any significant hysteresis. Cloud points can be tuned by changing the ratio of the two comonomers without sacrificing the reproducibility and sharpness.

RAFT polymerization was used to synthesize P(NAGA-AN) copolymers (Scheme 6.2-1). Block-kind copolymer structures were obtained since AN is preferably consumed at the beginning of the reaction. This was shown by GC kinetic studies and DSC measurements, which show two separated glass transition points.



Scheme 6.2-1: Copolymerization of NAGA and AN by using CMTD as chain transfer agent and AIBN as initiator.

Synopsis

In contrast to PNAGA, the synthesized P(NAGA-AN) copolymers show a narrow cooling/heating hysteresis in water, which can be tuned over a temperature range of < 5-40 °C, depending on the AN content (Figure 6.2-1A). In addition, it was shown that the cloud point in water does not change depending on the concentration (Figure 6.2-1B).

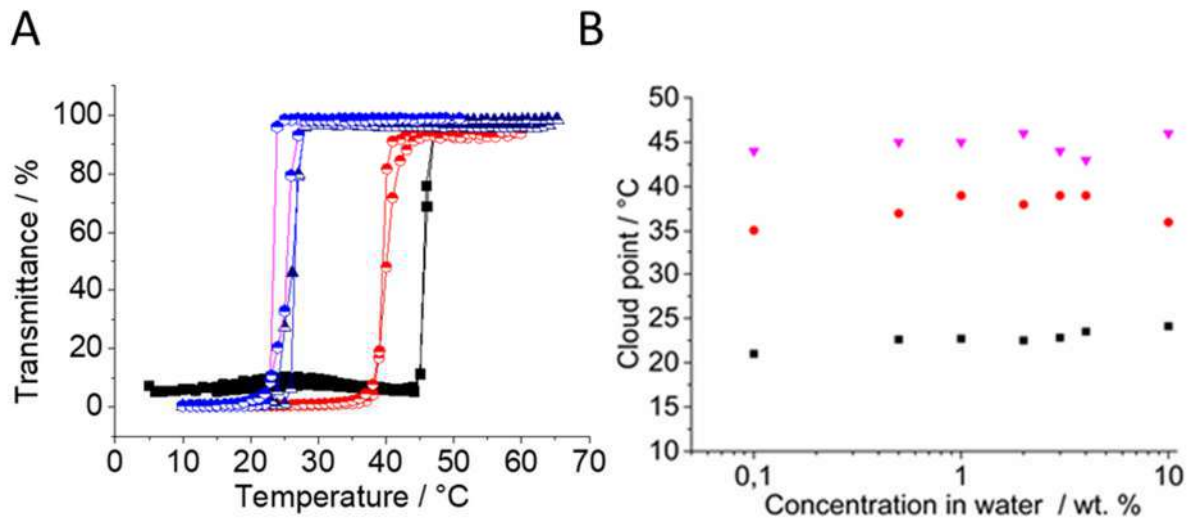


Figure 6.2-1:(A) hysteresis curves of the transmittance (%) versus temperature for 1 wt % P(NAGA-AN) in pure water, (B) cloud point (cooling) of the synthesized P(NAGA-AN) copolymers as a function of concentration in pure water. Heating rate 1 °C/min.

Furthermore, TEM and CryoTEM measurements showed the formation of micellar structures above and aggregation below the cloud point (Figure 6.2-2). In this case, the block-kind structure of the copolymer is probably the driving force for the formation of micellar structures above the cloud point. These micellar structures are presumably stabilized by strong hydrogen bonds, proven by the addition of unusually large amounts of urea which disturb the formation of hydrogen bonds, whereat the thermoresponsive behavior was maintained.

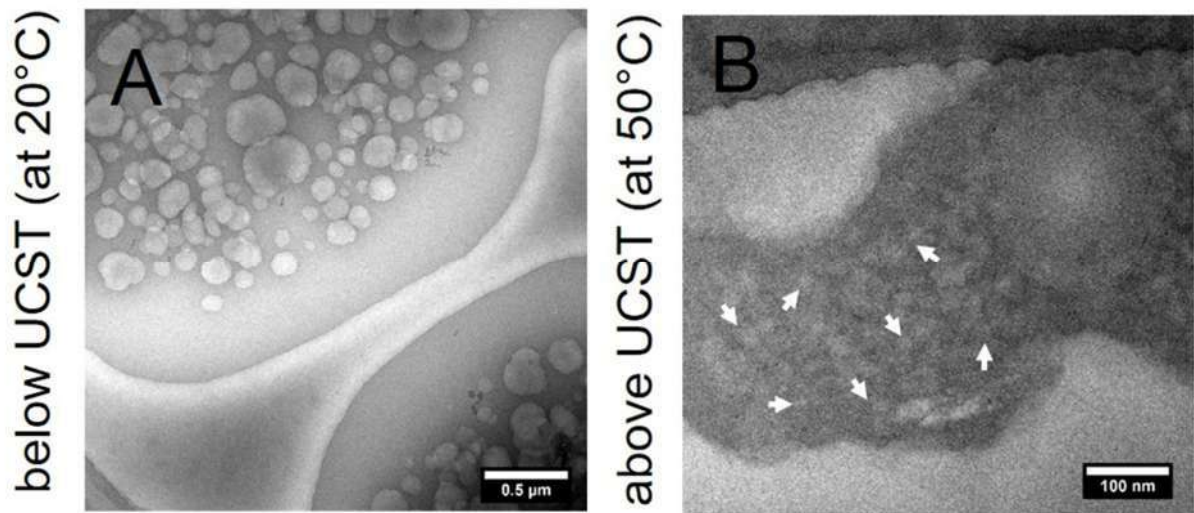


Figure 6.2-2: cryoTEM images of P(NAGA-AN) from a solution of concentration 0.1 wt % at temperature below (A at 20 °C) and above (B at 50 °C).

6.2.1 Individual Contribution to Joint Publications

The synthesis of the copolymers and its characterization were carried out by me. The manuscript was also written by me. The DLS and SLS studies were conducted by Arne Lerch. Prof. Dr. Seema Agarwal (corresponding author) was responsible for supervising, participating in the discussion, the designing concept and correcting the manuscript.

6.3 Let There be Light: Polymeric Micelles with Upper Critical Solution Temperature as Light-Triggered Heat Nanogenerators for Combating Drug-Resistant Cancer

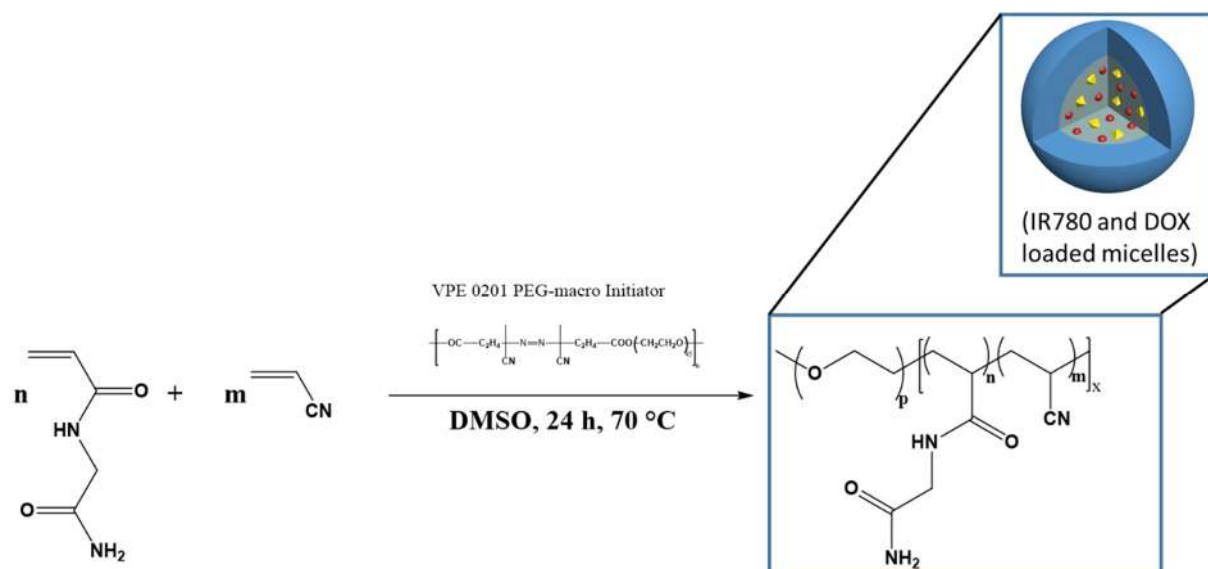
This work was **published** by Y. Deng⁺, **F. Käfer**,⁺ T. Chen, Q. Jin, J. Ji, S. Agarwal, in *Small* **2018**, 1802420.

[+] These authors contributed equally to this work.

In most cases, thermoresponsive polymeric micelles were constructed by lower critical solution temperature (LCST) polymers. Upon increasing the temperature to a temperature higher than LCST, polymeric micelles with LCST are not disassembled but shrunk, leading to an incomplete drug release. In this work, we show the first example of UCST-type polymeric micelles as drug nanocarriers to overcome drug resistance by light-triggered drug release and retention intracellularly.

By way of a free-radical polymerization of NAGA with acrylonitrile, using a poly(ethylene glycol) (PEG) macro-azoinitiator, a UCST copolymer was synthesized. The synthesized copolymer shows a cloud point at around 44 °C (cooling) in water as well as in PBS solution (0.1 M; pH = 7.4). Due to the microstructure of the PEG-*b*-P(NAGA-*co*-AN) copolymer, micelles are formed at RT, as shown by DLS and TEM measurements. The micelles were successfully used for the encapsulation of anticancer drug doxorubicin (DOX) and a photo-thermal agent (IR780) (Scheme 6.3-1).

Synopsis



Scheme 6.3-1: Schematic illustration of the synthesis of PEG-*b*-P(NAGA-AN) and the formation of DOX/IR780 loaded micelles.

By irradiation with an NIR laser, the micelles can be dissociated, which enables the spatiotemporal controlled release of DOX and prevents the efflux of DOX into drug resistant MCF-7/DOX cells. This allows an effective prevention of the growth of drug-resistant tumor cells which could be shown by *in vivo* studies with nude mice without any obvious side effects (Figure 6.3-1).

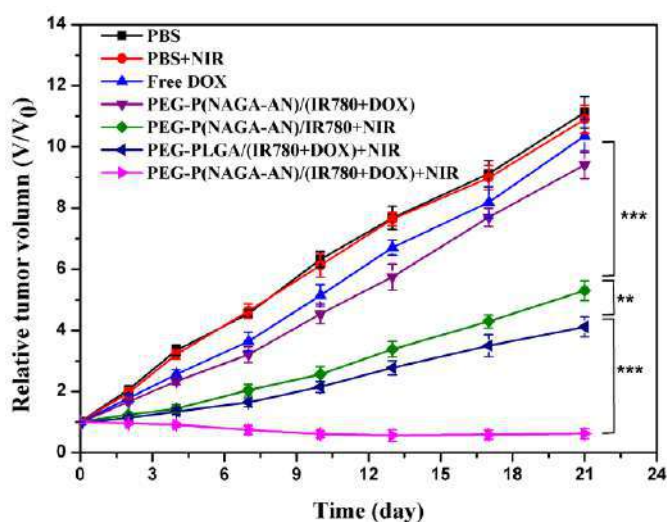


Figure 6.3-1: MCF-7/DOX tumor growth was evaluated by measuring the relative tumor volume after different treatments.

Synopsis

6.3.1 Individual Contribution to Joint Publications

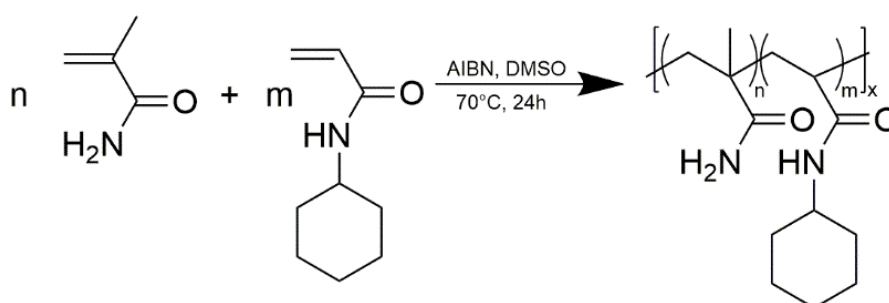
The synthesis of the copolymer and its characterization were carried out by me. The synthesis part of the manuscript was also written and revised by me. The *in vivo* release studies and cell experiments were carried out by Yongyan Deng under the supervision of Prof. Jin Qiao (corresponding author) and Prof. Dr. Jian Ji. Tingting Chen assisted in the discussion of the results and in the preparation of the art works. Prof. Dr. Jian Ji, Prof. Dr. Seema Agarwal (corresponding author) and Prof. Dr. Jin Qiao proposed the idea, helped write and correct the manuscript and were in charge of guiding and supervising this work.

6.4 Tuning the Phase Transition from UCST-Type to LCST-Type by Composition Variation of Polymethacrylamide Polymers

This work was **published** by **F. Käfer**, M. Pretscher, S. Agarwal, *Macromolecular Rapid Communication* **2018**, 1800640.

In this work, we show a rare example of composition-dependent thermoresponsive behavior of the copolymers of methacrylamide (MAAm) with hydrophobic comonomers such as *N*-cyclohexylacrylamide (NchAAM) and *N*-*tert*-butylacrylamide (NtbAAM). Polymethacrylamide (PMAAm) homopolymers show a UCST-type phase transition with a broad hysteresis.

Copolymers of methacrylamide (MAAm) were synthesized using free-radical polymerization (Scheme 6.4-1).



Scheme 6.4-1: Reaction scheme for the synthesis of copolymers of MAAm and NchAAM. Reactions were carried out in DMSO with AIBN as radical initiator.

While a broad UCST-type phase transition was observed with an increased T_{cp} with 2 mol % NchAAM in copolymer composition, with a copolymer with an NchAAM content of 5 mol %, the copolymer was already soluble in a temperature range of 5–80 °C when compared to PMAAm (Figure 6.4-1A). However, copolymer with an NchAAM content of 25 mol % showed an LCST-type phase transition with a narrow

Synopsis

cooling/heating hysteresis (Figure 6.4-1B). Ultimately, with a content of 50 mol % NchAAm, the copolymer was completely insoluble.

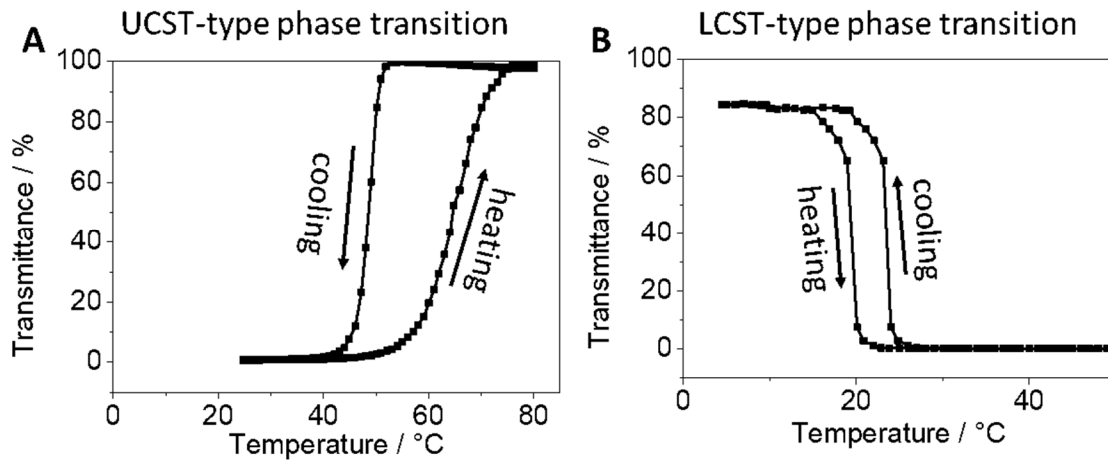


Figure 6.4-1: Phase separation in water as monitored by measuring Transmittance (%) at different temperatures during cooling and heating cycles **(A)** 1 wt % solution of PMAAm; **(B)** 1 wt % solution of a P(MAAm_{75%}-NchAAm_{25%}) copolymer.

With regard to the LCST-type copolymer, no significant effect on the concentration or the phase transition behavior was found. In contrast, the UCST copolymer showed a strong dependence on the T_{cp} in the concentration. At a concentration of 2 wt %, the polymer could no longer be dissolved (Figure 6.4-2).

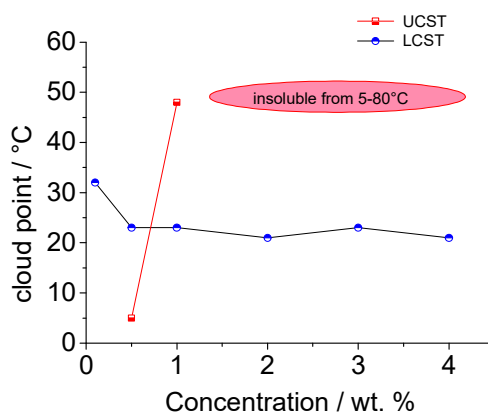


Figure 6.4-2: Cloud points as a function of concentration.

Synopsis

By adding urea, which disturbs the formation of hydrogen bonds, the role of hydrogen bonds on the phase transition behavior could be demonstrated. The T_{cp} of LCST-type transition increased with an increased amount of urea, whereas T_{cp} decreased with a UCST-type transition. Moreover, it was found that the hydrophobicity of the *N*-substituted comonomers has a considerable influence on the phase behavior, which could be shown by copolymerization of MAAm with different comonomers such as *N-tert*-butylacrylamide, *N-furfuryl*acrylamide or *N-n*-hexylacrylamide.

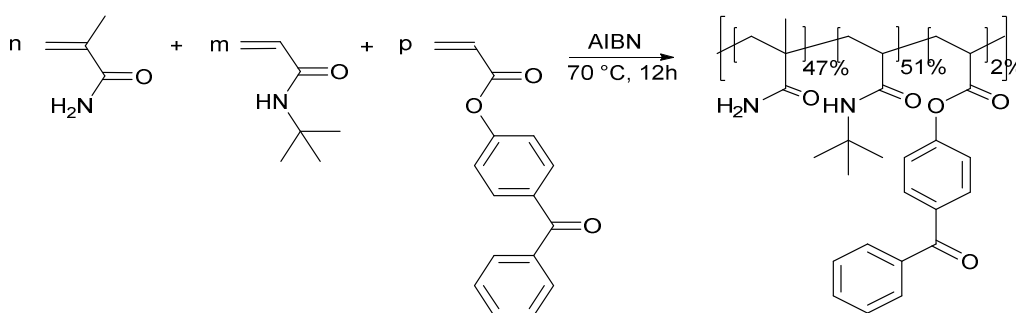
6.4.1 Individual Contribution to Joint Publications

The synthesis of the copolymers and its characterization were carried out by me. The manuscript was also written by me. Martin Pretschner helped with the synthesis and characterization as a student assistant under my guidance. Prof. Dr. Seema Agarwal (corresponding author) was responsible for supervising, participating in the discussion, the designing concept and correcting the manuscript.

6.5 Controlled-Release LCST-Type Nonwoven Depots via Squeezing-Out Thermal Response

This work **was published** by F. Käfer, R. Vilensky, G. Vasilyev, E. Zussman, S. Agarwal, *Macromolecular Materials and Engineering* **2019**, 304, (3), 1800606.

In this work, we demonstrate a proof-of-concept for the release of model nanoparticles from potential transdermal LCST-type nonwoven patch pores controlled by temperature. A LCST-type poly(methylacrylamide-co-*N*-*tert*-butylacrylamide-co-4-acryloylbenzo-phenone) P(MAAm-NtbAAm-ABP) copolymer was synthesized using free-radical copolymerization (Scheme 6.5-1). As a result of the photo cross-linker units and the polymer chain, the copolymer could be cross-linked under UV-light irradiation. Temperature-dependent rheology and turbidity measurements of the uncross-linked copolymer in solution as well as a micro-DSC measurement for the cross-linked polymerfilm showed an LCST-type phase transition at approximately 41 °C (heating) resp. 45 °C (cooling).



Scheme 6.5-1: Synthesis of the P(MAAm-NtbAAm-ABP) by free-radical polymerization at 70°C with AIBN a radical initiator and DMSO as solvent.

The copolymer was successfully electro-spun and subsequently cross-linked under UV-light irradiation to form a nano-fibrous matrix, which exhibits thermo-initiated LCST-

Synopsis

based contraction in an aqueous media. The nonwoven showed low contraction in cold water of around 20 % in the direction along the fibers axis and 5 % in the perpendicular direction. In contrast, at 40 °C, an additional strong contraction of 50 % in both directions was achieved due to the dehydration and formation of inter- and intramolecular hydrogen bonds. In order to demonstrate the temperature triggered contraction and the induced release, the nano-fibrous matrix was uploaded with fluorescently labeled carboxylated latex nanoparticles (c-NPs), 200 nm in size (Figure 6.5-1).

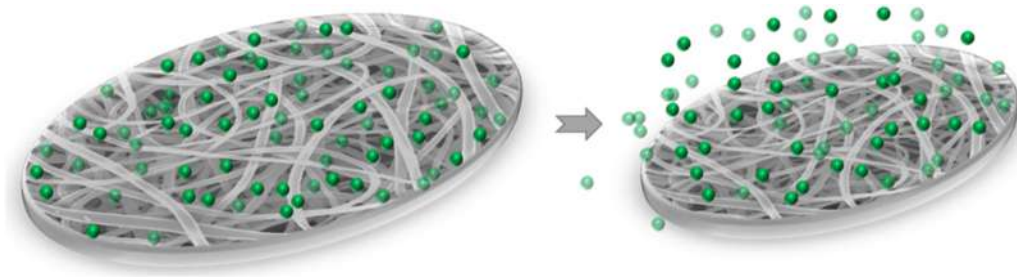


Figure 6.5-1: Schematics of the heat-induce fibrous matrix shrinkage and concurrent nanoparticles release.

The *in vitro* release was monitored using real time fluorescence microscopy. At around 28 °C, an extensive contraction occurred, accompanied by a burst release of the c-NPS. At 35 °C, the maximum of particles released was observed. Ultimately, after the first heating cycle, as much as 62 % of the c-NPS were released from the fibers mat.

Synopsis

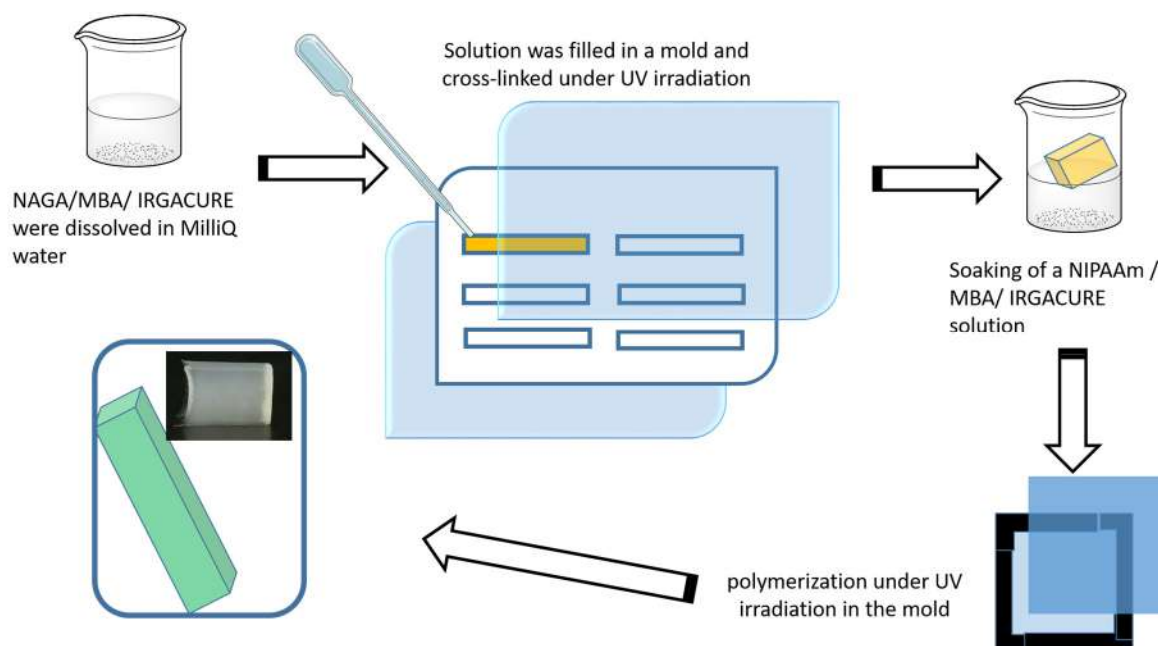
6.5.1 Individual Contribution to Joint Publications

The synthesis and the characterization of the copolymer were carried out by me. Turbidity DLS as well as micro DSC measurements were also performed by me. The rheology, TEM and contraction experiments were performed by Rita Vilensky and Gleb Vasilyev. The manuscript was written and revised by Rita Vilensky and me. Prof. Dr. Eyal Zussman and Prof. Dr. Seema Agarwal (corresponding author) were responsible for supervising, participating in the discussion, the designing concept and correcting the manuscript.

6.6 Interpenetrating Thermophobic, Thermophilic Dual Responsive Networks

This work **was published** by F. Käfer, Y. Hu, Y.J. Wang, Z. L. Wu, S. Agarwal, *Journal of Polymer Science Part A: Polymer Chemistry* **2019**, 57, 539–54.

In this work, we show the photo-induced radical polymerization of PNAGA gel in the first reaction step, followed by a second step for preparing the PNIPAAm network to achieve the IPN hydrogel structure of PNAGA/PNIPAAm (see Scheme 6.6-1). By changing the content PNIPAAm as the second network the swelling/deswelling behavior was changed from a broad UCST-type of a PNAGA hydrogel to a double thermoresponsive behavior for the prepared IPN hydrogels.



Scheme 6.6-1: Schematic preparation of PNAGA/PNIPAAm IPN hydrogels.

The IPN hydrogels showed a dual thermoresponsive swelling/deswelling behavior depending on the ratio of the 1st to 2nd network (weight ratio ω), which was

Synopsis

demonstrated by determination of the temperature dependent equilibrium swelling ratio (ESR) (Figure 6.6-1).

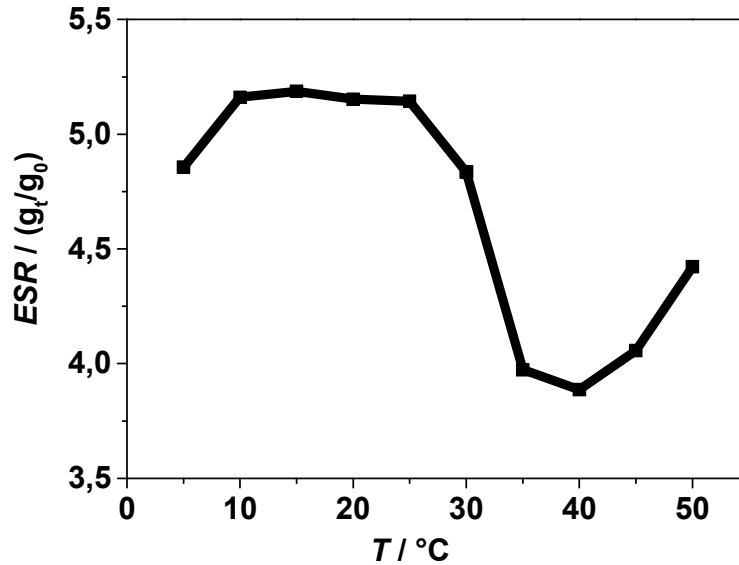


Figure 6.6-1: Equilibrium swelling rate of an IPN hydrogel with a NIPAAm weight ratio of $\omega = 0.7$.

Furthermore, stress/strain measurements under different environmental conditions were performed. The mechanical properties were affected by the temperature and by the PNIPAAm content. It turned out that an increasing temperature or a decreasing content of NIPAAm in the IPN hydrogel lead to better mechanical properties.

6.6.1 Individual Contribution to Joint Publications

The synthesis, the mechanically and thermoresponsive characterization of the IPN hydrogels were done by me and student assistant Yunfeng Hu under my guidance. Yan Jie Wang helped perform stress/strain measurements in an aqueous environment at different temperatures. The manuscript was written and revised by me. Prof. Dr. Seema Agarwal (corresponding author) and Prof. Dr. Zi Liang Wu were

Synopsis

responsible for supervising, participating in the discussion, the designing concept and correcting the manuscript.

7 Reprints of Publications

The manuscripts are reprinted in the form of journal articles with the permission of the respective publishers.

The corresponding author is marked with an asterisk.

7.1 LCST and UCST in One: Double Thermoresponsive Behavior of Block Copolymers of Poly(ethylene glycol) and Poly(acrylamide-co-acrylonitrile)

This work was published by **F. Käfer**, F. Liu, U. Stahlschmidt, V. Jérôme, R. Freitag, M. Karg, S. Agarwal, *Langmuir* **2015**, 31 (32), 8940-6.

Reprinted with permission; Copyright 2015 American Chemical Society

LCST and UCST in One: Double Thermoresponsive Behavior of Block Copolymers of Poly(ethylene glycol) and Poly(acrylamide-co-acrylonitrile)

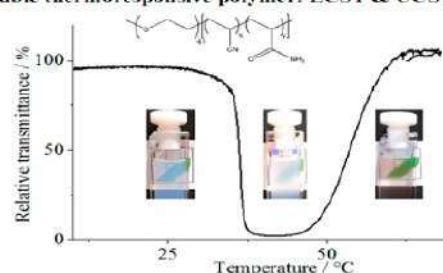
Florian Käfer,[†] Fangyao Liu,[†] Ullrich Stahlschmidt,[§] Valérie Jérôme,[§] Ruth Freitag,[§] Matthias Karg,[‡] and Seema Agarwal^{*,†}

[†]Macromolecular Chemistry II and Center for Colloids and Interfaces, [‡]Physical Chemistry I, and [§]Chair for Process Biotechnology, University of Bayreuth, Universitätsstraße 30, 95440 Bayreuth, Germany

Supporting Information

ABSTRACT: The change in thermoresponsive behavior from a single phase transition of upper critical solution temperature (UCST)-type of an acrylamide-acrylonitrile copolymer (AAm-co-AN) to a double responsive behavior (LCST-UCST-type (LCST, lower critical solution temperature)) in water by the introduction of a poly(ethylene glycol) (PEG) block is highlighted in the present work. The polymer is synthesized in a simple way by free-radical polymerization of acrylamide and acrylonitrile using a poly(ethylene glycol) (PEG) macro-azoinitiator. The dual thermoresponsive behavior was observed in a wide range of concentrations repeatable for many cycles with very small hysteresis depending upon the ratio of AAm, AN and PEG. Static light scattering (SLS) and dynamic light scattering (DLS) together with turbidity photometry and transmission electron microscopy confirmed a unique phase transition behavior due to the temperature dependent change in the morphology from micelles to agglomerates. The low cytotoxicity and two-in-one thermoresponsive behavior makes the polymer promising for biomedical applications in the future.

Double thermoresponsive polymer: LCST & UCST in one



INTRODUCTION

Polymers which exhibit a thermoresponsive behavior in water are well-known in the literature. This type of polymer can be classified in two groups, one which phase separates in water upon heating (lower critical solution temperature (LCST)-type)¹ and the other which shows phase separation upon cooling (upper critical solution temperature (UCST)-type).² Polymeric systems of LCST-type with a single phase transition temperature are very well studied. In the past few years, increasing attention has also been paid to polymers showing a UCST-type response with a single phase transition.³ A concentration dependent change from LCST to UCST in water is also known for polymers such as poly(trimethylene ether) glycol.⁴ At low concentrations (<15 wt %), the polymer showed LCST, and at high concentrations (>45 wt %) a UCST was observed. In the intermediate concentration range, the polymer was insoluble. The temperature dependent close-loop solubility behavior of poly(ethylene oxide) of a particular molar mass in water is also well studied.⁵

Progress has also been made in the preparation of block copolymers with one or more thermoresponsive blocks showing temperature dependent stepwise phase separation transitions of the Soluble–Insoluble–Insoluble type. In such cases the polymers show more than one cloud point of LCST-type as the individual blocks undergo phase-separation at

different temperatures.^{6,7} One of such polymers is an A–B block copolymer of poly(*N*-isopropylacrylamide) (NIPAAm) and poly(NIPAAm-co-(*N*-(hydroxymethyl)acrylamide) (HMAAm)) which showed a double thermoresponsive behavior with two cloud points.⁸ Many other block copolymers like poly(*N*-*n*-propylacrylamide)-*b*-poly(*N,N*-ethylmethacrylamide) (PnPA-*b*-PEMA) show a complex thermoresponsive behavior which is different from the stepwise phase separation behavior. The aqueous solution of (PnPA-*b*-PEMA) showed a change from transparent to turbid with intermediate transitions to cloudy and clear with increasing temperature.⁹ The block copolymer of poly(*N,N*-dimethylaminoethyl methacrylate) (PDMAEMA) and poly(ethylene glycol) (PEG) in water showed a change from a simple LCST-type, thermoresponsive behavior to a complex self-assembly process (soluble–insoluble–soluble; LCST-type transition at a lower temperature and a UCST-type transition at a higher temperature) with temperature on changing pH of the solution from neutral to pH 12.¹⁰ Dilute aqueous solutions of the block copolymer (poly(methoxytri(ethylene glycol) acrylate)-*b*-poly(4-vinylbenzyl methoxytris(oxyethylene) ether) (PTEGMA-*b*-PTEGSt)) also showed similar multiple reversible transitions, from

Received: February 3, 2015

Published: July 22, 2015

Table 1. Block Copolymers (PEG-*b*-poly(AAm-co-AN)) Made by Radical Polymerization of Acrylamide (AAm) and Acrylonitrile (AN) with PEG Macro-Azoinitiators

| entry | M_n | M_w | M_w/M_n | monomer/ initiator molar ratio | AN amount in polymer (mol %) | cloud points/°C ^a | |
|-------|--------|--------|-----------|--------------------------------|------------------------------|------------------------------|-----------------|
| | | | | | | LCST-type | UCST-type |
| 1 | 37 000 | 70 000 | 2.2 | 175:1 (PEG 2000 g/mol) | 9 | 30 | 50 |
| 2 | 30 000 | 53 000 | 1.8 | 175:1 (PEG 2000g/mol) | 12 | 50 | 68 ^b |
| 3 | 31 000 | 53 000 | 1.7 | 175:1 (PEG 2000g/mol) | 7 | 13 | 23 |
| 4 | 40 000 | 70 000 | 1.8 | 175:1 (PEG 6000 g/mol) | 13 | soluble | soluble |
| 5 | 58 000 | 85 000 | 1.5 | 1550:1 (PEG 6000 g/mol) | 11 | 20 ^c | 45 |

^aFirst cooling curves, concentration in pure water 7 wt %. ^bHydrolysis after three cycles. ^cDisappears after three cycles.

transparent, to cloudy, to clear bluish, and turbid, with the increase of temperature.¹¹ The corresponding homopolymers poly(TEGSt) and poly(TEGMA) showed only a LCST-type transition. A similar behavior was also shown for aqueous solutions of block copolymers consisting of a 2-ethyl-2-oxazoline block and another block consisting of a random copolymer of 2-ethyl-2-oxazoline and 2-*n*-propyl-2-oxazoline (PEtOx-*b*-poly(EtOx-*stat*-PropOx)).¹²

A combination of UCST- and LCST-type blocks in block copolymers provided complex self-assembly behavior with unimolecular dissolution of the polymers in water in the temperature range between the UCST and LCST of the corresponding blocks and phase separation below and above this temperature range (insoluble–soluble–insoluble; UCST-type transition at a lower temperature and a LCST-type transition at a higher temperature). Such a behavior was shown for a diblock copolymer consisting of poly(3-dimethyl(methacryloyloxyethyl) ammonium propanesulfonate) (PdMMAEAPS), as a UCST block, and poly(*N,N*-diethylacrylamide) (PdEA), as a LCST block,¹³ and quaternized block copolymers of 2-(2-methoxyethoxy)ethyl meth acrylate (MEO₂MA), oligo(ethylene glycol) methacrylate (OEGMA), and *N*-(3-(dimethylamino)propyl)methacrylamide (DMAPMA) (poly(OEGMA-co-MEO₂MA)-*b*-poly(DMAPMA)).¹⁴

Poly(acrylamide-co-acrylonitrile) poly(AAm-co-AN) is one of the rare examples of uncharged polymers showing a UCST-type single phase transition in water and physiological medium as shown in our previous work.¹⁵ In the present work, we show a simple method of making block copolymers of poly(ethylene glycol) (PEG) and poly(AAm-co-AN) using a PEG based macro-azoinitiator for a radical polymerization. The copolymer showed dual thermoresponsivity of LCST- and UCST-type in one system as investigated by turbidity and light scattering measurements in aqueous solution. The phase transition behavior and transition temperatures were found to depend on the PEG block length, polymer concentration, and ratio of AAm and AN. The temperature dependent change in the morphology from micelles to agglomerates and back to micelles was observed correlating well with the phase transition behavior. These changes are highly reproducible for many cycles.

MATERIALS AND METHODS

Chemical Reagents. PEG macro-azoinitiators with PEG molar mass (M_n) 2000 g/mol (VPE-0201) and 6000 g/mol (VPE 0601) were purchased from Wako and used without further purification. Acrylamide ($\geq 99.9\%$) was purchased from Sigma-Aldrich and freeze-dried. 2-Propenenitrile (99+%) was bought from ACROS Organics. Dimethyl sulfoxide (DMSO; $\geq 99.9\%$ ACS reagent) was purchased from Sigma-Aldrich. Ethylethanoate was distilled prior to use. Pure water was obtained from a Milli-Q Plus system (conductivity = 0.072

$\mu\text{S/cm}$). 3-(4,5-Dimethylthiazolyl-2)-2,5-diphenyl tetrazolium bromide (MTT) was purchased from Sigma-Aldrich. The cell culture materials were supplied by Greiner Bio-One; media and solutions were bought from Biochrome AG, Berlin, Germany.

Synthetic Procedure. The polymers were made by radical polymerization of AAm and AN using PEG macro-azoinitiators. The representative synthetic procedure is shown for entry 1 in Table 1. Other polymers given in Table 1 were made using similar procedure and using appropriate amounts of AAm, AN, and PEG initiators. In a 25 mL Schlenk flask, 123.2 mg of VPE-0201 (1 equiv), 0.599 g (78 mol %; 137 equiv) of acrylamide and 155 μL (22 mol %; 39 equiv) of acrylonitrile were dissolved in 10 mL of DMSO (feed ratio AAm/AN, 78:22). The solution was degassed via three freeze–pump–thaw cycles. The reaction flask was placed in an oil bath which was preheated to 70 °C and stirred for 24 h. The polymers were precipitated from the 10-fold excess volume of ethylethanoate. Afterward the polymers were centrifuged (7000 rpm, 10 min), washed three times with ethylethanoate and dried in a vacuum oven at 70 °C for 24 h.

¹H NMR (300 MHz, DMSO-*d*₆) δ /ppm: 1.22–2.18 (polymer backbone, –CH₂–), 2.1–2.9 (polymer backbone, –CH–CONH₂, –CH–CN–), 3.5 (–O–CH₂–CH₂–), 6.9 (–NH₂). ATR-FTIR: ν = 3650–3050 (mb, NH), 3000–2850 (w, CH₂), 2242 (w, –CN), 1659 (vs, CO), 1413 (m), 1348 (m), 1312 (m), 1118 (w) cm^{–1}.

Analytical Techniques. ¹H NMR spectra were recorded on a Bruker Ultrashield 300 machine with a 300 MHz operating frequency using DMSO-*d*₆ as solvent. The signals were calibrated to the DMSO signal at δ /ppm 2.5.

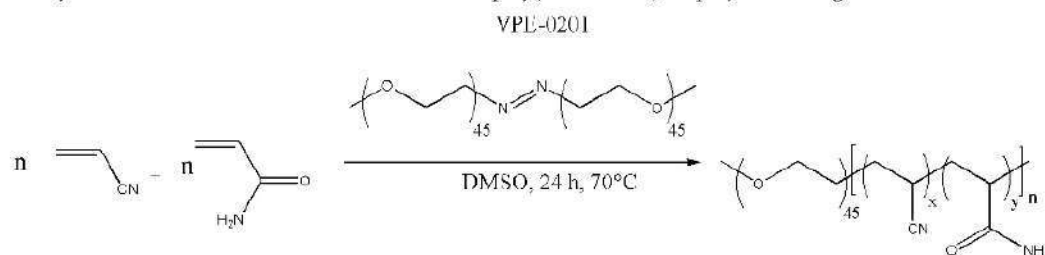
ATR-FTIR was used to determine the amount of acrylonitrile in copolymers. The measurements were conducted on a Digilab Excalibur Series FTS 3000 spectrometer with a diamond as ATR crystal. The spectra were analyzed by using the software WIN-IR PRO 3.3.

The differential scanning calorimetry (DSC) measurements were performed on a Mettler Toledo 821 DSC system. The system was calibrated with indium and zinc standards. All measurements were performed under nitrogen atmosphere with a heating/cooling rate of 10 °C/min.

The turbidity measurements were performed on a custom modified Tepper TP1-D spectrometer at a wavelength of 670 nm and with a cell path length of 10 mm under continuous stirring with a heating rate of 1.0 °C/min. The cloud points were determined at the point of inflection.

For determination of the molar mass and the molar mass distribution, gel permeation chromatography with DMSO as mobile phase was used. One PSS PolarSil PSA080505 (particle size 5 μm , dimension 8.0 mm \times 50 mm) as precolumn and two PSS PolarSil linear S (particle size 5 μm , dimension 8.0 mm \times 300 mm) columns calibrated with narrow Pullulan standards and a differential refractive index detector were employed. The flow rate was 0.7 mL/min at a temperature of 75 °C. The software PSS WinGPC Unity, Build 1321 was used for analyzing the spectra.

Transmission electron microscopy (TEM) measurements were performed on a Zeiss EM922 OMEGA EFTEM instrument. The micrographs were recorded by using a CCD camera (Ultrascan 1000,

Scheme 1. Synthetic Scheme for the Formation of PEG-*b*-poly(AAm-co-AN) Copolymers Using a PEG Macro-Azoinitiator

Gatan) and were processed with a digital image processing system (Gatan Digital Micrograph 3.9 for GMS 1.4).

Dynamic and static light scattering (DLS and SLS, respectively) measurements were performed on a 3D LS spectrometer of LS Instruments AG (Fribourg, Switzerland) in 2D operation using a HeNe laser (max. 35 mW constant output power at 632.8 nm) as light source. Two APD detectors in pseudo cross-correlation were used to detect the scattered light. The time average scattering intensities were measured at a scattering angle of 90°. The samples were filled in NMR tubes (VWR) with 5 mm outer diameter and measured at different temperatures. The temperature was adjusted with a stability of ± 100 mK by a heat controlled decalin bath. A FT100 thermoelement placed close to the sample position in the decalin bath was used to monitor the temperature. The DLS data were analyzed by inverse Laplace transformation (ILT) using the software AfterATV version 1.0d by Dullware providing the relaxation rate distributions.

RESULTS AND DISCUSSION

A PEG macro-azoinitiator (VPE 0201) was used for the free-radical polymerization of acrylamide (AAm) and acrylonitrile (AN) as shown in Scheme 1. The copolymers were structurally characterized using ^1H NMR and ATR-FTIR. The characteristic signals of $-\text{OCH}_2$ ($\delta = 3.5$ ppm), $-\text{C}(\text{O})\text{NH}_2$ ($\delta = 6.9$ ppm) and backbone protons in the lower ppm region clearly showed the presence of PEG and AAm in the copolymers (Figure 1). The characteristic absorption bands in the FTIR

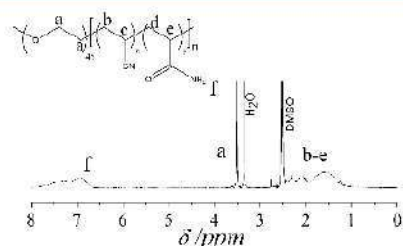


Figure 1. ^1H NMR spectrum of the PEG-*b*-poly(AAm-co-AN) copolymer (entry 1, Table 1; $M_n = 37\,000$ g/mol; PDI = 2.2) in $\text{DMSO}-d_6$ at 25 °C.

spectrum at 2242 and 1659 cm^{-1} substantiated the presence of cyano from AN and carbonyl groups from AAm in our copolymers. The comonomer molar ratio (AAm: AN) in the poly(AAm-co-AN) block was varied from 93:7 to 87:13 as determined by FTIR (shown in Supporting Information Figure 1). The polymers showed high molar masses ($M_n = 37\,000$ g/mol to 58 000 g/mol) and broad molar mass distributions (PDI = 1.5–2.2) as determined by gel permeation chromatography measurements (Supporting Information Figure 2). The differential scanning calorimetric measurements showed two separate thermal transitions. For example, a melting point at

24 °C corresponding to the PEG block and a glass transition temperature at 130 °C of the poly(AAm-co-AN) block for a copolymer with 9 mol % AN was seen (Supporting Information Figure 3). The initiation of AAm and AN copolymerization using PEG macro-azoinitiator could provide a A-B block copolymer (PEG-*b*-poly(AAm-co-AN)) by polymerization initiation by PEG radicals. Besides the formation of A-B block copolymers, the termination by radical combination and/or combination with PEG initiator radicals could also provide A-B-A block copolymers (PEG-*b*-poly(AAm-co-AN)-PEG). However, it is not possible to distinguish/quantify the amounts of each type (A-B and A-B-A) of block copolymers in the present work.

In one of our previous studies poly(AAm-co-AN) copolymers made by free-radical polymerization using azo-bis(isobutyronitril) (AIBN) as radical initiator were found to exhibit a single phase (insoluble-to-soluble) transition in water with increasing temperature. Hence a UCST-type behavior was observed. The cloud points could be easily varied by changing the copolymer composition.¹⁹ In the present work the presence of the PEG block led to a drastic change in the thermoresponsive behavior of poly(AAm-co-AN) from UCST-type (insoluble-to-soluble) to multiphase-type (soluble-insoluble-soluble; LCST at low temperature and UCST at higher temperature). The thermoresponsive behavior for block copolymers as observed by turbidity measurements (relative change in % transmittance with temperature) is shown in Figure 2.

For a block copolymer with 9 mol % AN at low temperatures, the relative transmittance is high and does not significantly change with increasing temperature up to about 25–30 °C where the transmittance drops dramatically. At around 40 °C, the transmittance starts to increase again and reaches even higher values than compared to the low temperature regime (below 25 °C). From this behavior two cloud points can be extracted. The LCST- and UCST-type cloud points were observed at around 30 and 50 °C, respectively. The phase transitions were reversible for at least nine cycles. Slight shifts of the LCST cloud point toward lower temperatures for increasing cycle numbers was found, and the UCST cloud point remained nearly unaffected. Independent of the cycle number the turbidity curves overlapped nicely for temperatures above 40 °C. The changes of the LCST cloud point might be related to kinetic effects during the self-assembly process, which is also affected by the heating rate (Supporting Information Figure 4). High molar mass poly(ethylene oxide) (PEO) also shows concentration dependent close-loop phase behavior in water with LCST and UCST at lower and higher temperatures, respectively, as documented in the literature.³ In any case, both LCST and UCST for PEO lie much above 100

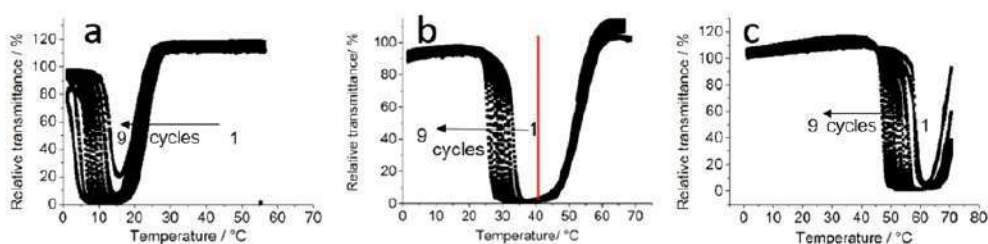


Figure 2. Turbidity measurements (cooling curves) of PEG-*b*-poly(AAm-*co*-AN) copolymer in pure water. The polymer concentration was 7 wt %, and AN amount in polymers was (a) 7 mol %, (entry 3, Table 1), (b) 9 mol % (entry 1, Table 1), and (c) 12 mol % (entry 2, Table 1).

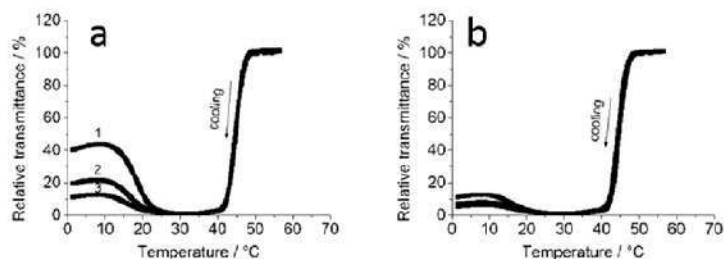


Figure 3. Turbidity measurements (cooling curves) of PEG-*b*-poly(AAm-*co*-AN) copolymer in water, concentration 7 wt %, PEG block length of 6000 g/mol (entry 5, Table 1), (a) first three cycles and (b) fourth to ninth cycle with nearly disappeared LCST.

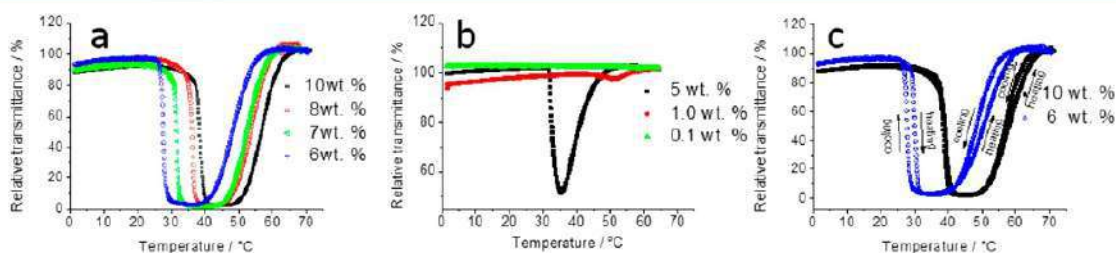


Figure 4. Cooling curves of the PEG-*b*-poly(AAm-*co*-AN) (entry 1, Table 1) copolymer with different concentrations in pure water, (a) 6–10 wt % and (b) 0.1–5 wt %; (c) hysteresis curves (heating and cooling) of the PEG-*b*-poly(AAm-*co*-AN) copolymer.

°C. Thermodynamically, the negative entropy of mixing and favorable enthalpy of formation (negative enthalpy) for specific hydrogen bonds between polymer and water molecules leads to solubility at low temperatures. At higher temperatures the unfavorable entropy term dominates and leads to phase separation (LCST-type phase transition). On increasing temperature further, the phase transition is dominated by combinatorial entropy and the components are completely miscible again (UCST-type phase transition).⁵

The increase in the amount of AN in block copolymers led to an increase in both cloud points (LCST-type varied from 13 to 50 °C and UCST-type changed from 23–68 °C) without affecting the multiphase solubility behavior (soluble–insoluble–soluble; LCST at low temperature and UCST at higher temperature) (entries 1–3, Table 1, Figure 2). This is in accordance with the tuning of the UCST-type cloud point of poly(AAm-*co*-AN) with change in ratio of AN and AAm as described by us in detail previously.⁵ The transitions were reversible for many cycles for copolymers with AN content up to about 9 mol % (Figure 2b). The block copolymers with 12 mol % AN (entry 2, Table 1) showed sharp LCST-type transitions for many cycles but led to decreased change in transmittance with temperature at high temperature (UCST-type transition) after three cycles. This is the inherent problem

of poly(AAm-*co*-AN) copolymers for compositions having a very high UCST-type cloud point due to hydrolysis of amide with time either during sample preparation or measurements.⁵ This particular block copolymer showed UCST-type cloud point of 68 °C in the first heating cycle. Although, there is some change in transmittance around UCST-type cloud point after nine cycles also but the change was not very strong. This means the block copolymers with AN content around 12 mol % show mostly LCST-type transition after few cycles. Besides ratio of AAm and AN, the PEG block length also affected phase transitions. The multiple phase transitions were highly sensitive to the length of PEG block. Increased PEG block length without changing the total molar mass of the block copolymer ($M_n \sim 37\,000$ g/mol) led to disappearance of thermoresponsivity. The polymer was soluble in water between 5 and 60 °C (entry 4, Table 1). Increase in the length of hydrophobic AAm-*co*-AN block in a block copolymer ($M_n \sim 58\,000$ g/mol) with PEG blocks of 6000 g/mol provided mainly UCST-type transition at around 45 °C after 3 cycles. In the first three cycles, weak multiple phase transitions were seen (Figure 3). After these three cycles the LCST is almost completely disappeared and a sharp UCST was seen.

The temperature dependent turbidity change of block copolymers of poly(AAm-*co*-AN) with a LCST-block poly-

(*N,N*-dimethylaminoethyl methacrylate) (PDMAEMA) made by RAFT-polymerization was recently shown. A temperature dependent aggregation was observed and copolymers showed transparency only between 22 and 41 °C.¹⁶

In addition, the cloud points (both LCST- and UCST-type) shifted to higher temperatures upon increase of the solution concentration in the range of 6–10 wt % (Figure 4a) with very small hysteresis in heating and cooling cycles (Figure 4c) as shown for entry 1, Table 1. The turbidity change for less concentrated solutions (<5 wt %) was not very drastic but similar soluble–insoluble–soluble transitions were seen (Figure 4b).

Further we performed light scattering experiments at a constant scattering angle of 90°. Figure 5 shows the static light scattering intensity recorded at different temperatures within a heating series.

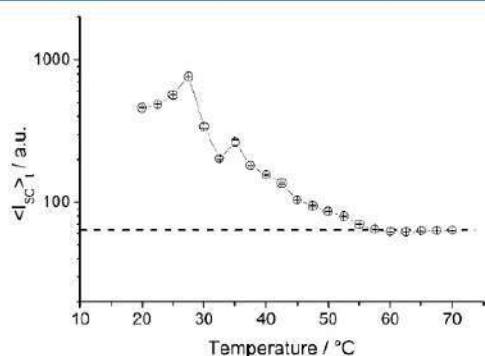


Figure 5. Static light scattering intensity (time average) of (entry 1, Table 1) with 7 wt % in water measured at different temperatures. Average of three measurements was taken. Dashed line highlights the average scattering intensity at temperatures above 60 °C.

Comparing the light scattering results with the turbidity measurements shown in Figure 2b, a very similar behavior is found. The scattering intensity increases at around 25–28 °C and then drops nearly continuously until reaching a plateau at around 60 °C. Above 60 °C the scattering intensity remains

nearly constant which is in very good analogy to the transmission of the sample as recorded by turbidity. It is worth noting that the turbidity experiments were performed with a constant heating rate and under continuous stirring of the sample. In contrast, the light scattering measurements were performed after equilibrating the sample for at least 10 min at each measured temperature and without stirring. Hence, the slightly different behavior, in particular in the LCST transition regime, is caused by the difference in sample treatment. To analyze whether these changes in the sample scattering behavior are related to structural changes, we performed dynamic light scattering experiments at different temperatures. Figure 6A shows intensity-time autocorrelation functions measured in the relevant temperature range.

At low temperatures, monomodal decays with similar decay rates are observed. In contrast, the correlation functions at 35 and 45 °C decay at significantly longer times, indicating slower dynamics in the sample. This can be attributed to larger structures. At 60 and 70 °C, the correlation functions decay at shorter times again, are very similar in their evolution, and show another fast contribution at shorter decay times. The autocorrelation functions were analyzed by the method of inverse Laplace transformation providing the hydrodynamic radius distribution functions (Figure 6b). Between 20 and 27.5 °C, the radius distributions are very similar in width and maximum position with only a slight increase in size. In contrast, at 35 °C, a second size population appears at significantly larger radii, indicating the formation of larger structures such as aggregates. This mode can also be observed at 45 °C. At 60 and 70 °C, the contribution at this larger size vanishes again and a second mode appears at significantly smaller sizes. Although a clear interpretation of the DLS data is difficult at this stage, not at least due to the relatively high sample concentration, the observed tendency is in very good agreement with the turbidity measurements. In addition, the results from DLS clearly show that structural transitions occur in the temperature range of 27.5–35 °C and in the range of 45–60 °C. These temperature intervals correspond to the LCST and the UCST cloud point regions. An in-depth study of the polymer morphology, for example, by means of small angle

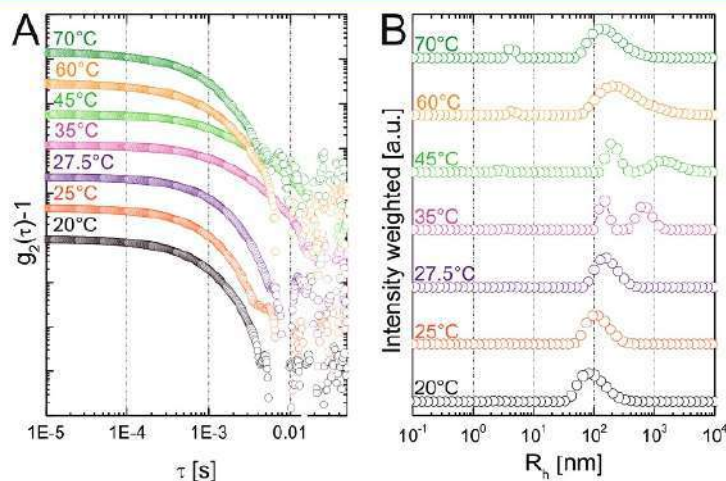


Figure 6. Results from DLS measurements at 90° scattering angle and different temperatures. (entry 1, Table 1) (A) Intensity-time autocorrelation functions as a function of the delay time τ . (B) Distributions of the hydrodynamic radius obtained from CONTIN analysis.

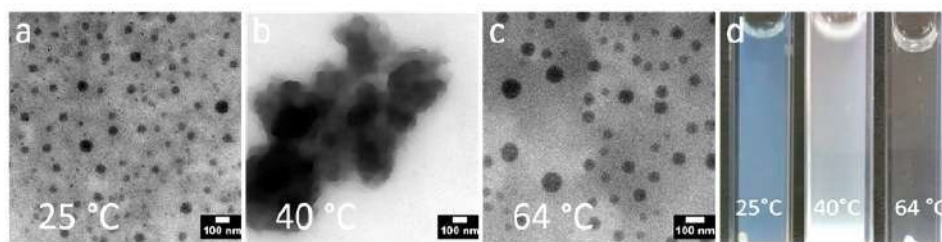


Figure 7. TEM images (a–c) of PEG-*b*-poly(AAm-co-AN) (entry 1, Table 1) from a solution of concentration 7 wt % at temperature (a) 25 °C, (b) 40 °C, and (c) 64 °C; (d) visual change of the polymer solution.

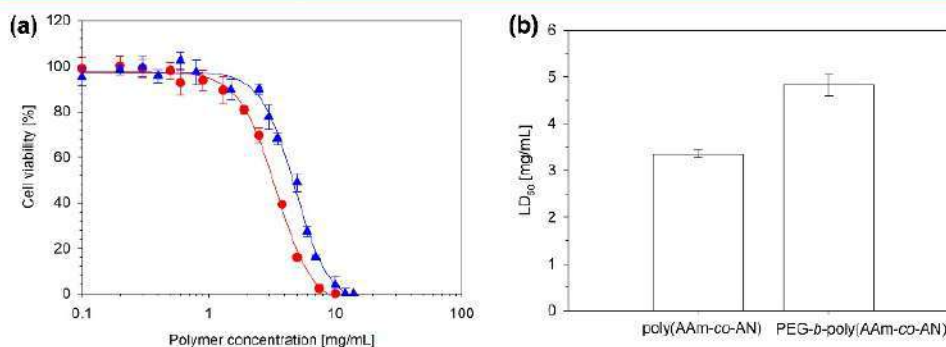


Figure 8. Cytotoxicity of the poly(AAm-co-AN)-based block copolymers (entry 1, Table 1) in L929 cells. (a) Incubation period was 24 h, and cell seeding density 1×10^5 cells per well: (red circles) poly(AAm-co-AN) and (blue up triangles) PEG-*b*-poly(AAm-co-AN). (b) LD₅₀ doses for the PEG-poly(AAm-co-AN) polymer and poly(AAm-co-AN) used as a reference. Data represent mean \pm SD from three independent experiments. There is a significant difference between the two means ($P \leq 0.001$; *t* test).

neutron scattering (SANS), is outside the scope of this paper and will be presented elsewhere in the future.

Further, TEM was used to study the morphology of the copolymer associates. TEM grids were prepared from solutions at different temperatures, followed by tempering for 24 h. Figure 7 shows the morphologies as observed by TEM.

At low temperature (25 °C) (Figure 7a), the polymer built small and spherical structures at high (7 wt %) concentrations. The diameter of these objects is below 30 nm, and a rather broad distribution in diameter is found. At this temperature, a core-shell micellar structure with the UCST-type block (poly(AAm-co-AN)) as core and a hydrophilic PEG as shell is quite possible. As explained before, the block copolymers were made by conventional radical polymerization and could lead to the formation of either AB or ABA block copolymers. This structural diversity may explain the polydispersity in size of the associated objects. An increase in temperature to 40 °C led to agglomeration (Figure 7b). These large agglomerates entail the change in turbidity from a bluish slightly turbid solution at 25 °C to a milky suspension at 40 °C as seen by the visual inspection (Figure 7d). On increasing temperature to 64 °C (Figure 7c, d), a clear solution was observed showing breakage of the aggregated polymeric network. Small spherical structures less than 100 nm in diameter were observed in TEM when the solution at 64 °C was allowed to dry on TEM grid at same temperature in an oven. This might be due to the self-assembly of the block copolymer during sample preparation although the solution visually and in turbidity measurement showed high transparency. The TEM images support the structural changes occurring in different temperature ranges as monitored by DLS and turbidity measurements. It is worth noting that the block copolymers in the present studies were

polydisperse but still could self-assemble and made stable temperature dependent micellar structures in a reproducible way. The unique thermoresponsive behavior gets support from the literature reference in which the polydispersity was intentionally introduced to make core-shell gyroid network mesostructure of a triblock terpolymer (PEG-(polystyrene-*b*-polyisoprene-polystyrene)) stable at a composition where it is not stable for the monodisperse analogue.¹⁷ It is worth mentioning that a simple blend of PEG and poly(AAm-co-AN; AN 18 mol %) shows only a UCST-type cloud point (50 °C for 7 wt % solution) reversible for many cycles without hysteresis similar to homo poly(AAm-co-AN) which shows a cloud point of 55 °C (Supporting Information Figure 5).

The block copolymers of PEG-*b*-poly(AAm-co-AN) showing multiphase transitions could be interesting for biomedical applications. In order to obtain an initial idea of its cytotoxicity toward mammalian cells and tissues, the standard MTT assay was performed and compared with poly(AAm-co-AN) used as reference. Therefore, the L929 cells were exposed to both polymers for 24 h. The addition of the polymers in the concentration range 0 to 14 mg/mL affects the cellular metabolic activity in a concentration-dependent manner (Figure 8). Under these conditions, the LD₅₀ values were 3.35 ± 0.09 mg/mL and 4.83 ± 0.24 mg/mL for cells treated with the poly(AAm-co-AN) and PEG-*b*-poly(AAm-co-AN), respectively. The block copolymer of PEG-*b*-poly(AAm-co-AN) have 1.5-fold higher LD₅₀ and is therefore less cytotoxic.

CONCLUSION

The successful synthesis of block copolymers of PEG and AAm-co-AN via conventional free-radical polymerization in a simple way using a PEG macro-azoinitiator was shown. The

introduction of a PEG block to random copolymers of AAm and AN (AAm-co-AN) led to a change in the thermoresponsive behavior from a single phase UCST-type transition of AAm-co-AN to a two-in-one (soluble-insoluble-soluble) LCST-UCST-type in water as shown by turbidity and light scattering studies. The phase transitions were dependent on the block lengths, ratio of AAm/AN, and the polymer concentration. The transitions were highly reproducible for many cycles with very small hysteresis. The unique two-in-one phase transition behavior was attributed to a temperature dependent change in the morphology from micelles to agglomerates and back to micelles. In the future, further experiments, like SANS, are necessary to get detailed information about the complex morphology change and the exact structures in the different temperature ranges. The low cytotoxicity and the double thermoresponsivity of the synthesized PEG-*b*-poly(AAm-co-AN) block copolymer makes it promising for applications for drug release.

■ ASSOCIATED CONTENT

● Supporting Information

The Supporting Information is available free of charge on the ACS Publications website at DOI: 10.1021/acs.langmuir.5b02006.

ATR-FTIR of synthesized PEG-*b*-poly(AAm-co-AN), GPC of PEG-*b*-poly(AAm-co-AN), DSC of a PEG-*b*-poly(AAm-co-AN), as well as turbidity measurements of 7 wt % solutions of PEG-*b*-poly(AAm-co-AN) by using different heating/cooling rates and of a poly(ethylene glycol)/poly(acrylamide-co-acrylonitrile) blend (PDF)

■ AUTHOR INFORMATION

Corresponding Author

*Telephone: +49-921-553397. Fax: +49-921-553393. E-mail: agarwal@uni-bayreuth.de.

Notes

The authors declare no competing financial interest.

■ ACKNOWLEDGMENTS

Thanks to Dr. Marina Krekhova, Department of Polymer Engineering at the University of Bayreuth, and Dr. Markus Drechsler, Department of Macromolecular Chemistry II, for the support in TEM measurement. We acknowledge the German Research Foundation (DFG) for financial support.

■ REFERENCES

- (1) Aseyev, V.; Tenhu, H.; Winnik, F. M. Non-ionic Thermoresponsive Polymers in Water. *Adv. Polym. Sci.* **2010**, *242*, 29–89.
- (2) Seuring, J.; Agarwal, S. Polymers with Upper Critical Solution Temperature in Aqueous Solution. *Macromol. Rapid Commun.* **2012**, *33*, 1898–1920.
- (3) Seuring, J.; Agarwal, S. Polymers with Upper Critical Solution Temperature in Aqueous Solution; Unexpected Properties from Known Building Blocks. *ACS Macro Lett.* **2013**, *2*, 597–600.
- (4) Lee, H.-N.; Rosen, B. M.; Penyvesi, G.; Sunkara, H. B. UCST and LCST Phase Behavior of Poly(trimethylene ether) Glycol in Water. *J. Polym. Sci., Part A: Polym. Chem.* **2012**, *50*, 4311–4315.
- (5) Kjellander, R.; Florin, E. Water Structure and Change in Thermal Stability of the System Poly(ethylene oxide)-Water. *J. Chem. Soc., Faraday Trans. 1* **1981**, *77*, 2053–2077.
- (6) Strandman, S.; Zhu, X. X. Thermo-responsive Block Copolymers with Multiple Phase Transition Temperatures in Aqueous Solutions. *Prog. Polym. Sci.* **2015**, *42*, 154–176.
- (7) Weiss, J.; Böttcher, C.; Laschewsky, A. Self-assembly of Double Thermoresponsive Block Copolymers end-capped with Complementary Trimethylsilyl Groups. *Soft Matter* **2011**, *7*, 483–492.
- (8) Kotsuchibashi, Y.; Kuboshima, Y.; Yamamoto, K.; Aoyagi, T. Synthesis and Characterization of Double Thermo-Responsive Block Copolymer Consisting *N*-isopropylacrylamide by Atom Transfer Radical Polymerization. *J. Polym. Sci., Part A: Polym. Chem.* **2008**, *46*, 6142–6150.
- (9) Jia, Y.-G.; Zhu, X. X. Complex Thermoresponsive Behavior of Diblock Polyacrylamides. *Polym. Chem.* **2014**, *5*, 4358–4364.
- (10) Han, X.; Zhang, X.; Yin, Q.; Hu, J.; Liu, H.; Hu, Y. Thermoresponsive Diblock Copolymer with Tunable Soluble-Insoluble and Soluble-Insoluble-Soluble Transitions. *Macromol. Rapid Commun.* **2013**, *34*, 574–580.
- (11) Hua, F.; Jiang, X.; Zhao, B. Temperature-Induced Self-Association of Doubly Thermosensitive Diblock Copolymers with Pendant Methoxytris (oxyethylene) Groups in Dilute Aqueous Solutions. *Macromolecules* **2006**, *39*, 3476–3479.
- (12) Trinh, L. T. T.; Lambermont-Thijs, H. M. L.; Schubert, U. S.; Hoogenboom, R.; Kjøniksen, A.-L. Thermoresponsive Poly(2-oxazoline) Block Copolymers Exhibiting Two Cloud Points: Complex Multistep Assembly Behavior. *Macromolecules* **2012**, *45*, 4337–4345.
- (13) Maeda, Y.; Mochiduki, H.; Ikeda, I. Hydration Changes during Thermosensitive Association of a Block Copolymer Consisting of LCST and UCST Blocks. *Macromol. Rapid Commun.* **2004**, *25*, 1330–1334.
- (14) Tian, H.-Y.; Yan, J.-J.; Wang, D.; Gu, C.; You, Y.-Z.; Chen, X.-S. Synthesis of Thermo-Responsive Polymers With Both Tunable UCST and LCST. *Macromol. Rapid Commun.* **2011**, *32*, 660–664.
- (15) Seuring, J.; Agarwal, S. First Example of a Universal and Cost-Effective Approach: Polymers with Tunable Upper Critical Solution Temperature in Water and Electrolyte Solution. *Macromolecules* **2012**, *45*, 3910–3918.
- (16) Zhang, H.; Tong, X.; Zhao, Y. Diverse Thermoresponsive Behaviors of Uncharged UCST Block Copolymer Micelles in Physiological Medium. *Langmuir* **2014**, *30*, 11433–11441.
- (17) Meuler, A. J.; Ellison, C. J.; Hillmyer, M. A.; Bates, F. S. Polydispersity-Induced Stabilization of the Core-Shell Gyroid. *Macromolecules* **2008**, *41*, 6272–6275.

LCST and UCST in one: Double thermoresponsive behavior of block copolymers of poly(ethylene glycol) and poly(acrylamide-*co*-acrylonitrile)

*Florian Käfer,[†] Fangyao Liu,[†] Ullrich Stahlschmidt,^{†††} Valérie Jérôme,^{†††} Ruth Freitag,^{†††}
Matthias Karg,^{††} and Seema Agarwal^{†*}*

[†] : University of Bayreuth, Macromolecular Chemistry II and Center for Colloids and Interfaces, Universitätsstraße 30, 95440 Bayreuth, Germany

^{††} : University of Bayreuth, Physical Chemistry I, Universitätsstraße 30, 95440 Bayreuth, Germany

^{†††} : University of Bayreuth, Chair for Process Biotechnology, Universitätsstraße 30, 95440 Bayreuth, Germany

Supporting Information

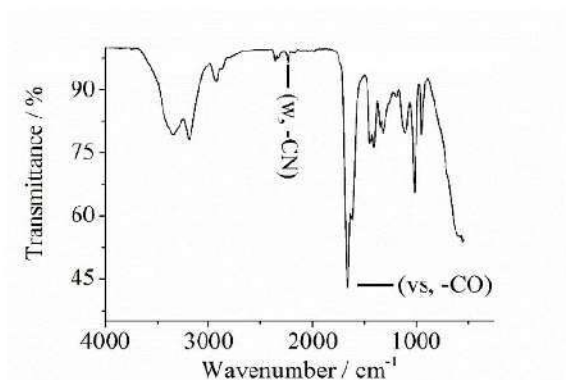


Figure 1. ATR-FTIR Spectrum of a PEG-*b*-poly(AAm-*co*-AN) copolymer with a molar ratio (AAm: AN) of 91:9 (entry 1, table 1). Determined by integrating the characteristic absorptions bands in the FTIR spectrum at 2242 cm^{-1} (-CN) and 1659 cm^{-1} (-C=O).

For calculation of the molar ratio a calibration function was employed as described previously.¹

Gel permeation chromatography

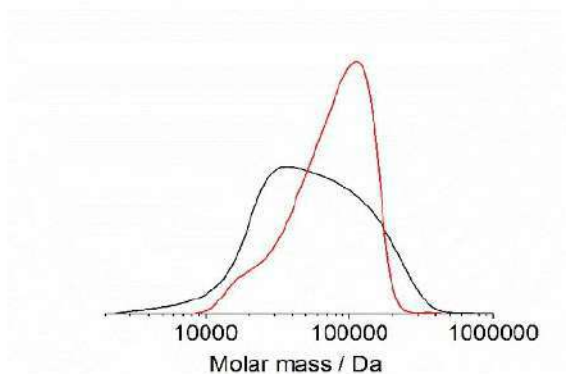


Figure 2. Molar mass distribution from DMSO GPC of PEG-*b*-poly(AAm-*co*-AN) copolymers, **black**: (entry 1, table 1, PEG unit = 2000 g/mol) with a molar ratio (AAm: AN) of 91:9; **red**: (entry 5, table 1, PEG unit = 6000 g/mol) with a molar ratio (AAm: AN) of 89:11.

Differential scanning calorimetry

The Differential scanning (DSC) measurements were performed on a Mettler Toledo 821 DSC system. The system was calibrated with indium and zinc standards. All measurements were performed under nitrogen atmosphere with a heating /cooling rate of 10 $^{\circ}\text{C}/\text{min}$.

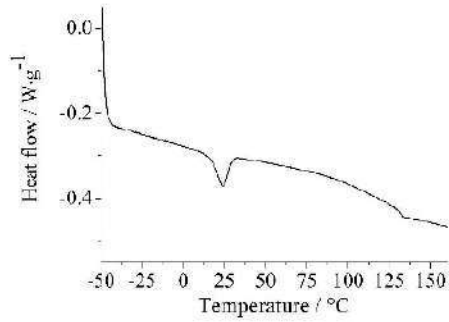


Figure 3. DSC curve of PEG-*b*-poly(AAm-*co*-AN) (entry 1, table 1) with melting point at 24 °C of the PEG block and a glass transition point at 130 °C of the poly(AAm-*co*-AN) block.

Turbidity measurements

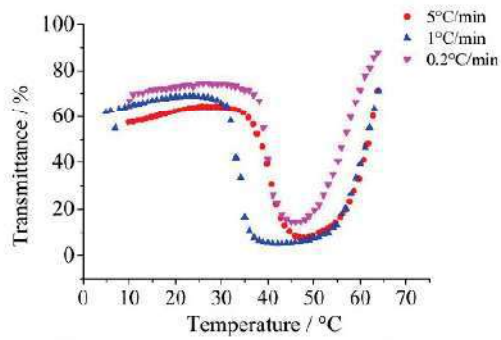


Figure 4. Cooling curves of PEG-*b*-poly(AAm-*co*-AN), (entry 1, table 1), concentration 7wt. % in pure water, ($M_n = 37,000$ g/mol, PDI = 2.2), with different heating rates.

Turbidity measurement of a poly(ethylene glycol) / poly(acrylamide-*co*-acrylonitrile) blend.

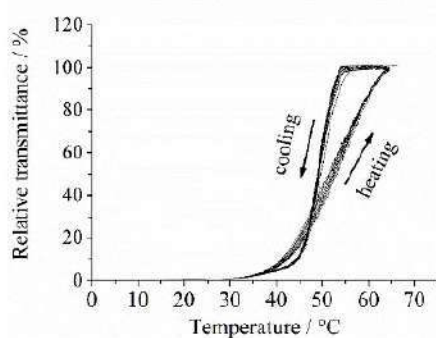


Figure 5. Hysteresis curves in turbidity measurement of a poly(ethylene glycol) ($M_n = 2,000$ g/mol), poly(acrylamide-*co*-acrylonitrile) ($M_n = 21,000$ g/mol) blend, ratio 2:1 (a:n).

References

1. Seuring, J.; Agarwal, S. First Example of a Universal and Cost-Effective Approach: Polymers with Tunable Upper Critical Solution Temperature in Water and Electrolyte Solution. *Macromolecules* **2012**, *45*, 3910-3918.

7.2 Tunable, Concentration-Independent, Sharp, Hysteresis-Free UCST
Phase Transition from Poly(*N*-Acryloyl Glycinamide-Acrylonitrile)
System

This work was published by **F. Käfer**, A. Lerch, S. Agarwal, *Journal of Polymer Science Part A: Polymer Chemistry* **2017**, *55* (2), 274-279.

Reprinted with permission; Copyright 2016 Wiley Periodicals, Inc.

Tunable, Concentration-Independent, Sharp, Hysteresis-Free UCST Phase Transition from Poly(*N*-Acryloyl Glycinamide-Acrylonitrile) System

Florian Käfer,¹ Arne Lerch,² Seema Agarwal¹

¹Macromolecular Chemistry II, University of Bayreuth, Bayreuth 95440, Germany

²Physical Chemistry I, University of Bayreuth, Bayreuth 95440, Germany

Correspondence to: S. Agarwal (E-mail: agarwal@uni-bayreuth.de)

Received 3 August 2016; accepted 12 September 2016; published online 5 October 2016

DOI: 10.1002/pola.28374

ABSTRACT: Poly(*N*-acryloylglycinamide-co-acrylonitrile) (poly(NAGA-AN)) copolymers were synthesized using reversible-addition-fragmentation transfer polymerization. In contrast to poly(NAGA) the thermoresponsive behavior of poly(NAGA-AN) shows a narrow cooling/heating hysteresis in water with a tunable cloud point, depending on the acrylonitrile amount in polymer. Furthermore, we showed that there is no significant effect of the solution concentration on the cloud point and stable phase transition behavior in electrolyte solutions, which is presumable controlled by forming stable micellar

like structures as a result of the block/graft-copolymer structure. This is in contrast to poly(NAGA) which shows a strong concentration dependent cloud point in aqueous solution with a broad cooling/heating hysteresis. © 2016 Wiley Periodicals, Inc. *J. Polym. Sci., Part A: Polym. Chem.* 2017, 55, 274–279

KEYWORDS: *N*-acryloyl glycinamide-acrylonitrile; micelle formation; RAFT polymerization; thermoresponsive polymers; UCST

INTRODUCTION Almost every compound is sensitive to the change in one or more of the external stimuli, such as light, pH, temperature, electric and magnetic fields, and chemicals, and shows a gradual change in properties. However, some compounds show a very significant and sudden change in the physical properties with a minor change in the stimuli, called stimuli responsive materials.^{1–3} Thermoresponsive polymers are one of the materials that change their properties with temperature.^{4–8} There are two types of phase separations from solution at a particular concentration due to the conformation change above and below a critical temperature and the corresponding polymers are called polymers of lower critical solution temperature (LCST) and upper critical solution temperature (UCST) types. Such behavior in water is of importance for drug release, targeted drug delivery, bio separation, smart implants, micro actuators, and so forth.^{9–12} A lot of polymers of LCST type are known and well studied.^{13,14} In contrast, studies related to the polymers showing UCST type transitions in water are quite limited but increasing in the last years. Although, some of the zwitterionic polymers and polyelectrolytes show UCST-type transitions in water, they are dominated by Coulomb interactions and the thermoresponsive behavior is highly dependent upon the molar mass, presence of salts, ionic strength and multivalent

ions.^{15–18} In the last few years more and more attention has been given to the nonionic polymers with phase transitions dominated by hydrogen (H)-bonding.^{19,20} Acrylamide and acrylonitrile random copolymers (poly(AAm-co-AN)) have emerged out as one of the promising systems with sharp and reversible phase transitions of UCST type and tunable cloud points (temperature at which phase separation occurs depending on polymer concentration) Acrylamide, small hysteresis, and tolerance toward electrolytes.^{4,19–23} Moreover, cross-linked poly(AAm-co-AN) could provide thermophilic hydrogels.²⁴ All these properties provide the poly(AAm-co-AN) system at present a place in the category of UCST-type polymers which is occupied by poly(*N*-isopropylacrylamide) (poly(NIPAM)) for polymers with LCST-type transitions. Both poly(NIPAM) and poly(AAm-co-AN) show non-significant changes in cloud points with concentration for very dilute solutions (0.01–1 wt%), but cloud point increases for poly(AAm-co-AN) and decreases for poly(NIPAM) with an increase in concentration.^{13,19} Poly(*N*-acryloylglycinamide) (poly(NAGA)) is another interesting nonionic polymer showing phase transition of UCST type due to thermally controlled reversible H-bonding interactions.^{25–28} The limitation of this system is the broad phase transition with hysteresis of more than 10 °C. Also, phase transition temperatures are strongly

Additional Supporting Information may be found in the online version of this article.

© 2016 Wiley Periodicals, Inc.

TABLE 1 Cloud Points and Composition of the Synthesized Copolymers of NAGA and AN Using CMDT as Chain Transfer Agent and AIBN as Initiator

| Entry | AN in Polymer (mol%) ^a | AN in Feed (mol%) | UCST (°C) ^{b,c} | UCST (°C) ^{b,d} | UCST (°C) in PBS ^{b,e} |
|-------|-----------------------------------|-------------------|--------------------------|--------------------------|---------------------------------|
| 1 | 32 | 35 | 45 | 45 | 43 |
| 2 | 30 | 33 | 39 | 40 | 41 |
| 3 | 27 | 30 | 24 | 24 | 23.5 |
| 4 | 22 | 25 | <5 | <5 | <5 |
| 5 | 43 | 45 | Insol. | Insol. | Insol. |

Monomer:CTA:initiator ratio (200:1:0.3).

^a Compositions were determined by ATR-FTIR using a calibration function.^b Cloud points determined for 1 wt% solutions in pure water with a heating rate 1.0 °C/min.^c Cooling.^d Heating.

influenced by concentration. For example, the cloud point changes from 7.6 to 25.4 °C on changing concentration from 0.25 to 5.4 wt%. At higher concentrations (more than 5–6 wt%), poly(NAGA) forms a physical gel in water.²⁷ Attempts were made to tune the properties of poly(NAGA) by copolymerization with *N*-acetylacrylamide (NAAAm). The cloud point of poly(NAGA) was further decreased below 12 °C (on cooling) depending upon the amount of NAAAm and disappeared on incorporation of more than 0.355 molar fraction of it. Moreover, the transitions were very broad with large hysteresis similar to that of the homopolymer poly(NAGA).²⁸ The copolymerization of NAGA with hydrophobic monomer, butyl acrylate (BA) provided complex effect on phase separation behavior with significant hysteresis, that is, cloud point decreased till about 10 mol% of BA and thereafter increased with the amount of BA. Unfortunately, the phase transition behavior was not reproducible and led to significant change in cloud point with each new cycle.¹⁹ In the present work, we provide a new polymer system showing highly reproducible, stable and sharp phase transitions for many cycles without any significant hysteresis based on NAGA and AN copolymer. Otherwise, the homopolymer of poly(NAGA) shows cloud points of 17 and 29 °C during heating and cooling, respectively, with a hysteresis of approximately 12 °C.²⁷ The cloud points can be tuned by changing the ratio of the two comonomers without sacrificing the reproducibility and sharpness. Interestingly, the system showed no significant effect of polymer concentration on cloud point for a very broad range (tested range: 0.1–10 wt%) making it different from other UCST-type nonionic polymers.

EXPERIMENTAL**Materials****Chemical Reagents**

S-Cyanomethyl-*S*-dodecyltrithiocarbonat (98%, HPLC) and dimethyl sulfoxide (DMSO) (≥99.9%, ACS reagent) were purchased from Sigma-Aldrich. 2-Propenenitrile (99+ %; Acros Organics) was purified by distillation. *N*-acryloyl glycinamide ($T_m = 141$ °C) was synthesized according to a published procedure.²⁷ 2,2'-Azobisisobutyronitrile (AIBN, Fluka) was recrystallized

from ethanol. Milli-Q Plus system (conductivity = 0.072 μS/cm) was used for getting pure water. Toluene (HPLC grade, >99.9%) for GC measurements was purchased from VWR Chemicals.

Synthetic Procedure

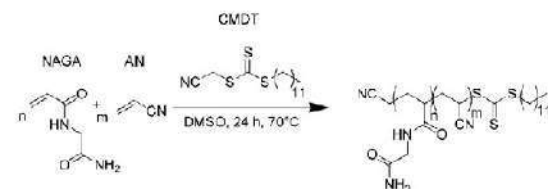
All polymerizations were carried out under argon. *N*-acryloyl glycinamide (NAGA) and acrylonitrile (AN) (in total 200 eq) and *S*-cyanomethyl-*S*-dodecyltrithiocarbonat (CMDT) (1 eq) were dissolved in 10 mL DMSO (feed ratio NAGA:AN, 65:35) in a Schlenk flask followed by degassing (three freeze-pump-thaw cycles). A AIBN/DMSO solution (0.3 eq of AIBN) was added. The reaction was carried out in an oil bath, preheated to 70 °C. The polymers were precipitated from methanol (tenfold volume). After polymerization, the polymers were centrifuged (7000 rpm, 10 minutes), washed few times with methanol and dried in a vacuum oven at 70 °C for 24 hours.

¹H NMR (300 MHz, DMSO-*d*₆) δ/ppm: 1.22–2.18 (polymer backbone, -CH₂-), 2.1–2.9 (polymer backbone, -CH-), 3.5 (-NH-CH₂-CONH₂); 6.9–9.2 (-NH₂); ATR-FTIR: ν = 3650–3050 (mb, NH), 3000–2850 (w, CH₂), 2242 (w, -CN), 1659 (vs, CO), 1413 (m, -CH-), 1348 (m, -CH-), 1312 (m, -CH-) 1118 (w, C-N) cm⁻¹.

Instrumentation and Analysis

Nuclear magnetic resonance (NMR) spectroscopy: Bruker Ultrashield 300 machine (300 MHz) was used for measuring ¹H NMR spectra.

Fourier-transform infrared spectroscopy (FT-IR): Spectra were recorded using a FTIR spectrometer (Digilab, Excalibur Series) with an attenuated total reflectance (ATR) unit.

**SCHEME 1** Copolymerization of NAGA and AN by using CMDT as chain transfer agent and AIBN as initiator.

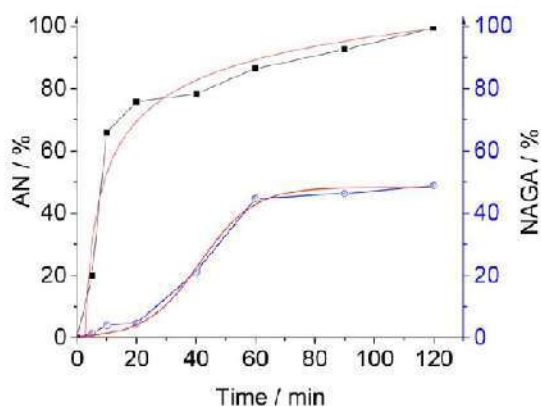


FIGURE 1 Influence of the reaction time on amount of NAGA (circles) and AN (squares) in copolymer (entry 2, Table 1). [Color figure can be viewed at wileyonlinelibrary.com]

To record the spectra the software WinIRPro (Digilab, version 3.3.1.014) was used. In order to evaluate the spectra, Origin 8.5 (OriginLab) was used.

Differential scanning calorimetry (DSC): Mettler Toledo 821 DSC system was used for DSC measurements under nitrogen atmosphere with a heating/cooling rate of 10 °C/min. A total of 6–8 mg of samples were used for measurements. The results were analyzed from the second heating cycle.

JASCO V-630 Spectrophotometer was used for the turbidity measurements at 660 nm with continuous stirring at a heating rate of 1.0 °C/min. The cell path length was 10 mm. The cloud points were determined at the point of inflection of % transmittance versus temperature curves. For measurements, first appropriate amounts of samples were dissolved in

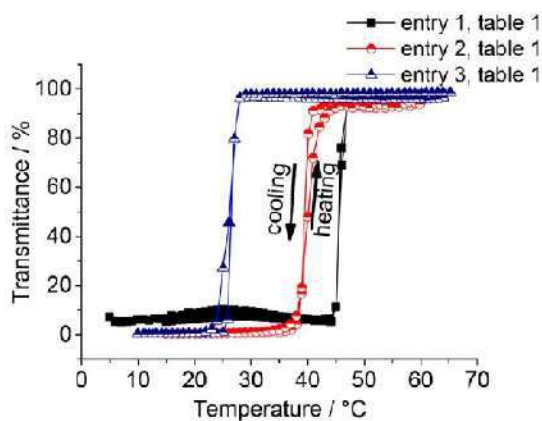


FIGURE 2 % transmittance versus temperature hysteresis curves for 1 wt% poly(NAGA-AN) in pure water. [Color figure can be viewed at wileyonlinelibrary.com]

Millipore-water/phosphate buffer by heating at 60 °C and measurement was started from cooling cycle.

GC measurements were performed on a SHIMADZU GC-2010 Plus. As stationary phase a column from Zebron ZB 5MS; $L = 30 \text{ m} \times L_d = 0.25 \text{ mm} \times df = 0.25 \text{ }\mu\text{m}$ was used.

Molar mass and the molar mass distribution were determined by gel permeation chromatography with dimethyl sulfoxide as eluent. A precolumn (SS PolarSil PSA080505; particle size 5 μm , dimension 8.0 mm \times 50 mm) and two PSS PolarSil linear S (particle size 5 μm , dimension 8.0 mm \times 300 mm) columns were used. Pullulan of different molar masses with narrow dispersities were used as standards. The flow rate was 0.7 mL/min at a temperature of 75 °C. As detector a differential refractive index detector was used. The software PSS WinGPC Unity, Build 1321, was used.

The morphologies were investigated by elastic bright-field transmission electron microscopy (TEM) and (cryo)TEM

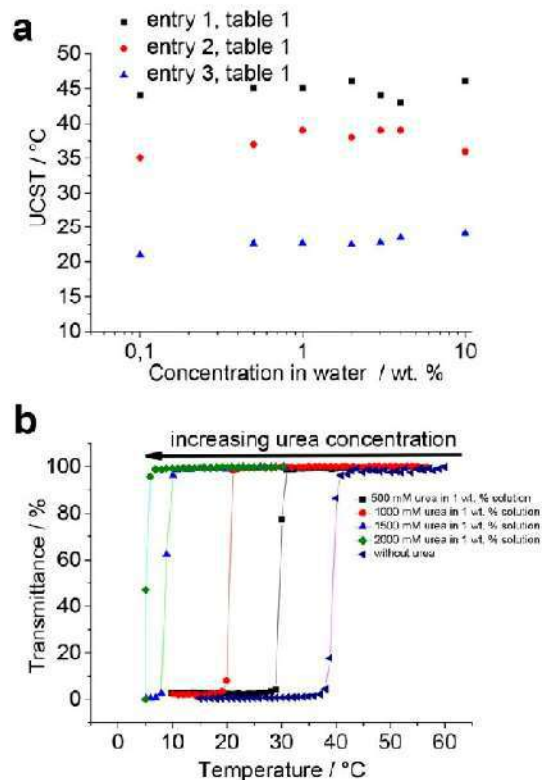


FIGURE 3 (a) Cloud point (cooling) of the synthesized poly(NAGA-AN) copolymers as a function of concentration in pure water. Heating rate 1 °C/min. (b) Cooling curves of poly(NAGA-AN) of (entry 2, Table 1) with a polymer concentration of 1% wt in aqueous solution with increasing amount (500–2000 mM) of urea. Heating rate 1 °C/min. [Color figure can be viewed at wileyonlinelibrary.com]

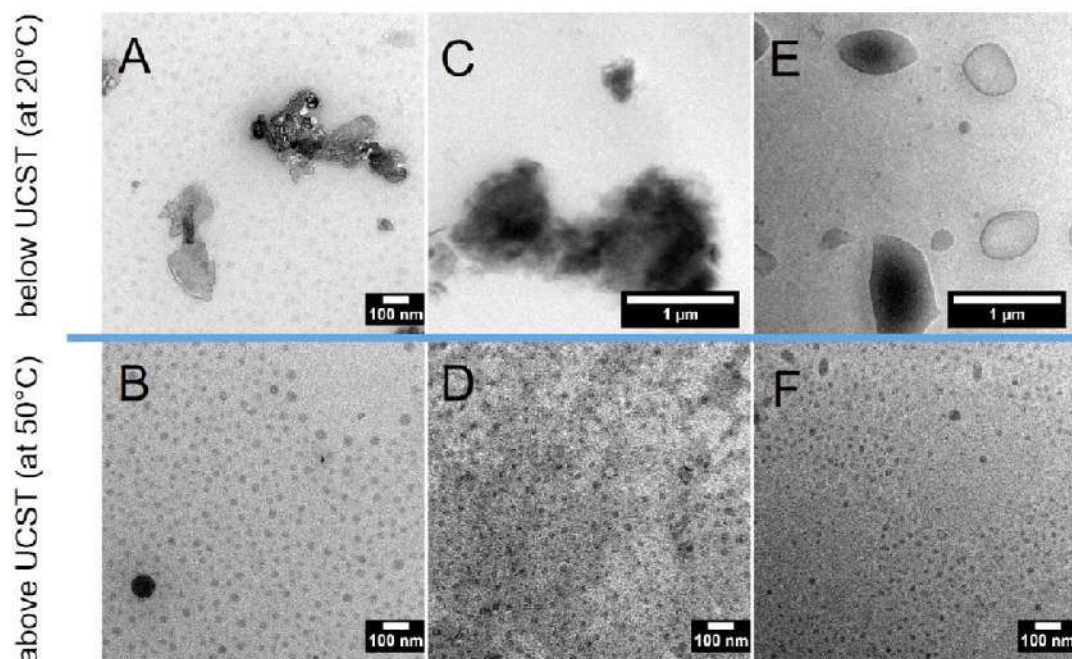


FIGURE 4 TEM images of poly(NAGA-AN) (A/B) (entry 1, Table 1), (C/D) (entry 2, Table 1), (E/F) (entry 3, Table 1) from a solution of concentration 1 wt% at temperature above (bottom row, at 50 °C) and below (top row, at 20 °C) of the UCST (determined by turbidity measurements). [Color figure can be viewed at wileyonlinelibrary.com]

using a ZEISS 922 Omega EFTEM (Zeiss NTS GmbH, Oberkochen, Germany) electron microscope operated at an acceleration voltage of 200 kV. Zero-loss filtered images were recorded with a CCD camera system (Ultrascan 1000, Gatan) and processed, using a digital imaging processing system (Gatan Digital Micrograph 3.9 for GMS 1.4. cryoTEM samples were vitrified at 20 and 50 °C in liquid ethane.

Dynamic light scattering (DLS) measurements of the copolymers (entries 1–3, Table 1) were performed on a 3D spectrometer from LS Instruments AG (Fribourg, Switzerland) operated in 3D modulated cross-correlation. A HeNe laser (maximum 35 mW constant power output at $\lambda = 632.8$ nm) was used as light source. Samples were prepared by dissolving the copolymers in MilliQ water in glass tubes at elevated temperature (60 °C) with concentrations of 0.1 wt%. After complete dissolution, all samples were filtered with PTFE filters of 5 μm pore size directly into dust-free cylindrical quartz cuvettes (diameter 10 mm). The scattered light was detected by two APD detectors. Three intensity-time autocorrelation functions were measured at a scattering angle of 90° with an acquisition time of 60 seconds. Temperature-dependent measurements below UCST and above UCST were performed at 20 and 50 °C, respectively. The sample temperature was adjusted by a heat controlled decalin bath with a stability of ± 100 mK. The temperature was monitored by a PT100 thermoelement, placed close to the sample position

in the decalin bath. The recorded data were analyzed by inverse Laplace transformation (ILT) with the AfterALV software (v.1.0d) by Dullware.

RESULTS AND DISCUSSION

In the present work, RAFT polymerization was used as a tool to make new copolymers of NAGA with AN (Scheme 1) in order to tailor cloud-points with almost no hysteresis. Different copolymers with varied ratio of the two comonomer units were made by changing their amount in the feed using CMDT as chain transfer agent and AIBN as radical initiator.

^1H NMR (Fig. S1) was not useful in determining copolymer composition due to overlapping peaks. Therefore, the copolymer composition was determined by ATR-FTIR (Figs. S2 and S3) and is shown in Table 1. This is an established method for copolymer composition determination.²⁷

The polymers had molar masses of 11,000–18,000 g/mol and molar mass dispersity of ~ 1.3 as determined from GPC measurements using Pullulan standards. All GPC curves were unimodal (Fig. S4 and Table S1). The polymers showed two glass transition temperatures as measured by DSC (Fig. S5 and Table S2). The first and second glass transition temperatures increased with the increase in the amounts of AN and NAGA, respectively, in the copolymers. The presence of two glass transition temperatures ruled out the formation of

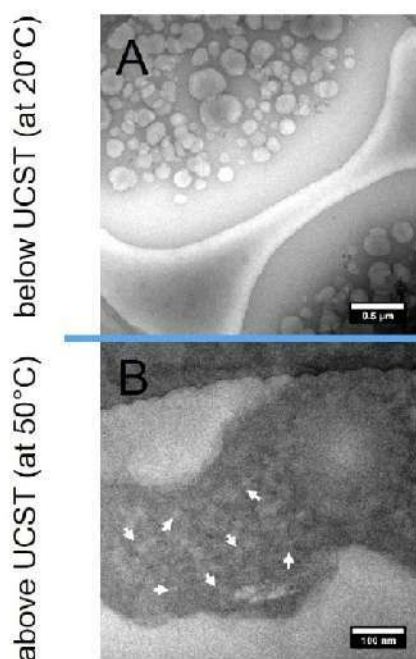


FIGURE 5 cryoTEM images of poly(NAGA-AN) (A/B) (entry 1, Table 1) (from a solution of concentration 0.1 wt% at temperature below (A at 20 °C) and above (B at 50 °C) the UCST (determined by turbidity measurements). [Color figure can be viewed at wileyonlinelibrary.com]

statistical copolymers. To follow the microstructure of the polymer, the copolymerization reaction was followed at different intervals of time. The reaction was stopped and the amount of unreacted AN was followed by GC (Figs. S6 and S7 and Table S3). Knowing the amount of unreacted AN by GC and the total yield of the reaction from gravimetric, the amount of unreacted NAGA could be calculated (Fig. 1).

Interestingly, a vast reactivity difference between NAGA and AN was observed. In the beginning till about 17% conversion, mainly AN was polymerized with very small amounts of NAGA, that is, after about 20 minutes of polymerization, around 80 wt% of AN was already consumed whereas less than 4 wt% NAGA was polymerized. This clearly rules out the formation of random copolymers. Since the monomer feed composition strongly changes with conversion, the reactivity ratios will depend upon the conversion and therefore, would not be meaningful in commenting about the copolymer structure.²⁹ The huge reactivity difference between AN and NAGA hint about the formation of block/gradient-type copolymers or a grafted copolymer structure with PAN backbone with grafts of NAGA. In RAFT polymerization the termination reactions are reduced, but not avoided completely, therefore both AB and ABA types of block structures are possible. The graft structure is possible by transfer reactions generating radicals on PAN backbone followed by NAGA polymerization. The

formation of block copolymers as well as a grafted copolymer structure by simultaneous polymerization of two comonomers in one-pot is rare, but already known in the literature for other comonomer systems.^{29,30} The formation of a blend of two homopolymers during polymerization or presence of homo PAN in copolymers is ruled out based on the combination of following facts: (a) monomodal GPC curves and (b) PAN homopolymer is not soluble in water at any temperature, whereas the polymer showed thermoresponsive behavior (described below) without traces of any insoluble part in the solution above cloud point.

The thermoresponsive behavior of the resulting polymers was tested by measuring % transmittance vs. temperature for 1 wt% polymer solutions in water. Sharp phase transitions were observed with cloud points depending upon the copolymer composition. The cloud points varied between <5 °C and about 40 °C depending upon the copolymer composition without any hysteresis between cooling and heating cycles (Fig. 2).

Additional experiments were done by adding intentionally definite amounts of homo-poly(NAGA) in a solution of copolymers in water and studied effect on thermoresponsive behavior. This experiment was done to have indirect check about the possibility of presence of some homo-poly(NAGA) in the copolymers and the effect on thermoresponsivity, if any. The presence of homo-poly(NAGA) till about 6 mol% had no significant effect on thermoresponsive behavior in terms of sharpness and hysteresis but large amounts lowered down the cloud points with broad transitions and hysteresis. Since thermal transitions observed for polymers were sharp, without hysteresis, rules out the presence of large amounts of homo-poly(NAGA) in the polymer samples prepared in this work (Figs. S8 and S9).

The cloud points were not affected by measurements in PBS buffer and showed almost similar cloud points as in water (Fig. S10). Thermoresponsive behavior was studied at different concentrations and interestingly showed a highly stable system with no significant change in the cloud points [Fig. 3(a)] for a very broad range of concentrations (0.1–10 wt%).

This is in contrast to most of the other thermoresponsive polymers based on thermoreversible H-bonding.¹⁸ Also, the present poly(NAGA-AN) copolymer system tolerated a huge amount of H-breaking agent (urea; 2 M) without complete disappearance of the UCST-type phase transition [Fig. 3(b)]. In a previous work, the use of 0.5 M H-bond disruptor was sufficient for disappearance of UCST-phase transition of a copolymer of NAGA and *N*-acetylacrylamide.²⁰ TEM measurements of the samples above the cloud points (at 50 °C) showed spherical particles of size between 10 and 60 nm, which agglomerate on cooling below the cloud points. Above cloud point, poly(NAGA) block is hydrophilic and PAN block hydrophobic leading to self-assembled micellar-like structures which agglomerate below cloud point due to change in hydrophilicity of the poly(NAGA) block (Fig. 4). The self-assembly of the poly(NAGA-AN) copolymers to micellar structures above a critical temperature appears to be

responsible for thermoresponsivity with sharp transitions. Moreover, the polymers in the present work are made by RAFT showing low (1.2–1.3) molar mass dispersity and expected to have compositional homogeneity leading to sharp transitions.³¹

The cryoTEM images (Fig. 5) of entry 1, vitrified at 20 and 50 °C (solution concentration 0.1 wt%) shows a similar morphology as seen by the TEM image (Fig. 4). At 20 °C, large agglomerates with sizes between 100 and 500 nm were observed. In addition to cryoTEM, we analyzed entries 1–3 at 20 °C in dispersion using DLS. The samples show monomodal, narrow size distributions and average radii between 100 and 400 nm (Fig. S11). Hence, the impression from cryoTEM is well-supported by DLS measurements in dispersion. At 50 °C, structures below 100 nm were observed in cryoTEM, which was dedicated to the formation of micellar-like structures. At this temperature, DLS results for entries 1–3 were found to be rather complex with many different contributions obtained by CONTIN analysis. Hence, a clear estimation of an object size by DLS is not easily possible pointing probably towards the presence of larger aggregates or network-like structures in addition to micellar structures. We want to note that, due to the intensity-weighting of the DLS data, the network structures may be present in minority only.

CONCLUSIONS

The RAFT copolymerization of NAGA and AN provided block-type/graft structure with AN preferably polymerized in the beginning. The structure was underpinned by DSC, showing two glass transition points and a reaction kinetic study, in which the time dependent amount of reacted acrylonitrile was followed by GC measurements. Turbidity measurements of the resulting polymers show a narrow hysteresis in water which can be tuned from <5 up to 40 °C. The thermoresponsive behavior was not disturbed in PBS buffer and showed similar cloud points as that in Millipore water. The cloud points were independent from the concentration in a wide range. This is in contrast to phase transition behavior of poly(NAGA), which shows a broad cooling/heating hysteresis in water with a significant effect of the concentration of the aqueous solution. The formation and aggregation of micellar structures above and below critical temperatures stabilized by H-bonding might be responsible for thermoresponsive behavior as the system tolerated unusually high concentrations of hydrogen bonding disturbing reactants like urea. The presence of spherical particles above critical temperature was evident from TEM and cryoTEM.

ACKNOWLEDGMENTS

We thank Deutsche Forschungsgemeinschaft for financial support. The authors acknowledge Matthias Karg (Heinrich-Heine-University Düsseldorf, Germany) for assistance with the DLS measurements and interpretation.

REFERENCES

- 1 P. Theato, S. B. Sumerlin, R. K. O'Reilly, T. H. Epps, *Chem. Soc. Rev.* **2013**, *42*, 7055–7056.
- 2 H. P. James, R. John, A. Alex, A. Sharma, *Acta Pharm. Sin. B* **2014**, *4*, 120–127.
- 3 M. A. Cohen Stuart, W. T. S. Huck, J. Genzer, M. Müller, C. Ober, M. Stamm, G. B. Sukhorukov, I. Szleifer, V. V. Tsukruk, M. Urban, F. Winnik, S. Zauscher, I. Iuzinov, S. Mink, *Nat. Mater.* **2010**, *9*, 101–113.
- 4 J. Seuring, S. Agarwal, *Macromol. Rapid Commun.* **2012**, *33*, 1898–1920.
- 5 J. Seuring, S. Agarwal, *ACS Macro Lett.* **2013**, *2*, 597–600.
- 6 M. A. Ward, T. K. Georgiou, *Polymers.* **2011**, *3*, 1215–1242.
- 7 V. Bütün, S. Liu, J. V. M. Weaver, X. Bories-Azeau, Y. Cai, S. P. Armes, *React. Funct. Polym.* **2006**, *66*, 157–165.
- 8 P. J. Roth, *Macromol. Chem. Phys.* **2014**, *215*, 825–838.
- 9 C. de las Heras Alarcón, S. Pennadam, C. Alexander, *Chem. Soc. Rev.* **2005**, *34*, 276–285.
- 10 H. P. James, R. John, A. Alex, K. R. Anoop, *Acta Pharm. Sin. B* **2014**, *4*, 120–127.
- 11 P. Bawa, V. Pillay, Y. E. Choonara, L. C. du Toit, *Biomed. Mater.* **2009**, *4*, 022001 (15 pp).
- 12 L. Liu, S. Jiang, Y. Sun, S. Agarwal, *Adv. Funct. Mater.* **2016**, *26*, 1021–1027.
- 13 S. Fujishige, K. Kubota, I. Ando, *Phys. Chem.* **1989**, *93*, 3311–3313.
- 14 V. Aseyev, H. Tenhu, F. M. Winnik, *Adv. Polym. Sci.* **2011**, *242*, 29–89.
- 15 T. Maji, S. Banerjee, Y. Biswas, T. K. Mandal, *Macromolecules* **2015**, *48*, 4957–4966.
- 16 M. Noh, S. Kang, Y. Mok, S. J. Choi, J. Park, J. Kingma, J. H. Seob, Y. Lee, *Chem. Commun.* **2016**, *52*, 509–512.
- 17 Y. Kohno, S. Saita, Y. Men, J. Yuan, H. Ohno, *Polym. Chem.* **2015**, *6*, 2163–2178.
- 18 N. Morimoto, K. Muramatsu, T. Wazawa, Y. Inoue, M. Suzuki, *Macromol. Rapid Commun.* **2014**, *35*, 103–108.
- 19 J. Seuring, S. Agarwal, *Macromolecules* **2012**, *45*, 3910–3918.
- 20 L. Mäkinen, D. Varadharajan, H. Tenhu, S. Hietala, *Macromolecules* **2016**, *49*, 986–993.
- 21 B. A. Pineda-Contreras, H. Schmalz, S. Agarwal, *Polym. Chem.* **2016**, *7*, 1979–1986.
- 22 L. Hou, P. Wu, *Soft Matter* **2015**, *11*, 7059–7065.
- 23 F. Käfer, F. Liu, U. Stahlschmidt, V. Jérôme, R. Freitag, M. Karg, S. Agarwal, *Langmuir* **2015**, *31*, 8940–8946.
- 24 F. Liu, S. Jiang, L. Ionov, S. Agarwal, *Polym. Chem.* **2015**, *6*, 2769–2776.
- 25 F. Liu, J. Seuring, S. Agarwal, *Macromol. Chem. Phys.* **2014**, *215*, 1466–1472.
- 26 F. Liu, S. Agarwal, *Macromol. Chem. Phys.* **2015**, *216*, 460–465.
- 27 J. Seuring, M. F. Bayer, K. Huber, S. Agarwal, *Macromolecules* **2012**, *45*, 374–384.
- 28 J. Seuring, S. Agarwal, *Macromol. Chem. Phys.* **2010**, *211*, 2109–2117.
- 29 P. B. Zetterlund, M. Takemura, A. F. Johnson, *Macromolecules* **2005**, *38*, 2173–2179.
- 30 Y. Shi, Z. Zheng, S. Agarwal, *Chem. Eur. J.* **2014**, *20*, 7419–7428.
- 31 B. A. Pineda Contreras, F. Liu, S. Agarwal, *J. Polym. Sci. A: Polym. Chem.* **2014**, *52*, 1878–1884.

Supporting Information

Tunable, concentration independent, sharp, hysteresis free UCST phase transition from poly(*N*-acryloyl glycinamide-acrylonitrile) system

Florian Käfer,¹ Arne Lerch,² Seema Agarwal^{1*}

¹Department of Macromolecular Chemistry II, University of Bayreuth, 95440 Bayreuth, Germany

²Department of Physical Chemistry I, University of Bayreuth, 95440 Bayreuth, Germany

*Correspondence to: Seema Agarwal (E-mail: agarwal@uni-bayreuth.de)

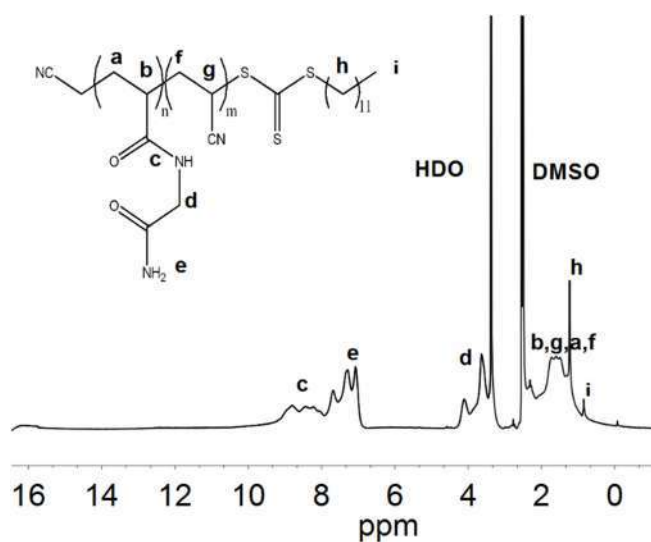


FIGURE S1 ^1H NMR spectrum of the poly(NAGA-AN) copolymer (entry 1, table 1; $M_n = 16\ 000\ \text{g/mol}$; $D = 1.3$). The sample was dissolved in DMSO-d_6 and measurement was done at $25\ ^\circ\text{C}$.

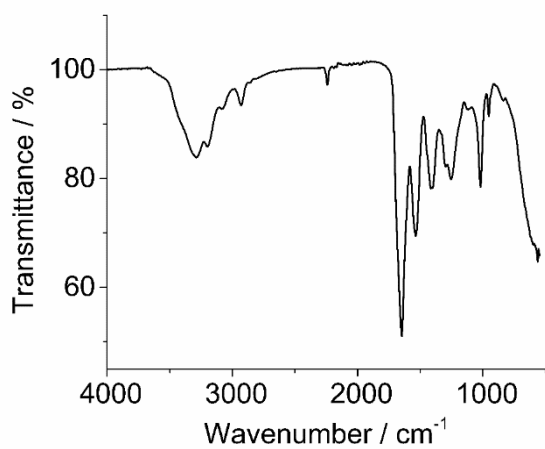


FIGURE S2 ATR-FTIR spectra of (entry 1, table 1) with the $-\text{CN}$ band at $2242\ \text{cm}^{-1}$ and the $-\text{C}(\text{O})-$ band at the wavenumber of $1658\ \text{cm}^{-1}$.

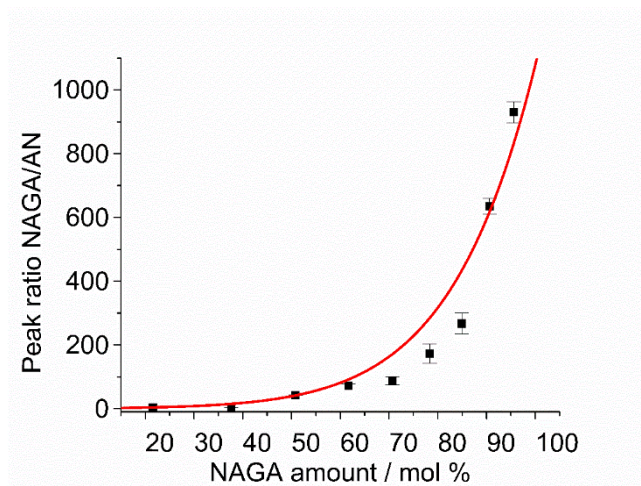


FIGURE S3 ATR-FTIR calibration function for determination of copolymer composition.

Calibration curve was made by using poly(NAGA)/poly(AN) blends. Both homopolymers were synthesized using RAFT polymerization

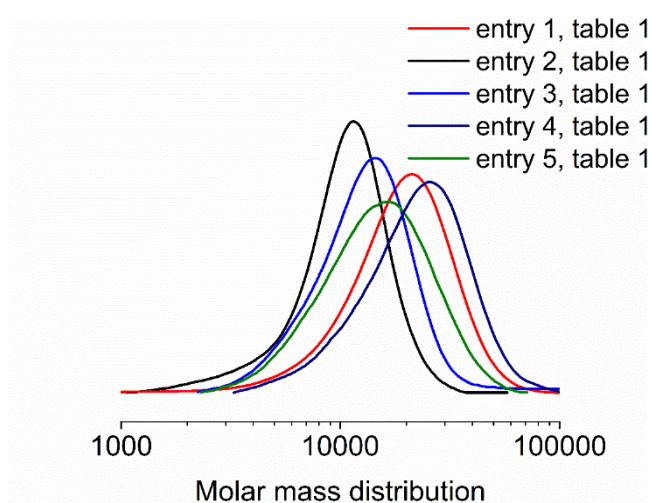


FIGURE S4 Molar mass distribution curves (entry 1-5, table 1).

TABLE S1 M_n and molar mass distributions of NAGA/AN copolymers measured by GPC using DMSO as solvent.

| Entry | M_n | D |
|--------------|-------------------------|-----------------------|
| 1 | 16 000 | 1.3 |
| 2 | 11 000 | 1.3 |
| 3 | 14 000 | 1.2 |
| 4 | 18 500 | 1.4 |
| 5 | 12 300 | 1.4 |

TABLE S2 Glass transition temperatures of poly(NAGA-AN) and poly(NAGA) determined by DSC.

| Entry | $Tg_1 / ^\circ\text{C}$ | $Tg_2 / ^\circ\text{C}$ |
|--------------|---|---|
| 1 | 108 | 147 |
| 2 | 103 | 140 |
| 3 | 87 | 153 |
| 4 | 107 | 160 |
| 5 | 110 | - |

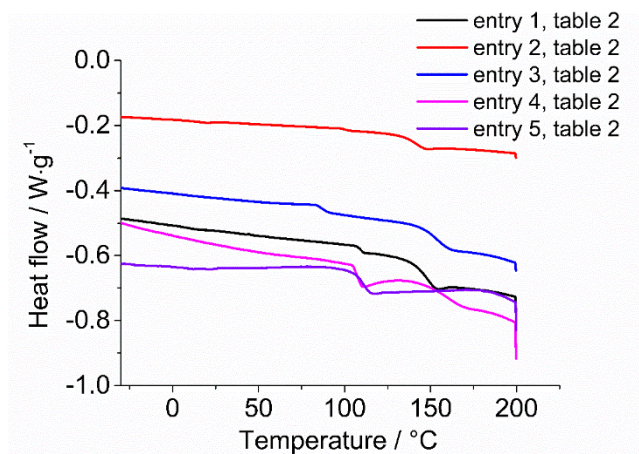


FIGURE S5 Glass transition temperatures of poly(NAGA-AN) and poly(NAGA) determined by DSC (entry 1-5, Table 2).

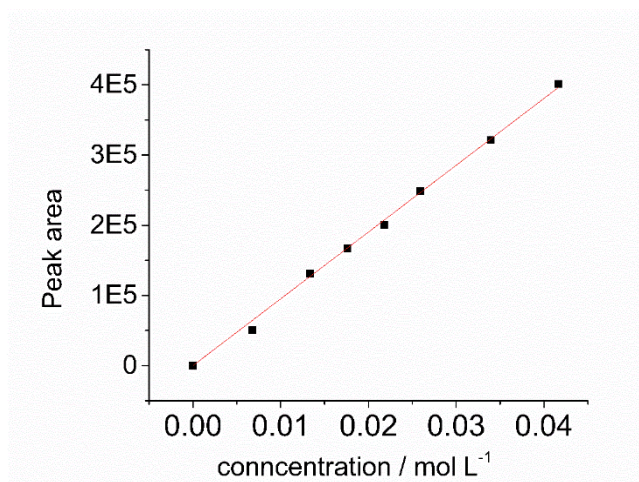


FIGURE S6 Calibration function of acrylonitrile in toluene. $R^2= 0.9992$

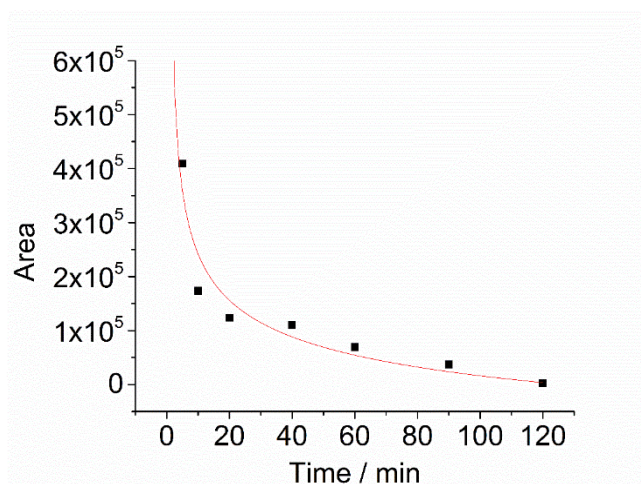


FIGURE S7 Peak areas of the GC measurements of unreacted acrylonitrile in toluene as solvent depending on reaction time, (entry 1, table 1).

TABLE S3 Yields, reacted amounts of N-acryloyl glycinamide in copolymer after different time periods m_0 (NAGA) = 525 mg, m_0 (AN) = 117 mg

| Entry | Time / min | Yield / % | NAGA / % | AN / % |
|--------------|-------------------|------------------|-----------------|---------------|
| 1 | 0 | 0 | 0 | 0 |
| 2 | 5 | 5 | 1.5 | 19.9 |
| 3 | 10 | 15 | 4 | 66 |
| 4 | 20 | 17 | 4.6 | 75.7 |
| 5 | 40 | 31 | 21.1 | 78.4 |
| 6 | 60 | 52 | 44.6 | 86.4 |
| 7 | 90 | 54 | 46.3 | 92.6 |
| 8 | 120 | 58 | 48.8 | 99.5 |

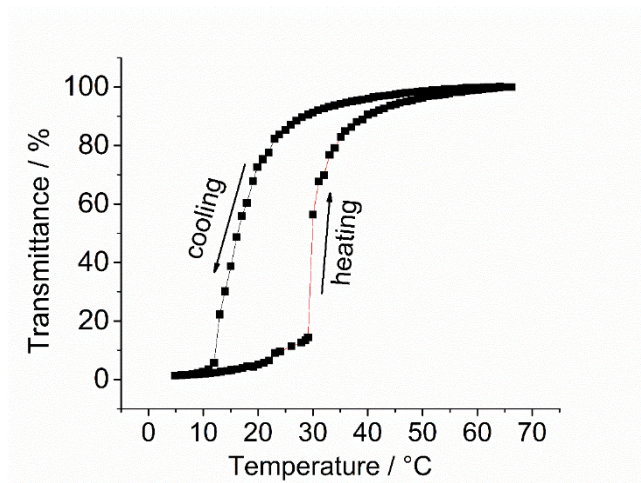


FIGURE S8 Hysteresis curve of poly(NAGA) in pure water, concentration 1 wt.%.

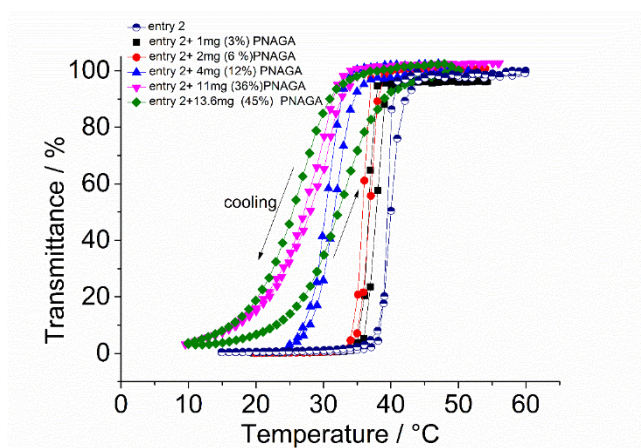


FIGURE S9 Effect of poly(NAGA) in different amounts on the hysteresis and cloud point of (entry 2, table 1), concentration of (entry 2, table 1) was 1 wt.%.

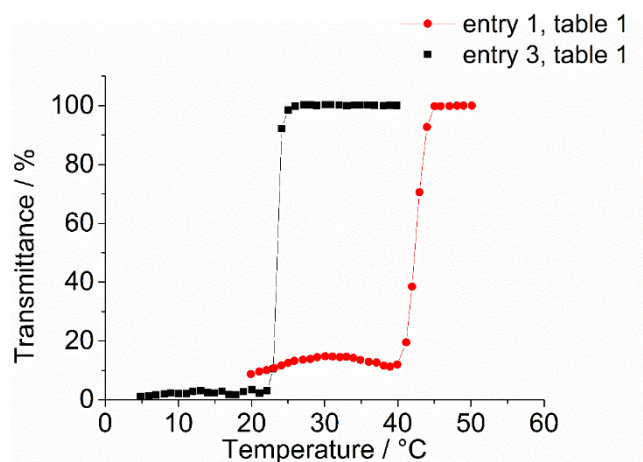


FIGURE S10 Cooling curves of (entry 1 and 3, table 1) in PBS puffer solution, concentration 1 wt. %

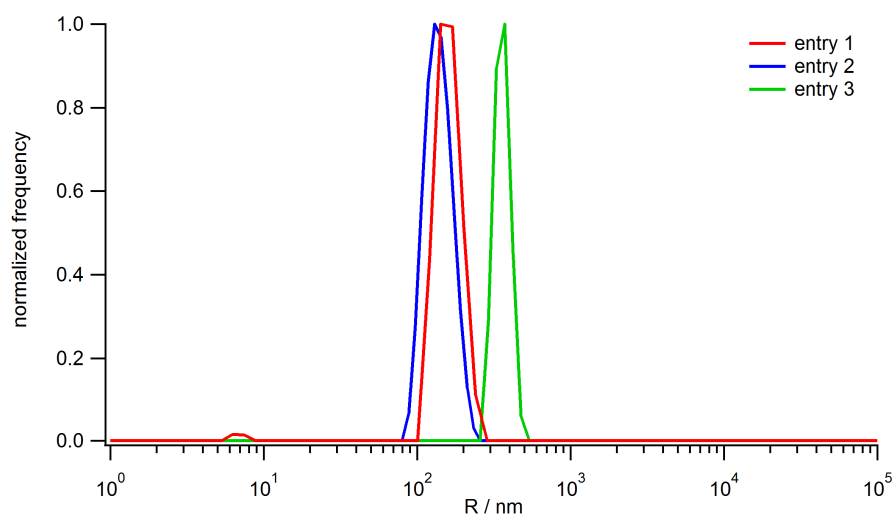


FIGURE S11 Radius distribution functions obtained from CONTIN analysis of intensity-time autocorrelation functions measured with DLS for entries 1, 2 and 3 at 20°C. The samples were measured at a scattering angle of 90° at concentrations of 0.1 wt. %.

7.3 Let There be Light: Polymeric Micelles with Upper Critical Solution Temperature as Light-Triggered Heat Nanogenerators for Combating Drug-Resistant Cancer

This work was published by Y. Deng⁺, **F. Käfer**,⁺ T. Chen, Q. Jin, J. Ji, S. Agarwal, *Small* **2018**, 1802420.

[+] These authors contributed equally to this work.

Reprinted with permission; Copyright 2018 WILEY-VCH Verlag GmbH & Co. KGaA, Weinheim

Let There be Light: Polymeric Micelles with Upper Critical Solution Temperature as Light-Triggered Heat Nanogenerators for Combating Drug-Resistant Cancer

Yongyan Deng, Florian Käfer, Tingting Chen, Qiao Jin,* Jian Ji, and Seema Agarwal*

Complete drug release and efficient drug retention are two critical factors in reversing drug resistance in cancer therapy. In this regard, polymeric micelles with an upper critical solution temperature (UCST) are designed as a new exploration to reverse drug resistance. The amphiphilic UCST-type block copolymers are used to encapsulate photothermal agent IR780 and doxorubicin (DOX) simultaneously. The integrated UCST-type drug nanocarriers show light-triggered multiple synergistic effects to reverse drug resistance and are expected to kill three birds with one stone: First, owing to the photothermal effect of IR780, the nanocarriers will be dissociated upon exposure to laser irradiation, leading to complete drug release. Second, the photothermal effect-induced hyperthermia is expected to avoid the efflux of DOX and realize efficient drug retention. Last but not least, photothermal ablation of cancer cells can be achieved after laser irradiation. Therefore, the UCST-type drug nanocarriers provide a new strategy in reversing drug resistance in cancer therapy.

1. Introduction

Chemotherapy is considered as one of the most important options after surgical resection of the primary tumor in clinic. Unfortunately, the therapeutic efficacy of conventional chemotherapy is always unsatisfactory mainly owing to the severe drug resistance of cancer cells.^[1,2] How to reverse the drug resistance has been considered as the bottleneck problem in cancer chemotherapy.^[3] Nanodrug delivery systems have received increased attention to overcome drug resistance in cancer therapy.^[4–10] However, although various drug nanocarriers with different architectures were fabricated, how to realize spatiotemporal

on-demand release in tumor sites and subsequent efficient intracellular retention of the drugs are still big challenges for nanodrug delivery systems.^[11]

In recent years, various stimuli-responsive nanocarriers were developed for smart drug delivery.^[12,13] Compared to endogenous stimuli (pH, redox potential, enzyme, etc.), exogenous stimuli (temperature, light, etc.)-responsive drug nanocarriers might be more advantageous for spatiotemporally controlled on-demand drug release.^[14,15] For example, thermoresponsive polymeric micelles were prepared as drug nanocarriers since the end of last century.^[16] In most of the cases, thermoresponsive polymeric micelles were constructed by lower critical solution temperature (LCST) polymers, such as poly(*N*-isopropylacrylamide) and poly(oligo-(ethylene glycol) methacrylate).^[17,18] Upon increasing the

temperature to higher than LCST, polymeric micelles with LCST will not be disassembled but shrunk, leading to incomplete drug release. In contrast, polymeric micelles exhibiting an upper critical solution temperature (UCST) will be dissociated when the temperature is higher than UCST, leading to complete drug release, which might be more promising in drug delivery.^[19–21] The biomedical applications of UCST polymers are strongly impeded due to the sensitivity to ionic strengths and polymer concentrations as most of the UCST polymers were based on polyzwitterions.^[22–24] Recently, we synthesized a series of noncharged UCST-type polymers with tunable cloud points based on copolymers of *N*-acryloylglycinamide and acrylonitrile, which were independent on ionic strengths and polymer concentrations.^[25] Block and graft copolymers of noncharged UCST-type segments with hydrophilic poly(ethylene glycol), poly(dimethylacrylamide), and poly(*N,N*-dimethylaminoethyl methacrylate) provide temperature dependent micellar structures which opens up an interesting future direction of thermoresponsive polymers in biomedical applications.^[26–28] In order to achieve thermoresponsive drug release *in vivo*, how to heat up the UCST-type drug nanocarriers is a big challenge. Compared to conventional microwave and radiofrequency radiation which are very difficult to control effective area of hyperthermia and show less precise site-specific controllability,^[26,29] photothermal action of near-infrared (NIR) laser irradiation might be a much better candidate for precision medicine and site-specific drug release due to its outstanding spatiotemporal controllability.^[30–33]

Y. Deng, T. Chen, Dr. Q. Jin, Prof. J. Ji
 MOE Key Laboratory of Macromolecule Synthesis and Functionalization
 of Ministry of Education
 Department of Polymer Science and Engineering
 Zhejiang University
 Hangzhou 310027, China
 E-mail: jinjqiao@zju.edu.cn
 F. Käfer, Prof. S. Agarwal
 Macromolecular Chemistry II and Center for Colloids and Interfaces
 University of Bayreuth
 Universitätsstraße 30, 95440 Bayreuth, Germany
 E-mail: agarwal@uni-bayreuth.de

The ORCID identification number(s) for the author(s) of this article can be found under <https://doi.org/10.1002/smll.201802420>.

DOI: 10.1002/smll.201802420

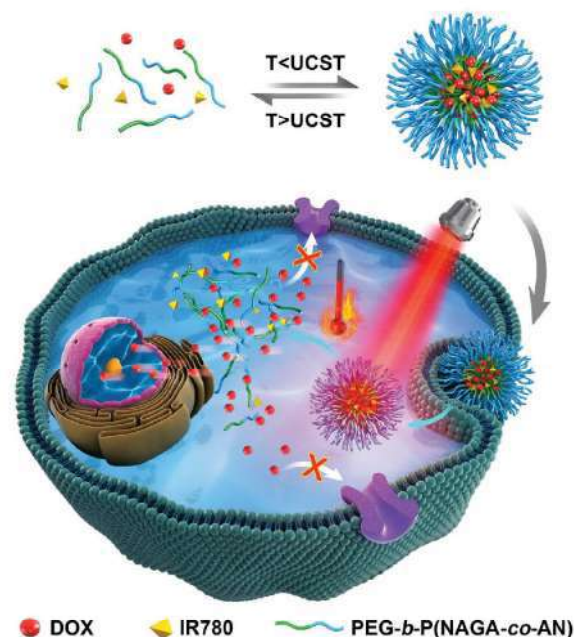
In this work we show the first example of UCST-type polymeric micelles as drug nanocarriers to overcome drug resistance by light-triggered drug release and retention intracellularly. Poly(ethylene glycol)-*b*-poly(*N*-acryloylglycinamide-*co*-acrylonitrile) (PEG-*b*-P(NAGA-*co*-AN)) with a cloud point of 44 °C was synthesized to encapsulate photothermal agent IR780 and anticancer drug doxorubicin (DOX) simultaneously. PEG-*b*-P(NAGA-*co*-AN) can form micelles at room temperature. Micelles will be disassembled upon NIR irradiation owing to the photothermal effect of IR780, which will result in complete release of DOX. Moreover, the photothermal effect induced hyperthermia is expected to avoid the efflux of DOX intracellularly. Therefore, owing to the photothermal effect of IR780, UCST-type polymeric nanocarriers can achieve spatiotemporally controlled drug release and efficient drug retention intracellularly, thus overcoming the drug resistance in cancer treatment (Scheme 1).

2. Results and Discussion

2.1. Preparation, Characterization, and Drug Release Behavior of UCST-type Nanocarriers

The UCST polymer PEG-*b*-P(NAGA-*co*-AN) was synthesized by radical polymerization as shown in Scheme S1 (Supporting Information). The number-average molecular weight (M_n) and the molar ratio of NAGA/AN in PEG-*b*-P(NAGA-*co*-AN) were 36 kDa and 2:1, respectively (Figures S1–S3, Supporting Information). The thermoresponsive behavior was studied by turbidity measurements. The transmittance of a 1 wt% aqueous solution of PEG-*b*-P(NAGA-*co*-AN) dramatically increased with the increase of temperature, indicating typical UCST-type phase transition behavior with a cloud point of 44 °C (Figure S4, Supporting Information). Interestingly, the cloud point of PEG-*b*-P(NAGA-*co*-AN) in phosphate buffered saline (PBS) was almost the same with that in water (Figure 1A), which is very important for its biomedical applications.

PEG-*b*-P(NAGA-*co*-AN) could readily self-assemble into nanosized micelles in aqueous solution at room temperature (25 °C) with the number-average hydrodynamic diameter of 109.7 nm as confirmed by dynamic light scattering (DLS) (Figure 1B). The transmission electron microscopy (TEM) image in Figure S5 (Supporting Information) further confirmed the spherical structure of PEG-*b*-P(NAGA-*co*-AN) micelles. It should be noted that the hydrodynamic diameter of core-shell micelles is influenced by many factors, including temperature, the length of hydrophilic block, the length of hydrophobic block, the compactness of the micelles, hydrophilicity/hydrophobicity ratio, and so on. It is reasonable that PEG-*b*-P(NAGA-*co*-AN) micelles have the hydrodynamic diameter of 109.7 nm, which was also observed for PEG-based core-shell micelles by many other researchers.^[34–36] Meanwhile, the PEG-*b*-P(NAGA-*co*-AN) solution showed clear evidence of the Tyndall effect (Figure 1C, insets) in phosphate buffer (pH 7.4), indicating the existence of nanoaggregates. As expected, the micelles showed thermoresponsive behavior. The hydrodynamic diameter of the micelles dramatically decreased to 7.2 nm and the Tyndall effect was not observed anymore when the temperature was above UCST,



Scheme 1. Scheme illustration for combating cancer drug resistance using NIR laser-triggered UCST-type nanocarriers.

indicating thermotriggred dissociation of UCST-type micelles (Figure 1C). Meanwhile, the nonresponsive poly(ethylene glycol)-*block*-poly(lactide-*co*-glycolide) (PEG-*b*-PLGA) micelles were prepared as a control with the size of 103 nm (Figure S6, Supporting Information). DOX and IR780 were subsequently encapsulated into PEG-*b*-P(NAGA-*co*-AN) micelles. The hydrodynamic diameter and drug loading content (DLC) of DOX loaded PEG-*b*-P(NAGA-*co*-AN) micelles (NP_{UCST}/DOX), IR780 loaded PEG-*b*-P(NAGA-*co*-AN) micelles ($NP_{UCST}/IR780$), IR780, and DOX coloaded PEG-*b*-P(NAGA-*co*-AN) micelles ($NP_{UCST}/(IR780+DOX)$), IR780 and DOX coloaded PEG-*b*-PLGA micelles ($NP_{PLGA}/(IR780+DOX)$) were shown in Table 1. $NP_{UCST}/(IR780+DOX)$ exhibited both the characteristic absorption of IR780 and DOX confirmed by UV-vis-NIR spectrum (Figure 1D), which proved successful encapsulation of IR780 and DOX simultaneously. It should be noted that $NP_{UCST}/(IR780+DOX)$ was very stable in physiological environment (phosphate buffer saline, pH 7.4) and lysosomal pH (pH 5.5), which is very important for its biomedical applications (Figure S7, Supporting Information). Owing to the photothermal effect of IR780, the solution temperature of $NP_{UCST}/(IR780+DOX)$ increased with light intensity-dependent 808 nm NIR irradiation (Figure 2A). If 4.0 W cm⁻² laser was used, the solution temperature would increase to as high as 60 °C after 3 min irradiation, which is high enough for photothermal triggered on-demand drug release as well as photothermal therapy (PTT).

The controlled release of DOX was studied in different temperatures to confirm the thermoresponsive behavior of the nanocarriers. As shown in Figure 2B, the release velocity of DOX from $NP_{UCST}/(IR780+DOX)$ was very slow at 37 °C. Only 25% of DOX was released after 24 h. However, the drug

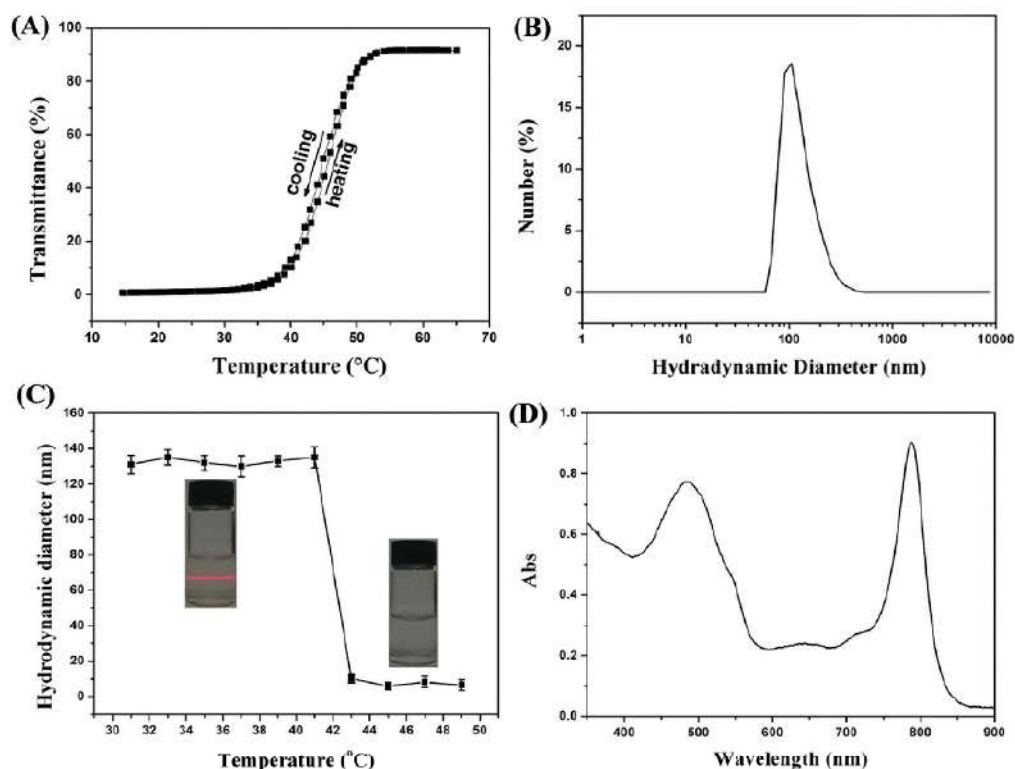


Figure 1. A) Turbidity measurement of 1.0 wt% PEG-*b*-P(NAGA-*co*-AN) in PBS buffer solution with heating rate of 1 °C min⁻¹. B) The DLS result of 0.1 mg mL⁻¹ PEG-*b*-P(NAGA-*co*-AN) micelles in aqueous solution at 25 °C. C) The DLS measurement of 0.1 mg mL⁻¹ PEG-*b*-P(NAGA-*co*-AN) in phosphate buffer (pH 7.4) at different temperatures. The insets showed the Tyndal effect. D) The UV-vis-NIR spectrum of NP_{UCST}/(IR780+DOX). The concentration of NP_{UCST}/(IR780+DOX) was 2.0 mg mL⁻¹.

release from NP_{UCST}/(IR780+DOX) was greatly accelerated when the temperature was above UCST (50 °C), which might be ascribed to thermotriggred dissociation of PEG-*b*-P(NAGA-*co*-AN) micelles. More than 80% of DOX was released after 4 h. In contrast, the release of DOX was very slow and did not show significant difference between 37 and 50 °C if DOX was loaded in conventional PEG-*b*-PLGA micelles. The NIR laser triggered drug release was then investigated. After NP_{UCST}/(IR780+DOX) was irradiated with 808 nm NIR laser for 5 min at 37 °C, the hydrodynamic diameter of the micelles increased from 136.8 nm to more than 1 μm (Figure 2C). The large aggregates might be attributed to the aggregation of DOX and IR780 after released from the micelles. As expected, spherical micelles were not observed any more in TEM images (Figure S8, Supporting Information). Moreover, the cumulative drug release profile in Figure 2D showed fast release of DOX upon exposed to NIR irradiation, owing to the photothermal-triggered dissociation of NP_{UCST}/(IR780+DOX). It should be noted that 5 min NIR laser irradiation (4.0 W cm⁻²) is enough to achieve a relative enhancement of drug release. The UCST-type nanocarriers showed limited drug leakage at normal body temperature (37 °C), while exhibited fast drug release upon 808 nm laser irradiation. Therefore, spatiotemporally controlled “on-demand” drug release can be achieved upon NIR laser irradiation. At the

same time, the release of DOX from PEG-*b*-P(NAGA-*co*-AN) micelles was very slow at pH 7.4 with 10% FBS or at pH 6.8 (Figure S9, Supporting Information), which indicated minimal leakage of DOX from PEG-*b*-P(NAGA-*co*-AN) micelles before their internalization by cancer cells.

2.2. Cellular Uptake and Measurement of Drug-Resistance Reversal

In order to investigate if DOX and IR780 could be effectively uptaken by cancer cells, confocal laser scanning microscope (CLSM) was applied to investigate the cellular internalization and distribution of DOX and IR780 in DOX-sensitive MCF-7 and DOX-resistant MCF-7/DOX breast cancer cells. After MCF-7 cells were incubated with free DOX, strong red fluorescence of DOX was observed in the cell nucleus of MCF-7 cells (Figure S10, Supporting Information). However, as shown in Figure 3, the red fluorescence of DOX could almost not be observed in MCF-7/DOX cells after incubation with free DOX, which might be attributed to the strong drug efflux by P-glycoprotein (P-gp).^[37] Furtherly, if NP_{UCST}/(IR780+DOX) was incubated with DOX-resistant MCF-7/DOX cells without NIR laser exposure, DOX was not observed in MCF-7/DOX cells as well. However, IR780 could be uniformly distributed

Table 1. DLS results and drug loading content (DLC) of drug loaded micelles.

| Samples | Hydrodynamic diameter [nm] | PDI | DLC (DOX) [wt%] | DLC (IR780) [%] |
|---------------------------------|----------------------------|------|-----------------|-----------------|
| NP _{UCST} /DOX | 136.3 | 0.22 | 10.1 | – |
| NP _{UCST} /IR780 | 134.5 | 0.19 | – | 5.4 |
| NP _{UCST} /(IR780+DOX) | 136.8 | 0.28 | 8.7 | 4.8 |
| NP _{PLGA} /(IR780+DOX) | 128.6 | 0.16 | 9.4 | 5.1 |

in the cytoplasm of MCF-7/DOX cells. MCF-7/DOX cells incubated with NP_{UCST}/(IR780+DOX) were then irradiated with NIR laser. Whether photothermal effect-induced hyperthermia could influence the expression of P-gp was investigated at first by western blot analysis. As shown in Figure 4, high P-gp protein level was detected in MCF-7/DOX cells. When MCF-7/DOX cells were incubated with NP_{UCST}/(IR780+DOX), the expression of P-gp was almost not changed with no significant difference. Interestingly, if MCF-7/DOX cells were incubated with NP_{UCST}/(IR780+DOX) under NIR exposure, remarkably high P-gp level downregulation was detected with 72% decrease of P-gp expression, which might be ascribed

to the photothermal effect-induced hyperthermia. Therefore, photothermal effect can inhibit P-gp protein expression and avoid drug efflux to overcome drug resistance. The uptake of NP_{UCST}/(IR780+DOX) by MCF-7/DOX cells under NIR exposure was then investigated. On the one hand, DOX can be completely released from the micelles due to the photothermal effect-triggered dissociation of UCST-type micelles. On the other hand, the photothermal effect-induced hyperthermia could achieve efficient intracellular retention by depressing the expression of P-gp. Therefore, DOX can be completely released and efficiently retained in MCF-7/DOX cells. Strong fluorescence of DOX could be observed in MCF-7/DOX cells. The intracellular DOX fluorescence could also be greatly influenced by NIR laser irradiation if NP_{UCST}/(IR780+DOX) was incubated with MCF-7 cells. Relative weak DOX fluorescence was observed in MCF-7 cells without NIR irradiation due to the fluorescence quenching when DOX was accumulated in the micellar core. However, the intracellular DOX fluorescence was significantly enhanced after DOX was released from the micelles after NIR irradiation. On the other hand, if MCF-7/DOX cells were incubated with conventional NP_{PLGA}/(IR780+DOX) under NIR exposure, only relatively weak intracellular DOX fluorescence was observed since DOX cannot be

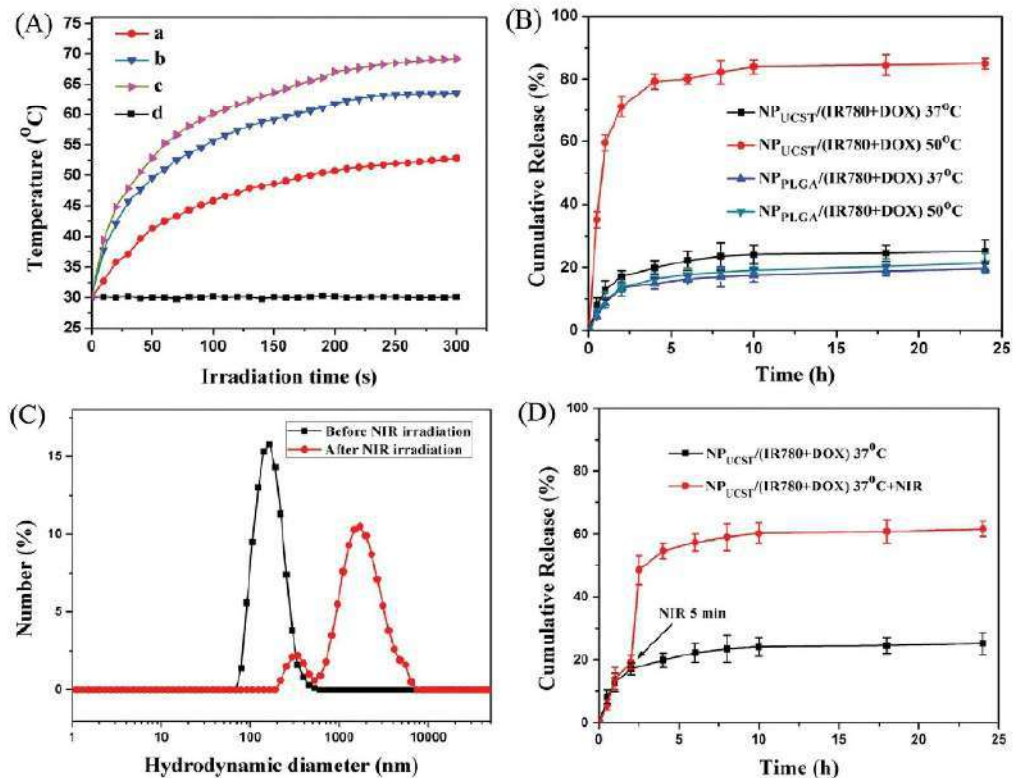


Figure 2. A) Temperature profiles of NP_{UCST}/(IR780+DOX) (0.2 mg mL⁻¹ IR780 equivalent) under 808 nm laser irradiation with light intensities of a) 2.0 W cm⁻², b) 4.0 W cm⁻², and c) 6.0 W cm⁻². NP_{UCST}/DOX d) was used as negative control under 808 nm laser irradiation with a light intensity of 6.0 W cm⁻². B) In vitro drug release profiles of NP_{UCST}/(IR780+DOX) and NP_{PLGA}/(IR780+DOX) at 37 and 50 °C. C) The hydrodynamic diameter of NP_{UCST}/(IR780+DOX) before and after NIR laser exposure at 37 °C. D) In vitro light-triggered cumulative release of DOX from NP_{UCST}/(IR780+DOX) in PBS at 37 °C. To assess how irradiation affects drug release from the micelles, 5 min NIR laser exposure (4 W cm⁻²) was applied at 2 h post incubation.

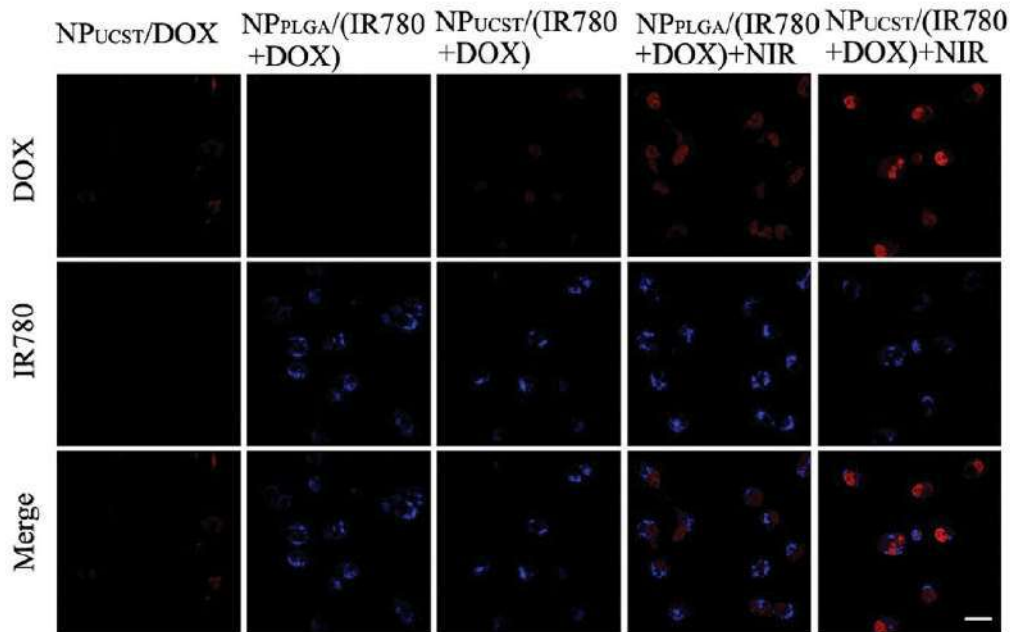


Figure 3. Cellular uptake of different nanocarriers ($\approx 5.0 \mu\text{g mL}^{-1}$ IR780, $\approx 10.0 \mu\text{g mL}^{-1}$ DOX) after incubation with MCF-7/DOX cells for 6 h. Some samples were irradiated with NIR laser (4 W cm^{-2}) for 5 min. Scale bar: 25 μm .

effectively released from micelles. Flow cytometry was further used to investigate the accumulation of DOX in MCF-7/DOX cells. As shown in Figure S11 (Supporting Information), NIR laser exposure could remarkably increase the red fluorescence of DOX in MCF-7/DOX cells. The strongest DOX fluorescence was observed after incubation with NP_{UCST}/(IR780+DOX) under NIR exposure due to the double benefits of photothermal effects, which was consistent with the CLSM results. Therefore, both effective drug release and minimal drug efflux are crucial for effective accumulation of DOX in MCF-7/DOX cells, which is the prerequisite in reversing the drug resistance.

2.3. In Vitro Cytotoxicity Studies

The cytotoxicity of the nanocarriers with or without NIR laser exposure was evaluated by the 3-(4,5-dimethyl-thiazol-2-yl)-2,5-diphenyl tetrazolium bromide (MTT) assay. When the nanocarriers or free DOX were incubated with DOX-sensitive MCF-7 cells, the proliferation of MCF-7 cells was significantly inhibited since DOX can be accumulated in MCF-7 cells in all the groups (Figure S12, Supporting Information). However, as shown in Figure S13 (Supporting Information), all of the nanocarriers did not show obvious cytotoxicity to MCF-7/DOX cells in the absence of NIR exposure even if the DOX concentration

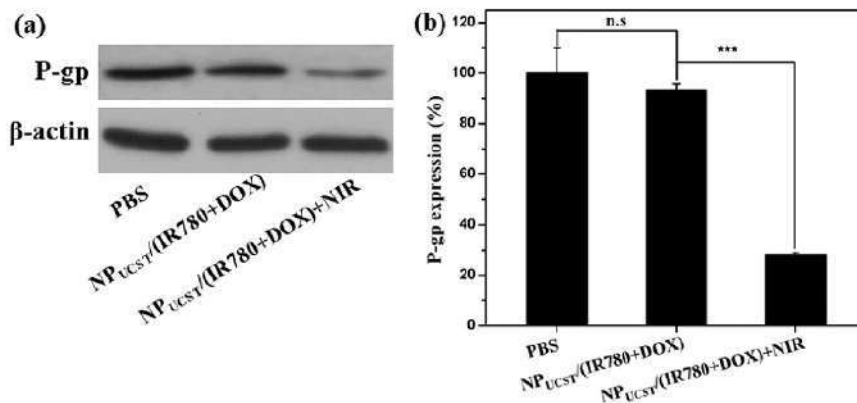


Figure 4. a) The expression of P-gp after different treatments was measured by western blot. b) Quantitative analysis of the expression of relative P-gp after different treatments.

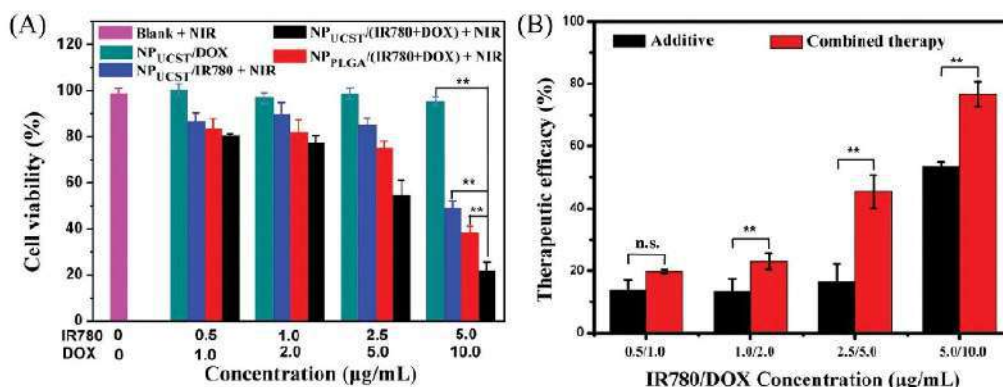


Figure 5. A) Proliferation inhibitions toward MCF-7/DOX cells after different treatments by MTT assay. B) Therapeutic efficacy evaluation of NP_{UCST}/DOX, NP_{UCST}/IR780 with NIR irradiation, and NP_{UCST}/(IR780+DOX) with NIR irradiation. * $p < 0.05$; ** $p < 0.01$.

was as high as $10.0 \mu\text{g mL}^{-1}$. MCF-7/DOX cells cannot be killed by DOX without laser irradiation probably due to the strong drug efflux by P-gp. Further, it should be noted that the viabilities of MCF-7/DOX cells were almost not influenced if blank MCF-7/DOX cells were suffered from 808 nm NIR laser exposure (4.0 W cm^{-2}) for 5 min, which indicated that laser irradiation at this light intensity could not influence the viability of MCF-7/DOX cells. After MCF-7/DOX cells were incubated with NP_{UCST}/IR780 under NIR irradiation, hyperthermia-induced cancer cell ablation was observed due to the photothermal effect of IR780 (Figure 5A). The cell viability of MCF-7/DOX cells treated with NP_{UCST}/IR780 ($5.0 \mu\text{g mL}^{-1}$ IR780 equivalent) under NIR irradiation was 49.0%. Moreover, NP_{UCST}/(IR780+DOX) showed significantly enhanced cytotoxicity under NIR irradiation. The cell viability was remarkably decreased to 21.5% when the concentrations of IR780 and DOX were 5.0 and $10.0 \mu\text{g mL}^{-1}$, respectively. The 50% inhibitory concentration (IC₅₀) of NP_{UCST}/(IR780+DOX) (DOX equivalent) evaluated by MCF-7/DOX cells was about $5.2 \mu\text{g mL}^{-1}$. The effective cellular growth inhibition of NP_{UCST}/(IR780+DOX) after laser irradiation might be ascribed to effective intracellular accumulation of DOX by photothermal-triggered complete drug release and minimal drug efflux, which is the prerequisite to overcome drug resistance and improve chemotherapeutic efficacy. The synergistic effect of IR780-based hyperthermia (NP_{UCST}/IR780 with NIR irradiation) and DOX-based chemotherapy (NP_{UCST}/DOX) was then investigated by calculating the therapeutic efficacy of each group (Figure 5B). Therapeutic efficacy was calculated by deducting the cell viability from 100%. Meanwhile, the additive therapeutic efficacies of chemotherapy and photothermal therapy were calculated by the equation $T_{\text{additive}} = 100\% - (f_{\text{chemo}} \times f_{\text{photothermal}}) \times 100\%$, where f was the fraction of surviving cells after every treatment.^[38] The results suggested that the combined therapy group (NP_{UCST}/(IR780+DOX) with NIR irradiation) had notably higher therapeutic efficacy than the merely additive therapeutic efficacy of IR780-based photothermal therapy (NP_{UCST}/IR780 with NIR irradiation) and DOX-based chemotherapy (NP_{UCST}/DOX), indicating excellent synergistic effect to overcome drug resistance. Furthermore, compared to NP_{UCST}/(IR780+DOX) with NIR irradiation, the conventional NP_{PLGA}/(IR780+DOX) with

NIR irradiation showed much weaker cytotoxicity, probably owing to incomplete drug release.

Live/dead cell viability assay was further employed to visualize cytotoxic effects of hyperthermia assisted chemotherapy against MCF-7/DOX cells. The fluorescein diacetate/propidium iodide (FDA/PI) double staining was applied to identify live and dead/apoptotic cells after different treatments. As shown in Figure 6, when MCF-7/DOX cells were incubated with NP_{UCST}/(IR780+DOX) or NP_{PLGA}/(IR780+DOX) in the absence of NIR laser exposure, red fluorescence was almost not observed, indicating negligible lethal effects. When MCF-7/DOX cells were incubated with NP_{UCST}/IR780 and NIR laser was irradiated for 5 min, partial cell death was observed, owing to IR780 triggered photothermal cytotoxicity. Meanwhile, NP_{PLGA}/(IR780+DOX) can also induce some cell death after laser irradiation. However, NP_{PLGA}/(IR780+DOX) was not as effective as NP_{UCST}/(IR780+DOX) to kill MCF-7/DOX cells, which might be ascribed to the inefficient drug release of NP_{PLGA}/(IR780+DOX). If MCF-7/DOX cells treated with NP_{UCST}/(IR780+DOX) were suffered from NIR irradiation, almost all of the cells were killed. All the results were in good agreement with MTT assay.

2.4. In Vivo Tumor Growth Inhibition

The in vivo performance of drug nanocarriers was accessed on nude mice bearing MCF-7/DOX tumors as the xenograft model. The efficient accumulation of DOX in tumor site was very important for improved therapeutic efficacy and minimal side effect. The in vivo biodistribution was first evaluated by the noninvasive optical imaging technique. As shown in Figure 7A, stronger NIR fluorescence from NP_{UCST}/(IR780+DOX) was observed in tumor site 4 h after injection compared with that of free IR780. Notable fluorescent signal from NP_{UCST}/(IR780+DOX) could still be detected in tumor site even after 72 h postinjection, which indicated that the drug nanocarriers could be effectively accumulated in tumor site. Furthermore, the DOX accumulation in main organs and tumors at 24 h postinjection was carried out by ex vivo fluorescent imaging. The mice treated with NP_{UCST}/(IR780+DOX) showed much

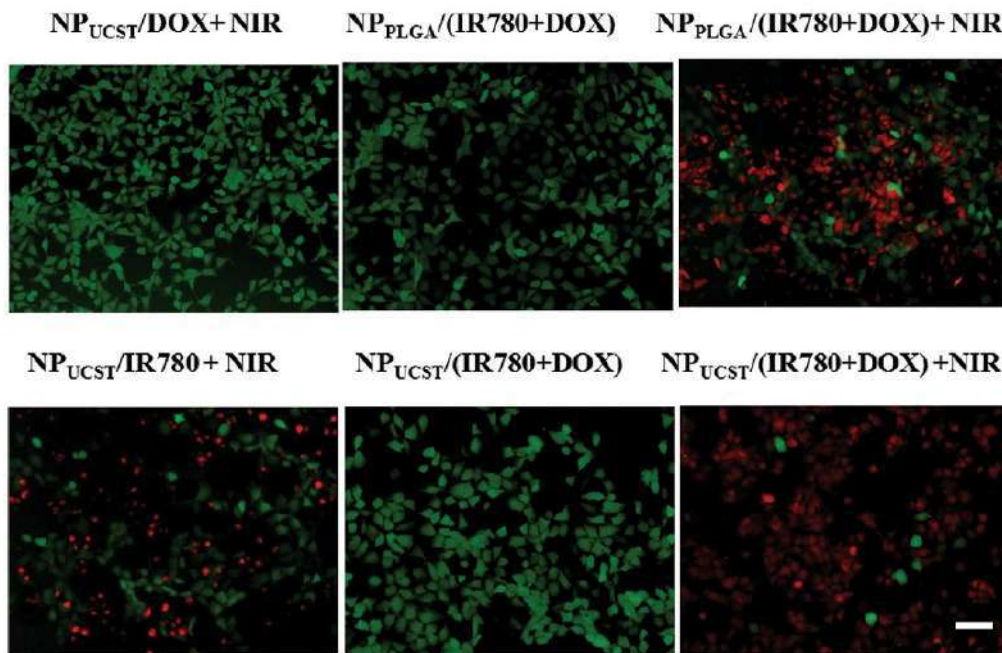


Figure 6. Evaluation of the cytotoxicity by fluorescent microscopy using FDA/PI double staining after different treatments. Dead cells: red fluorescence of PI; live cells: green fluorescence of FDA. Scale bar: 25 μ m.

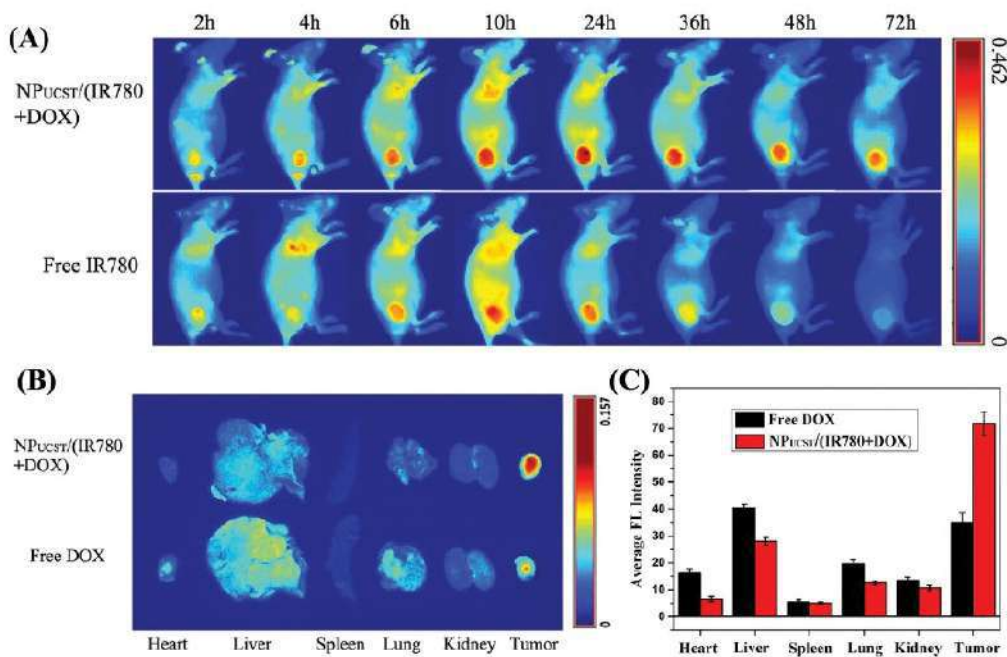


Figure 7. A) In vivo time-dependent whole body NIR fluorescent imaging of MCF-7/DOX tumor-bearing mice after intravenous administration of NP_{UCST}/((IR780+DOX)) or free IR780. B) Ex vivo fluorescence images of main organs and tumor after administration of NP_{UCST}/((IR780+DOX)) or free DOX for 24 h. C) Quantification of average fluorescent signals of DOX in main organs and tumor site after administration of NP_{UCST}/((IR780+DOX)) or free DOX for 24 h.

stronger fluorescence of DOX in tumor site than that treated with free DOX (Figure 7B,C). In contrast, mice treated with NP_{UCST}/(IR780+DOX) showed much weaker fluorescence of DOX in main organs than that treated with free DOX.

The in vivo antitumor behavior was then evaluated by tracking the tumor growth rate after different treatments. At first, the increase of temperature in tumor site after treated with nanocarriers plus laser irradiation was studied by infrared (IR) thermal imaging. After irradiated with 808 nm laser for 5 min, both of the NP_{UCST}/(IR780+DOX) and NP_{PLGA}/(IR780+DOX) groups had an obvious tendency to heat up (Figure 8A). The temperature in tumor tissue could be higher than 50 °C after 3 min irradiation, which is sufficient to induce irreversible tissue damage.^[39] The antitumor effect of chemo-photothermal therapy was then investigated. As shown in Figure 8B, the free DOX and NP_{UCST}/DOX groups can only slightly inhibited the tumor growth without significant difference, which might be attributed to the strong drug resistance of MCF-7/DOX cells. NP_{UCST}/IR780 with NIR irradiation could partially inhibit the tumor growth with 4–5 times increase of tumor sizes, owing to IR-780 induced photothermal therapy. Interestingly, NP_{UCST}/(IR780+DOX) with NIR irradiation presented remarkable tumor regression with a statistically significant difference ($p < 0.001$). The excellent antitumor effect could be attributed to the synergistic effect of hyperthermia and chemotherapy by

photothermal-induced complete drug release, minimal drug efflux and photothermal therapy. In contrast, since DOX cannot be completely released from NP_{PLGA}/(IR780+DOX) after NIR irradiation, the antitumor effect was significantly attenuated with 3 times increase of tumor size. The mice were sacrificed 21 days postinjection. The tumor tissues were harvested and weighted. The tumor weight of each group was in accordance with the results of the tumor growth rate (Figure S14, Supporting Information). The tumor inhibition ratio (TIR) was then calculated. The TIR of the NP_{UCST}/(IR780+DOX) group after NIR irradiation was 94.4%, which was much higher than other groups (Figure 8C). Meanwhile, the mean body weight of mice after different treatments did not exhibit significant change compared with the control group, which indicated that the DOX concentration in these groups was well tolerant (Figure S15, Supporting Information). The potential cardiotoxicity after different treatments was further investigated by hematoxylin–eosin (H&E) staining. All the treatments did not cause apparent histopathological cardiotoxicity, demonstrating negligible side effects in these treatments (Figure S16, Supporting Information). In order to further investigate the antitumor performance after different treatments, the levels of proliferation and apoptosis in tumor tissues were then analyzed by immunohistochemistry, including H&E staining, Ki67 assay, and terminal deoxynucleotidyl transferase (TdT)-mediated dUTP

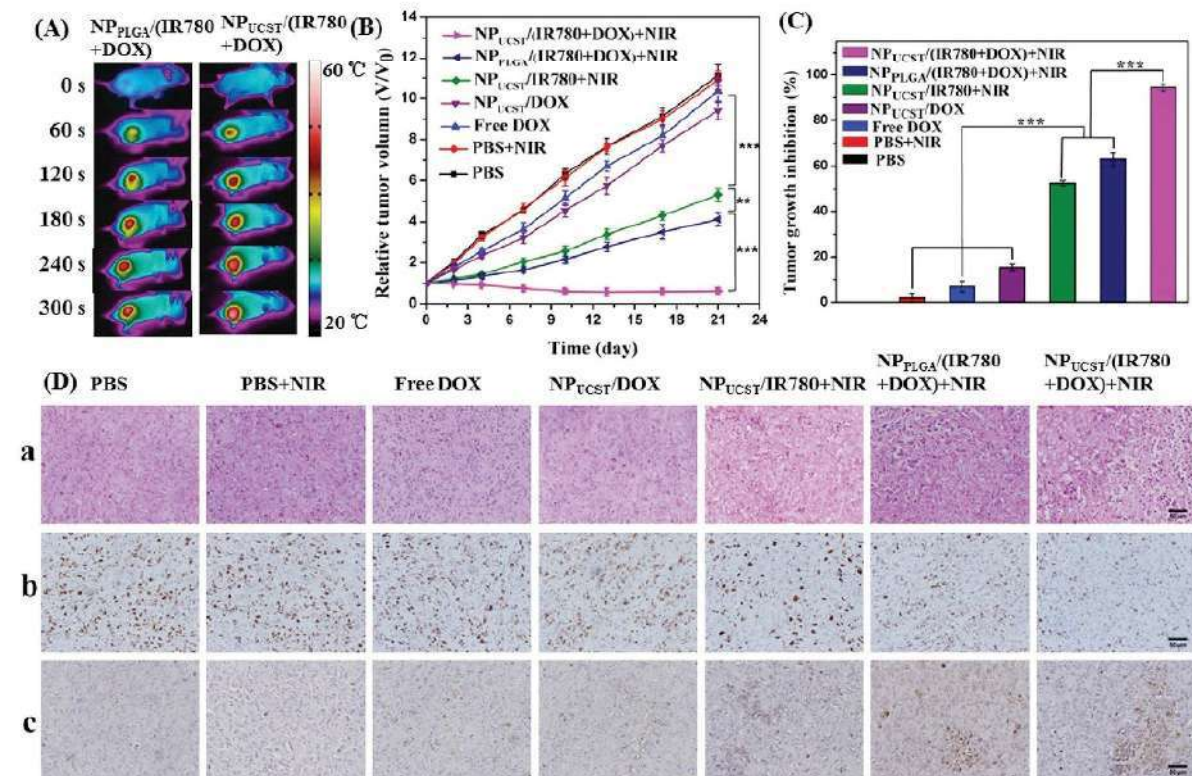


Figure 8. A) Infrared (IR) thermal images of MCF-7/DOX tumor-bearing mice exposed to 808 nm NIR laser for 5 min (4 W cm⁻²). B) MCF-7/DOX tumor growth was evaluated by measuring the relative tumor volume after different treatments. C) Tumor growth inhibition ratio after different treatments. D) Representative H&E a), Ki67 b), and TUNEL c) staining of tumor tissues after treating with different formulations. Scale bar: 50 μm.

nick-end labeling (TUNEL) assay. As depicted in Figure 8D by the histological H&E staining, the NP_{UCST}/(IR780+DOX) group after NIR irradiation showed much better suppression of tumor cell proliferation than other groups. Specifically, the percentage of proliferating cells in tumor tissue treated with the NP_{UCST}/(IR780+DOX) group after NIR irradiation was less than other groups detected by Ki67 assay. Meanwhile, the percentage of apoptotic cells in tumor tissue treated with the NP_{UCST}/(IR780+DOX) group after NIR irradiation was much higher than other groups detected by the TUNEL assay. Therefore, the levels of proliferation and apoptosis in tumors after different treatments were in good agreement with the TIR results. Therefore, taking advantage of UCST-type drug nanocarriers, efficient intracellular accumulation of DOX by complete drug release and minimal drug efflux played an important role in overcoming drug resistance and improving the therapeutic efficacy both in vitro and in vivo.

3. Conclusion

In conclusion, a new UCST-type drug nanocarrier was fabricated for combating drug-resistant cancer. The UCST-type PEG-*b*-P(NAGA-co-AN) micelles with cloud point of 44 °C were successfully constructed to encapsulate IR780 and DOX simultaneously. Owing to the photothermal effect of IR780, micelles would be dissociated upon NIR laser exposure, leading to spatiotemporally controlled efficient release of DOX. Meanwhile, the photothermal effect induced hyperthermia could avoid the efflux of DOX in drug resistant MCF-7/DOX cells. Therefore, significantly increased intracellular DOX accumulation was achieved in MCF-7/DOX cells by efficient drug release and minimal drug efflux. The IR780-based hyperthermia and DOX-based chemotherapy exhibited excellent synergistic effects in reversing drug resistance in cancer therapy. Specific NIR laser exposure after systemic administration of NP_{UCST}/(IR780+DOX) could efficiently inhibit MCF-7/DOX tumor growth without causing obvious side effect in tumor-bearing nude mice. Such UCST-type drug nanocarriers not only expanded the biomedical applications of thermal-responsive polymers, but also provided a new strategy to overcome drug resistance in cancer treatment.

Supporting Information

Supporting Information is available from the Wiley Online Library or from the author.

Acknowledgements

Y.D. and F.K. contributed equally to this work. Financial support from the National Natural Science Foundation of China (21774110, 51573160) and Deutsche Forschungsgemeinschaft is gratefully acknowledged. All in vivo experiments were carried out according to the "Principles of Laboratory Animal Care" (NIH publication no.86-23, revised 1985) and the guidelines for Lab Animal Welfare and Research Committee, Zhejiang University.

Conflict of Interest

The authors declare no conflict of interest.

Keywords

drug resistance, hyperthermia, light-triggered drug release, photothermal effect, UCST

Received: June 25, 2018

Revised: July 29, 2018

Published online:

- [1] C. Holohan, S. Van Schaeybroeck, D. B. Longley, P. G. Johnston, *Nat. Rev. Cancer* **2013**, *13*, 714.
- [2] M. M. Gottesman, T. Fojo, S. E. Bates, *Nat. Rev. Cancer* **2002**, *2*, 48.
- [3] G. Szakács, J. K. Paterson, J. A. Ludwig, C. Booth-Gentle, M. M. Gottesman, *Nat. Rev. Drug Discovery* **2006**, *5*, 219.
- [4] Y. Min, C. Mao, S. Chen, G. Ma, J. Wang, Y. Liu, *Angew. Chem., Int. Ed.* **2012**, *51*, 6742.
- [5] Y. Yan, M. Björnmalm, F. Caruso, *ACS Nano* **2013**, *7*, 9512.
- [6] Q. Yin, J. Shen, Z. Zhang, H. Yu, Y. Li, *Adv. Drug Delivery Rev.* **2013**, *65*, 1699.
- [7] Z. Li, H. Wang, Y. Chen, Y. Wang, H. Li, H. Han, T. Chen, Q. Jin, J. Ji, *Small* **2016**, *12*, 2731.
- [8] A. R. Kirtane, S. M. Kalscheuer, J. Panyam, *Adv. Drug Delivery Rev.* **2013**, *65*, 1731.
- [9] Y. Yuan, L. Wang, W. Du, Z. Ding, J. Zhang, T. Han, L. An, H. Zhang, G. Liang, *Angew. Chem., Int. Ed.* **2015**, *54*, 9700.
- [10] W. H. Chen, G. F. Luo, W. X. Qiu, Q. Lei, L. H. Liu, D. W. Zheng, S. Hong, S. X. Cheng, X. Z. Zhang, *Chem. Mater.* **2016**, *28*, 6742.
- [11] S. R. MacEwan, A. Chilkoti, *Angew. Chem., Int. Ed.* **2017**, *56*, 6712.
- [12] Y. P. Torchilin, *Nat. Rev. Drug Discovery* **2014**, *13*, 813.
- [13] H. J. Han, D. Valdepérez, Q. Jin, B. Yang, Z. H. Li, Y. L. Wu, B. Pelaz, W. J. Parak, J. Ji, *ACS Nano* **2017**, *11*, 1281.
- [14] N. Rapoport, *Prog. Polym. Sci.* **2007**, *32*, 962.
- [15] G. Yang, J. Liu, Y. Wu, L. Feng, Z. Liu, *Coord. Chem. Rev.* **2016**, *320–321*, 100.
- [16] M. Bikram, J. L. West, *Expert Opin. Drug Delivery* **2008**, *5*, 1077.
- [17] P. Hernández, A. Lucero-Acuña, C. A. Gutiérrez-Valenzuela, R. Moreno, R. Esquivel, *e-Polymers* **2017**, *17*, 399.
- [18] D. Roy, W. L. A. Brooks, B. S. Sumerlin, *Chem. Soc. Rev.* **2013**, *42*, 7214.
- [19] J. Seuring, S. Agarwal, *ACS Macro Lett.* **2013**, *2*, 597.
- [20] M. Arotçarèna, B. Heise, S. Ishaya, A. Laschewsky, *J. Am. Chem. Soc.* **2002**, *124*, 3787.
- [21] F. Käfer, F. Liu, U. Stahlschmidt, V. Jérôme, R. Freitag, M. Karg, S. Agarwal, *Langmuir* **2015**, *31*, 8940.
- [22] J. Seuring, S. Agarwal, *Macromol. Rapid Commun.* **2012**, *33*, 1898.
- [23] C. Ju, H. Kang, *RSC Adv.* **2017**, *7*, 56426.
- [24] W. M. Wan, F. Cheng, F. Jäkle, *Angew. Chem., Int. Ed.* **2014**, *53*, 8934.
- [25] F. Käfer, A. Lerch, S. Agarwal, *J. Polym. Sci., Part A: Polym. Chem.* **2017**, *55*, 274.
- [26] W. Li, L. Huang, X. Ying, Y. Jjian, Y. Hong, F. Hu, Y. Du, *Angew. Chem., Int. Ed.* **2015**, *54*, 3126.
- [27] G. Huang, H. Li, S. T. Feng, X. Li, G. Tong, J. Liu, C. Quan, Q. Jiang, C. Zhang, Z. Li, *Macromol. Chem. Phys.* **2015**, *216*, 1014.
- [28] H. Zhang, X. Tong, Y. Zhao, *Langmuir* **2014**, *30*, 11433.
- [29] K. Zhang, P. Li, H. Chen, X. Bo, X. Li, H. Xu, *ACS Nano* **2016**, *10*, 2549.
- [30] H. Yu, Z. Cui, P. Yu, C. Guo, B. Feng, T. Jiang, S. Wang, Q. Yin, D. Zhong, X. Yang, Z. Zhang, Y. Li, *Adv. Funct. Mater.* **2015**, *25*, 2489.
- [31] L. Hui, S. Qin, L. Yang, *ACS Biomater. Sci. Eng.* **2016**, *2*, 2127.
- [32] A. J. Zhu, K. Miao, Y. B. Deng, H. T. Ke, H. He, T. Yang, M. Guo, Y. L. Li, Z. Q. Guo, Y. Y. Wang, X. L. Yang, Y. L. Zhao, H. B. Chen, *ACS Nano* **2015**, *9*, 7874.
- [33] W. Qiu, L. H. Liu, S. Y. Li, Q. Lei, G. F. Luo, X. Z. Zhang, *Small* **2017**, *13*, 1603956.

Reprints of Publications

- [34] D. Kim, E. S. Lee, K. T. Oh, Z. G. Gao, Y. H. Bae, *Small* **2008**, *4*, 2043.
- [35] A. Alkan, S. Wald, B. Louage, B. R. De Geest, K. Landfester, F. R. Wurm, *Langmuir* **2017**, *33*, 272.
- [36] Y. Zhang, Y. Lu, F. Wang, S. An, Y. Zhang, T. Sun, J. Zhu, C. Jiang, *Small* **2017**, *13*, 1602494.
- [37] L. Wang, X. Lin, J. Wang, Z. Hu, Y. Ji, S. Hou, Y. Zhao, X. Wu, C. Chen, *Adv. Funct. Mater.* **2014**, *24*, 4229.
- [38] H. Park, J. Yang, J. Lee, S. Haam, I. H. Choi, K. H. Yoo, *ACS Nano* **2009**, *3*, 2919.
- [39] C. Peng, Y. Shih, P. Lee, T. M. Hsieh, T. Luó, M. Shieh, *ACS Nano* **2011**, *5*, 5594.



Supporting Information

for *Small*, DOI: 10.1002/sml.201802420

Let There be Light: Polymeric Micelles with Upper
Critical Solution Temperature as Light-Triggered Heat
Nanogenerators for Combating Drug-Resistant Cancer

Yongyan Deng, Florian Käfer, Tingting Chen, Qiao Jin, Jian
Ji, and Seema Agarwal**

Copyright WILEY-VCH Verlag GmbH & Co. KGaA, 69469 Weinheim, Germany, 2016.

Supporting Information

Let there be light: Polymeric micelles with upper critical solution temperature as light-triggered heat nanogenerators for combating drug-resistant cancer

Yongyan Deng,⁺ Florian Käfer,⁺ Tingting Chen, Qiao Jin,^{} Jian Ji, Seema Agarwal^{*}*

Experimental Section

Materials

IR-780 iodide and 3-(4,5-dimethyl-thiazol-2-yl)-2,5-diphenyl tetrazolium bromide (MTT) were bought from Sigma-Aldrich. Poly(ethylene glycol) methyl ether-block-poly(lactide-co-glycolide) (PEG-PLGA, PEG Mn 2,000, PLGA Mn 5,000) was bought from Xi'an ruixi Biological Technology Co., Ltd. Doxorubicin hydrochloride (DOX·HCl) was obtained from Dalian Meilun Biotech Co., Ltd. RMPI-1640, penicillin-streptomycin, and Fetal bovine serum (FBS) were purchased from Gibco Life Technologies (USA). MCF-7/DOX cells were supplied by Keygen Biotech Co. Ltd (China). All other chemical reagents and solvents were analytically pure and used directly without further purification. DOX-resistant human breast cells MCF-7/DOX were purchased from Keygen Biotech Co. Ltd (Shanghai, China). PEG-azo macroinitiator VPE-0201 (PEG unit Mn = 2,000 g mol⁻¹) was obtained from Wako and used without further purification. N-acryloylglycinamide (NAGA) was synthesized according to our previous work.^[1] 2-propenenitrile was purchased from ACROS Organics and distilled under reduced pressure.

Measurements

¹H-NMR spectra were recorded on a Bruker Ultrashield 300 spectrometer. FTIR spectroscopic imaging in attenuated total reflection (ATR) mode was used to calculate the amount of acrylonitrile in the copolymers on a Digilab Excalibur Series FTS 3000 spectrometer. To determine the polymer composition the peaks at 2244 (-CN) cm⁻¹ and the

1654 (-CO) cm^{-1} were integrated and the ratio (-CO)/(-CN) was calculated. The copolymer composition was determined using an IR calibration function made by mixing both homopolymers in different ratios. The spectra were analyzed by using the software WIN-IR PRO 3.3. The turbidity measurements were carried out on a JASCO V-630 Spectrophotometer at 660 nm with continuous stirring at a heating rate of 1.0 $^{\circ}\text{C min}^{-1}$. The cell path length was 10mm spectrometer. The polymer was dissolved at 60 $^{\circ}\text{C}$ under continuous stirring for 15 min. For the measurement the sample was heated up to 60 $^{\circ}\text{C}$ and the measurement was started with the cooling curve. Gel permeation chromatography (GPC) was used to determine the molecular weight and molecular weight distribution with dimethyl sulfoxide as mobile phase. The flow rate was set as 0.7 mL min^{-1} and the temperature was 75 $^{\circ}\text{C}$. The fluorescence emission spectra were determined on a Shimadzu RF-530 spectrometer. In order to measure the fluorescent intensity of DOX, the excitation wavelength was set at 488 nm and the emission spectra were recorded from 510 to 750 nm. Dynamic light scattering (DLS) measurements were performed using a Malvern Zetasizer Nano-ZS which was equipped with a He-Ne laser at a wavelength of 633 nm. The samples were cleaned by a 0.45 μm Millipore filter before DLS measurements. The temperature of the samples was balanced for 2 min for every measurement. Number-average hydrodynamic diameter (D_h) was used in this research. Transmission electron microscopy (TEM) measurements were performed on a HT7700 TEM (HITACHI, Japan) operated at an accelerating voltage of 100 kV. TEM The cellular uptake experiments were recorded by confocal laser scanning microscope (Leica TCS SP5). Live/dead cell viability assay and immunofluorescence staining analysis were performed on a fluorescence microscope (Olympus IX81). Flow cytometry analysis of cell uptake was analyzed by a BD FACS-CaliburTM flow cytometer. In vivo whole body NIR fluorescent imaging was obtained with a CRI Maestro in vivo imaging system which was equipped with a tunable liquid-crystal filter and a cooled scientific-grade monochrome CCD camera. The light source for light irradiation is an 808 nm laser with

tunable light intensity (Lasever Inc., China). The change of the temperature after NIR laser exposure was recorded by an IR thermal imaging camera (FLIR E60, Flir System Inc., USA).

Synthesis of PEG-*b*-P(NAGA-co-AN)

For the synthesis of the copolymer, NAGA and acrylonitrile (AN) (distilled under reduced pressure) were dissolved in 10 mL dimethyl sulfoxide (DMSO) with a total monomer concentration of 1M (feed ratio NAGA:AN, 65:35; n:n) in a Schlenk flask followed by degassing (three freeze-pump-thaw cycles). A VPE-0201/DMSO solution (0.3 wt. % of VPE-0201) was added to the reaction solution. The reaction was carried out at 70°C for 24 h. The polymer was precipitated from methanol. The polymer was centrifuged (6,000 rpm, 15 minutes), and afterwards dialyzed against water for two days by changing the water twice per day. Finally, the polymer was lyophilized.

Preparation of PEG-*b*-P(NAGA-co-AN) and PEG-*b*-PLGA micelles

The UCST-type PEG-*b*-P(NAGA-co-AN) micelles were readily prepared by the cosolvent approach. Briefly, 10 mg of PEG-*b*-P(NAGA-co-AN) was dissolved in 2 mL of DMSO. The solution was stirred for 1 h. Distilled water (2 mL) was then added to the solution dropwise. The solution was stirred for another 3 h and dialyzed against water for at least 48 h (MWCO 3,500). The PEG-*b*-PLGA micelles was prepared the same as PEG-*b*-P(NAGA-co-AN) micelles.

Preparation of drug loaded micelles

In order to prepare NP_{UCST}/(IR780+DOX), 15 mg of PEG-*b*-P(NAGA-co-AN) was dissolved in 2 mL of DMF by stirring for 1 h. 3 mg of Doxorubicin hydrochloride and 1.5 mg of IR780 were then added. After that, 20 µL of triethylamine (TEA) was added by microsyringe. The solution was stirred for another 2 h. The solution was transferred to a dialysis bag and dialyzed against distilled water for at least 48 h. For the determining of the total content of DOX in the micelles, the micellar solution was freeze-dried and the solid was then dissolved in methanol/DMSO (1:1). The DOX content was determined by a UV-vis spectrum taking

advantage of the characteristic UV absorbance at 480 nm. In order to measure the IR780 content in the micelles, the micellar solution was lyophilized and then dissolved in the mixture of methanol and DMSO (v/v 1:1). The content of IR-780 was then determined by UV-vis-NIR spectrum at 780 nm. The drug loading content (DLC) of DOX and IR780 were calculated by the follow Equations 1.

$$\text{DLC (\%)} = \frac{\text{weight of loaded drug}}{\text{weight of polymer} + \text{weight of loaded drug}} \times 100\% \quad (1)$$

NP_{UCST}/IR780, NP_{UCST}/DOX and NP_{PLGA}/(IR780+DOX) were prepared the same as NP_{UCST}/(IR780+DOX) unless different kinds of drugs were used.

Characterizations on in vitro photothermal effects

The in vitro photothermal conversion effects of NP_{UCST}/(IR780+DOX) were characterized by monitoring the temperature rises of NP_{UCST}/(IR780+DOX) (0.2 mg mL⁻¹ IR780 equivalent) in aqueous solution during a 5 min irradiation with 808 nm NIR laser at varying light intensities. The solution temperature was recorded by an IR thermal imaging camera (FLIR E60, Flir System Inc., USA).

In vitro drug release experiments

In order to study the in vitro drug release, 2 mL of 1 mg mL⁻¹ NP_{UCST}/(IR780+DOX) or NP_{PLGA}/(IR780+DOX) solution was added into a dialysis bag (MWCO 3,500). The dialysis bag was then soaked in 20 mL of phosphate buffer saline (PBS) solution. The solution was kept at 37 °C or 50 °C in a constant temperature shaking table with constant shaking (100 rpm). The external buffer solution (0.5 mL) was taken out at different time (0.5 h, 1 h, 2 h, 4 h, 6 h, 8 h, 10 h, 18 h, 24 h) and 0.5 mL of fresh medium was added. The release of DOX was calculated by determining the fluorescent intensities at 595 nm ($\lambda_{\text{ex}} = 488$ nm). The cumulative release ratio at every time point was calculated by dividing the cumulative amount of DOX released with the initial amount of DOX added into the dialysis bag.

In order to assess how photothermal effects affect the release of DOX from NP_{UCST}/(IR780+DOX), a 5 min NIR laser irradiation (6.0 W cm⁻²) was applied to

NP_{UCST}/(IR780+DOX) solution at 2 h after initiation of incubation at 37 °C. The release of DOX was measured by determining the fluorescence intensities at 595 nm ($\lambda_{\text{ex}} = 488 \text{ nm}$).

Cell Culture

The DOX-resistant MCF-7/DOX human breast cancer cells were cultured in complete RPMI 1640 medium supplemented with 10% FBS, 100 U mL⁻¹ penicillin and 100 mg mL⁻¹ streptomycin with addition of 1.0 $\mu\text{g mL}^{-1}$ DOX at 37 °C under a humidified atmosphere containing 5% CO₂. The DOX-sensitive MCF-7 cells were incubated the same as MCF-7/DOX cells unless 1.0 $\mu\text{g mL}^{-1}$ DOX was not added.

Cellular uptake studies

In order to study the cellular internalization and distribution, MCF-7 cells or MCF-7/DOX cells were seeded at 5×10^4 cells per well. After 24 h incubation, the cells were treated with free DOX (10 $\mu\text{g mL}^{-1}$), NP_{UCST}/DOX (DOX 10 $\mu\text{g mL}^{-1}$), NP_{UCST}/IR780 (IR780 5 $\mu\text{g mL}^{-1}$), NP_{UCST}/(IR780+DOX) (DOX 10 $\mu\text{g mL}^{-1}$, IR780 5 $\mu\text{g mL}^{-1}$) or NP_{PLGA}/(IR780+DOX) (DOX 10 $\mu\text{g mL}^{-1}$, IR780 5 $\mu\text{g mL}^{-1}$) for 6 h. After washing the cells with PBS for three times, the cells were fixed with 4% paraformaldehyde for about 20 min. In another group, MCF-7 cells or MCF-7/DOX cells were firstly incubated with NP_{UCST}/IR780 (IR780 5 $\mu\text{g mL}^{-1}$), NP_{UCST}/(IR780+DOX) (DOX 10 $\mu\text{g mL}^{-1}$, IR780 5 $\mu\text{g mL}^{-1}$) or NP_{PLGA}/(IR780+DOX) (DOX 10 $\mu\text{g mL}^{-1}$, IR780 5 $\mu\text{g mL}^{-1}$) for 2 h. The cells were then irradiated with 808 nm NIR laser (4 W cm⁻²) for 5 min. The cells were then incubated for 4 h. After washing the cells with PBS for three times, the cells were fixed with 4% paraformaldehyde for about 20 min. The fixed cells were then observed by CLSM (Leica TCS SP5).

The quantitative evaluation of intracellular DOX was studied by flow cytometry. MCF-7/DOX cells were at first seeded in a 24-well plate at a density of 1×10^5 cells per well. After incubation for 24 h, the cells were treated with NP_{UCST}/(IR780+DOX) (DOX 10 $\mu\text{g mL}^{-1}$, IR780 5 $\mu\text{g mL}^{-1}$) or NP_{PLGA}/(IR780+DOX) (DOX 10 $\mu\text{g mL}^{-1}$, IR780 5 $\mu\text{g mL}^{-1}$). 6 h later, the cell culture medium was removed. The cells were then washed with cold PBS for three

times. Another group of MCF-7/DOX cells were firstly treated with NP_{UCST}/(IR780+DOX) (DOX 10 $\mu\text{g mL}^{-1}$, IR780 5 $\mu\text{g mL}^{-1}$) or NP_{PLGA}/(IR780+DOX) (DOX 10 $\mu\text{g mL}^{-1}$, IR780 5 $\mu\text{g mL}^{-1}$) for 2 h. The cells were irradiated with 808 nm NIR laser (4 W cm^{-2}) for 5 min and then incubated for 4 h. After removing the cell culture medium, the cells were washed with cold PBS for three times. Trypsin was used to digest the cells. The cells were collected in a centrifuge tube by centrifuging for 5 min (1,000 rpm). The cells in the bottom were resuspended in 0.5 mL of PBS for flow cytometry measurement. The blank cells without any treatment were used as negative control.

Western Blot Assay

Western blot assay was used to detect the expression of P-gp in MCF-7/DOX cells after different treatments. MCF-7/DOX cells were incubated in a 12-well plate and treated with PBS, NP_{UCST}/(IR780+DOX) (DOX 10 $\mu\text{g mL}^{-1}$, IR780 5 $\mu\text{g mL}^{-1}$), and NP_{UCST}/(IR780+DOX) (DOX 10 $\mu\text{g mL}^{-1}$, IR780 5 $\mu\text{g mL}^{-1}$) with 5 min NIR irradiation, respectively. After that, the MCF-7/DOX cells were lysed and proteins were extracted from cells. The total protein was quantified using BCA Protein Quantification Kit. The proteins of each sample were then resolved by 10% sodium dodecyl sulfate polyacrylamide gel electrophoresis (SDS-PAGE) and then electrotransferred onto the polyvinylidene fluoride membrane. The membrane was incubated with TBST containing 5% nonfat dry milk for 1 h and then incubated with relevant primary antibodies (P-gp and β -actin, 1:1000 dilutions) at 4 °C overnight. After that, the membranes were washed three times with TBST and hybridized with relevant secondary antibody (1:5000 dilutions) for 1 h. The bands were visualized by chemiluminescence using an enhanced chemiluminescence detection kit.

Cytotoxicity studies

The cell viability was determined by conventional MTT assay. The cytotoxicity of different nanocarriers without laser irradiation was evaluated at first. MCF-7/DOX cells were seeded into a 96-well plate at 8,000 cells per well. After 12 h, the cell culture medium was replaced

with fresh cell culture medium containing different nanocarriers and incubated for 48 h in dark. After that, 20 μL of MTT in the concentration of 5 mg mL^{-1} was added to each well. The cells were incubated for another 4 h. Finally, 150 μL of dimethyl sulfoxide was added to every well to replace the culture medium and formazan absorbance was determined by a microplate Bio-Rad reader (Thermo Fisher Scientific) at 490 nm. Data were presented as average \pm SD ($n = 5$).

To assess the efficacy of chemo-photothermal treatment, MCF-7/DOX cells were seeded into a 96-well plate at 8,000 cells per well. After 12 h, fresh cell culture medium containing different nanocarriers was used to replace the cell culture medium and incubated for 48 h in dark. For some samples, the cells were at first cultured for 6 h and then irradiated with NIR laser (4 W cm^{-2}) for 5 min and cultured for 42 h. After that, 20 μL MTT in the concentration of 5 mg mL^{-1} was added to each well. The cells were then incubated for another 4 h. Finally, 150 μL of dimethyl sulfoxide was added to every well to replace the culture medium and formazan absorbance was determined by a microplate reader at 490 nm. Data were presented as average \pm SD ($n = 5$). The cytotoxicity of different nanocarriers or free DOX towards MCF-7 micelles was measured the same as MCF-7/DOX cells.

In order to observe the therapeutic efficacy after different treatment directly, MCF-7/DOX cells were incubated with different nanocarriers ($10 \mu\text{g mL}^{-1}$ of DOX, $5 \mu\text{g mL}^{-1}$ of IR780) in the presence or absence of NIR laser exposure (4 W cm^{-2}) for 5 min. After that, PBS was used to wash the cells. The cells were then stained with FDA for visualising live cells and PI for visualising dead cells. The images were obtained by fluorescent microscopy immediately.

Xenograft tumor mouse model

All in vivo experiments were carried out according to the “Principles of Laboratory Animal Care” (NIH publication no.86-23, revised 1985) and the guidelines for Lab Animal Welfare and Research Committee, Zhejiang University. 4-6 weeks old female BALB/c nude mice were obtained from Vital River Laboratory Animal Technology Co. Ltd. MCF-7/DOX cells

(1×10^7) were injected subcutaneously into the mice. The volume of the tumor was estimated by the Equation 2.

$$\text{Volume} = (\text{Tumor Length}) \times (\text{Tumor Width})^2 / 2 \quad (2)$$

In vivo whole body imaging and biodistribution

Once the MCF-7/DOX xenografts reached around 150 mm^3 , the tumor-bearing nude mice were divided into different groups randomly (3 mice per group). Two groups of the mice were intravenously administrated with $100 \mu\text{L}$ free IR-780, and $100 \mu\text{L}$ NP_{PLGA}/(IR780+DOX) (0.2 mg mL^{-1} IR-780 equivalent) respectively. The in vivo whole body NIR fluorescent imaging was then carried out at different time intervals by collecting the IR-780 signals.

In order to study the biodistribution of DOX, two groups of mice were tail vein injected with $100 \mu\text{L}$ free DOX, and $100 \mu\text{L}$ NP_{PLGA}/(IR780+DOX) (0.4 mg mL^{-1} equivalent) respectively. The mice were sacrificed after 48 h injection and the main organs (heart, liver, spleen, lung, kidney) and tumor tissue were harvested for bio-distribution analysis by collecting the DOX signals.

In vivo tumor growth inhibition

The nude mice bearing MCF-7/DOX tumor were divided into seven groups randomly (five mice every group). After that, the mice were tail vein injected with $100 \mu\text{L}$ of PBS, free DOX (0.4 mg mL^{-1}), NP_{UCST}/IR780 (IR780 0.2 mg mL^{-1}), NP_{UCST}/DOX (DOX 0.4 mg mL^{-1}), NP_{UCST}/(IR780+DOX) (DOX 0.4 mg mL^{-1} , IR780 0.2 mg mL^{-1}) or NP_{PLGA}/(IR780+DOX) (DOX 0.4 mg mL^{-1} , IR780 0.2 mg mL^{-1}), respectively. After 24 h post-injection, some tumors were exposed to NIR laser (4 W cm^{-2}) for 5 min. The increase of the temperature can be recorded by an infrared thermal imaging camera. All of the treatments including injection and irradiation were repeated two times at a time interval of 2 days. The tumor volume and body weight of every mouse were recorded regularly. At 21 days after first injection, the treated tumor-bearing nude mice were sacrificed. The hearts were harvested and fixed for H&E staining assay. The tumors were harvested and weighted.

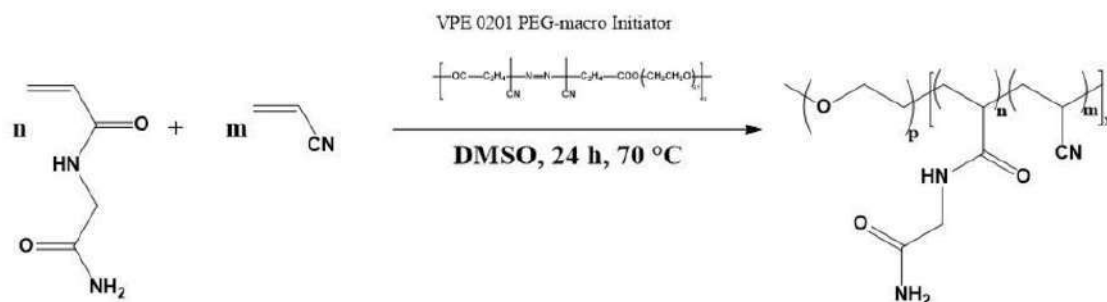
To study the levels of proliferation and apoptosis in tumor tissues after treating with different formulations, Immunohistochemistry was used. The tumor tissues were collected at 24 h after different treatments. The tissue samples were fixed for H&E, Ki67, and TUNEL assay.

Statistical Analysis

Data were expressed as mean \pm SD. The one-way ANOVA analysis was used to determine the statistical significance using no significance: n.s, *P < 0.05, **P < 0.01, ***P < 0.001.

References

[1] J. Seuring, M. F. Bayer, K. Huber, S. Agarwal. *Macromolecules* **2012**, *45*, 374-384.



Scheme S1. Schematic illustration of the synthesis of PEG-*b*-P(NAGA-*co*-AN).

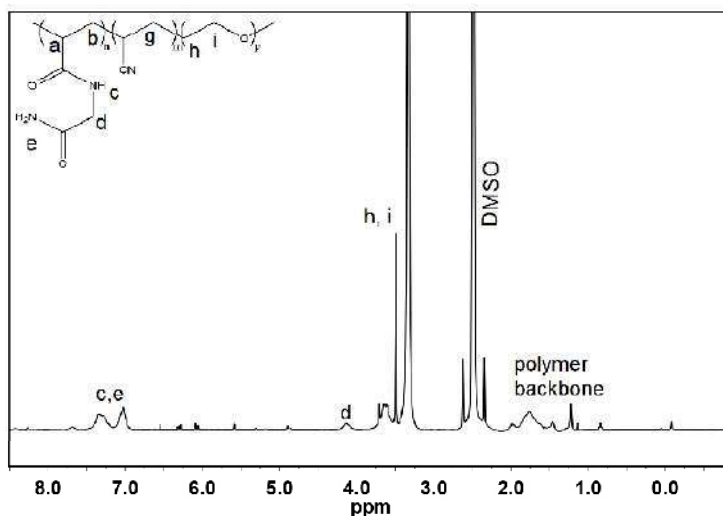


Figure S1. ^1H NMR spectrum of PEG-*b*-P(NAGA-*co*-AN) in DMSO- d_6 . (300 MHz, DMSO- d_6) δ /ppm: 1.2–2.1 (polymer backbone, $-\text{CH}_2-$), 2.1–2.6 (polymer backbone, $-\text{CH}-$), 3.5 ($-\text{OCH}_2$); 4.2 ($-\text{NH}-\text{CH}_2$); 6.9–7.3 ($-\text{NH}$, $-\text{NH}_2$).

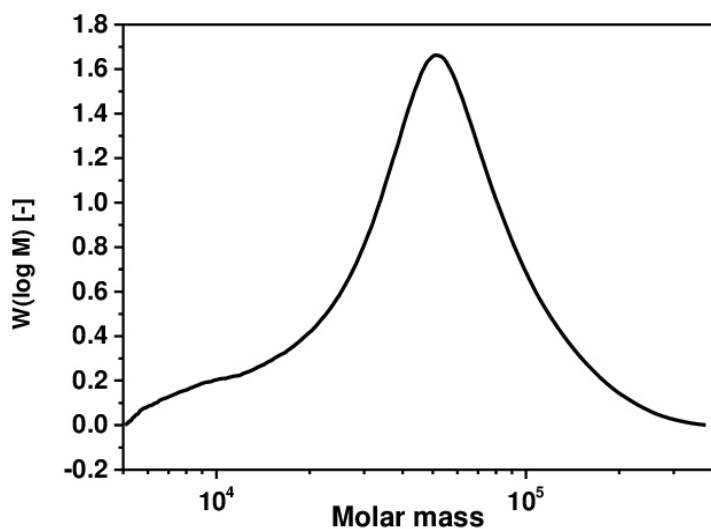


Figure S2. The GPC trace of PEG-*b*-P(NAGA-*co*-AN) measured in DMSO. $M_n = 36,000$, $M_w/M_n = 1.7$.

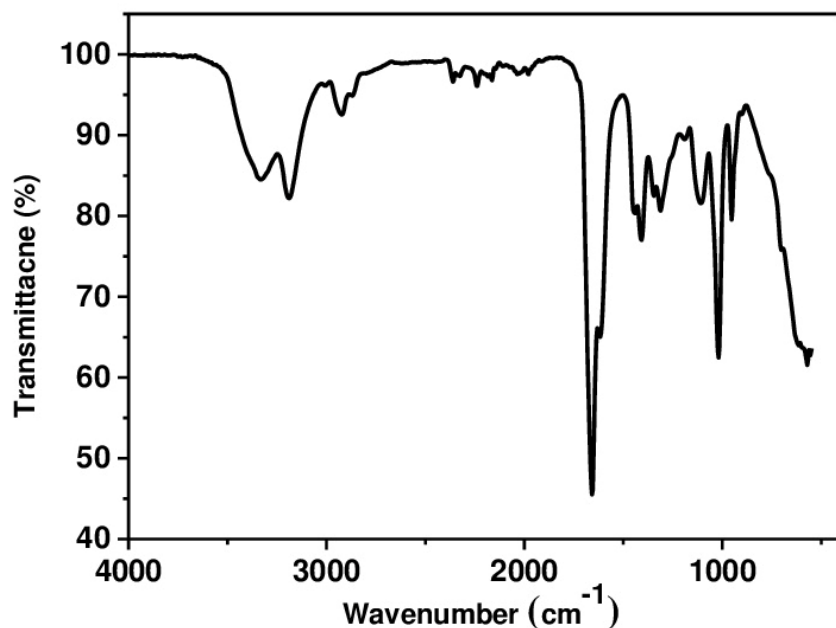


Figure S3. FT-IR spectrum of PEG-*b*-P(NAGA-*co*-AN). ATR-FTIR: 3650–3050 (mb, -NH), 3000–2850 (w, -CH₂), 2244 (w, -CN), 1654 (vs, -CO), 1413 (m, -CH-), 1348 (m, -CH-), 1312 (m, -CH-), 1118 (w, -C-N), 1018 (w, -C-O-C) cm⁻¹. Copolymer composition: 32-mol % acrylonitrile, 68-mol % *N*-acryloylglycinamide.

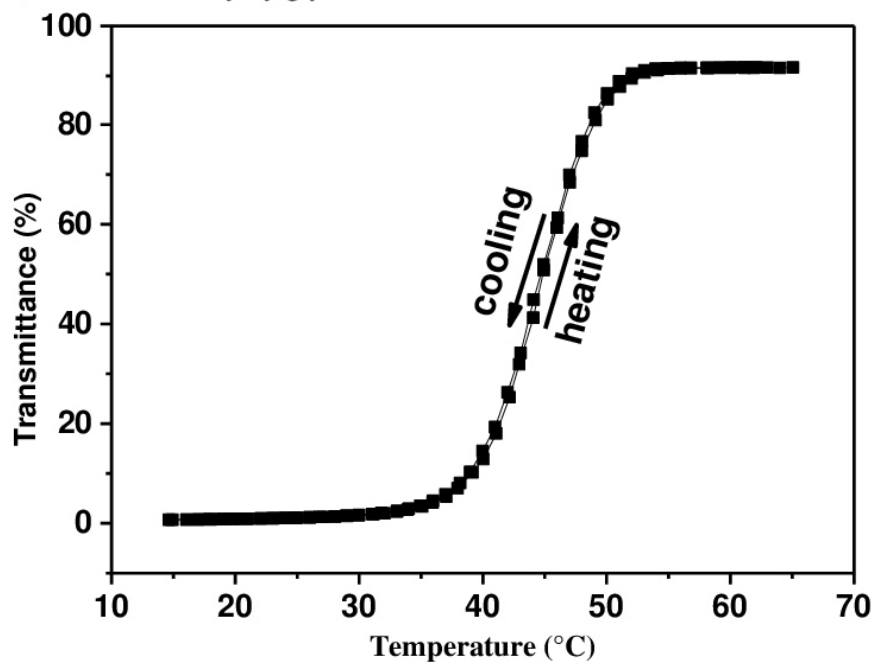


Figure S4. Turbidity measurement of PEG-*b*-P(NAGA-*co*-AN) in aqueous solution with a concentration of 1 wt. %. The cloud point was taken at the point of inflection of the curve.

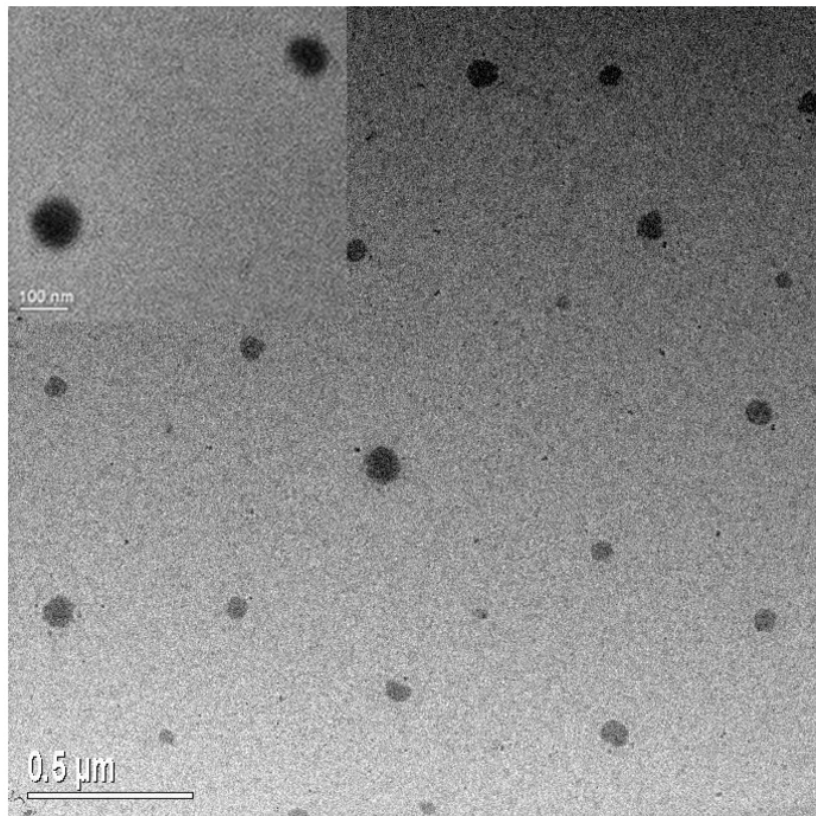


Figure S5. The TEM image of PEG-*b*-P(NAGA-*co*-AN) micelles at 25 °C. Inset shows the magnified TEM image of PEG-*b*-P(NAGA-*co*-AN) micelles.

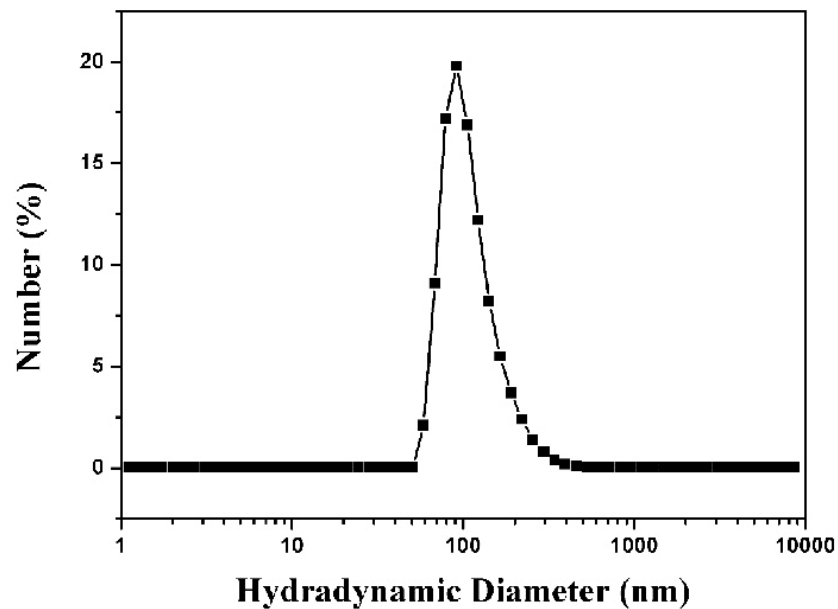


Figure S6. The DLS result of PEG-*b*-PLGA micelles in aqueous solution.

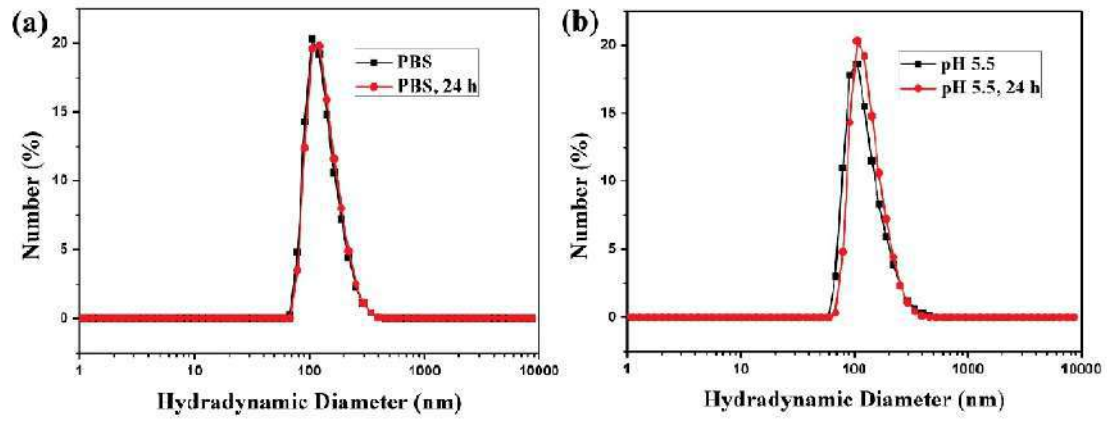


Figure S7. The DLS results of $\text{NP}_{\text{UCST}}/(\text{IR780}+\text{DOX})$ micelles in PBS and lysosomal pH (pH 5.5).

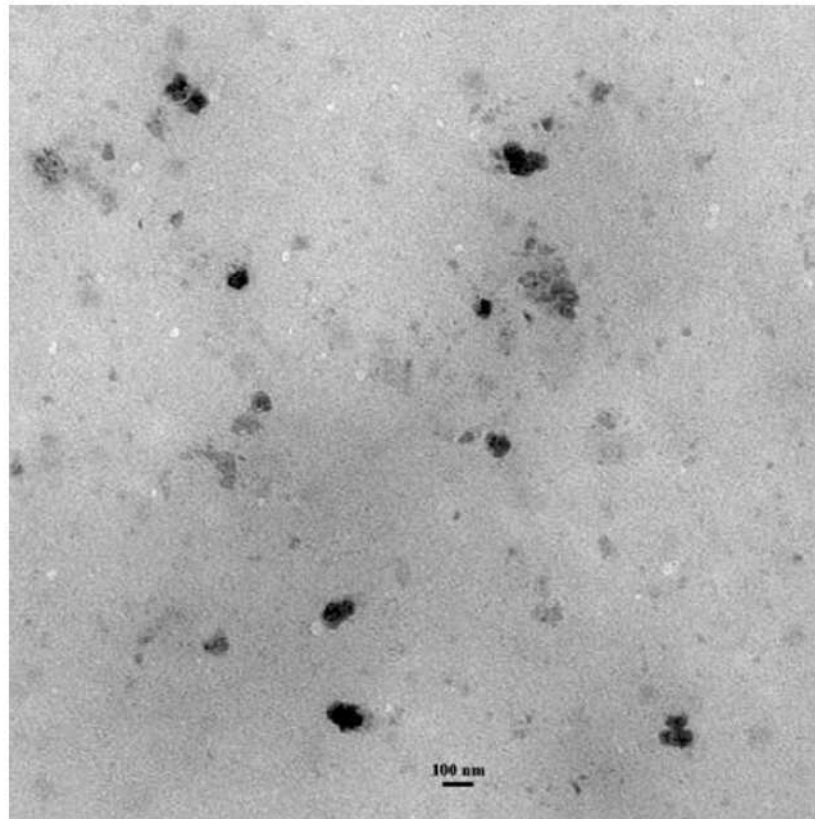


Figure S8. The TEM image of $\text{NP}_{\text{UCST}}/(\text{IR780}+\text{DOX})$ micelles after 5 min NIR laser irradiation.

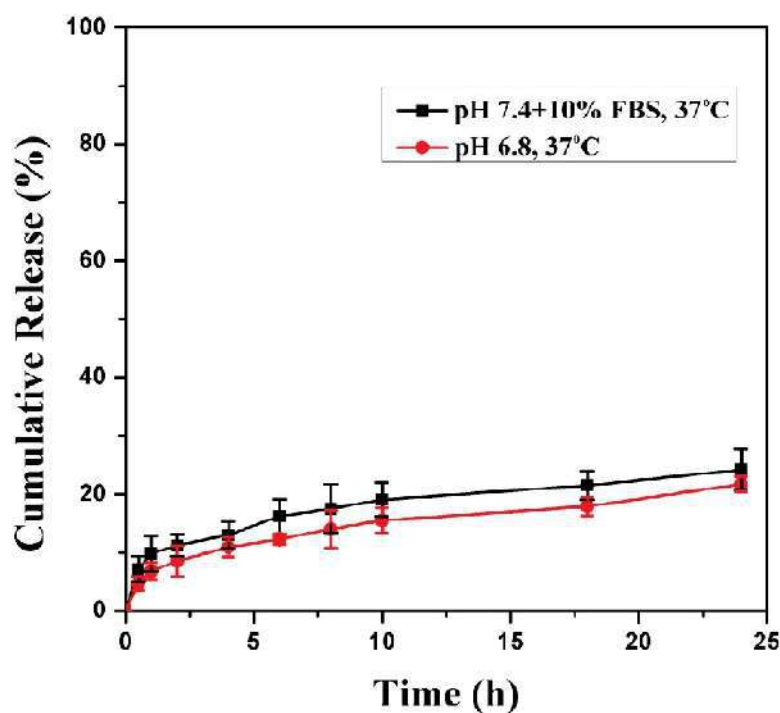


Figure S9. In vitro release of DOX from PEG-*b*-P(NAGA-*co*-AN) micelles at pH 7.4 with 10% FBS or at pH 6.8 at 37°C.

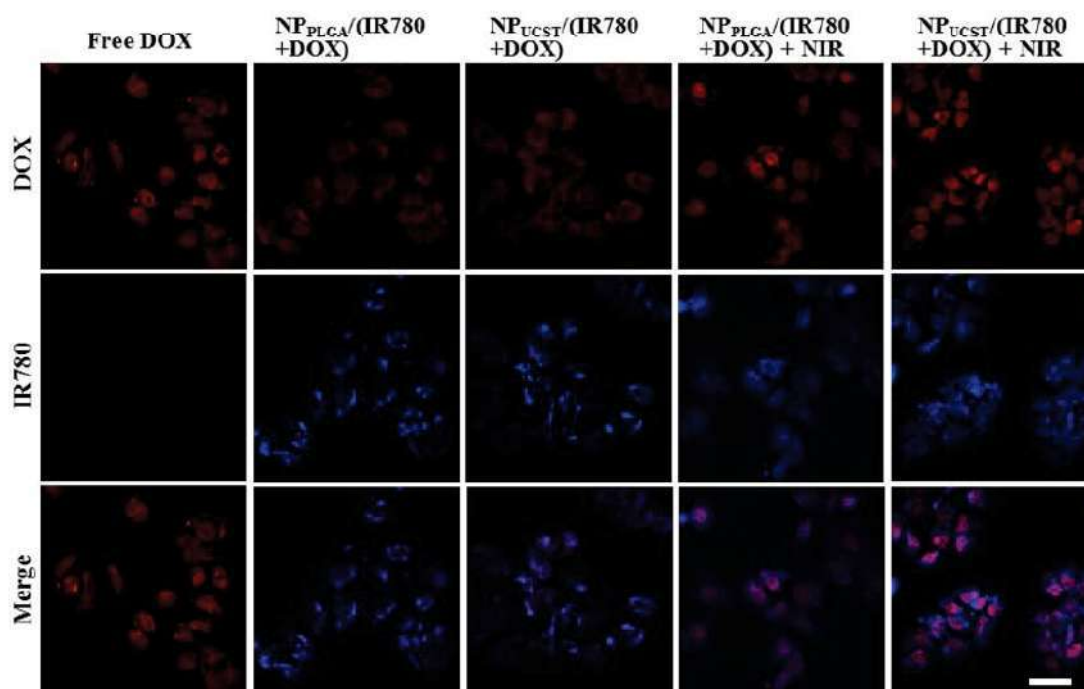


Figure S10. Cellular uptake of different nanocarriers ($\sim 5.0 \mu\text{g mL}^{-1}$ IR780, $\sim 10.0 \mu\text{g mL}^{-1}$ DOX) after incubation with MCF-7/DOX cells for 6 h. Some samples were irradiated with NIR laser (4 W cm^{-2}) for 5 min. Scale bar: 25 μm .

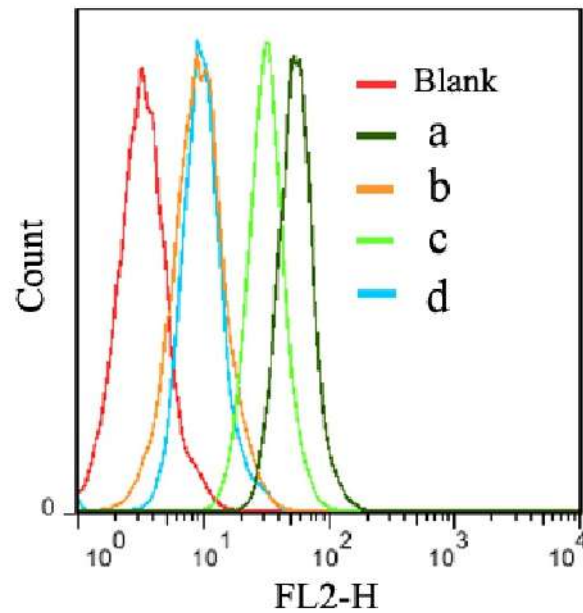


Figure S11. Flow cytometry analysis of intracellular DOX fluorescence after incubation of $\text{NP}_{\text{UCST}}/(\text{IR780}+\text{DOX})$ with MCF-7/DOX cells for 2 h with (a) or without (b) laser irradiation. $\text{NP}_{\text{PLGA}}/(\text{IR780}+\text{DOX})$ with (c) or without (d) laser irradiation was used as control.

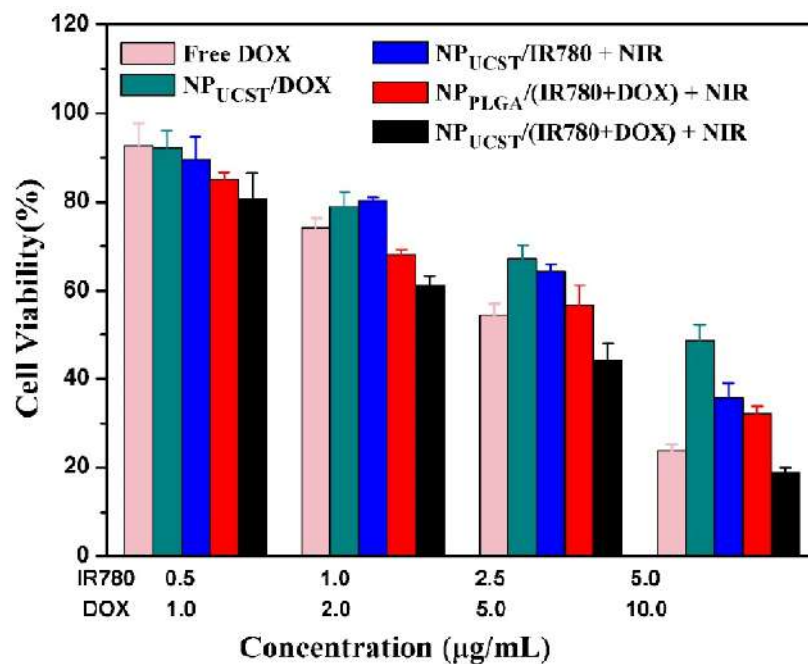


Figure S12. Proliferation inhibitions toward MCF-7 cells after different treatments by MTT assay.

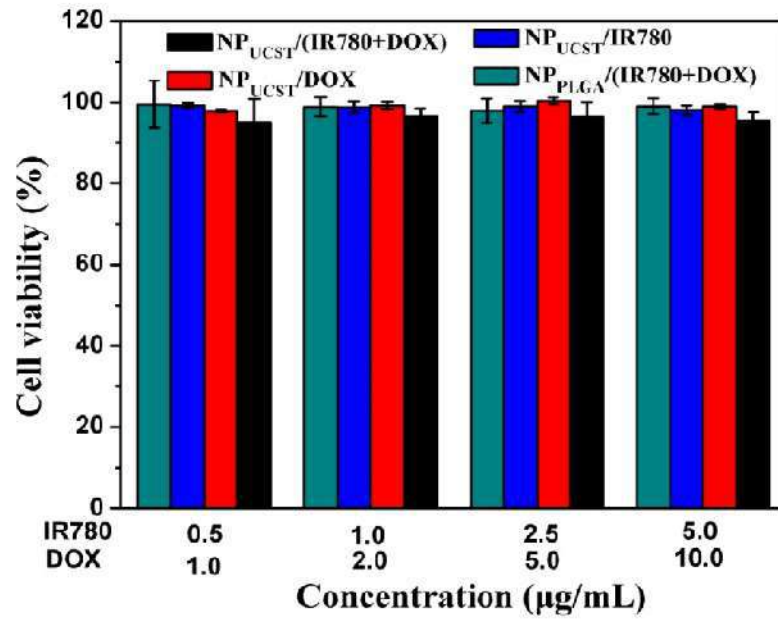


Figure S13. Quantitative evaluation of cell viability of MCF-7/DOX cells after different treatments.

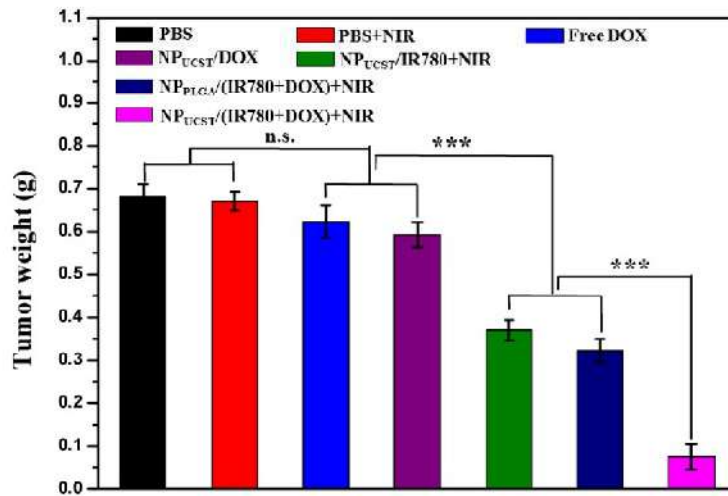


Figure S14. Average tumor weights after different treatments.

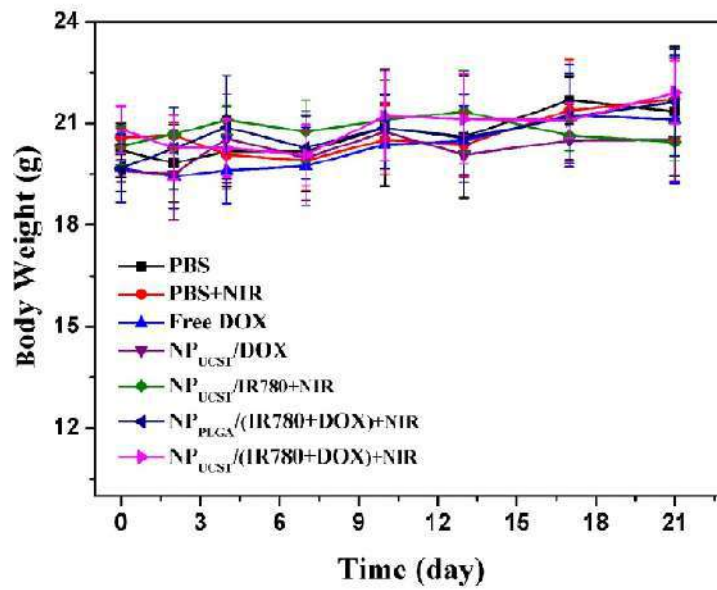


Figure S15. Body weight curves of MCF-7/DOX tumor bearing mice after different treatments.

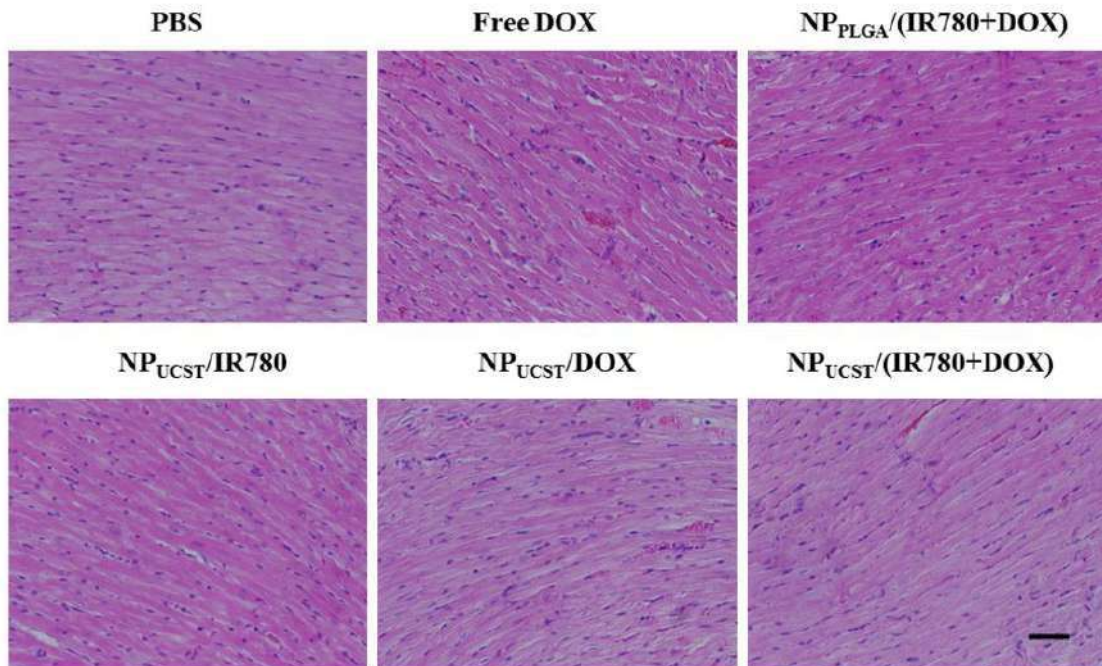


Figure S16. H&E stained images of hearts harvested from the mice with different treatments. Scale bar: 50 μ m.

7.4 Tuning the Phase Transition from UCST-Type to LCST-Type by Composition Variation of Polymethacrylamide Polymers

This work was published by **F. Käfer**, M. Pretscher, S. Agarwal, *Macromolecular Rapid Communication* **2018**, 1800640.

Reprinted with permission; Copyright 2018 WILEY-VCH Verlag GmbH & Co. KGaA,
Weinheim



Tuning the Phase Transition from UCST-Type to LCST-Type by Composition Variation of Polymethacrylamide Polymers

Florian Käfer, Martin Pretscher, and Seema Agarwal*

Polymethacrylamide copolymers with hydrophobic *N*-substituted acrylamides, such as *N*-cyclohexylacrylamide and *N*-*tert*-butylacrylamide, are rare examples of polymers showing composition-dependent thermoresponsive behavior in water. They show unexpected behavior different from the conventional copolymers of a thermoresponsive polymer with hydrophobic comonomers. On increasing the amount of the hydrophobic comonomer in the polymer, there is a change from UCST-type phase behavior to complete solubility, followed by compositions showing LCST-type transition and insolubility in water (U-S-L-I-type change). At 50 mol% of less hydrophobic *N*-*tert*-butyl acrylamide (logP 0.87) in contrast to ≈25 mol% of *N*-cyclohexylacrylamide (logP 1.51), the broad UCST-type transition of polymethacrylamide is turned to LCST-type transitions with very narrow hysteresis in water and PBS buffer. The use of H-bond and water-structure breaker showed the role of H-bonding and hydrophobic interactions in phase transitions of UCST-type and LCST-type, respectively. This work is an important add-on to the infant field of nonionic polymers of UCST-type.

Thermoresponsive polymers showing lower critical solution or upper critical solution temperatures (LCST and UCST, respectively) in water as well as in electrolyte solutions are of great interest in a wide field of applications.^[1–7] In the last more than two decades, a lot of research efforts were devoted toward finding out new examples of polymers exhibiting LCST-type transition, tuning of their critical temperatures, understanding the mechanism of phase transitions and applications.^[7,8] The research regarding nonionic polymers showing UCST-type transitions in water undisturbed by the presence of electrolytes has picked up pace only in the last 5–6 years.^[9–16] Copolymers of acrylamide (AAm) and *N*-acryloylglycinamide (NAGA) each with acrylonitrile (AN) are one of the universal examples showing sharp UCST-type transitions with narrow hysteresis in water and buffer solutions.^[17,18] The cloud point could be tuned in a wide temperature range by changing the copolymer composition which is also a very well observed phenomenon in polymers with LCST-type transitions.^[19] The effect of molar mass, chain ends, polymer concentration, and the effect of

comonomers on cloud points is studied for UCST-type copolymers based on AAm and NAGA homo- and copolymers.^[16,20]

Thermoresponsive polymers depending upon their structure clearly show either LCST-type or UCST-type transitions. Multiple transitions in one system are possible in case of block copolymers and polymer-clay composites.^[21–23] A unique phenomenon, such as the change in the thermoresponsive behavior (i.e., LCST-type to UCST-type or vice versa) of a polymer in water, is seen in some specific examples due to the change in the hydrophilicity/hydrophobicity ratio. One of such examples is a graft copolymer of poly(vinyl alcohol) and poly(*p*-dioxanone) (PDO) which shows either UCST-type or LCST-type transition in water depending upon the length of the PDO graft.^[24]

In this work, we show a rare example of composition-dependent thermoresponsive

behavior of the copolymers of methacrylamide (MAAm) with hydrophobic comonomers, such as *N*-cyclohexylacrylamide (NchAAm) and *N*-*tert*-butylacrylamide (NtbAAm). Polymethacrylamide (PMAAm) homopolymer shows a UCST-type phase transition with a broad hysteresis. Copolymerization with hydrophobic comonomers in different feed ratios showed a unique behavior, which was different from the conventional copolymers. The conventional and routine chemistry is expected to simply change the cloud points (temperature of phase transition for a particular concentration) on copolymerization with hydrophobic comonomer in different amounts. For UCST-type transitions, the hydrophobic comonomer should decrease the cloud point on increasing the amount of the comonomer. However, in our case, it is not only the cloud points. Altogether, the phase transition-type changed. The thermoresponsive behavior can be tuned to UCST-type with different cloud points, LCST-type, and temperature-independent solubility just by changing the copolymer composition. This effect is different from the commonly observed phenomenon of changed cloud points on use of hydrophobic comonomer in thermoresponsive polymers and is rarely observed.^[25,26]

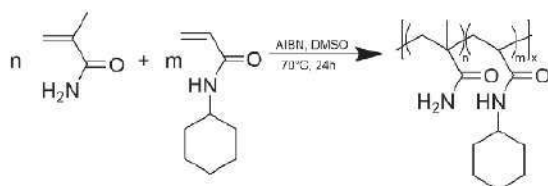
Copolymers of MAAm with NchAAm were synthesized using free radical polymerization (Scheme 1).

The copolymers were structurally characterized using ¹H NMR spectroscopy. The polymer backbone protons of MAAm and NchAAm (protons marked in Figure S1a–d, Supporting Information) and –CH₂ protons of cyclohexane ring of NchAAm (protons marked in Figure S1f, Supporting Information)

F. Käfer, M. Pretscher, Prof. S. Agarwal
Macromolecular Chemistry II and Bayreuth Center for Colloids
and Interfaces, Universitätsstrasse 30
95440, Bayreuth, Germany
E-mail: agarwal@uni-bayreuth.de

The ORCID identification number(s) for the author(s) of this article can be found under <https://doi.org/10.1002/marc.201800640>.

DOI: 10.1002/marc.201800640



Scheme 1. Reaction scheme for the synthesis of copolymers of MAAM and NchAAM. Reactions were carried out in dimethylsulfoxide (DMSO) with azobisisobutyronitrile (AIBN) as radical initiator.

overlapped between 0.5 and 2.3 ppm. $-\text{CH}$ (ϵ proton) of NchAAM was observed as a distinct signal centered at 3.5 ppm. Using the integral for the copolymer backbone protons (Figure S1a–d,f, Supporting Information) and the integral of ϵ proton of NchAAM, the copolymer composition was determined as shown in (Table 1). Furthermore, the reactivity ratios were calculated, $r_{\text{MAAM}} = 0.24$ and $r_{\text{NchAAM}} = 0.07$ using the Fineman–Ross method, indicating a statistical distribution of comonomers (Figure S2, Table S1, Supporting Information). The molar masses of the copolymers were determined by performing GPC measurements using DMSO as solvent. The copolymers showed molar masses in a range of around $M_n = 27800$ to 48500 depending upon the copolymer composition (Figure S3, Supporting Information). Differential scanning calorimetric measurements (Figure S4, Supporting Information) showed only one glass transition temperature for the copolymers which increased from $T_g = 160$ °C for P(NchAAM) homopolymer up to $T_g = 248$ °C for the composition MAAM:NchAAM, 98:2 with the lowest amount of NchAAM, whereas PMAAM itself showed a $T_g = 251$ °C.^[27]

The phase transition behavior was investigated by monitoring transmittance (%) at different temperatures. PMAAM displays a sharp transition of soluble-to-insoluble (UCST-type) on cooling a transparent solution with cloud point around 35 °C. The sample showed a broad hysteresis and the cloud point during heating was ≈ 55 °C (Figure 1a).

This was previously reported by the authors.^[17] The formation and breakage of intermolecular H-bonding interactions due to the amide units with change in temperature is responsible for the UCST-type transition. P(NchAAM) itself is insoluble in water in the tested temperature range of 5–80 °C. On

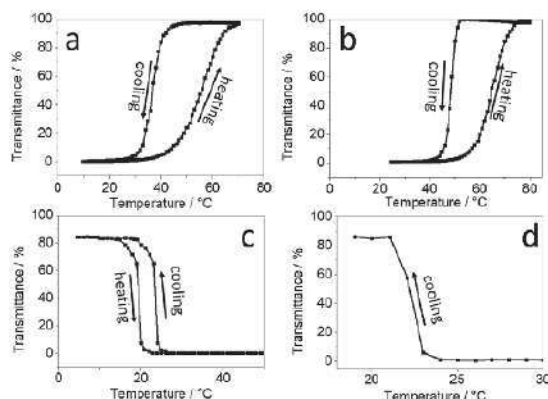


Figure 1. Phase separation in water as monitored by measuring transmittance (%) at different temperatures during cooling and heating cycles: a) 1 wt% (PMAAM); b) 1 wt% (Table 1, entry 2); c) 1 wt% (Table 1, entry 5); d) cloud point (cooling) of (Table 1, entry 5) in PBS. Heating rate: 1 °C min⁻¹.

the contrary, the copolymers interestingly showed a change in the thermoresponsive behavior depending upon the copolymer composition, that is, it varies from UCST-type phase transition of PMAAM to sharp LCST-type transitions with less hysteresis (Figure 1b,c). The copolymer containing about 2 mol% of hydrophobic NchAAM showed UCST-behavior similar to that of homo-PMAAM, but with increased cloud points on heating and cooling (48/65 °C cooling/heating) due to the increased hydrophobicity (Figure 1b). The increase in the cloud point on incorporation of hydrophobic comonomer is, by now, a well-studied phenomenon for acrylamide-based UCST-type copolymers in which the increased amount of acrylonitrile AN led to a continuous increase in the cloud point.^[17]

For MAAM copolymers with hydrophobic comonomer, a different observation was made. Further, increasing the amount of NchAAM in the copolymers up to 10 mol% led to the formation of soluble polymers in water. For 1 wt% solution in water, no transmittance change with temperature was observed in the temperature range from 5 to 80 °C. It seems that bulky cyclohexane groups hindered the polymer–polymer interactions of H-bonding-type between the amide units of PMAAM and made the polymer soluble till about a particular copolymer composition. On increasing the amount of NchAAM to about 25 mol% in the copolymer, a different phase transition behavior was observed. It changed to a soluble–insoluble-type (LCST-type) transition (Figure 1c). The polymer–water interactions outweighed till a critical temperature (cloud point) providing solubility. On increasing the temperature beyond the critical temperature, the polymer–polymer interactions (hydrophobic interactions) dominated leading to phase separation. For 1 wt% solution, the cloud point on cooling was about 23 °C and a very narrow hysteresis of about 3–4° was observed. Furthermore, the cloud point was not changed significantly in PBS buffer (0.1 M) (Figure 1d).

The phase transition behavior of MAAM and NchAAM copolymers in the presence of urea changed significantly for both UCST-type (Figure 2a) and LCST-type (Figure 2b) transitions depending upon the concentration.

Table 1. Copolymers of MAAM and NchAAM and their thermoresponsive behavior.

| Entry | NchAAM in polymer [mol%] | T_g [°C] | Cloud point cooling/heating [°C] | D | M_n |
|-------|--------------------------|------------|----------------------------------|-------------------|--------|
| 1 | 0 | 251 | UCST 35/55 | N/A ^{a)} | N/A |
| 2 | 2 | 248 | UCST 48/ 65 | N/A | N/A |
| 3 | 5 | 223 | Soluble | N/A | N/A |
| 4 | 10 | 210 | Soluble | 1.6 | 33 800 |
| 5 | 25 | 212 | LCST 23/20 | 1.6 | 48 500 |
| 6 | 50 | 180 | Insoluble | 1.9 | 27 800 |

^{a)}N/A, not determined due to insolubility in DMSO.

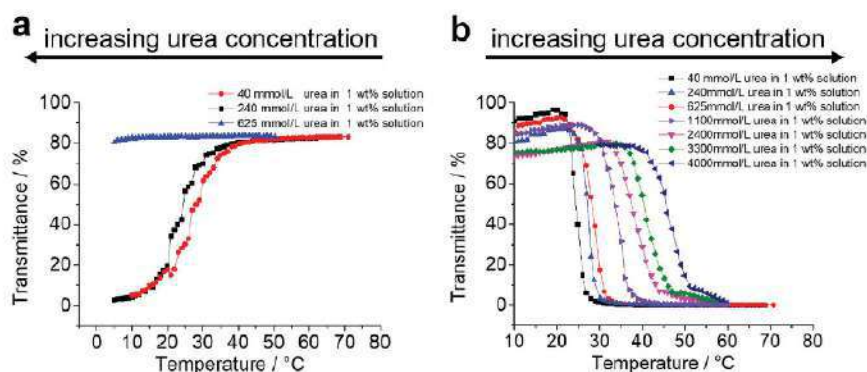


Figure 2. a) Cooling curves (of Table 1, entry 2) with a polymer concentration of 1 wt% in aqueous solution with increasing amount (40–625 mM) of urea; b) cooling curves (of Table 1, entry 5) with a polymer concentration of 1 wt% in aqueous solution with increasing amount (40–4000 mM) of urea. Heating rate: 1 °C min⁻¹.

The cloud point is decreased significantly from 48 °C (cooling) to 25 °C (cooling) with a concentration of urea (40 mM) for a copolymer with 2 mol% of NchAAm (Table 1, entry 2). By further increasing the urea concentration to 625 (mM), the UCST disappeared completely and the polymer did not separate out on cooling and remained soluble. The urea is an H-bond breaker and decreased the polymer–polymer interactions and hence there was an increase in solubility in water on increasing its concentration. This proves the role of H-bonding interactions in UCST-type transition of the PMAAm and its copolymers with NchAAm.

For LCST-type transitions, beyond the critical point, entropy-unfavorable ordering of water molecules around the nonpolar polymer supports stronger hydrophobic interactions and hence the phase separation at higher temperature.^[28] The well-known water-structure breaker urea changed the cloud point depending upon its concentration for the copolymer with 25 mol% of NchAAm (Figure 2b). In general, the cloud point of LCST-type increased on adding urea in water. The cloud point could be increased from 23 °C (cooling) without urea to about 50 °C with a concentration of ($c_{\text{urea}} = 4 \text{ M}$). In addition, a decrease in the maximum transmittance (%) below LCST could be observed with increasing concentration of urea. This is attributed to the disturbed hydrogen bonds between acrylamide units with water molecules below LCST due to the presence of urea. A copolymer with 50 mol% and more of NchAAm was insoluble in water due to the strong hydrophobic effect of NchAAm units in the resulting copolymer.

The change in enthalpy (ΔH) during the phase transition plays a considerable role for the phase transition of LCST-type polymers.^[29] This is in contrast to most of the polymers which are showing a UCST-type transition in aqueous solution.^[4] For these polymers, the entropic change (ΔS) is the major factor. The enthalpy change of the polymers as detected by the micro-DSC measurements is presented in Figure 3. For the copolymer showing LCST-type phase transition (Table 1, entry 5), a strong change in the enthalpy during the phase transition is apparent. It is well-known that the LCST polymers form a well-ordered hydration shell at lower temperatures, which will be disordered upon heating resulting in a positive ΔH .^[29] According to

the expectation, almost no change in ΔH upon heating of the UCST-type copolymer was measured.

Poly(*N*-isopropylacrylamide (PNiPAAm) is one of the known examples showing concentration-independent phase transition in the concentration range 0.01–1 wt%.^[30] The copolymer with molar ratio of MAAm:NchAAm, 75:25 (Table 1, entry 5) also showed no significant effect of polymer concentration on cloud point or phase transition behavior. At low concentration (0.1 wt%), the phase transition was broad (Figure 4, Figures S5 and S6, Supporting Information). This is in contradistinction to the copolymer composition MAAm:NchAAm, 98:2 that show UCST-type phase transition. With increasing concentration, an increase of the cloud point could be determined, whereby from a concentration of 2 wt% the polymer can no longer be dissolved in a temperature range of 5–80 °C.

Further, few other hydrophobic comonomers were tested for studying their influence on thermoresponsive properties of PMAAm. A comparable phase transition behavior could be observed for copolymers of MAAm and NtbAAm (Figure 5, Table 2).

The copolymers were characterized by ¹H NMR, GPC measurements (Figures S7 and S8, Supporting Information). In this case too, the change in copolymer composition changed the phase transition behavior in water. Although the general trend of effect of polymer composition in changing UCST-type transitions for copolymers with less amount of the comonomer (NchAAm and NtbAAm) to the LCST-type transitions for large amount of the comonomer in copolymers remained same,

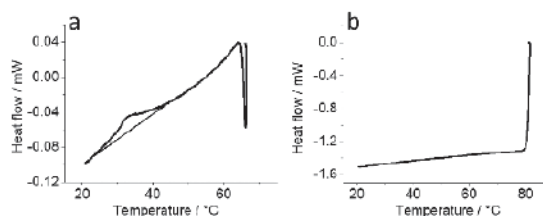


Figure 3. Cooling curves of a μ DSC measurements of a) LCST-type (Table 1, entry 5); b) UCST-type (Table 1, entry 2). Heating rate: 0.25 °C min⁻¹.

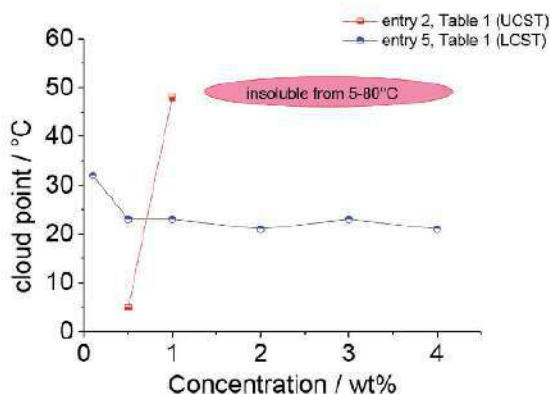


Figure 4. Cloud points as a function of concentration (of Table 1, entry 2 and Table 1, entry 5). Heating rate: $1\text{ }^{\circ}\text{C min}^{-1}$.

the composition at which it occurred was different. Change of *N*-cyclohexyl group with *N*-tert butyl group brought a change in the hydrophobicity of the polymer chain and the steric hindrance from the side chain. The $\log P$ (partition coefficient in 1-octanol-water), a symbol of hydrophobicity of monomers as calculated by ChemDraw, is 1.51 and 0.84 for NchAAm and NtbAAm, respectively. This shows lower hydrophobicity of NtbAAm. Therefore, the copolymers with much higher content (50 mol%) of NtbAAm in comparison to NchAAm copolymers showed LCST-type transition. The similar behavior was seen in the copolymers of NAGA and diacetone acrylamide (DAAM)^[25] showing LCST-type transitions for higher amounts (45–65 mol%) of the DAAM in the copolymers. This system is one of the first examples showing copolymer composition-dependent change in the thermoresponsive behavior.

By copolymerization with other *N*-substituted acrylamide comonomers, such as *N*-*n*-hexylacrylamide ($\log P = 2.04$), *N*-furfurylacrylamide ($\log P 0.37$), no change in phase transition behavior could be observed. The synthesized copolymers were either insoluble or completely soluble in a temperature range of 5–80 $^{\circ}\text{C}$. This indicates a complex hydrophobic/hydrophilic balance effect, with the size and hydrophobicity of the *N*-substituents representing the decisive influencing variables. In order to better comprehend these influencing variables in the future, further detailed research is required. Here, the use of dynamic light scattering (DLS) and neutron scattering could give a detailed impression of the dynamic at the phase transition as well as the change in morphology due to the influencing variables mentioned above.

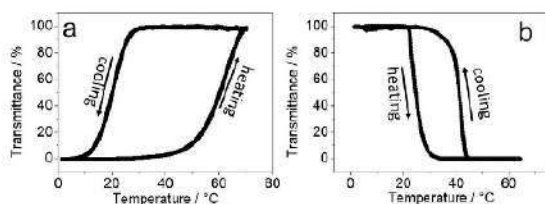


Figure 5. Transmittance (%) versus temperature hysteresis curves in pure water: a) 1 wt% (Table 2, entry 1); b) 1 wt% (Table 2, entry 5). Heating rate $1\text{ }^{\circ}\text{C min}^{-1}$ for all measurements.

Table 2. Copolymers of MAAM and NtbAAm and their thermoresponsive behavior.

| Entry | NtbAAm in polymer [mol%] | Cloud point cooling/heating [$^{\circ}\text{C}$] | \bar{M}_w | M_n |
|-------|--------------------------|--|-------------------|--------|
| 1 | 2 | UCST 11/60 | N/A ¹⁾ | N/A |
| 2 | 5 | Soluble | 2.5 | 13 000 |
| 3 | 10 | Soluble | 1.5 | 41 000 |
| 4 | 25 | Soluble | 1.5 | 30 000 |
| 5 | 50 | LCST 41/24 | 2.2 | 19 500 |
| 6 | 100 | Insoluble | N/A | N/A |

¹⁾N/A, not determinable due to insolubility in DMSO.

The unique polymer example showing a rare phenomenon of switching the type of thermoresponsive phase transition in water from UCST-type to LCST-type through completely soluble and insoluble states dependent upon the copolymer composition is given in **Figure 6**.

The copolymers of MAAM with hydrophobic NchAAm and NtbAAm monomers made by conventional radical polymerization showed this peculiar behavior. PMAAM homopolymer showed a UCST-type transition in water with a broad hysteresis. The addition of a hydrophobic comonomer in the form of a copolymer till a definite composition retained UCST-type transition with increased cloud point. Further increase in the comonomer amount led to compositions that were completely soluble in water. After a critical composition, the copolymer showed LCST-type transition with narrow hysteresis followed by completely insoluble polymers on increasing the amount of the comonomer. The composition at which transition from UCST-type to LCST-type phase transition shifted was dependent upon the hydrophobicity of the comonomer. The role of H-bonding in thermoresponsive transitions is shown by studying phase transitions in the presence of urea. The cloud point of LCST-type increased with increased amount of urea, whereas for

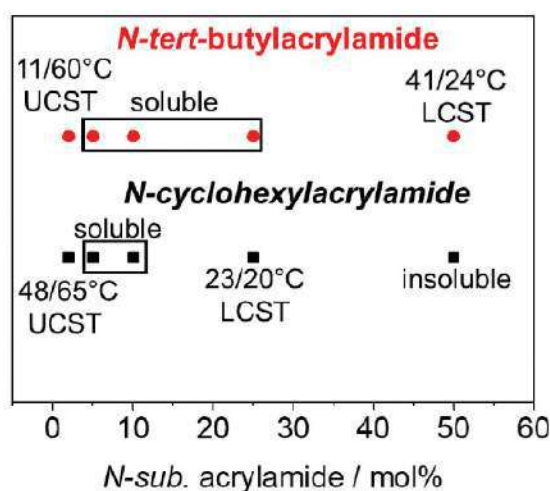


Figure 6. Composition-dependent change in the solubility of methacrylamide copolymers.



UCST-type transition was decreased. This interesting and rare example should be further studied by light and neutron scattering measurements in the future for understanding the transitions in detail.

Experimental Section

Materials: Dimethyl sulfoxide (DMSO) ($\geq 99.9\%$ ACS reagent) and *N*-*tert*-butylacrylamide (NtbAAm) (97%) were purchased from Sigma-Aldrich. NtbAAm was recrystallized from ethanol to remove the stabilizer. *N*-cyclohexylacrylamide (NchAAm) was synthesized according to the procedure described below. 2,2'-Azobisisobutyronitrile (AIBN, Fluka) was recrystallized from ethanol. A Milli-Q Plus system (conductivity = $0.072 \mu\text{S cm}^{-1}$) was used for getting pure water.

Synthesis of *N*-Cyclohexylacrylamide (NchAAm): *N*-cyclohexylacrylamide was synthesized by the condensation of acryloyl chloride (Sigma Aldrich $>97\%$) purified by distillation under reduced pressure and cyclohexylamine (Sigma Aldrich 99.9%, recrystallized from ethanol). The reaction was carried out in dichloromethane. Therefore, cyclohexylamine (5 g, 1 eq) was dissolved in 40 mL dichloromethane and cooled down to 0°C followed by the addition of triethylamine (5.6 g, 1.1 eq). To this solution, acryloyl chloride (5.3 mL, 1.2 eq) was added dropwise over 60 min. The reaction solution was stirred further for 14 h at room temperature. After 14 h, the solution was washed first three times with Milli-Q water followed by 0.1 molar NaOH/water solution and was brined three times. The dichloromethane phase was collected and reduced at rotary evaporator. The raw product was purified by column chromatography using silica gel as column material with dichloromethane/methanol (3:1 v/v) as eluting solvent and was dried afterward under vacuum at room temperature. Yield: 89%. $^1\text{H NMR}$ (500 MHz, $\text{DMSO-}d_6$, δ): 7.94 (s, H, NH), 6.19 (3H; $-\text{CH}=\text{CH}_2$), 3.71 (1H; $-\text{NH}-\text{CH}-$, cyclohexene), 1.70–1.16 (d, 10H, cyclohexene $-\text{CH}_2$) ppm.

Synthesis of Copolymers of Methacrylamide (MAAm) with *N*-Cyclohexylacrylamide (NchAAm) and *N*-*tert*-Butylacrylamide (NtbAAm): The copolymers were made by free-radical polymerization using different ratios of the comonomers. The detailed procedure is described for a copolymer of MAAm and NchAAm with feed molar ratio MAAm:NchAAm, 75:25. NchAAm (76.6 mg) and MAAm (128 mg) were dissolved in 2 mL of DMSO and degassed by three freeze-thaw pump cycles. Afterward, AIBN (1 mg [0.3 eq] based on the total monomer amount) was added as a solution (10 mg AIBN dissolved in 1 mL DMSO) and the polymerization was carried out at 70°C for 24 h. The polymers were precipitated in methanol, washed three times, and dialyzed against water for 3 days to remove monomer impurities. Afterward, the solution was lyophilized. The same procedure was used for making copolymers with other feed compositions and copolymers of MAAm with NtbAAm. To determine the copolymerization parameters, the reactions were stopped at low conversions, less than 20%.

Characterization: The glass transition points (T_g) were determined using differential scanning calorimetry (DSC, Type DSC 821e, Mettler Toledo). The measurements were carried out under N_2 atmosphere from 0 to 300°C with a heating rate of $10^\circ\text{C min}^{-1}$. The results were analyzed from the second heating cycle.

Turbidity measurements were performed on a JASCO V-630 Spectrophotometer at 660 nm with continuous stirring at a heating rate of $1.0^\circ\text{C min}^{-1}$. The cell path length was 10 mm. The cloud points were determined at the point of inflection of transmittance (%). For measurements, the samples were dissolved in Millipore water/phosphate buffer and the measurement was started from cooling cycle in the temperature range from 5 to 80°C .

The molar mass and the molar mass distribution \bar{M} were determined by gel permeation chromatography (DMSO) as eluent. A precolumn (PolarSil PSA080505; particle size 5 mm, dimension 8.0×3 50 mm) and two PSS PolarSil linear S (particle size 5 mm, dimension $8.0 \times 3 \times 300$ mm) columns were used. Pullulan of different molar

masses with narrow dispersity were used as standards. The flow rate was 0.7 mL min^{-1} at a temperature of 75°C . As detector, a differential refractive index detector was used. The software PSS WinGPC Unity, Build 1321, was used in order to determine the molar mass and \bar{M} . $^1\text{H-NMR}$ measurements were performed on a 500 MHz Bruker Avance III HD 500 with $\text{DMSO-}d_6$ as solvent.

Supporting Information

Supporting Information is available from the Wiley Online Library or from the author.

Acknowledgements

The authors would like to thank Deutsche Forschungsgemeinschaft (DFG) for the financial support.

Conflict of Interest

The authors declare no conflict of interest.

Keywords

composition, LCST, polymethacrylamide, thermoresponsive polymers, UCST

Received: August 30, 2018
Revised: September 19, 2018
Published online:

- [1] V. Aseyev, H. Tenhu, F. M. Winnik, *Adv. Polym. Sci.* **2011**, 242, 29.
- [2] A. Gandhi, A. Paul, S. O. Sen, K. K. Sen, *Asian J. Pharm. Sci.* **2015**, 10, 99.
- [3] R. Liu, M. Fraylich, B. R. Saunders, *Colloid Polym. Sci.* **2009**, 287, 627.
- [4] J. Seuring, S. Agarwal, *Macromol. Rapid Commun.* **2012**, 33, 1898.
- [5] N. Shimada, M. Nakayama, A. Kano, A. Maruyama, *Biomacromolecules* **2013**, 14, 1452.
- [6] S.-H. Jung, H.-I. Lee, *Bull. Korean Chem. Soc.* **2014**, 35, 501.
- [7] D. Roy, W. L. Brooks, B. S. Sumerlin, *Chem. Soc. Rev.* **2013**, 42, 7214.
- [8] D. Crespy, R. M. Rossi, *Polym. Int.* **2007**, 56, 1461.
- [9] Y. Di, X. Ma, C. Li, H. Liu, X. Fan, M. Wang, H. Deng, T. Jiang, Z. Yin, K. Deng, *Macromol. Chem. Phys.* **2014**, 215, 365.
- [10] M. Qi, K. Li, Y. Zheng, T. Rasheed, Y. Zhou, *Langmuir* **2018**, 34, 3058.
- [11] H. Zhang, X. Tong, Y. Zhao, *Langmuir* **2014**, 30, 11433.
- [12] G. Meiswinkel, H. Ritter, *Macromol. Rapid Commun.* **2013**, 34, 1026.
- [13] N. Higashi, R. Sonoda, T. Koga, *RSC Adv.* **2015**, 5, 67652.
- [14] J. Seuring, S. Agarwal, *ACS Macro Lett.* **2013**, 2, 597.
- [15] B. A. Pineda-Contreras, F. Liu, S. Agarwal, *J. Polym. Sci. A Polym. Chem.* **2014**, 52, 1878.
- [16] F. Liu, J. Seuring, S. Agarwal, *J. Polym. Sci. A Polym. Chem.* **2012**, 50, 4920.
- [17] J. Seuring, S. Agarwal, *Macromolecules* **2012**, 45, 3910.
- [18] F. Käfer, A. Lerch, S. Agarwal, *J. Polym. Sci. A Polym. Chem.* **2017**, 55, 274.
- [19] K. Skrabania, J. Kristen, A. Laschewsky, Ö. Akdemir, A. Hoth, J.-F. Lutz, *Langmuir* **2007**, 23, 84.
- [20] J. Seuring, S. Agarwal, *Macromol. Chem. Phys.* **2010**, 211, 2109.



- [21] S. Strandman, X. X. Zhu, *Prog. Polym. Sci.* **2015**, *42*, 154.
- [22] M. Xia, Y. Cheng, Z. Meng, X. Jiang, Z. Chen, P. Theato, M. Zhu, *Macromol. Rapid Commun.* **2015**, *36*, 477.
- [23] F. Kafer, F. Liu, U. Stahlschmidt, V. Jerome, R. Freitag, M. Karg, S. Agarwal, *Langmuir* **2015**, *31*, 8940.
- [24] G. Wu, S.-C. Chen, Q. Zhan, Y.-Z. Wang, *Macromolecules* **2011**, *44*, 999.
- [25] W. Sun, Z. An, P. Wu, *Macromolecules* **2017**, *50*, 2175.
- [26] H. Zhang, J. Zhang, W. Dai, Y. Zhao, *Polym. Chem.* **2017**, *8*, 5749.
- [27] S.-W. Kuo, H.-C. Kao, F.-C. Chang, *Polymer* **2003**, *44*, 6873.
- [28] R. Silveston, B. Kronberg, *J. Phys. Chem.* **1989**, *93*, 6241.
- [29] Y. Okada, F. Tanaka, *Macromolecules* **2005**, *38*, 4465.
- [30] S. Fujishige, K. Kubota, I. Ando, *J. Phys. Chem.* **1989**, *93*, 3311

Reprints of Publications

Copyright WILEY-VCH Verlag GmbH & Co. KGaA, 69469 Weinheim, Germany, 2018.



Supporting Information

for *Macromol. Rapid Commun.*, DOI: 10.1002/marc.201800640

**Tuning the Phase Transition from UCST-Type to LCST-Type
by Composition Variation of Polymethacrylamide Polymers**

Florian Käfer, Martin Pretscher, and Seema Agarwal*

Copyright WILEY-VCH Verlag GmbH & Co. KGaA, 69469 Weinheim, Germany, 2018.

Supporting Information

for Macromol. Rapid Commun., DOI: 10.1002/marc.201800640

Tuning the phase transition from UCST-type to LCST-type by composition variation of Poly(methacrylamide) polymers.

Florian Käfer, Martin Pretscher, Seema Agarwal*

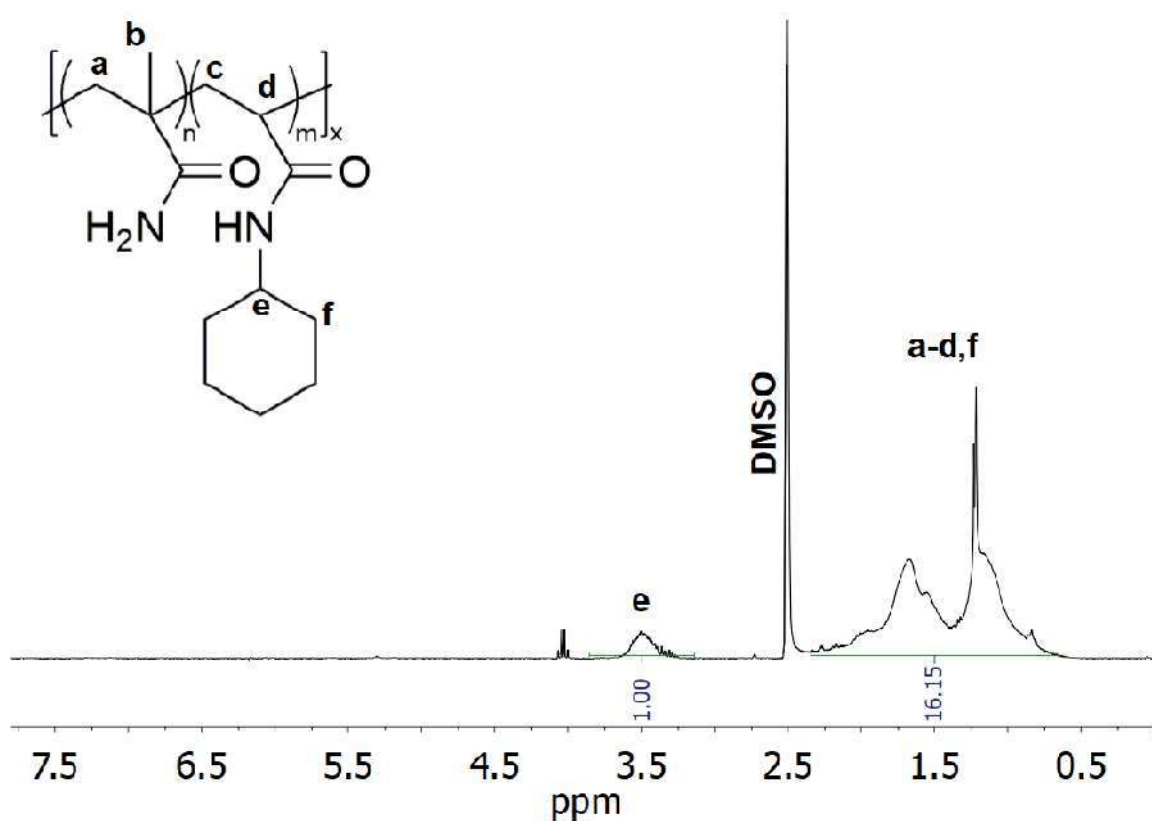


Figure S1. ¹H-NMR of P(MAAm-NchAAm) (entry 5, Table S1) in DMSO-d₆ with trifluoroacetic acid (TFA). TFA was used in order to shift water to a higher ppm region.

Reprints of Publications

Table S1. Synthesis of P(MAAm-NchAAm) copolymers to determine the reactivity ratio.

| Entry | m (MAAm) [mg] | m (NchAAm) [mg] | n (MAAm) [eq] | n (NchAAm) [eq] | Yield [%] |
|-------|------------------|---------------------|------------------|--------------------|--------------|
| 1 | 64 | 268 | 0.3 | 0.7 | 15 |
| 2 | 21 | 344 | 0.1 | 0.9 | 11 |
| 3 | 191 | 38 | 0.9 | 0.1 | 3 |
| 4 | 149 | 115 | 0.7 | 0.3 | 6 |

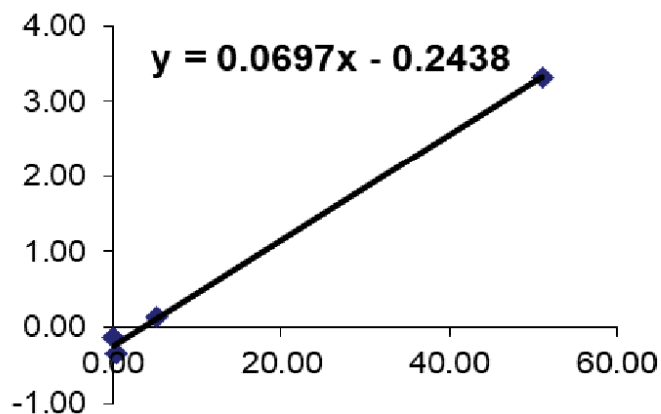


Figure S2. Fineman-Ross plot for determination of the reactivity ratio of MAAm and NchAAm.

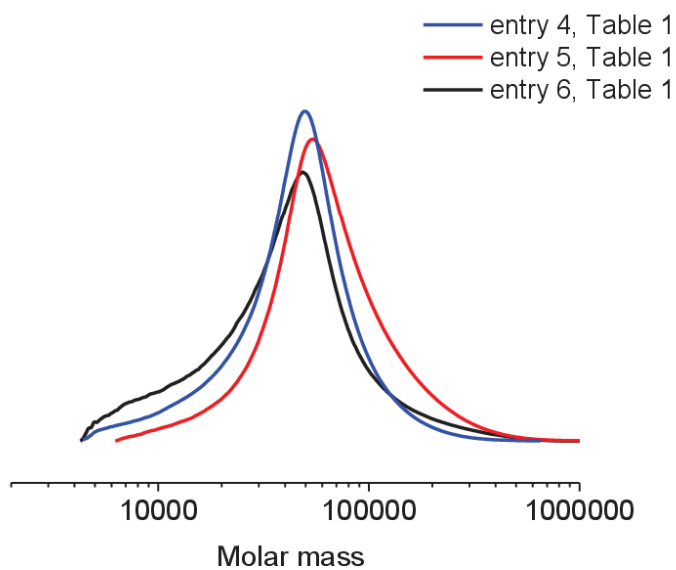


Figure S3. DMSO-GPC traces of the synthesized copolymers (entry 4-6, Table 1).

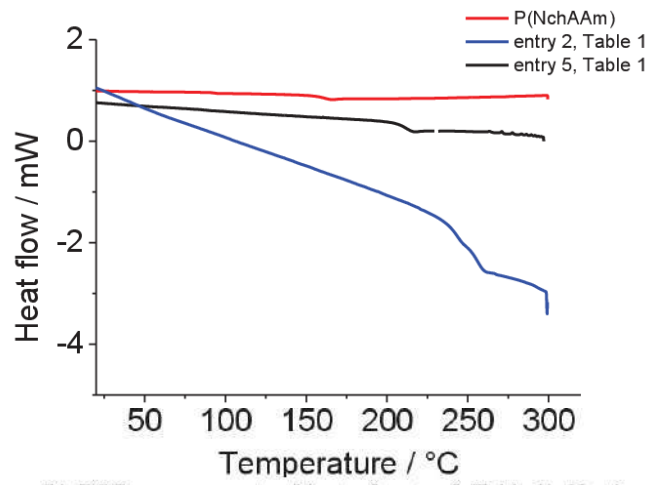


Figure S4. DSC measurements of (entry 2, entry 5, Table 1). Heating rate 10°C/min.

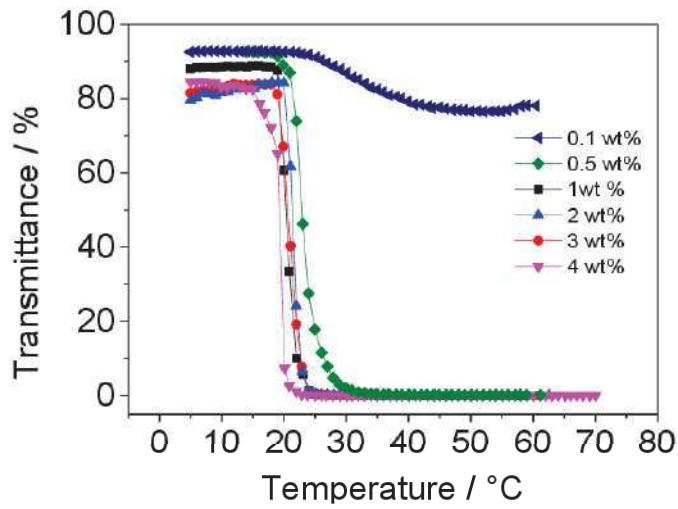


Figure S5. Cooling curves of (entry 5, Table 1) as a function of concentration in pure water. Heating rate 1°C/min.

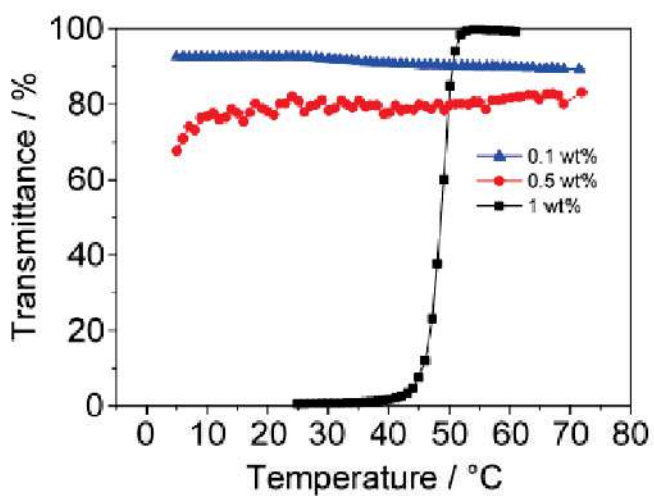


Figure S6. Cooling curves of (entry 2, Table 1) as a function of concentration in pure water. Heating rate 1°C/min.

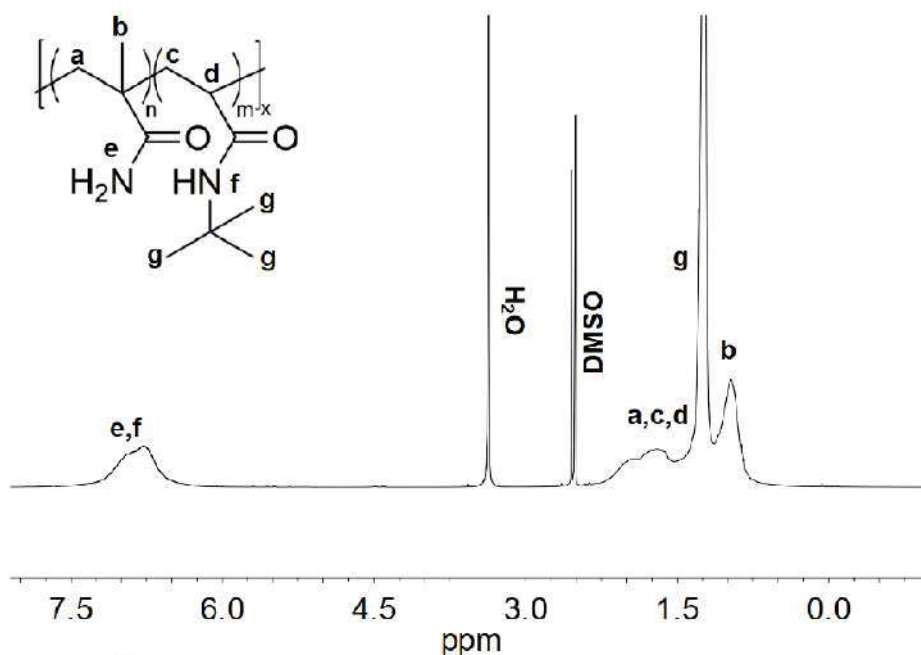


Figure S7. $^1\text{H-NMR}$ of P(MAAm-NtbAAm) (entry 5, Table 2) in DMSO-d_6 .

P(MAAm-NtbAAm): $^1\text{H NMR}$ (500 MHz, DMSO-d_6 , δ): 6.92-6.77 (d, 4H, NH_2), 2.28-1.46 (polymer backbone; $-\text{CH}_2-\text{CH}_2-$), 1.23 (9H; -tert butyl $-\text{C}(\text{CH}_3)_3$), 0.97 (3H, $-\text{CH}_3$) ppm.

Reprints of Publications

P(MAAm-NchAAm). Using the integral of **g** for the 3 methyl groups (9 protons) from NtbAAm and the integral of **b** for the methyl group of MAAm (3 protons), the copolymer composition was determined by the integral **g** by nine and integral **b** divided by three.

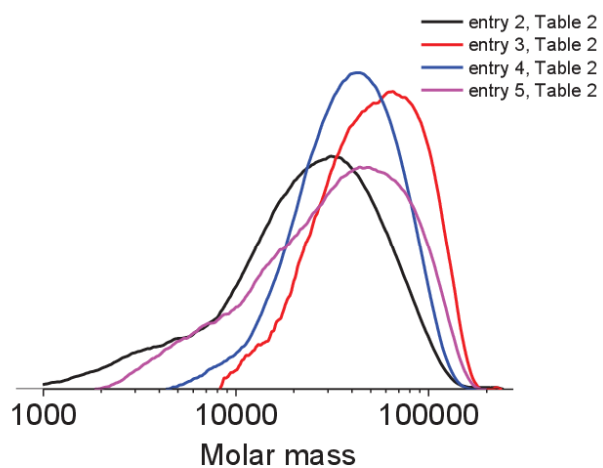


Figure S8. DMSO-GPC traces of the synthesized copolymers (entry 2-5, Table 2).

7.5 Controlled-Release LCST-Type Nonwoven Depots via Squeezing-Out Thermal Response

This work was published by **F. Käfer**, R. Vilensky, G. Vasilyev, E. Zussman, S. Agarwal, *Macromolecular Materials and Engineering* **2019**, 304, (3), 1800606.

Reprinted with permission; Copyright 2018 WILEY-VCH Verlag GmbH & Co. KGaA, Weinheim

Controlled-Release LCST-Type Nonwoven Depots via Squeezing-Out Thermal Response

Florian Käfer, Rita Vilensky, Gleb Vasilyev, Eyal Zussman,* and Seema Agarwal*

A novel thermoresponsive fibrous matrix as controlled release depots upon heating is described. The matrix is composed of electrospun fibers of a lower critical solution temperature (LCST)-type poly(methacrylamide-*co*-*N*-*tert*-butylacrylamide-*co*-4-acryloylbenzophenone) P(MAAm-NtbAAm-ABP) copolymer. Spherical particles, simulating depots of drugs, are embedded with liquid-filled inter-fiber spaces (pores). On heating above 25 °C up to 45 °C, the nanofibers undergo a contraction of about 40%. This solid deformation is attributed to the LCST transition. Fibrous matrix contraction drives expulsion of depots and water solution stored in the pores of the matrix, as evidenced by in situ observations. The liquid flow in the deformable porous medium demonstrates liquid drainage from the matrix as a function of temperature. Experimental results reveal that 70% of the particles are expelled from the matrix upon heating to 45 °C from room temperature. The presented particles encapsulation and release model system using LCST-type fibrous matrix can be used as a transdermal patch.

among others,^[8–10] for the release of encapsulated drug from monolithic fibers or core-shell fibers,^[11–13] relying in general on solute diffusion, polymeric matrix swelling, and degradation. Alternatively, electrospun fibers were designed to achieve controlled release upon specific stimuli such as pH when using polyelectrolytes,^[14,15] or thermal when using thermo-responsive polymers (TPs) with a lower critical solution temperature (LCST) such as poly(*N*-isopropylacrylamide) (PNIPAAm) with a phase transition temperature at around 32 °C.^[16]

In this work, we demonstrate a temperature-controlled release of model nanoparticles from pores of potential transdermal nonwoven patch. The transdermal delivery of drugs and bioactive molecules has lot of implications not only for the local skin disease therapy but also for systemic delivery of drugs.^[17] Till now, nano-sized carrier systems

such as micelles, polymeric nanoparticles, or liposomes are the main skin-delivery systems to facilitate drug delivery by topical application.^[18,19] Nano-carriers may facilitate transportation and/or allow creating depots of drugs in the skin for a sustained or stimuli-induced release using external triggers based on temperature, pH, light, magnetic field, ultrasound, or electrical.^[18,20]

The patch in our work is made of a thermoresponsive electrospun fibrous matrix with a LCST-type phase transition temperature at 45 °C for a controlled release above the body temperature, which is not possible with PNIPAAm. Nanoparticles are encapsulated in the inter-fiber pores surrounded by a medium. When raising the ambient temperature above the LCST, the fibrous matrix shrink and as a result the encapsulated medium with the suspended particles is released to the immediate environment where the fibrous patch is applied onto the skin surface (Scheme 1).

At first, we demonstrate the synthesis, characterization, and preparation of electrospun fibers of an LCST-type poly(methylacrylamide-*co*-*N*-*tert*-butylacrylamide-*co*-4-acryloylbenzophenone) P(MAAm-NtbAAm-ABP) copolymer. The copolymer was successfully electrospun to form a nano-fibrous matrix, which exhibits thermo-initiated, LCST-based shrinkage in aqueous media. Then, for the demonstration of the temperature-triggered-release, the fibrous matrix was uploaded at room temperature with nano-carriers (fluorescently labeled carboxylated latex nanoparticles, 200 nm in diameter) and in situ release while heating was monitored using real-time fluorescence microscopy. The thermo-responsive fibrous matrix demonstrated controlled nano-carriers release due to rapid and reversible swelling and shrinking, in aqueous media.

1. Introduction

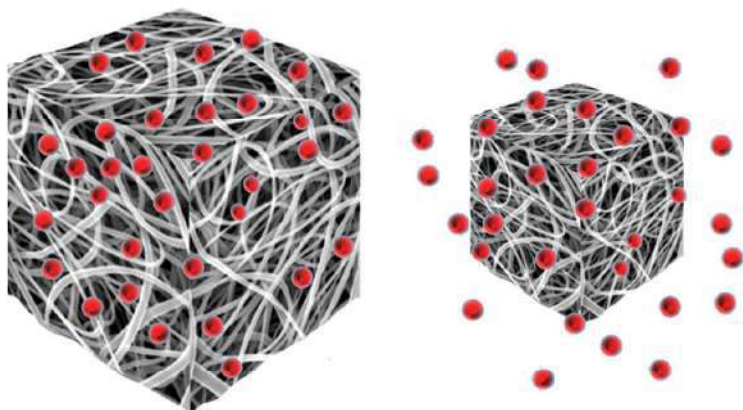
Electrospinning of polymer solutions is a versatile method of making fibrous matrix composed of fibers with nano-to-microscale diameter, high inter-fiber pores, pore interconnectivity, and large surface area to volume ratio.^[1–3] The porosity of the fibrous matrix is highly dependent on fiber diameter^[4] that is mainly determined by the polymer concentration and process parameters such as the electrostatic field strength and flow rate of the solution.^[5,6] Another feature of electrospun fibers is the intra-fiber porosity that is mainly affected by the surface energy and the solvent evaporation rates.^[7] The advantages of the high specific area and high porosity were applied in drug release applications,

F. Käfer, Prof. S. Agarwal
Macromolecular Chemistry II
Bavarian Polymer Institute and Bayreuth Center for Colloids and Interfaces
University of Bayreuth
Universitätsstrasse 30
Bayreuth 95440, Germany
E-mail: agarwal@uni-bayreuth.de

Dr. R. Vilensky, Dr. G. Vasilyev, Prof. E. Zussman
NanoEngineering Group, Faculty of Mechanical Engineering
Technion—Israel Institute of Technology
Haifa 32000, Israel
E-mail: meeyal@technion.ac.il

The ORCID identification number(s) for the author(s) of this article can be found under <https://doi.org/10.1002/mame.201800606>.

DOI: 10.1002/mame.201800606



Scheme 1. Schematics of the transdermal fibrous patch with encapsulated nanoparticles in the inter-fiber pores (left). Upon heating stimulation, LCST-type phase transition occurs resulting in the fibrous matrix shrinkage and concurrently expelling of the nanoparticles and the medium from the pores (right).

2. Experimental Section

2.1. Materials

Dimethyl sulfoxide (DMSO) ($\geq 99.9\%$ ACS reagent), (NtbAAm) as well as (MAAm) (98%) were purchased from Sigma-Aldrich. 4-acryloyloxybenzophenon (ABP) was synthesized in the lab. Both acrylamides were recrystallized from ethanol. 2,2'-Azobisisobutyronitrile (AIBN, Fluka) was recrystallized from ethanol. Milli-Q Plus system (conductivity = $0.072 \mu\text{S cm}^{-1}$) was used to obtain deionized water. *N,N'*-dimethylformamide (DMF) (99.8%) was obtained from Sigma-Aldrich. All materials were used as received, without further purification.

2.2. Polymer Synthesis

Methacrylamide (1.06 g, 0.5 eq), *N-tert*-butylacrylamide (1.59 g, 0.5 eq), and 4-acryloyloxybenzophenon (126 mg, 0.02 eq to the total monomer amount) were dissolved in 25 mL DMSO ($c = 1 \text{ M}$). To degas the reaction solution Ar was bubbled through the mixture for 30 min. Afterward, an AIBN/DMSO solution (12 mg, 0.3 mol% to the total amount of monomer) was added. The polymerization was carried out at 70°C for 12 h, and afterward the polymer was precipitated in toluene, purified by three washing steps, and dried under reduced pressure at 30°C for at least 24 h. ^{13}C -NMR (500 MHz, $\text{DMSO-}d_6$, δ): 180 (s, $-\text{C}=\text{O}$, MAAm), 175 (s, $-\text{C}=\text{O}$, NtbAAm), 141-121(-benzene ABP), 49.8 (s, $-\text{C}-\text{CH}_2-\text{CH}-$), 45.5 (s, $-\text{CH}_2-(\text{CH}-\text{CH}_3)-\text{CH}_2-$), 40.2 (m, polymer backbone), 29.7 (s, $-\text{NH}-\text{C}-(\text{CH}_3)_3$), 17.6 (s, $-\text{CH}_2-(\text{CH}-(\text{CH}_3)-\text{CH}_2-$) ppm.

2.3. Electrospinning of P(MAAm-NtbAAm-ABP)

The P(MAAm-NtbAAm-ABP) copolymer was dissolved in DMF to obtain a 36 wt% solution. The resulted solution was

electrospun onto a rotating disc with a tangential velocity of 16 m s^{-1} under electrostatic field of 1.25 kV cm^{-1} and a constant flow rate of 0.2 mL h^{-1} controlled by a Harvard Apparatus PHD 2000 syringe pump to produce 0.3–1 mm-thick, oriented fibres mat. The resulted fibrous mats were dried in a vacuum oven at 40°C for 1 h to remove any residual solvent followed by photocrosslinking of nanofibers with a UV lamp for 2 h.

The alignment degree of the fibres was determined using Herman's orientation function,^[21,22] $f_{||} = (3(\cos^2 \phi) - 1)/2$ where ϕ is the angle between the equator and the meridian. The porosity of the matrix was calculated as $P = (1 - \rho_{\text{sample}}/\rho_{\text{polymer}})$, where ρ_{sample} is the density of the fibrous matrix, and ρ_{polymer} is the density of the polymer.

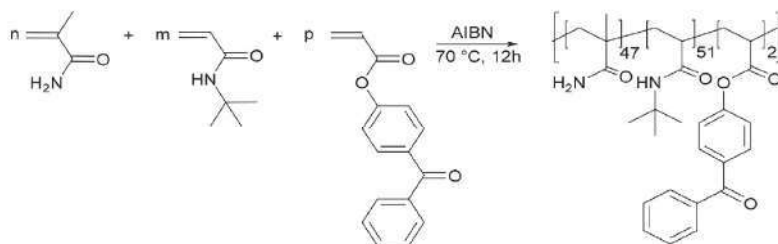
2.4. Characterization

The molar mass was determined using GPC with DMSO as solvent and eluent. A precolumn (SS PolarSil PSA080505; particle size 5, 8.0, 350 mm) and two PSS PolarSil linear S (particle size 5 mm, dimension 8.0 mm 3300 mm) columns were used. Pullulan (narrow molar mass distribution of different molar masses) were used as standards. The flow rate was 0.7 mL min^{-1} at a temperature of 75°C . A differential refractive index detector was used. The software PSSWinGPC Unity, Build 1321, was used to determine the molar masses and distribution.

The copolymer composition was determined using a quantitative reversed-gated-decoupling ^{13}C -NMR measurement performed on a 500 MHz Bruker Avance III HD 500 in $\text{DMSO-}d_6$ as a solvent. Integrating the peaks of the carbonyl carbon of MAAm (180 ppm) and the carbonyl carbon of NtbAAm (175 ppm), the copolymer composition was determined.

The change in transmittance with temperature was followed by a JASCO V-630 Spectrophotometer with a cell path length of 10 mm and a wavelength of 660 nm, heating rate 1°C min^{-1} , using a 2 wt% solution of the copolymer. Therefore, the polymer was dissolved in the pure water below room temperature. The turbidity measurement showed a LCST with a cloud point of 37°C , determined at the point of inflection (cooling), and 41°C (heating). To determine the cloud point for the cross-linked polymer, the polymer was dissolved in ethanol, casted in the form of film and cross-linked under UV irradiation for around 30 min. A part of the resulting polymer film was given into pure water for $\approx 12 \text{ h}$ to equilibrate it at room temperature. Afterward, a micro-DSC measurement was performed on a Setaram Micro DSC 3 with a 0.6 mL cell and a heating/cooling rate of $0.25^\circ\text{C min}^{-1}$.

Rheological measurements of a 2 wt% copolymer aqueous solution were performed using a Discovery DHR-2 rotational rheometer (TA Instruments, USA) under steady-state shear deformation. The preferred geometry was cone-and-plate, with a cone diameter of 40 mm and a surface-plate angle of 1° . The



Scheme 2. Synthesis of the P(MAAm-NtbAAm-ABP) by free radical polymerization at 70 °C with AIBN, a radical initiator and DMSO as a solvent.

Nikon, Tokyo, Japan) equipped with an Intensilight illuminator. A petri-dish with the tested sample was placed on an ITO heating control unit and mounted on the microscope stage. The temperature in the aqueous medium was monitored using thermocouple connected to Pico-TC 08 thermocouple data logger. The images were analyzed using ImageJ to determine the mean intensity in the region of interest (ROI).

tests were carried out at the temperature range of 5–39 °C. The solution was stored at 4 °C and incubated at the desired temperature for 15 min prior to measurement.

Structural characterization of 2 wt% polymer aqueous solution was performed using cryo-TEM. Specimens were prepared in a controlled environment vitrification system (CEVS) at 6, 12, 25, and 37 °C (temperature variance ± 2 °C) and 100% relative humidity.^[23] Samples were examined in a FEI T12 G2 microscope operated at 120 kV, using a Gatan 626 cryo-specimen holder. Specimens were equilibrated in the microscope below -180 °C, and then examined in the low-dose imaging mode to minimize electron beam radiation damage.

LS instruments AG (Fribourg, Switzerland) 3D spectrometer was used for the dynamic light scattering (DLS) measurements in 3D modulated cross-correlation mode. The light source was a HeNe laser. Samples were prepared in MilliQ water by heating at 15 and 60 °C with concentrations of 0.1 wt%.

High resolution SEM images of the as-spun and dried fibers were obtained using Carl Zeiss Ultra Plus HRSEM. The accelerating voltage of 1 keV was used. A secondary electrons detector was used to study the morphology and surface topography.

Tensile tests were carried out on a custom-made horizontal tensile machine which had a Sensotec 2N load cell (model 31/1435-03). This machine is equipped with a bath, which allows for testing in a fluid medium at a controlled temperature. The dry sample (15 × 7 mm) was mounted on a sample holder using rubber clamps, strained to a fixed length, and immersed in the water bath. The water reservoir was heated using an immersed heating element. Throughout the experiment, the stress was recorded as a function of time and temperature. The engineering stress was calculated over the initial cross-sectional area.

For the release experiments, dry fibrous matrix (10 × 10 × 1 mm) was first fixed to the bottom of petri-dish. Then, suspension of fluorescently labeled, carboxylated, polystyrene nanoparticles (c-NPs), 0.2 μm in diameter (Magsphere, Inc), with a concentration of 0.25% solid in water, (5×10^{11} beads mL⁻¹), were added dropwise to the matrix. Real time imaging release of c-NPs from the fiber-mesh was obtained using an upright epifluorescence microscope (AZ100 multizoom,

3. Results and Discussion

A UV-crosslinkable poly(methacrylamide-*co*-*N*-*tert*-butylacrylamide-*co*-4-acryloylbenzophenone) P(MAAm-NtbAAm-ABP) copolymer was synthesized using free radical polymerization with AIBN as a radical initiator (**Scheme 2**).

The ¹H-NMR showed several overlapping peaks, therefore quantitative ¹³C-NMR was used for the copolymer structure characterization. Integrating the specific signals for $-C=O$ of MAAm (182 ppm)^[24] and $-C=O$ of NtbAAm (175 ppm)^[25] allows calculating the copolymer composition (Figure S1, Supporting Information). The copolymer shows a peak molar mass (Mp) of around = 71 000 g mol⁻¹ as determined by gel permeation chromatography (Figure S2, Supporting Information). The polymers showed the thermoresponsive behavior of LCST-type in water as seen by the change in transmittance of a 2 wt% solution by UV-vis spectroscopy (**Figure 1a**). The turbidity curve in showing a change of around 20% in transmittance assumed due to the formation of a polymer “network” structure at 42 °C. Furthermore, the thermo-responsive behavior of the cross-linked copolymer was shown by a microDSC measurement (Figure 1b).

Comparing the LCST-type phase transition of the polymer solution, and the cross-linked polymer film a small shift in the cloud point, as well as, a change in the broadness of the phase transition was observed. The slight change in the cloud point from 41 °C (heating) for the polymer solution, and 45 °C (heating) for the cross-linked polymer film, and the change in the broadness of the phase transitions, is due to the difference in the heating rates of 1 °C min⁻¹ for the turbidity measurement,

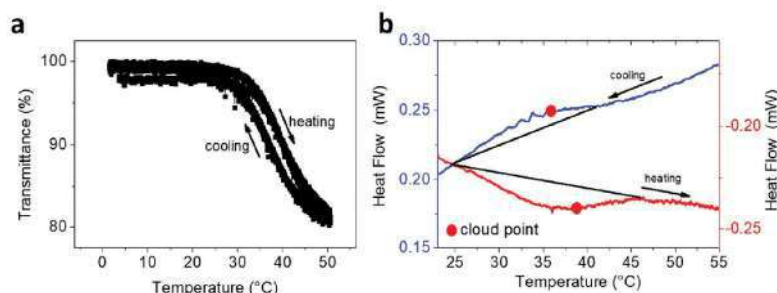


Figure 1. a) Turbidity measurement, cooling/heating cycle of a 2 wt% copolymer solution in pure water with a heating rate of 1 °C min⁻¹; b) micro-DSC measurement of the cross-linked polymer film in pure water. Heating rate 0.25 °C min⁻¹.

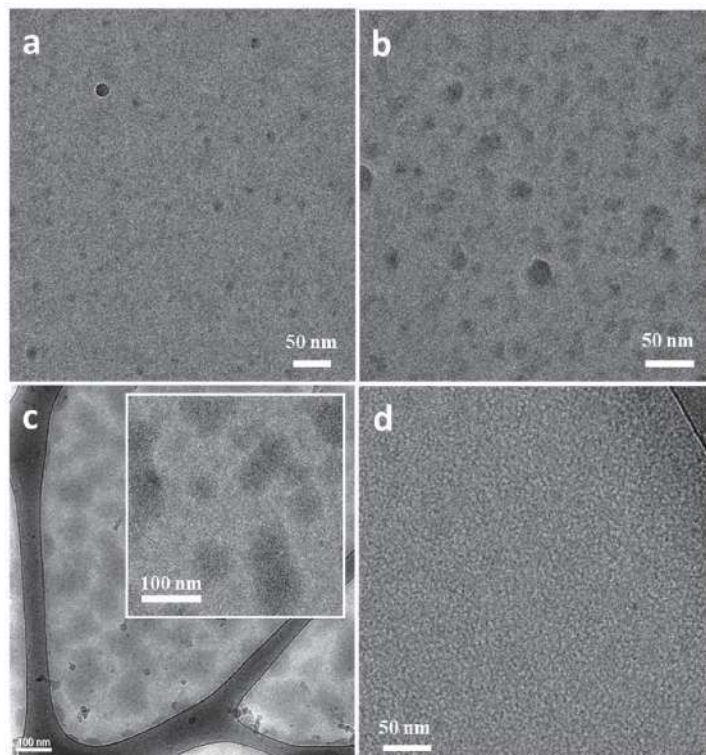


Figure 2. Cryo-TEM images of 2% copolymer in water at different temperatures: a) 6 °C; b) 12 °C; c) 20 °C; d) 37 °C.

and 0.25 °C min^{-1} for the micro-DSC measurement. In order to study the structural evolution of the copolymer as a function of temperature, in aqueous solution, cryo-TEM and DLS measurements were carried out. Samples for cryo-imaging were prepared at different temperatures: 6, 12, 20, and 37 °C. **Figure 2** shows the structural evolution of 2 wt% copolymer in water, with increasing temperature.

At 6 °C, spherical individual micelles of 15–20 nm in diameter were observed. As the temperature increased (12 °C), spherical aggregates increase in size up to 30–50 nm, while further increase in temperature leads to larger, overlapping aggregates, which form percolated continuous domains. The DLS measurements confirmed the results of the cryo-TEM measurements. At 15 °C single micelles with an average size of $r_H = 11\text{ nm}$ and already bigger aggregates were observed whereas significant larger aggregates with a size of approximately $r_H = 60\text{ nm}$ were seen at a temperature of 60 °C (Figure S3, Supporting Information). Such an aggregation of water-soluble copolymers at low temperature is quite unexpected, nevertheless, individual micelles were observed in aqueous solution at a temperature as low as 6 °C, which is considerably lower than the LCST of the copolymer ($\approx 40\text{ °C}$). Note that for a random copolymer of AAm and NtbAAm which is comparable to our copolymer structure, the determined reactivity ratios $r(\text{AAm}) = 1.5$; $r(\text{NtbAAm}) = 0.5$ indicate a random copolymer with hydrophobic NtbAAm rich segments, which enables the formation of

micellar structures.^[26] Furthermore, the formation of micellar structures of random LCST-type copolymers was shown in several examples,^[27] among them is the work by Dan et al. that presents the formation of micelles of a random LCST-type methacrylate-type (hydrophobic) and methacrylamide-type (hydrophilic units) copolymer.^[28] The formation of these micelles was explained by a hydrophilic/hydrophobic balance whereas the hydration of the amide groups was shown to play a major role. In our case, the formation of micelles at 6 °C can be attributed to hydrophobic NtbAAm rich domains which dominates the aggregation at low temperature, while at a higher temperature $>12\text{ °C}$, structural rearrangements and further assembly are driven by differences in hydration degree of the copolymer units. Based on our observations, we assume that the micelles that were observed at 6 °C possibly adopt core-corona structure. As the temperature increases ($T > 12\text{ °C}$) P(MAAm-NtbAAm-ABP) becomes less hydrated, that is, more hydrophobic, leading to reorganization and incorporation of additional chain segments and polymer chains into spherical aggregates. Further increase in temperature induces further association and formation of network-kind structures (Figure 2c). At 37 °C cryo-TEM image showed no presence of large aggregates. This result could be attributed to precipitation of large aggregates, or their disassembly. Flow curves (viscosity vs shear stress) of the copolymer solution in the temperature range from 5

to 39 °C are shown in **Figure 3a**.

For all the tested temperatures, the polymer solution demonstrated a complex rheological behavior, which confirm the formation of network. Therefore, the solution viscosity was measured as a function of temperature at a shear stress of 0.15 Pa (in most cases a pseudo-Newtonian behavior with almost constant viscosity was registered at this stress). It is evident that the curve can be divided into four distinct regions (Figure 3b). A decrease in the viscosity with temperature was observed in Region I, at 5–12 °C followed by a significant viscosity rise at 12–22 °C. Then, viscosity goes through a maximum and decreases until the temperature reaches $\approx 37\text{ °C}$. Finally, in Region IV, at temperatures higher than 37 °C the viscosity starts to increase once again. It is possible to distinguish between typical shapes of the flow curves when considering the different regions of viscosity versus temperature curve. This difference can be explained in terms of the transformation of the copolymer microstructure with temperature in aqueous media as observed by cryo-TEM. Spherical individual micelles could be clearly seen at low temperatures. The amount of these micelles is not high, thus one can conclude that not all the copolymer chains were involved in the self-assembly and individual solubilized macromolecules coexist together with the micelles.^[29] Flow curves of the solution at these temperatures demonstrate a weak yield behavior in the region of low stresses, which is typical for structured systems.^[30] As the amount of the micelles is limited,

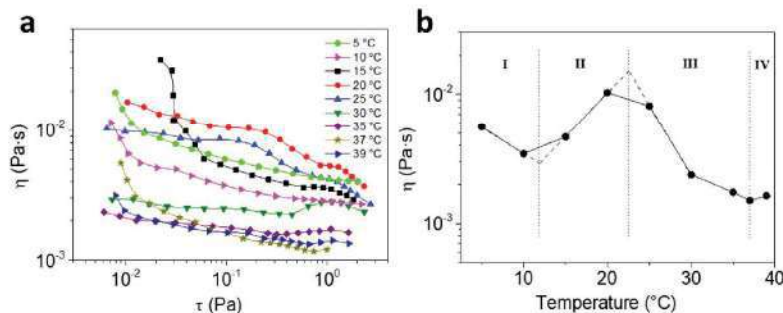


Figure 3. a) Flow curves of 2 wt% copolymer solution at different temperatures; b) viscosity at a shear stress of 0.15 Pa versus temperature.

it is reasonable to assume that interactions between dissolved copolymer chains and the chains fragments, forming corona of the micelles, are the origin of this behavior. When increasing the temperature above 22 °C macromolecular mobility increases and as a result, the viscosity and yield stress decrease. At the same time, the morphology of the solution in terms of micelles concentration and their respective size remains almost unchanged in Region I,^[31] as indicated by the parallel flow curves at 5 and 10 °C. Intermolecular association of hydrophobic segments of the copolymer becomes stronger as the temperature rises.^[32] Therefore, more chains take part in the self-assembling process and both the amount of the micelles and their size increase, forming micellar clusters as a result (Region II). This leads to enhancement of the yield behavior and overall viscosity increase. In addition, a plateau region followed by shear thinning appears at stresses 0.6–1.3 Pa. Finally, agglomeration of the clusters causes the formation of a continuous percolated “network” consisting of the copolymer micelles interconnected via entanglements formed by polar parts of the corona. Apparently, the formation of this percolated structure occurs in the vicinity of the maximum of the viscosity-temperature curve. After that, viscosity progressively decreases (Region III) with temperature according to Arrhenius law. At these conditions yield stress gradually disappears and double steps shape of the curves reflects a complex structure of the solution. The first step corresponds to disentangling of micellar coronas and breaking of clusters into smaller structures, while the origin of the second step is not fully understood. It should be noted that similar curves with two inflection points were previously presented for hydrophobically associating block copolymers in aqueous media at the semi-dilute unentangled regime.^[33,34] Flow with a very weak shear thinning at stresses below 0.5 Pa was registered at 30 and 35 °C. Then, a mild shear thickening takes place followed by more pronounced shear thinning. This effect is usually attributed to shear-induced switching from intra- to intermolecular interactions of associating groups. In particular, for telechelic associative block copolymers, which forms a flower-like micelles it is assumed that stretching of the bridging chains in micellar clusters occurs at a certain shear stress followed by a loop-to-bridge transition. These bridges can be destroyed at higher stresses and thus an opposite bridge-to-loop transition leading to break-up of the clusters takes place, and resulting in the shear thinning. In the case of the studied copolymer only spherical “hairy” micelles

can be formed and, therefore, the explanation of the phenomenon should be slightly different. Apparently, a part of intramolecular $-C=O \cdots H-N$ hydrogen bonds can be broken under the action of the shear field and then reformed as intermolecular or intermicellar bonds acting as temporal cross-linkers, which can be destroyed at further stress increase. This process should start at temperatures, at which enlargement and interaction between micelles begin (Region II, Figure 3b). Therefore, the high stress plateau at 0.6–1.3 Pa should be treated as masked shear thickening phenomenon as they situated at the same range of stresses (Figure 3a).

Above stress of ≈ 1.3 Pa shear thinning takes place, thus this value can be considered as the strength of the structure formed in the solution as a result of the re-associations described above. At the same time, at temperatures >15 °C shear rate corresponding to the onset of the structure destruction progressively increases reflecting a shortening of a lifetime of the bonds with temperature. At temperatures higher than 37 °C (Region IV, Figure 3b) yield behavior in the range of low stresses appears again. This feature evidences the onset of macroscopic phase separation in the solution (apparently, to some extent this process has already started at 35 °C). At the same time, the structure formed by clusters of the micelles is still preserved as the shear thickening effect is clearly seen. Viscosity versus temperature curve has local minima and maximum reflecting a complex phase behavior of the copolymer in aqueous media. Previously similar non-monotonic curve was reported for PNIPAAm water solution, and was attributed to macroscopic phase separation.^[32] In our case, the reorganization of the copolymer structure on the microscopic level was detected at temperatures prior to macroscopic phase separation (LCST). The P(MAAm-NtbAAm-ABP) copolymer was electrospun to form a fibrous matrix composed of fibers with an average diameter of 0.85 ± 0.1 μm , with an alignment distribution of ± 9 (Figure 4a).

Shrinking and swelling tests have been carried out to characterize the behavior of individual cross-linked fibers using cryo-SEM images after vitrification process (Figure 4b,c). The average measured diameter of the fibers that were soaked in cold water (20 °C) was 0.97 ± 0.12 μm , while the average diameter of fibers soaked in hot water (45 °C) was 0.78 ± 0.09 μm showing a decrease of about 20% in the diameter of the fiber. A macroscopic overview of the contraction effect was demonstrated when working with a sample of the cross-linked fibrous matrix. At first, the sample was immersed in cold water at 6 °C, after 20 min the matrix became gel-like and transparent and shrank by $\approx 30\%$ in the direction along the fibers axis and by $\approx 4\%$ in the perpendicular direction (Figure 4e). Apparently, the contraction of the fibrous matrix in the direction parallel to the fibers axis is attributed to the relaxation of the stretched electrospun polymer chains via solvent-driven relaxation mechanism.^[22,35] The thermoresponsive fibers contraction and expansion in water with temperature is utilized in the literature for actuation purpose.^[36] Upon heating the water media to 40 °C (LCST) the fibrous matrix showed an additional contraction

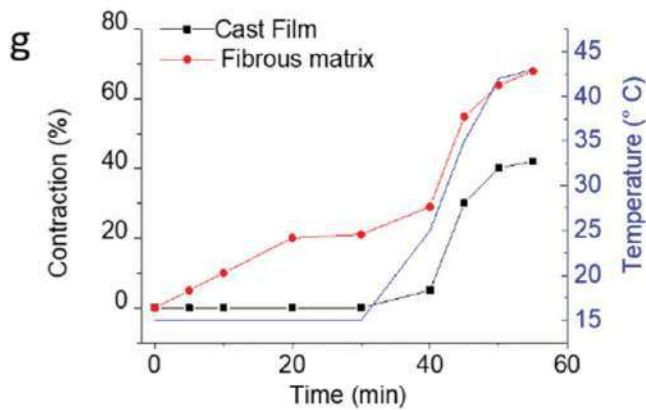
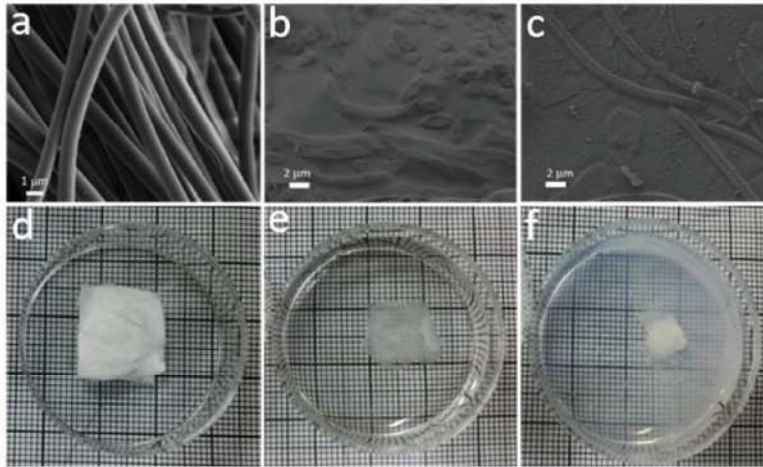


Figure 4. HR-SEM images of a) the as-spun fibers; b) cryo-SEM images of the fibers soaked in water at 20 °C; c) cryo-SEM images of the fibers soaked in water at 45 °C; d) optical image of the as-spun fibrous matrix; e) after soaked in water at 6 °C; f) after heating to 40 °C; g) contraction of the fibrous matrix (in the direction along the fiber axis) and cast film as a function of temperature.

of about 50% parallel and perpendicular to the fibers axis (Figure 4f). In order to verify the origin of the contraction phenomena upon wetting, the fibrous matrix obtained by significant stretching was compared to cast film (Figure 4g). Also in this experiment, fibrous matrix exhibits contraction of about 20% after 30 min in water while the cast film shows no contraction, implying the observed initial contraction is due to stress relaxation. Upon heating up to 40 °C both types of samples exhibit contraction of about 50%, where in both samples the contraction rate was isotopically at this range of temperature and was found to be $0.025 \pm 0.01 \text{ mm s}^{-1}$. Stress–temperature relationship as a result of a strain controlled test, of the fibrous matrix immersed in a water bath, is presented (Figure 5).

Upon wetting, at constant temperature (6 °C), an initial decrease in stress was observed. Then, the stress increased until a steady stress was achieved. The decrease in stress, and the following increase at constant temperature could be related to two competing effects: enhanced mobility of the

chains due to chains hydration followed by contraction of the electrospun fibers due to solvent-induced relaxation.^[35,37] As the water bath is heated an increase of the stress is monitored, while the highest rate of stress/temp is observed at a temperature >30 °C. At about 38 °C the stress reaches a plateau then rapid relaxation at high temperature occurs. Real-time fluorescence microscopy imaging was used to visualize the nano-carriers (c-NPs) release. Figure 6 displays images of the heat-induced contraction of the fibrous matrix, accompanied by the substantial c-NPs outburst.

The streamlines that can be visualized during matrix contraction suggest pressure-driven flow. The measured velocity along various streamlines was $u = 0.05 \pm 0.01 \text{ mm s}^{-1}$. While the driving force for the fluid expulsion was attributed to contraction following increasing temperatures, a more thorough analysis is required to confirm the dominance of this effect over other possible forces capable of driving fluid release on heating up to 45 °C. A possible effect is a natural convection due to the difference of the liquid density, as a result of the temperature gradient along the matrix. However, since the Rayleigh number, $R_a \ll 1$, natural convection is negligible. Also, capillary rise of the liquid in the porous matrix upon heating should be considered. However, a simple calculation using Darcy law can demonstrate that the time required for the capillary rise is in the scale of seconds while our experimental results demonstrate that complete liquid expulsion required ≈ 3 min.

It is important to emphasize that the suspension of the c-NPs (0.2 μm in diameter) is assumed to be sufficiently dilute so that there are no direct or hydrodynamic

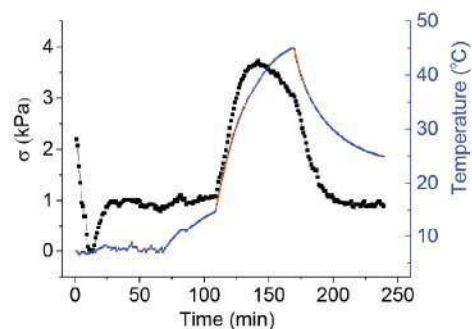


Figure 5. Stress–temperature relationship measured during strain-controlled test. Maximal stress is obtained at 38 °C.

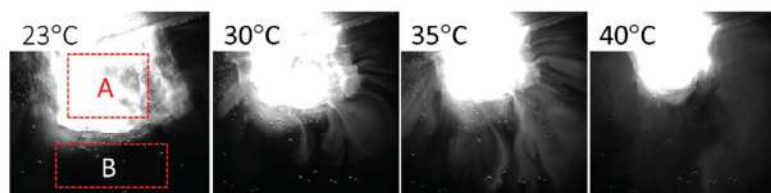


Figure 6. Fluorescence images of the fibrous matrix loaded with fluorescently labeled c-NP at different temperatures, specifying regions A and B, in the center of the fibrous matrix and in the vicinity of it, respectively.

interactions between the particles. Additionally, the enhanced hydrophobicity of the polymer at elevated temperatures lead to a weakening of polymer-particles interactions. Upon heating, the fibrous matrix contracts and the entrapped suspension starts to flow. For particles of such small dimensions, the creeping flow approximation is expected to hold locally, while the center of mass is “frozen” into the moving solvent. Thus, translational motion of the particles relative to the solvent is impossible. When considering a circumscribed sphere of the tested sample (fibrous matrix) with equivalent radius of R , with typical pore with radius r , and contraction rate of the sphere due to heating is dR/dt , and the number of pores is n , then the terminal velocity of released particle through a capillary of diameter r is

$$u = \frac{4}{n} \left(\frac{R}{r} \right)^2 \frac{dR}{dt} \quad (1)$$

When considering a typical sample with $R = 5$ mm, $dR/dt = 0.025$ mm s⁻¹, typical capillary diameter of $r = 0.004$ mm, and the number of pores $n = 6 \cdot 10^5$, considering homogeneous packing (coverage) of the pores on the sphere with porosity of 87%, then the estimated velocity of a particle is $u = 0.04$ mm s⁻¹ which is slower in nearly 20% than the average measured velocity. Noticeably the estimated velocity is affected by the porosity of the free surface of the circumscribed sphere and the average capillary's radius. To quantify the extent of the c-NPs release, fluorescence intensity was analyzed within two areas of interest: region A (within the fibrous matrix) and region B (in the surrounding media) (Figure 6). Figure 7 presents the concentration of particles (based on intensity), in region B as a function of temperature/time.

The presence of c-NPs in the surrounding media at $t = 0$ and the followed decrease at constant temperature, results from c-NPs spontaneous desorption from fibrous matrix free surface after immersing the sample in the water reservoir and due to photo-bleaching of the FITS-fluorescent dye. According to intensity analysis in region A (Figure S4, Supporting Information), within the first 10 min, only 2% of the c-NPs diffused from the fibrous matrix to the surround media. Next, the temperature of the media was raised, at a rate of 4 °C min⁻¹. As the temperature rose above 28 °C, extensive matrix shrinkage has begun, accompanied by substantial particles exclusion from the matrix to the surrounding media. The maximal rate of c-NPs release was observed above 35 °C. After the first

heating cycle, about 60% of the particles were excluded from the matrix.

4. Conclusions

We demonstrated a fibrous matrix which can shrink/swell and release nano-carriers as a function of temperature. The matrix is made of a thermo-responsive electrospun fibrous matrix characterized with LCST-type phase transition. Nanoparticles encapsulated in the inter-fiber pores surrounded by a medium and released in a nearly constant rate in the range of 30–42 °C. Fibers were made from a UV light cross-linkable P(MAAM-NtbAAM-ABP) copolymer which was synthesized and structurally characterized using quantitative ¹³C-NMR. Temperature-dependent rheology and turbidity measurements of the uncross-linked copolymer in solution showed an LCST-type phase transition at ≈41 °C. Micro-DSC measurements of the cross-linked polymer film showed an LCST phase transition at about 45 °C. Swelling tests of the matrix showed a low contraction of 20% in the cold water in the direction along the fibers axis and 5% in the perpendicular direction. At 40 °C an additional strong contraction of 50% in both directions was achieved due to the dehydration and formation of inter- and intra-molecular hydrogen bonds.

The presented Inter-fiber encapsulation and temperature-regulated release can be used as a transdermal patch, allowing the release of whole particles towards a lesion or various therapeutic drugs. The suggested drug transport relies mainly on the matrix-squeezing rate, but also on the matrix porosity and typical pore dimension. This is unlike typical release mechanisms from polymers matrices, which rely on matrix hydrolysis and solid-state diffusion of the encapsulated compound from the fibers/matrix into the surrounding aqueous bath.^[14]

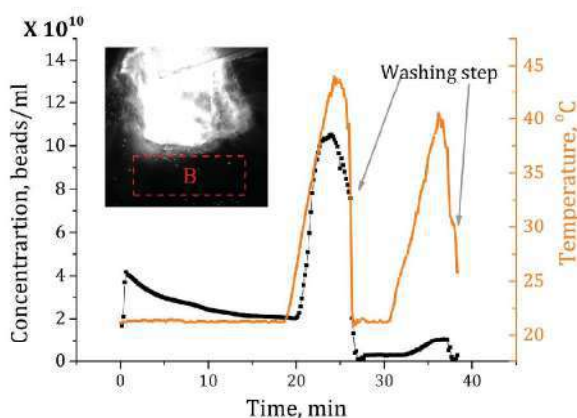


Figure 7. Release concentration of fluorescently labeled c-NP as a function of temperature/time. In the first 20 min the release occurs at constant temperature increase at $t > 20$ min.



Supporting Information

Supporting Information is available from the Wiley Online Library or from the author.

Acknowledgements

The authors are indebted to the GIP program of the German Research Foundation (DFG), for their financial support. The authors also thank the Russell Berrie Nanotechnology Institute (RBNI) at the Technion. E.Z. acknowledges the support of the Winograd Chair of Fluid Mechanics and Heat Transfer at Technion.

Conflict of Interest

The authors declare no conflict of interest.

Keywords

drug delivery, electrospinning, fiber matrix, lower critical solution temperature, nanoparticles

Received: October 10, 2018

Revised: November 10, 2018

Published online: December 17, 2018

- [1] S. Agarwal, A. Greiner, J. H. Wendorff, *Prog. Polym. Sci.* **2013**, *38*, 963.
- [2] A. Greiner, J. H. Wendorff, *Angew. Chem., Int. Ed.* **2007**, *46*, 5670.
- [3] Y. J. Hwang, S. Choi, H. S. Kim, *e-Polym.* **2018**, *18*, 339.
- [4] S. J. Eichhorn, W. W. Sampson, *J. R. Soc., Interface* **2005**, *2*, 309.
- [5] S. A. Theron, E. Zussman, A. L. Yarin, *Polymer* **2004**, *45*, 2017.
- [6] J. M. Deitzel, J. Kleinmeyer, D. Harris, N. C. Beck Tan, *Polymer* **2001**, *42*, 261.
- [7] P. Dayal, J. Liu, S. Kumar, T. Kyu, *Macromolecules* **2007**, *40*, 7689.
- [8] R. Haloui, A. Moldavsky, Y. Cohen, R. Semiat, E. Zussman, *J. Membr. Sci.* **2011**, *379*, 370.
- [9] S. Jiang, H. Hou, S. Agarwal, A. Greiner, *ACS Sustainable Chem. Eng.* **2016**, *4*, 4797.
- [10] A. Greiner, J. H. Wendorff, A. L. Yarin, E. Zussman, *Appl. Microbiol. Biotechnol.* **2006**, *71*, 387.
- [11] R. Srikar, A. L. Yarin, C. M. Megaridis, A. V. Bazilevsky, E. Kelley, *Langmuir* **2008**, *24*, 965.
- [12] S. K. Tiwari, R. Tzezana, E. Zussman, S. S. Venkatraman, *Int. J. Pharm.* **2010**, *392*, 209.
- [13] A. Abu Ammar, M. Gruber, P. Martin, O. Stern, F. Jahshan, O. Ertracht, E. Sela, S. Srouji, E. Zussman, *J. Controlled Release* **2018**, *272*, 54.
- [14] M. Boas, A. Grady, G. Vasilyev, M. Burman, E. Zussman, *Soft Matter* **2015**, *11*, 1739.
- [15] O. A. Inozemtseva, Y. E. Salkovskiy, A. N. Severyukhina, I. V. Vidyasheva, N. V. Petrova, H. A. Metwally, I. Y. Stetsciura, D. A. Gorin, *Russ. Chem. Rev.* **2015**, *84*, 251.
- [16] J. Seuring, S. Agarwal, *Macromol. Rapid Commun.* **2012**, *33*, 1898.
- [17] A. Vogt, C. Wischke, A. T. Neffe, N. Ma, U. Alexiev, A. Lendlein, *J. Controlled Release* **2016**, *242*, 3.
- [18] M. Amjadi, S. Sheykhsari, B. J. Nelson, M. Sitti, *Adv. Mater.* **2018**, *30*, 1704530.
- [19] T. Naolou, E. Rühl, A. Lendlein, *Eur. J. Pharm. Biopharm.* **2017**, *116*, 1.
- [20] C. Guo, R. H. Khengar, M. Sun, Z. Wang, A. Fan, Y. Zhao, *Pharm. Res.* **2014**, *31*, 3051.
- [21] R. Dersch, T. Liu, A. K. Schaper, A. Greiner, J. H. Wendorff, *J. Polym. Sci., Part A: Polym. Chem.* **2003**, *41*, 545.
- [22] L. Liu, H. Bakhshi, S. Jiang, H. Schmalz, S. Agarwal, *Macromol. Rapid Commun.* **2018**, *39*, 1800082.
- [23] D. Danino, A. Bernheim-Groswasser, Y. Talmon, *Colloids Surf. A* **2001**, *183–185*, 113.
- [24] K. Hatada, T. Kitayama, K. Ute, *Polym. Bull.* **1983**, *9–9*, 241.
- [25] B. de Lambert, M.-T. Charreyre, C. Chaix, C. Pichot, *Polymer* **2005**, *46*, 623.
- [26] N. S. Save, M. Jassal, A. K. Agrawal, *Polymer* **2003**, *44*, 7979.
- [27] L. Li, K. Raghupathi, C. Song, P. Prasad, S. Thayumanavan, *Chem. Commun.* **2014**, *50*, 13417.
- [28] M. Dan, Y. Su, X. Xiao, S. Li, W. Zhang, *Macromolecules* **2013**, *46*, 3137.
- [29] L. C. Pham Trong, M. Djabourov, A. Ponton, *J. Colloid Interface Sci.* **2008**, *328*, 278.
- [30] A. Y. Malkin, A. I. Isayev, *Concepts, Methods and Applications*, ChemTec Publishing, Toronto **2006**.
- [31] M. Sahn, T. Yildirim, M. Dirauf, C. Weber, P. Sungur, S. Hoepfener, U. S. Schubert, *Macromolecules* **2016**, *49*, 7257.
- [32] K. C. Tam, X. Y. Wu, R. H. Pelton, *J. Polym. Sci., Part A: Polym. Chem.* **1993**, *31*, 963.
- [33] M. Pabon, J.-M. Corpart, J. Selb, F. Candau, *J. Appl. Polym. Sci.* **2002**, *84*, 1418.
- [34] T. Aubry, M. Moan, *J. Rheol.* **1994**, *38*, 1681.
- [35] L. Liu, S. Jiang, Y. Sun, S. Agarwal, *Adv. Funct. Mater.* **2016**, *26*, 1021.
- [36] S. Agarwal, S. Jiang, Y. Chen, *Macromol. Mater. Eng.* **2018**, 1800548 <https://doi.org/10.1002/mame.201800548>.
- [37] G. Vasilyev, M. Burman, A. Arinstein, E. Zussman, *Macromol. Mater. Eng.* **2017**, *302*, 1600554.

Reprints of Publications

Copyright WILEY-VCH Verlag GmbH & Co. KGaA, 69469 Weinheim, Germany, 2018.



Supporting Information

for *Macromol. Mater. Eng.*, DOI: 10.1002/mame.201800606

Controlled-Release LCST-Type Nonwoven Depots via
Squeezing-Out Thermal Response

Florian Käfer, Rita Vilensky, Gleb Vasilyev, Eyal Zussman,*
and Seema Agarwal*

Copyright WILEY-VCH Verlag GmbH & Co. KGaA, 69469 Weinheim, Germany, 2018.

Supporting Information

for *Macromol. Mater. Eng.*, DOI: 10.1002/mame.201800606

Controlled-release LCST-type nonwoven depots via squeezing-out thermal response

Florian Käfer, Rita Vilensky, Gleb Vasilyev, Eyal Zussman,* Seema Agarwal*

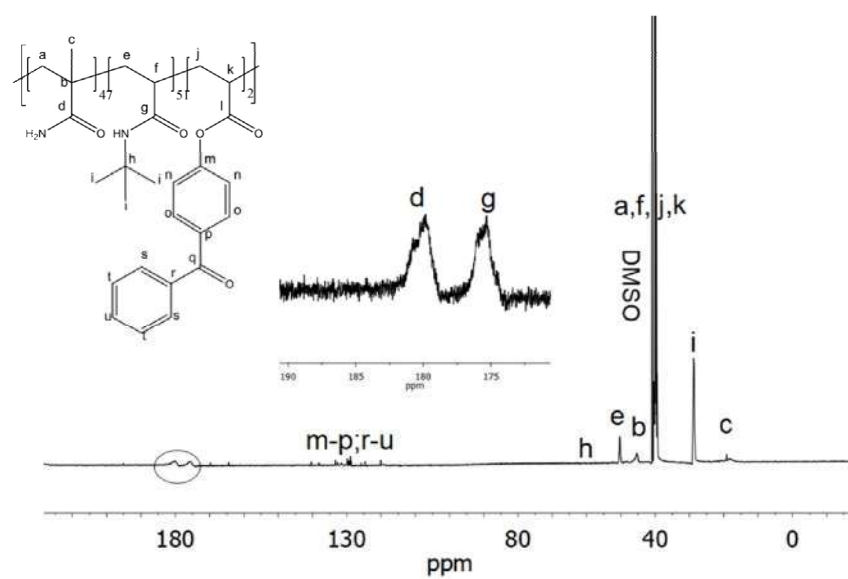


Figure S1. Quantitative ¹³C-NMR of the P(MAAm-NtbAAm-ABP) copolymer.

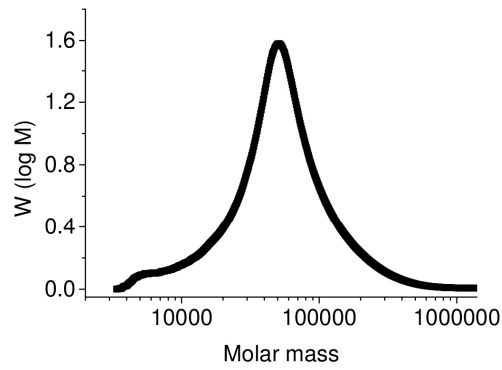


Figure S2. GPC measurement of the synthesized P(MAAm-NtbAAm-ABP) copolymer; $M_p = 71\ 000$.

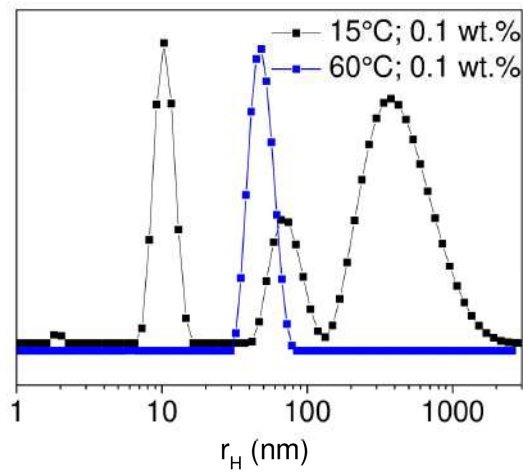


Figure S3. DLS measurement of the P(MAAm-NtbAAm-ABP) copolymer at 15°C (**black**) with an average $r_H = 11$ nm; 60°C (**blue**) with an average $r_H = 60$ nm.

Reprints of Publications

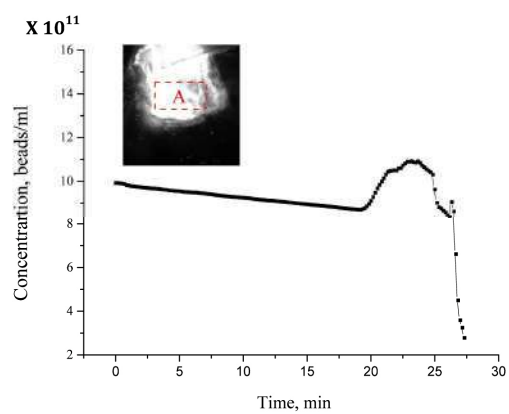


Figure S4. Concentration of the of c-NPs within the fibrous matrix (Area A) at constant temperature of $\sim 23^{\circ}\text{C}$ (0-20 min) and at elevated temperature ($t > 20$ min and at $T > 28^{\circ}\text{C}$).

7.6 Interpenetrating Thermophobic, Thermophilic Dual Responsive Networks

This work was published by **F. Käfer**, Y. Hu, Y.J. Wang, Z. L. Wu, S. Agarwal, *Journal of Polymer Science Part A: Polymer Chemistry* **2019**, 57, 539–54.

Reprinted with permission; Copyright 2018 Wiley Periodicals, Inc.

Interpenetrating Thermophobic and Thermophilic Dual Responsive NetworksFlorian Käfer,¹ Yunfeng Hu,² Yan Jie Wang,² Zi Liang Wu,² Seema Agarwal ²¹Macromolecular Chemistry II and Bayreuth Center for Colloids and Interfaces, Universitätsstrasse 30, 95440, Bayreuth, Germany²Department of Polymer Science and Engineering, Zhejiang University, Hangzhou 310027, China

Correspondence to: S. Agarwal (E-mail: agarwal@uni-bayreuth.de)

Received 24 October 2018; Accepted 13 November 2018; published online 29 November 2018

DOI: 10.1002/pola.29292

ABSTRACT: Poly(*N*-acryloyl glycinamide) (PNAGA)/poly(*N*-isopropyl acrylamide) (PNIPAAm) interpenetrating network (IPN) hydrogels were made by UV-light initiated radical polymerization in two-steps. The IPN hydrogels showed a double thermoresponsive behavior due to the combination of PNIPAAm (thermophobic) and PNAGA (thermophilic) networks. Increasing the content of the thermophobic PNIPAAm network leads to a change from a broad thermophilic volume phase transition temperature of PNAGA to a thermophilic–thermophobic-type dual transition for the prepared IPN. Due to the double thermoresponsive character

of the IPN gels, the mechanical properties are dependent upon temperature as demonstrated by performing tensile tests in water at 15 and 50 °C. Furthermore, the IPN hydrogels were characterized using turbidity measurements, SEM, and the determination of the equilibrium swelling ratio. © 2018 Wiley Periodicals, Inc. *J. Polym. Sci., Part A: Polym. Chem.* **2019**, *57*, 539–544

KEYWORDS: gels; IPN; mechanical properties; phase transitions; thermoresponsive

INTRODUCTION Hydrogels which are responsive to change in the environment like pH, temperature, ionic strength, or magnetic field have received a broad interest in different fields of applications like drug release, tissue engineering, or catalytic systems.¹ Especially for drug release applications multifunctionality of the used gels is often required.² The combination of a thermoresponsive and pH responsive functionality in one system was shown for hydrogels, particles as well as for soft actuators.^{3–5} A widely used method for the production of multi responsive hydrogels for many applications is the synthesis of hydrogels with an interpenetrating network (IPN) structure, shown by many known literature examples.^{6–10} One example for an IPN hydrogel with pH and thermoresponsive behavior was shown by Zhang et al. using poly(methacrylic acid) as a pH responsive network and poly(*N*-isopropyl acrylamide) (PNIPAAm) as a thermoresponsive network, which is well-known for the LCST-type phase transition in water.^{11,12} The corresponding IPN hydrogel showed a change in the swelling behavior at around 32 °C and at a pH = 5.5. Kim et al. prepared an IPN hydrogel by combining poly(vinyl alcohol) with PNIPAAm. The IPN gels show a relatively high swelling ratio in the range from 180 to 300% at 35 °C, depending on the pH and the temperature.¹³ An example for IPN hydrogel with robust mechanical and thermoresponsive properties was shown by Means et al. using poly(2-acrylamido-2-methylpropane sulfonic

acid (PAMPS) as the first network and poly(NIPAAm-co-[2-(methacryloyloxy)ethyl]dimethyl-(3-sulfopropyl)ammonium hydroxide) as the second network.¹⁴ A strong double network hydrogel was shown by Gong et al. using PAMPS and poly(acrylamide) which leads to significant increase in mechanical properties compared to the corresponding single network gels.¹⁵ Wu et al. described a conductive and highly stretchable hydrogel using poly(*N*-acryloyl glycinamide-co-2-acrylamide-2-methylpropanesulfonic) hydrogels and PEDOT/PS to form the IPN structure.¹⁶ In a previous publication they showed the good mechanical properties of PNAGA hydrogels which were prepared by photoinitiated radical polymerization of a concentrated *N*-acryloyl glycinamide (NAGA) solution in water.¹⁷

In this work we show a dual thermoresponsive IPN made by sequentially forming PNAGA and PNIPAAm networks by photo-induced radical polymerization. Changing the content of PNIPAAm as the second network, the swelling/deswelling behavior was changed from a broad thermophilic (positive) volume phase transition temperature (VPTT) of a PNAGA hydrogel to a double thermoresponsive behavior for the prepared IPN hydrogels. The change of mechanical properties of these IPN hydrogels was investigated by tensile tests at 15 and 50 °C. Further, the IPN hydrogels were characterized using FTIR, turbidity, and rheology measurements to study the mechanical and swelling behaviors.

Additional supporting information may be found in the online version of this article.

© 2018 Wiley Periodicals, Inc.

EXPERIMENTAL**Materials**

Glycinamide hydrochloride (98%, Acros Organics, America, China), acryloyl chloride (99%, Sigma-Aldrich), potassium carbonate, *N*-isopropylacrylamide (98%, Sigma-Aldrich), 2-hydroxy-4'-(2-hydroxyethoxy)-2-methylpropiophenone (IRGACURE D-2959, 98%, Sigma-Aldrich), and *N,N'*-methylenebisacrylamide (MBA) (99%, Sigma-Aldrich) were used as received. All other chemicals and solvent are analytical reagents. NAGA has been prepared according to our previous work.¹⁸

Preparation of PNAGA Hydrogels

PNAGA hydrogels were prepared via photoinitiated polymerization using a concentrated precursor solution containing NAGA and IRGACURE D-2959 as photo initiator. Therefore, 0.2 g NAGA were dissolved in 794 μ L MilliQ water. Afterward 6 mg IRGACURE D-2959 (3 wt % relative to NAGA) was added into the solution. The precursor solution was injected into steel rectangle molds (inner width 3 mm, length 25 mm, thickness 1 mm, eight molds in one steel sheet). For bigger hydrogel sheets the solution was filled in a mold with a size of $100 \times 100 \times 1$ mm. The time for UV irradiation was adjusted to 1 min at 25 °C. The obtained hydrogel was washed thoroughly with water to remove impurities and kept in water at room temperature.

Preparation of IPN Hydrogels

A 20 wt % NIPAAm solution containing IRGACURE D-2959 (3 wt % relative to the amount of NIPAAm) and cross-linker (MBA) (20 mol % relative to NIPAAm) was prepared. The PNAGA gel prepared above was soaked in this solution at 35 °C for 24 h. After removing the surface water using a filter paper, the swollen gels were weighed, sandwiched between two glass substrates and then placed atop a bed of ice. A UV lamp with max power of 60 mW cm^{-2} was used to crosslink the second network at 0 °C for 1 min. The IPN gels were purified using dialysis for 2 days. In order to determine the weight ratio of the two components in IPN, the amount of PNIPAAm after dialysis and drying the IPN were calculated as follows:

$$m(\text{PNIPAAm}) = m(\text{IPN}) - m(\text{PNAGA}).$$

$m(\text{PNAGA})$ was determined by weighing after dialysis and drying the PNAGA gel in vacuum.

The weight ratio could be determined as follows:

$$\omega = \frac{m_{\text{PNIPAAm}}}{m_{\text{PNAGA}}}.$$

Differential Scanning Calorimetry

Mettler Toledo 821 DSC module was used for DSC measurements under nitrogen atmosphere (flow rate = 80 mL min^{-1}) at a heating rate of 10 °C min^{-1} .

Fourier-transform infrared spectroscopy

IR spectroscopic measurements were done on a Digilab Excalibur Series FTS 3000 spectrometer by the attenuated total reflection technique employing a diamante crystal.

Equilibrium Swelling Ratio

IPN gels with different weight ratio of PNIPAAm and PNAGA were placed in a glass vial containing 5 mL MilliQ water. The glass vials were kept in a controlled temperature (5–50 °C) water bath for 24 h. Afterward the surface water was blotted out and the samples were immediately weighed (W_i). Afterward, each gel was vacuum dried (Heraeus Vacutherm, 40 °C, 24 h) and weighed (W_d). The equilibrium swelling ratio (ESR) was calculated as ratio of the two (W_i/W_d).

Transparency Measurements

JASCO V-630 Spectrophotometer was applied for the turbidity measurements. The measurements were performed at a wavelength of 660 nm with halter equipped with two quartz glasses (Hellma Analytics, Germany), fixing the sample in-between. The heating rate was set to 1 °C min^{-1} .

Kinetic Swelling and Deswelling Studies

The gels were placed in sealed vial containing 5 mL MilliQ water at the starting temperature until the equilibrium mass (W_0) was constant. Then the gels were transferred immediately into a water bath heated to 20 and 40 °C, respectively. After defined time intervals, each gel was taken out from vial, blotted with Kim Wipe paper, and immediately weighed (W_t) and returned to vial for subsequent measurements. After the gels showed no weight change, the gels were dried in vacuum oven (Heraeus Vacutherm, 40 °C, 24 h) and weighed (W_d) afterward. The water retention was calculated as follows: $W_R = (W_t - W_d)/W_s$.

Mechanical Property

Mechanical tests of hydrogels were carried out on a Zwick Roell BT1-FR0 5TN.D14 tensile test device at room temperature. The stress-strain measurements at 15 and 50 °C in water were performed on a commercial tensile tester (Instron 3343). Before the measurements, all samples were fully equilibrated in Millipore-water. The samples were cut into dumb-bell shape with an initial gauge length of 12 mm and a width of 2 mm. The extension rate was set at 50 mm min^{-1} . All samples were measured three times.

Rheological Measurements

The rheological measurements were performed on an Anton Paar MCR 302 using a plate PP25 with a diameter of 25 mm. For the measurement a constant force of $F = 0.15$ N was set. The sample thickness was 1 mm. A cooling/heating cycle (5–50 °C) was performed, beginning with cooling. The heating rate was 1 °C min^{-1} .

RESULTS AND DISCUSSION

The IPN hydrogels were obtained with a two-step preparation technique starting with the synthesis of PNAGA gels, performing a photoinitiated free-radical polymerization using a concentrated aqueous NAGA solution. Sequentially, a second step, including the soaking of NIPAAm, cross-linker, and initiator solution, and the UV-light initiated polymerization was performed to obtain IPN PNAGA/PNIPAAm, as shown in Scheme 1.

In order to show the effect of the second network, the amount of NIPAAm was varied. IPNs with different weight ratios of NIPAAm and NAGA were prepared ($\omega = 0.1, 0.2, 0.4, \text{ and } 0.7$ were prepared).

FTIR spectra (Supporting Information Fig. S1) confirmed the existence of both polymers in the IPN, due the observed signals of the amide group at $\delta = 3271 \text{ cm}^{-1}$ (s, NH_2), 1555 cm^{-1} (vs, NH) and isopropyl functional group from PNIPAAm at $\delta = 1380 \text{ cm}^{-1}$. Further, the presence of the two glass transition temperatures at $135 \text{ }^\circ\text{C}$ (PNIPAAm) and $175 \text{ }^\circ\text{C}$ (PNAGA) showed the existence of two networks^{19,20} (Supporting Information Fig. S2).

In order to demonstrate the thermoresponsive properties of the IPN hydrogels, temperature-dependent turbidity measurements were performed (Fig. 1). PNAGA gel with physical cross-linking via H-bonding in water at room temperature ($20 \text{ }^\circ\text{C}$) was transparent with high transmittance (93%) and showed a continuous thermophilic-type change of around 10% transmittance in a temperature range from 0 to $60 \text{ }^\circ\text{C}$. By contrast, the transmittance change for the IPNs was dependent upon the amount of PNIPAAm. The IPN 1 with a weight ratio of $\omega = 0.1$ showed clearly two phase transitions: a thermophilic transition showing a continuous sharp and significant change in the transmittance reaching a maximum at about $30 \text{ }^\circ\text{C}$ followed by a small decrease in transmittance. Increasing the PNIPAAm content resulted in a thermophilic transition followed by a sharp decrease in the transmittance. In general, the change in transmittance for the thermophilic transition decreased on increasing the amount of PNIPAAm, that is, on going from IPN1 to IPN4. The sharp phase transition at $32 \text{ }^\circ\text{C}$ of the IPN gels matched well with the LCST-type phase transition of PNIPAAm, indicating a successful introduction of a PNIPAAm network and dual thermoresponsivity of IPNs.²¹

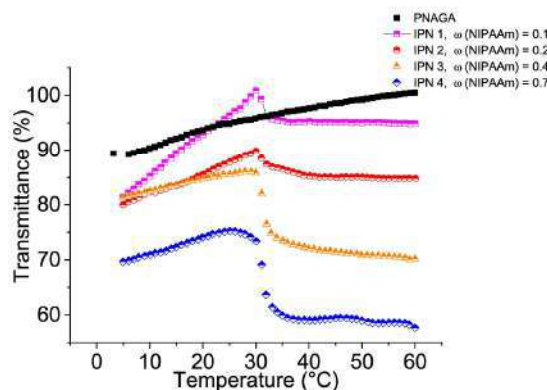
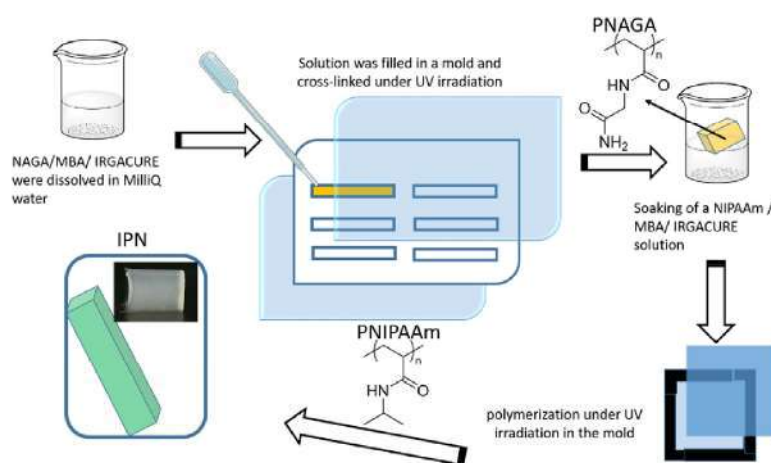


FIGURE 1 Temperature dependence of transmission of PNAGA; IPN 1–4, $\omega = 0.1$ – 0.7 . All curves were obtained from first cooling process. [Color figure can be viewed at wileyonlinelibrary.com]

Furthermore, the temperature-dependent ESR of the IPN gels was also investigated. As shown in Figure 2(A), PNAGA gel showed a continuous swelling when the temperature increased from 5 to $50 \text{ }^\circ\text{C}$, indicating a broad thermophilic phase transition. For IPN 1 ($\omega = 0.1$) and IPN 2 ($\omega = 0.2$) with a low weight fraction of PNIPAAm, the ESR was similar to the ESR of the PNAGA. In contrast, a sharper transition of ESR was observed when the percentage of the second network (PNIPAAm) increased above a critical ratio [Fig. 2(D)]. Particularly, IPN 4 ($\omega = 0.7$) exhibited a significant decrease by around 25% in ESR, beginning at $30 \text{ }^\circ\text{C}$ and reaching a plateau at around $35 \text{ }^\circ\text{C}$. Below the VPTT, PNIPAAm was in the hydrophilic open coil state, and the increase in temperature weakened the H-bonding between PNAGA chains and thus led to swelling of the IPN hydrogel. At around $30 \text{ }^\circ\text{C}$ the



SCHEME 1 Schematic preparation of PNAGA/PNIPAAm IPN hydrogels. [Color figure can be viewed at wileyonlinelibrary.com]

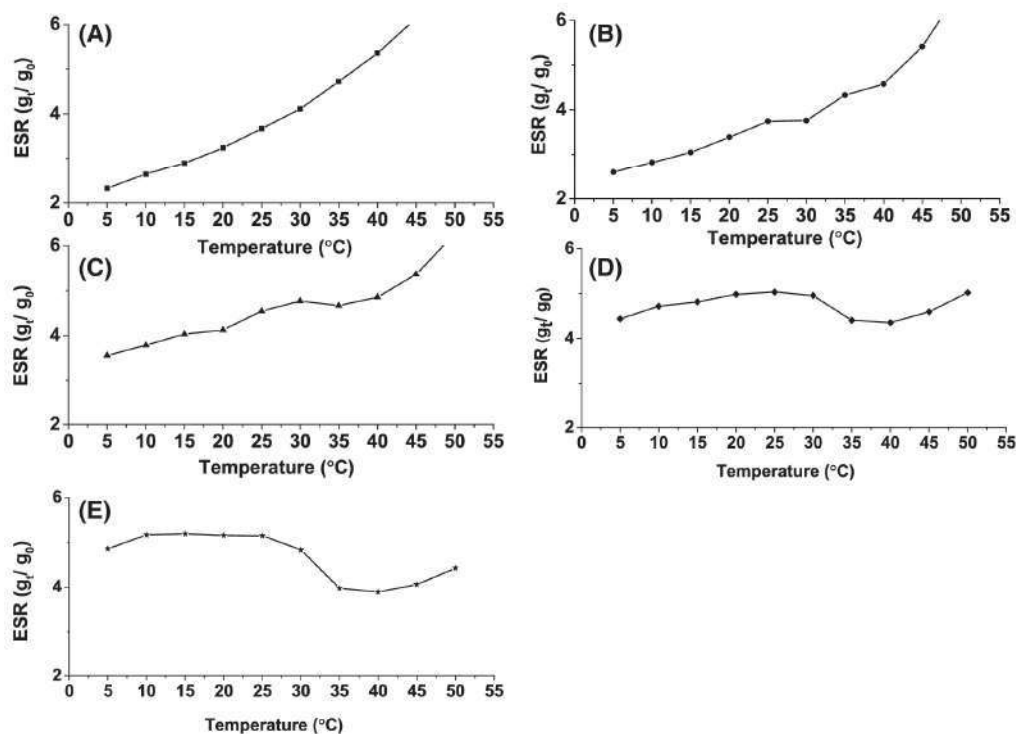


FIGURE 2 Temperature dependence of equilibrium swelling ratio of (A) PNAGA; IPN 1–4 with different weight ratio (B) IPN 1, $\omega = 0.1$ (C) IPN 2, $\omega = 0.2$ (D) IPN 3, $\omega = 0.4$ (E) IPN 4, $\omega = 0.7$.

conformation of PNIPAAm is changing from an open coil to a globule state causing an increase in hydrophobicity and deswelling of the IPN. A second swelling step was occurred above 45 °C, which is corresponding to the swelling of PNAGA whereas PNIPAAm goes into the globule state. The change of the conformation of PNAGA and PNIPAAm from an open coil state to a globule state was shown in the literature.^{22,23} In general, the IPN hydrogels with a weight ratio of $\omega = 0.4$ (IPN3) and $\omega = 0.7$ (IPN4) showed a two-stage transition, including a broad thermophilic-type and a thermophobic-type VPTT.

Furthermore, the IPN showed fast swelling–deswelling as shown for IPN 4 sample with a weight ratio of $\omega = 0.7$. A rapid swelling from 40 to 20 °C and deswelling from 20 to 40 °C were obtained (Fig. 3).

Besides, rheology measurements of PNAGA and IPN 4 were performed (Fig. 4). For PNAGA a temperature-dependent change in the storage module G' was observed at 12 °C during the cooling and 25 °C during the heating [Fig. 4(A)]. This corresponds to the cloud points of a PNAGA solution.¹⁸ For IPN 4 a decrease in G' at around 25 °C followed by an increase in G' at 15 °C in the cooling cycle was observed due the dual responsive IPN [Fig. 4(B)]. The measurements

could not be performed during heating cycle due to the lack of proper closed measuring cell avoiding evaporation of water during heating. Nevertheless, IPN4 showed a double transition due to the coexistence of PNAGA and PNIPAAm networks.

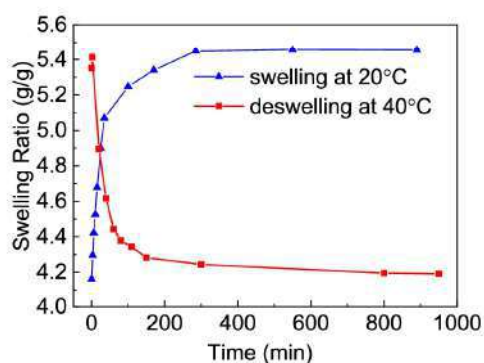


FIGURE 3 Swelling and deswelling kinetics of IPN 4 at 20 °C (swelling) and 40 °C (deswelling) in MilliQ water. [Color figure can be viewed at wileyonlinelibrary.com]

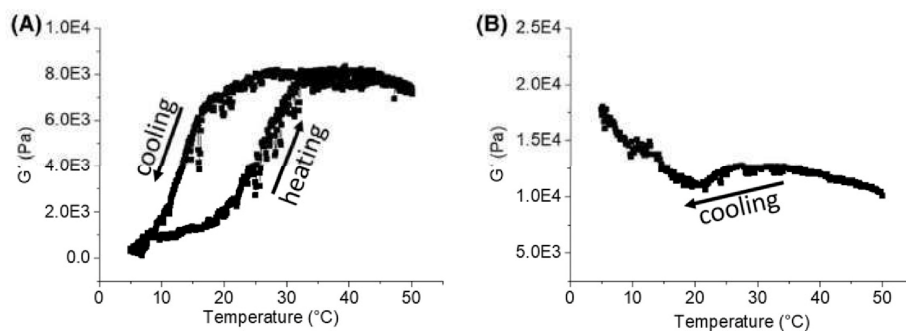


FIGURE 4 Cooling/heating cycle (5–50 °C) rheology measurements of PNGA and IPN 4 with a constant force of 0.15 N.

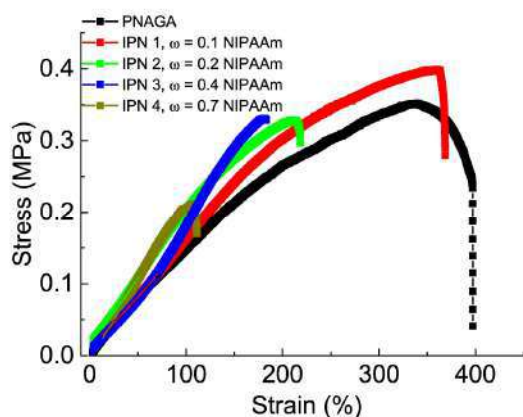


FIGURE 5 Stress–strain curves of PNAGA/PNIPAAm IPN gels in the equilibrated state at 25 °C of samples PNAGA and IPN 1–4. [Color figure can be viewed at wileyonlinelibrary.com]

Tensile measurements were performed after equilibration in water at room temperature (22 ± 1 °C) (Fig. 5).

Although, there was a decrease in the breaking strain on increasing the amount of NIPAAm in the IPNs, still the IPN with a weight ratio of $\omega = 0.4$ (IPN3) showed a high breaking strain of $183 \pm 5\%$. In comparison, the PNIPAAm hydrogel had a low breaking strain of around 35% in the swollen state and around 70% in the collapsed state.^{24,25} Owing to the thermoresponsive behavior of the IPN gels, the mechanical properties were influenced by the temperature. Tensile measurements were also carried out in water at 15 and 50 °C, below the VPTT of PNIPAAm and above of the VPTT of PNAGA, respectively (Fig. 6, Supporting Information Table S1). The IPN with lower amount of NIPAAm (IPN1-2, $\omega = 0.1$ –0.2) showed increased breaking strain from $211 \pm 39\%$ (IPN 1) to $340 \pm 85\%$ with decreased breaking stress from 0.34 to 0.26 MPa when the temperature increased from 15 to 50 °C, which led to destruction of the H-bonds between PNAGA chains.¹⁷ The same trend was observed for IPN2 ($\omega = 0.2$). Further increase in the amount of PNIPAAm resulted in decrease in mechanical properties of the IPN gel (IPN3-4, $\omega = 0.4$ –0.7), almost in the same range as that of pure PNIPAAm.²²

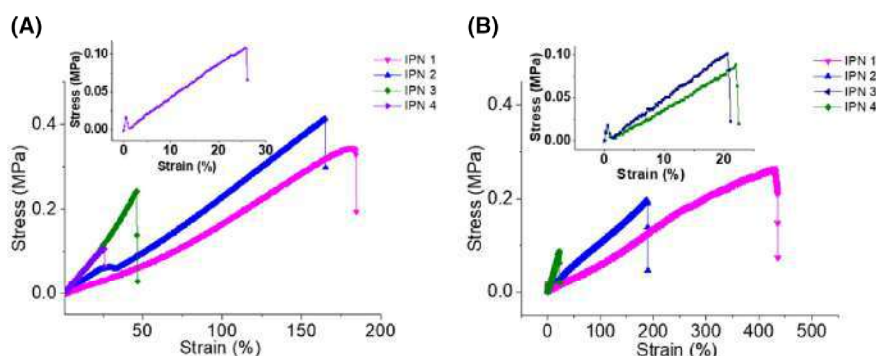


FIGURE 6 Stress–strain curves of PNAGA/PNIPAAm IPN gels. (A) Stress/strain measurements in water at 15 °C of IPN samples; (B) stress strain measurements in water at 50 °C of IPN sample. [Color figure can be viewed at wileyonlinelibrary.com]

CONCLUSIONS

In this work, we showed the preparation and characterization of new dual thermoresponsive IPN hydrogels combining thermophilic phase transition of PNAGA with thermophobic transition of PNIPAAm. The dual responsivity is dependent upon the weight ratio of the two networks. Turbidity, rheology, and ESR measurements were performed to show the effect of the PNIPAAm content on the thermoresponsive behavior, which changed from a thermophilic phase transition behavior to a double thermoresponsive behavior of the IPN hydrogels by increasing the weight ratio of PNIPAAm. The tensile measurements showed the gels with breaking stress of 0.2–0.4 MPa and breaking strain of 100–400% depending upon the amount of PNIPAM in the IPN. Furthermore, temperature-dependent mechanical properties were found in these IPN gels. The IPN gel (IPN 1–2) showed improved breaking strain yet almost constant breaking stress when the temperature increased from 15 to 50 °C. Therefore, a series of IPN hydrogels including those with good mechanical properties (low PNIPAAm content) and a dual thermoresponsive behavior (high PNIPAAm content) were obtained, which can be used depending on the application requirements.

ACKNOWLEDGMENT

The authors would like to thank Deutsche Forschungsgemeinschaft (DFG) for the financial support.

REFERENCES AND NOTES

- 1 E. M. Ahmed, *J. Adv. Res.* **2015**, *6*, 105.
- 2 T. R. Hoare, D. S. Kohane, *Polymer* **2008**, *49*, 1993.
- 3 C. Zhao, X. Zhuang, P. He, C. Xiao, C. He, J. Sun, X. Chen, X. Jing, *Polymer* **2009**, *50*, 4308.
- 4 T. Wan, Q. Chen, Q. Zhao, R. Huang, L. Liao, J. Xiong, L. Tang, *J. Appl. Polym. Sci.* **2015**, *132*, 42139.
- 5 L. Liu, H. Bakhshi, S. Jiang, H. Schmalz, S. Agarwal, *Macromol. Rapid Commun.* **2018**, *39*, 1800082.
- 6 S. Suri, C. E. Schmidt, *Acta Biomater.* **2009**, *5*, 2385.
- 7 Y. Shi, L. Peng, G. Yu, *Nanoscale* **2015**, *7*, 12796.
- 8 E. S. Dragan, *Chem. Eng. J.* **2014**, *243*, 572.
- 9 D. Myung, D. Waters, M. Wiseman, P.-E. Duhamel, J. Noolandi, C. N. Ta, C. W. Frank, *Polym. Adv. Technol.* **2008**, *19*, 647.
- 10 K. Yasuda, J. P. Gong, Y. Katsuyama, A. Nakayama, Y. Tanabe, E. Kondo, M. Ueno, Y. Osada, *Biomaterials* **2005**, *26*, 4468.
- 11 C. Boutris, E. G. Chatzi, C. Kiparissides, *Polymer* **1997**, *38*, 2567.
- 12 J. Zhang, N. A. Peppas, *Macromolecules* **2000**, *33*, 102.
- 13 S. J. Kim, S. J. Park, S. I. Kim, *React. Funct. Polym.* **2003**, *55*, 61.
- 14 A. K. Means, D. A. Ehrhardt, L. V. Whitney, M. A. Grunlan, *Macromol. Rapid Commun.* **2017**, *38*, 1700351.
- 15 J. P. Gong, Y. Katsuyama, T. Kurokawa, Y. Osada, *Adv. Mater.* **2003**, *15*, 1155.
- 16 Q. Wu, J. Wei, B. Xu, X. Liu, H. Wang, W. Wang, Q. Wang, W. Liu, *Sci. Rep.* **2017**, *7*, 41566.
- 17 X. Dai, Y. Zhang, L. Gao, T. Bai, W. Wang, Y. Cui, W. Liu, *Adv. Mater.* **2015**, *27*, 3566.
- 18 J. Seuring, F. M. Bayer, K. Huber, S. Agarwal, *Macromolecules* **2011**, *45*, 374.
- 19 R. G. Sousa, W. Magalhães, R. Freitas, *Polym. Degrad. Stab.* **1998**, *61*, 275.
- 20 M. Noh, S. Kang, Y. Mok, S. J. Choi, J. Park, J. Kingma, J. H. Seo, Y. Lee, *Chem. Commun.* **2016**, *52*, 509.
- 21 H. C. Haas, N. W. Schuler, *J. Polym. Sci., Part B: Polym. Lett.* **1964**, *2*, 1095.
- 22 C. Wu, X. Wang, *Phys. Rev. Lett.* **1998**, *80*, 4092.
- 23 M. Taylor, P. Tomlins, T. Sahota, *Gels* **2017**, *3*, 4.
- 24 M. A. Haq, Y. Su, D. Wang, *Mater. Sci. Eng. C* **2017**, *70*, 842.
- 25 T. Takigawa, T. Yamawaki, K. Takahashi, T. Masuda, *Polym. Gels Networks* **1998**, *5*, 585.

Supporting Information for

Interpenetrating thermophobic, thermophilic dual responsive networks

Florian Käfer,¹ Yunfeng Hu,² Yan Jie Wang², Zi Liang Wu², Seema Agarwal²

¹Macromolecular Chemistry II and Bayreuth Center for Colloids and Interfaces, Universitätsstrasse 30, 95440 Bayreuth, Germany

²Department of Polymer Science and Engineering Zhejiang University Hangzhou 310027, China
Correspondence to: Seema Agarwal (E-mail: agarwal@uni-bayreuth.de)

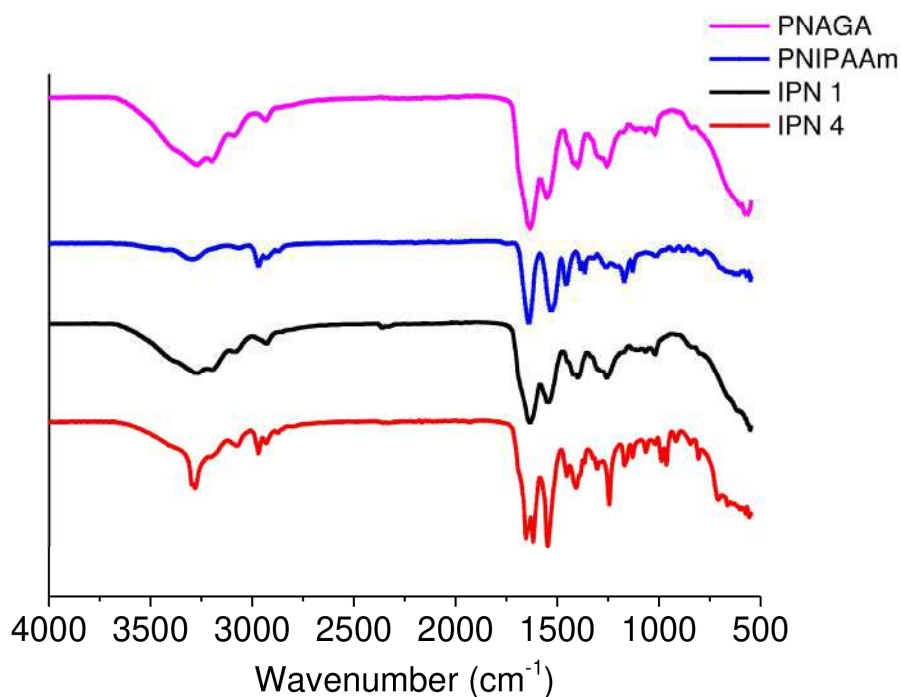


Figure S1 FTIR spectra of PNAGA, PNIPAAm and the prepared IPN hydrogels with the lowest (IPN 1) respectively with highest (IPN 5) content, PNIPAAm and PNIPAAm; 3271 (s, NH₂), 3202 (m, NH), 3090 (m, NH), 1632 (vs, C=O), 1555 (vs, NH), 1380-1370 (s, iso propyl), cm⁻¹.

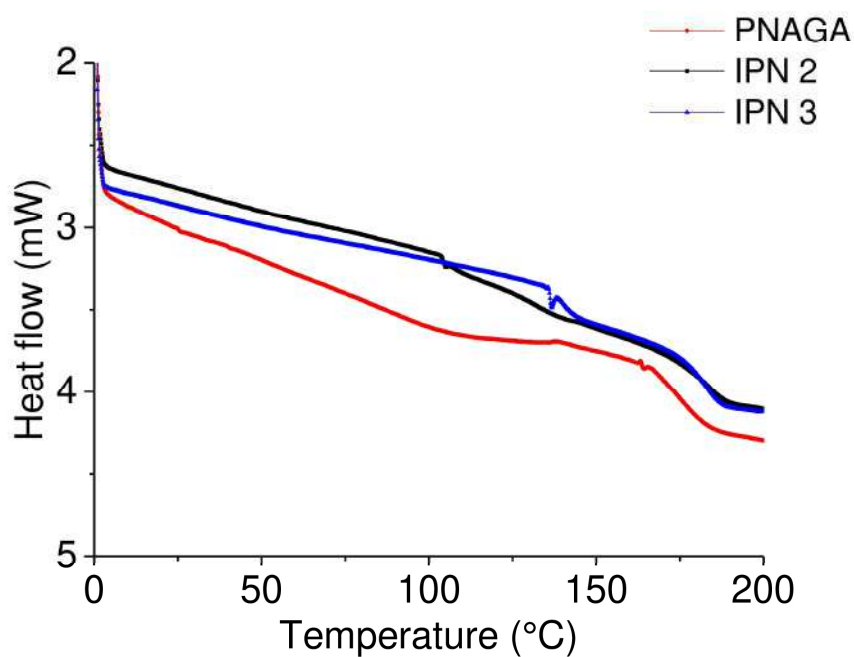


Figure S2: Differential calorimetry measurements of PNAGA, IPN 2 and IPN 3. Heating rate 10 °C/min. The T_g was determined from the second heating curve.

TABLE S1 Prepared IPN gels using a two-step technique using photo-initiated free radical polymerization.

| Entry ^a | $\omega(\text{PNIPAAm})$ | breaking strain 15°C (%) | breaking strain 50°C (%) | Young's modulus (MPa) at 15°C | Young's modulus (MPa) at 50°C |
|--------------------|--------------------------|--------------------------|--------------------------|---|---|
| IPN 1 | 0.1 | 211±39 | 340±85 | $1.3 \cdot 10^{-3} \pm 4.5 \cdot 10^{-5}$ | $5.7 \cdot 10^{-4} \pm 1.9 \cdot 10^{-5}$ |
| IPN 2 | 0.2 | 154±11 | 173±17 | $2.3 \cdot 10^{-3} \pm 8.7 \cdot 10^{-5}$ | $6.4 \cdot 10^{-4} \pm 4.4 \cdot 10^{-5}$ |
| IPN 3 | 0.4 | 53±6 | 21±2 | $4.2 \cdot 10^{-3} \pm 3.1 \cdot 10^{-4}$ | $6.2 \cdot 10^{-3} \pm 3.8 \cdot 10^{-4}$ |
| IPN 4 | 0.7 | 23±4 | 21±11 | $5.3 \cdot 10^{-3} \pm 1.6 \cdot 10^{-4}$ | $3.7 \cdot 10^{-3} \pm 2.2 \cdot 10^{-4}$ |

^a breaking strain PNAGA swollen at RT 360±47 %, Young's modulus $1.69 \cdot 10^{-3} \pm 2.2 \cdot 10^{-5}$ MPa

8 Outlook

As it is shown in this dissertation by use of a number of examples, thermoresponsive polymers are attracting a growing interest in research as well as in a wide range of applications. In recent years, considerable progress has been made in understanding UCST phase transition behavior. Nevertheless, a number of questions remain to which there is no answer and which require further and more precise studies. In this case, novel acrylamide-based *N*- or α -substituted comonomers could play an important role as they can show a significant impact on the phase transition behavior. The hydrophobicity and size of the substituents seem to be the main factors influencing the formation of hydrogen bonds and complex structures, which, in the future, should be characterized by neutron and dynamic light scattering studies using the copolymers synthesized in this thesis, and by using new synthesized acrylamide-based α -substituted comonomers.

Moreover, the temperature-controlled change of the polymer morphology from micelles to aggregates and to micelles again opens a broad field of possible applications in the field of biomedicine, as shown in this thesis. Furthermore, the application of thermoresponsive IPN hydrogels is highly considerable in this field. Nevertheless, due to promising applications such as hydrogel microactuators, artificial muscles, etc., thermoresponsive fiber mats which show a strong contraction when the ambient temperature is changed should not be forgotten. Such a system could be used for wound care and a temperature-controlled release of drugs into open skin lesions.

9 Conferences participation

2015 Bayreuther Polymer Symposium, Bayreuth (**poster presentation**)

2016 99th Canadian Chemistry Conference and Exhibition, Halifax Canada (poster presentation) **2nd poster award**

2016 99th Canadian Chemistry Conference and Exhibition, Halifax Canada (Oral presentation)

2017 German-Israel-Palestine trilateral cooperation (GIP) meeting, Rhodes Greek (part of a presentation)

2017 Bayreuther Polymer Symposium, Bayreuth

2018 Macromolecular Colloquium Freiburg

2018 4-week research exchange to Zhejiang University with Prof. Zi Liang Wu, Hangzhou China

10 Acknowledgment

I would particularly like to thank my supervisor Prof. Seema Agarwal for her dedication to improve my scientific skills and for everything I have learned and experienced with her support during this time.

I would also like to thank Prof. Dr. Andreas Greiner and Dr. Holger Schmalz for helpful discussions, their guidance and very useful pieces of advice.

Thanks to Prof. Dr. Matthias Karg, Prof. Dr. Eyal Zussman, Prof. Dr. Zi Liang Wu and everyone else for the good and valuable cooperation.

Furthermore, I would like to thank the entire MC 2 group for the good time and the great support. Special thanks to Dr. Holger Pletsch, Dr. Fangyao Liu, Dr. Amanda Pineda, Dr. Markus Langer, Steffen Reich, Matthias Burghardt, Tobias Moss, Amir Bagheri, Dr. Judith Schöbel, Dr. Hadi Bakhshi, Marius Feldmann, Thomas Schmitt, Rika Schneider, Bianca Uch and all my student assistants for their support and suggestions. I would particularly like to thank Martin Pretscher for his great work as my student assistant.

I am very grateful to Dr. Li Liu and Mahsa Mafi for the deep friendship and the great time we shared together.

Ultimately, I would like to express deep gratitude to my family for their continuous support.

11 (Eidesstattliche) Versicherung und Erklärungen

(§ 9 Satz 2 Nr. 3 PromO BayNAT)

Hiermit versichere ich eidesstattlich, dass ich die Arbeit selbständig verfasst und keine anderen als die von mir angegebenen Quellen und Hilfsmittel benutzt habe (vgl. Art. 64 Abs. 1 Satz 6 BayHSchG).

(§ 9 Satz 2 Nr. 3 PromO BayNAT)

Hiermit erkläre ich, dass ich die Dissertation nicht bereits zur Erlangung eines akademischen Grades eingereicht habe und dass ich nicht bereits diese oder eine gleichartige Doktorprüfung endgültig nicht bestanden habe.

(§ 9 Satz 2 Nr. 4 PromO BayNAT)

Hiermit erkläre ich, dass ich Hilfe von gewerblichen Promotionsberatern bzw. –vermittlern oder ähnlichen Dienstleistern weder bisher in Anspruch genommen habe noch künftig in Anspruch nehmen werde.

(§ 9 Satz 2 Nr. 7 PromO BayNAT)

Hiermit erkläre ich mein Einverständnis, dass die elektronische Fassung meiner Dissertation unter Wahrung meiner Urheberrechte und des Datenschutzes einer gesonderten Überprüfung unterzogen werden kann.

(§ 9 Satz 2 Nr. 8 PromO BayNAT)

Hiermit erkläre ich mein Einverständnis, dass bei Verdacht wissenschaftlichen Fehlverhaltens Ermittlungen durch universitätsinterne Organe der wissenschaftlichen Selbstkontrolle stattfinden können.

Bayreuth, den 26.06.2019



Florian Käfer